The Role of TRIM71 in Male Germ Cell Development

- Dissertation -

zur
Erlangung des Doktorgrades (Dr. rer. nat.)
der
Mathematisch-Naturwissenschaftlichen Fakultät
der
Rheinischen Friedrich-Wilhelms-Universität Bonn

vorgelegt von

Yasmine Port

aus Lich

Bonn, Mai 2020

Angefertigt mit Genehmigung der Mathematisch-Naturwissenschaftlichen Fakultät der Rheinischen Friedrich-Wilhelms-Universität Bonn

1. Gutachter: Prof. Dr. Waldemar Kolanus

2. Gutachter: PD Dr. Heike Weighardt

Tag der Promotion: 14.08.2020

Erscheinungsjahr: 2020

Table of contents

Preliminary remarks

According to the common practice in English scientific writing, the present dissertation is partially written using the first-person plural narrator.

The thesis has been written without the assistance of third parties using only the indicated sources with appropriate reference made to the work of others.

All experiments described in this work have been performed by me except for the Illumina MiSeq analysis (excluding sample preparation and data analysis) which has been conducted at the Next Generation Sequencing (NGS) Core Facility of the Medical Faculty at the University Bonn (Dr. André Heimbach, Life & Brain Center, University Bonn).

List of figures

List of abbreviations

%	percent
°C	degrees Celsius
µ	micro
7-AAD	7-aminoactinomycin D
a	ammonium persulfate
A	Austria
A488	Alexa488 fluorophore
A_{al}	$A_{aligned}$
AGO	Argonaute
ANOVA	analysis of variance
AP	alkaline phosphatase
APC	Allophycocyanin
A_{pr}	A_{paired}
A_s	A_{single}
B	Belgium
BCA	bicinchoninic acid
BIM	BCL2-like 11 (BCL2L11)
BLIMP1	B lymphocyte-induced maturation protein 1
bp	base pair
BSA	bovine serum albumin
C. elegans	*Caenorhabditis elegans*, nematode
Cas	CRISPR-associated protein
CC	coiled-coil
CDK	cyclin-dependent kinase
CDKN1A	cyclin-dependent kinase inhibitor 1A
cDNA	complementary DNA
CH	Switzerland
CHC	choriocarcinoma
c-KIT	KIT proto-oncogene receptor tyrosine kinase
CRISPR	clustered regularly interspaced short palindromic repeats
crRNA	CRISPR RNA
CsCl	caesium chloride
Cy3	cyanine3 fluorophore
d	day
D	Germany
D. melanogaster	*Drosophila melanogaster*, fruit fly
D. rerio	*Danio rerio*, zebrafish
DAPI	4',6-diamidino-2-phenylindole
ddH_2O	double distilled water
DIC	differential interference contrast
DMEM	Dulbecco's Modified Eagle's Medium
DMSO	dimethyl sulfoxide
DNA	deoxyribonucleic acid
dNTP	deoxyribonucleotide triphosphate
DSB	double strand break
dsDNA	double-stranded DNA
DTT	dithiothreitol
E	embryonic day
E. coli	*Escherichia coli*, bacterium
e.g.	for example
EC	embryonal carcinoma
ECL	enhanced chemiluminescence
EDTA	ethylenediaminetetraacetic acid
EGC	embryonic germ cell
eGFP	enhanced green fluorescent protein
EGR1	early growth response 1
EpiLC	epiblast-like cells
ESC	embryonic stem cell
et al.	*et alli* (Latin: and others)
EtBr	ethidium bromide

etc.	*etcetera* (Latin: and other, similar)
EV	empty vector
f	forward
FACS	fluorescence activated cell sorting
FCS	fetal calf serum
FGF	fibroblast growth factor
FRAGILLIS	interferon induced transmembrane protein 3 (IFITM3)
FSC	forward scatter
g	gram
GCNIS	germ cell neoplasia *in situ*
GFP	green fluorescent protein
GRHL3	grainyhead-like transcription factor 3
h	hour
H&E	hematoxylin and eosin
HBS	HEPES buffered saline
HDR	homology-directed repair
HEK	human embryonic kidney
HEPES	hydroxyethylpiperazineethane sulfonic acid
HMGA2	high mobility group AT-hook 2
HPRT	hypoxanthine phosphoribosyltransferase
HRP	horseradish peroxidase
IgG	immunoglobulin G
indels	insertion and deletion mutations
INHBB	inhibin subunit beta B
iPSC	induced pluripotent stem cell
IT	Italy
IVC	individually ventilated cage
JP	Japan
kb	kilo bases
kDa	kilodalton
KLF4	kruppel-like factor 4
KO	knockout
l	litre
LB	lysogeny broth
let-7	lethal 7
LIN28	abnormal cell lineage 28
LIN-41	abnormal cell lineage 41
LPA	linear polyacrylamide
m	milli; metre
M	molar
M. musculus	*Mus musculus*, mouse
MedFI	median fluorescence intensity
MFI	mean fluorescence intensity
min	minute
miRNA	micro RNA
mRNA	messenger RNA
n	nano, number of experimental repetitions
NANOS3	nanos C2HC-type zinc finger 3
NHEJ	non-homologous end joining
NMD	nonsense-mediated decay
ns	non-significant
nts	nucleotides
OCT4	octamer-binding protein 4
OD	optical density
P	postnatal day
p	pico; p-value (probability value)
P/S	Penicillin/Streptomycin
PAGE	Polyacrylamide Gel Electrophoresis
PAM	protospacer adjacent motif
P-bodies	processing bodies
PBS	phosphate buffered saline
PBST	phosphate buffered saline plus Triton X-100

PCR	polymerase chain reaction
PFA	paraformaldehyd
PGC	primordial germ cell
PGCLC	PGC-like; primordial germ cell like
pH	pondus hydrogenii
PLXNB2	plexin B2
PMSF	phenylmethanesulfonyl fluoride
Prdm14	PR domain containing 14
PUMA	p53-upregulated modulator of apoptosis
qRT-PCR	quantitative real time PCR
r	reverse
RBL	retinoblastoma-like
RBP	RNA binding protein
RING	really interesting new gene
RIPA	radioimmunoprecipitation assay buffer
RNA	ribonucleic acid
rpm	revolutions per minute
RPMI	Roswell Park Memorial Institute Medium
RT	reverse transcriptase
s	second
S. pyogenes	*Streptococcus pyogenes*
SCF	stem cell factor
SCO	sertoli-cell-only
SD	standard deviation
SDS	sodium dodecyl sulfate
SEM	standard error of the mean
sgRNA	single guide RNA
SHCBP1	SHC SH2-domain binding protein 1
siRNA	small interfering RNA
SOX2	SRY (sex determining region Y)-box 2
SPF	specific-pathogen free
SSC	spermatogonial stem cell
SSC	sideward scatter
STELLA	developmental pluripotency associated 3 (DPPA3)
TALEN	transcription activator-like effector nuclease
TBST	tris-buffered saline plus Tween 20
TEMED	tetramethylethylenediamine
TER	teratoma
TFAP2C	transcription factor AP-2 gamma
TGCT	testicular germ cell tumour
TNAP	tissue non-specific alkaline phosphatase
tracrRNA	trans-activating RNA
TRIM	tripartite motif
TRIM71	tripartite motif containing 71
Tris	tris (hydroxymethyl) aminomethane
U	enzymatic units
UK	United Kingdom
USA	United States of America
UTR	untranslated region
UV	ultraviolet
V	volt
v/v	volume per volume
w/v	weight per volume
WB	Western blot
WHO	World Health Organisation
WT	wild type
YST	yolk sac tumour
ZFN	zinc finger nuclease

1 Introduction

Reproduction is the key to continuation of life. Every new life in sexual reproducing organisms starts with the fusion of a male (sperm) and female (oocyte) gamete giving rise to a totipotent zygote. Although the understanding of mammalian germ cell development has advanced significantly, infertility still remains a problem in modern society with 15 % of couples being unable to conceive within one year [4, 119]. Genetic defects during (embryonic) germ cell development are a major cause of infertility which also increases the susceptibility to testicular germ cell tumours (TGCT) in adolescent and young adult men [165, 229, 324]. Therefore, understanding the genetics of germ cell determination and differentiation is of high importance for elucidating the causes of infertility. The present work investigates TRIM71, a member of the TRIM-NHL protein family, as a genetic factor involved in male germ cell development in mice and human.

1.1 Murine embryonic germ cell development

Germ cells are the only cell type capable of generating an entirely new living multi-cellular organism ensuring the transmission of genetic and epigenetic information from one generation to the next [181, 250]. In mammals, gametes are derived from precursor cells called primordial germ cells (PGCs). During early mouse embryogenesis, at around embryonic day 6.25 (E6.25), PGCs start to develop from the proximal epiblast and are set aside from the somatic lineage for unique development [147]. The murine germ cell development can be divided into four stages: induction, specification, migration and sexual differentiation of the germ cells (Figure 1.1).

1.1.1 Induction of germ cell development

In the first stage of germ cell development, germ cell competence is induced in cells of the proximal posterior epiblast between E5.5 and E6.25 in response to extraembryonic signals (reviewed in [18, 97, 147, 212]). The acquirement of germ cell competence is the gain of PGC fate and the prerequisite for these cells to escape the somatic differentiation. Active BMP signalling induces the gene expression of the interferon-inducible transmembrane protein *Fragilis* (or *Ifitm3*) in the pluripotent proximal epiblast cells demarcating them from somatic neighbours and marking the onset of germ cell competence [247].

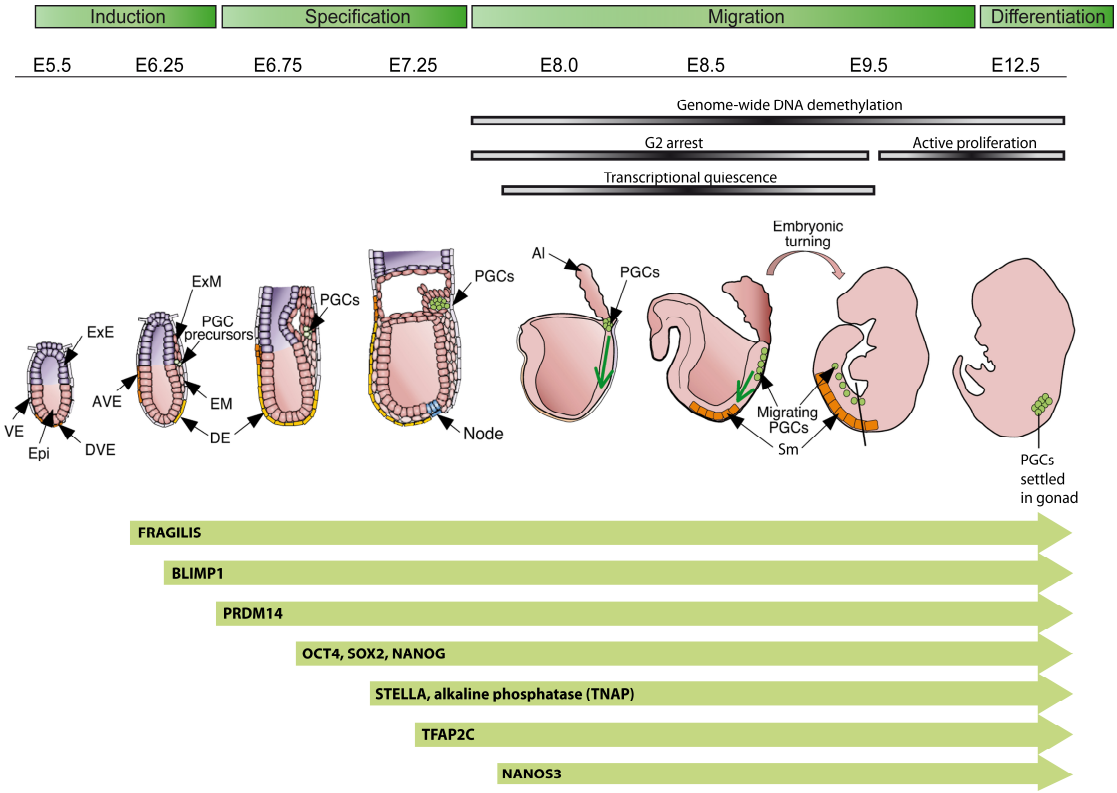

Figure 1.1 – Overview of the embryonic germ cell development in mice
Primordial germ cells (PGCs) are specified at E6.25 in the proximal posterior epiblast and migrate along the hindgut and through the mesentery to the genital ridges until E12.5. PGCs are illustrated as green circles. The direction of PGC migration is depicted by a green arrow and the timing of key germ cell marker expression is denoted by light green bold arrows below. Al = allantois; AVE = anterior visceral endoderm; DE = distal endoderm; DVE = distal visceral endoderm; EM = embryonic mesoderm; Epi = epiblast; ExE = extra-embryonic ectoderm; ExM = extra-embryonic mesoderm; PGCs = primordial germ cells; Sm = somite; VE = visceral endoderm. Adapted with permission from Development, originally published in Saitou *et al.* [248].

1.1.2 Specification of primordial germ cells

At E6.25 the FRAGILIS-positive cells of the proximal epiblast as well as the somatic neighbours display a similar gene expression profile associated with the mesodermal cell fate [147]. Germ cell specification occurs only in a subpopulation of these cells marked by the expression of the key transcriptional regulator *Blimp1* (or *Prdm1*) which is also induced by BMP signalling around E6.25 [212, 299]. In FRAGILIS-positive cells, BLIMP1 represses the somatic mesodermal differentiation programme [191, 212, 249]. Hence, lineage restriction of the proximal epiblast cells towards the germ cell fate is induced. Besides repression of the somatic mesodermal programme, BLIMP1 is important for the lineage-specific upregulation of germ cell specification genes, such as *Tfap2c* (or *AP2γ*), *Nanos3* and *c-Kit* [138, 139].

Whereas BLIMP1 is required for the repression of mesoderm-related genes, PRDM14 is responsible for the re-expression of pluripotency-associated genes (*Sox2*, *Oct4*, *Nanog*) in

germ cells [311, 313]. *Prdm14* gene expression is also induced by BMP signals as early as E6.5 [313]. TFAP2C is the third key regulator in germ cell specification, which is expressed in PGCs from E7.25 to E12.5 and essential for embryonic germ cell maintenance [304]. At E7.5, when PGC specification is complete, a total of ~40 lineage-restricted PGCs can be recognised that are characteristically expressing the DNA binding protein STELLA (DPPA3) [247] and the alkaline phosphatase TNAP [81].

1.1.3 Germ cell migration

Only shortly after specification, the PGCs start to migrate. In general, the migration can be divided into three successive phases. In the first phase (E7.5 – E9.0) PGCs initially migrate from the primitive streak into the adjacent posterior embryonic endoderm (future hindgut) [10] followed by migration from the base of the allantois along the hindgut (reviewed in [69, 237]). During the second phase (E9.5 - E10.5), the PGCs leave the hindgut and migrate bilaterally into the dorsal mesentery towards the genital ridges [194]. In the third migratory phase (E10.5 - E12.5) the PGCs reach the genital ridges (E10.5) and colonise them to form the embryonic gonad (reviewed in [69, 237]). Germ cells that are not migrating normally and remain in ectopic locations are eliminated by intrinsic apoptosis signalling involving the pro-apoptotic protein BAX [244, 272]. Germ cell apoptosis is activated in the absence of the c-Kit ligand Steel (or stem cell factor, SCF) whose expression is lost in the midline and becomes restricted to the lateral domains between E9.5 and E10.5 [244]. This process is of high importance as ectopic PGCs, which escape apoptosis along the midline, have been proposed as the origin of extragonadal germ cell tumours [254, 293]. In addition, in developing PGCs expression of *Nanos3* is detectable from E7.75 until shortly after their settlement in the gonads (E14.5 in male, E13.5 in female embryos) [276, 291]. NANOS3 is essential for the maintenance of the germ cell lineage as *Nanos3*$^{-/-}$ mouse embryos show an early loss of germ cells due to apoptosis in BAX-dependent and -independent mechanism [276].

While migrating to the genital ridges, PGCs initially proliferate before undergoing a cell cycle arrest in G2-phase and transcriptional quiescence between E7.5 and E9.5 [248, 259]. Once the PGCs have reached the genital ridges by E10.5, they have re-entered the cell cycle and proliferate extensively [248, 259]. At the beginning of migration, a cluster of ~40 founder PGCs are detectable whereas at E9.5 there exist 350 germ cells and at E10.5 there are already 1000 germ cells present [279]. After settlement in the gonads, shortly before becoming mitotically arrests (E13.5), approximately 25,000 PGCs are located in the gonads [279].

1.1.4 Sexual differentiation of the germ cells

Thus far, no sexual dimorphism of the gonadal structures is noticed. Sexual differentiation of the PGCs begins after colonization of the genital ridges at E10.5. Within one day of entering the genital ridge, epigenetic reprogramming takes place. In both female and male PGCs the biparental genomic imprinting pattern is erased [86, 149] and new sex-specific epigenetic patterns are re-established during gametogenesis [7]. Starting at E12.5 in female PGCs, now termed oocytes, the first meiotic division (E13.5) is initiated in response to retinoic acid [132]. The oocytes progress through leptotene, zygotene and pachytene stages before arresting in diplotene stage of prophase I of meiosis [100, 269]. Oogenesis is completed after birth upon hormonal stimulation with each reproductive cycle. In contrast, male PGCs, now referred to as gonocytes, enter mitotic arrest and stay quiescent in G0/G1 phase of the cell cycle from ~E12.5 onwards [100, 307]. One to two days after birth, in male mice, gonocytes resume proliferation with subsequent initiation of meiosis/spermatogenesis [182, 197, 245]. Importantly, the failure of male PGCs to enter mitotic arrest is assumed as one of the main causes of TGCT [18].

1.1.5 Spermatogenesis

Spermatogenesis is a precisely organised process – both temporally and spatially - that generates spermatozoa (Figure 1.2 and Figure 1.3). In mammals, spermatogenesis proceeds inside the seminiferous tubules of the testis. Within the seminiferous tubules, the germ cells are surrounded by somatic Sertoli cells which support spermatogenesis. The basement membrane, the border between the lumen of the seminiferous tubules and the interstitial tissue, contains peritubular myoid cells and macrophages. In the interstitial spaces between the tubules, blood vessels are situated which are surrounded by testosterone-producing Leydig cells as wells as macrophages and lymphoid epithelial cells [101, 245] (Figure 1.2).

Shortly after birth, gonocytes re-enter mitosis and migrate from the centre of the seminiferous tubule towards the basement membrane, where they differentiate into spermatogonial stem cells (SSCs) [20, 47, 110, 128, 197, 252, 298]. These cells are characterised by their potential to tightly regulate the balance of self-renewal and differentiation. SSCs are very rare as they divide only once every three to four days and thus, comprise only 0.03 % of all germ cells in the mouse testis [109, 111, 162–164, 283].

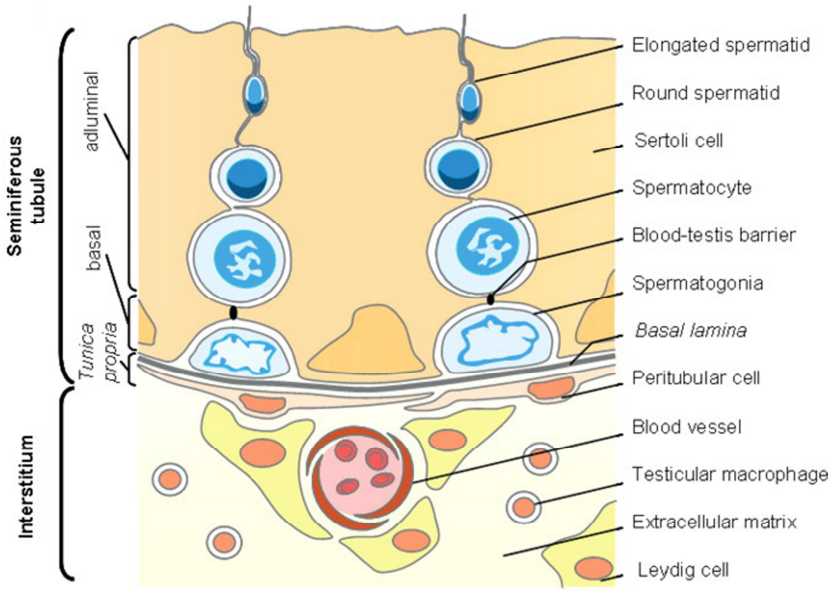

Figure 1.2 – Schematic representation of the mammalian testicular anatomy
The seminiferous tubules are defined by a basal membrane (*basal lamina*) from the interstitium and contain somatic Sertoli cells as well as germ cells at various developmental stages. Within the seminiferous tubule, spermatogenesis occurs from the basal membrane towards the lumen. The basal compartment contains the spermatogonia and primary spermatocytes (not depicted). Mature spermatocytes and spermatids reside in the adluminal compartment. In the highly vascularised interstitial compartment, testosterone-producing Leydig cells, macrophages and epithelial cells are located. Originally published in Molecular and Cellular Proteomics. Lagarrigue *et al.* [144] © the American Society for Biochemistry and Molecular Biology.

During spermatogenic lineage development, SSCs, also designated as undifferentiated A_{single} spermatogonia (A_s) [108, 208], undergo mitotic division generating two daughter cells which either complete cytokinesis and become two new A_s or remain connected by an intercellular bridge producing a pair of spermatogonia (A_{paired}, A_{pr}). Subsequently, A_{pr} spermatogonia undergo further mitotic divisions forming chains of 4, 8 or 16 interconnected $A_{aligned}$ spermatogonia (A_{al}) (reviewed in [220, 238, 240, 241, 245]). Stem cell renewal is also suggested to be obtained by so-called clonal fragmentation which describes A_{pr} as well as chains of A_{al} spermatogonia fragmenting into smaller clones consisting of 1, 2, 4, or 8 cells [91, 198, 199]. Collectively, A_s, A_{pr} and A_{al} spermatogonia are often referred to as undifferentiated spermatogonia (Figure 1.3). After the multiple rounds of mitosis to clonally amplify the pool of undifferentiated cells, the A_{al} spermatogonia differentiate without further division into A_1 spermatogonia (A_1), the first generation of the so-called differentiating spermatogonia. A_1 spermatogonia are irreversibly committed towards meiosis. In the following five sequential mitotic divisions type A_2, A_3, A_4, Intermediate and B spermatogonia are produced, which fill the entire seminiferous tubule (reviewed in [11, 68, 238–241]). B spermatogonia divide once again to produce primary spermatocytes. Next, the two meiotic divisions of the primary spermatocytes give rise to secondary spermatocytes (Meiosis I)

followed by round spermatids (Meiosis II) (reviewed in [68, 89, 238]). The differentiation of spermatogonia occurs in a highly synchronised manner towards the lumen of the seminiferous tubules [238, 318]. In the final step of spermatogenesis, spermatids undergo a morphological differentiation, so-called spermiogenesis, to generate mature sperm (spermatozoa) (reviewed in [209, 245]). In the subsequent process termed spermiation the mature spermatozoa are released from the supporting somatic Sertoli cells into the lumen of the seminiferous tubule (reviewed in [210]).

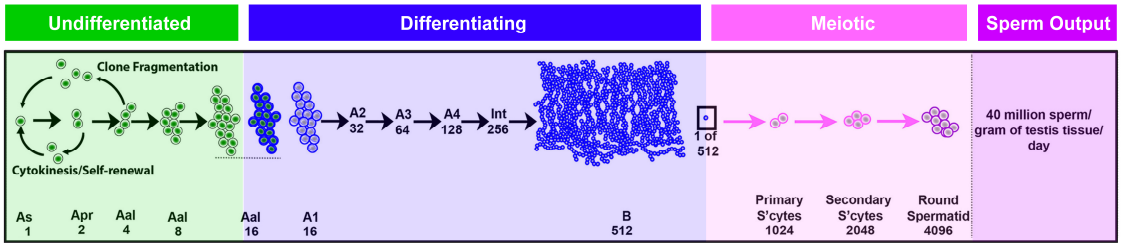

Figure 1.3 – Spermatogenetic lineage development in mice
During spermatogenic development in mice, undifferentiated spermatogonia (A_s, A_{pr} and A_{al}) undergo mitotic divisions to clonally amplify the pool of undifferentiated cells, thereby remaining interconnected. This is followed by six consecutive amplifying mitotic divisions in the pool of differentiating spermatogonia (A_1, A_2, A_3, A_4, Intermediate and B spermatogonia) giving rise to primary spermatocytes. By two subsequent meiotic divisions round spermatids are produced which undergo spermiogenesis to generate mature sperm. Modified with permission from Elsevier, originally published in Fayomi *et al.* [68].

1.2 Testicular germ cell tumours

As mentioned above, germ cell specification, development and maturation are tightly regulated, the failure of which can lead to infertility or the development of cancer. Testicular cancer accounts for approximately 1 % to 2 % of all neoplasms in young and adult men with over 71,000 new cases and about 9,500 deaths worldwide in 2018 [28, 70]. Yet, they are the most common malignancy in reproductive men aged 20 to 40 [70]. In general, testicular cancer incidences have been increasing over the last 30 to 40 years [44, 112] with highest incidences in men of European descent [29, 70, 216]. Approximately 95 % of malignant testicular tumours are accounted by germ cell tumours [27, 32].

Human germ cell tumours represent a heterogenous group of neoplasms that are not only localised in the testis but also the ovaries and in different extragonadal sizes along the midline of the body and brain [213, 214]. TGCT can be divided into three groups based on the age, anatomical site and genomic imprinting: (I) tumours of new-borns and infants (teratomas and yolk sac tumours), (II) tumours of adolescents and young adults (seminomas and non-seminomas) and (III) spermatocytic seminoma of elderly men (≥50 years) [213]. As risk factors of TGCTs the presence of the testicular dysgenesis syndrome

(cryptorchidism, azoospermia and testicular atrophy) as well as familial predisposition and environmental influences has been described [2, 49, 99, 213].

All TGCTs are thought to arise from a common precursor lesion, termed testicular germ cell neoplasia *in situ* (GCNIS) according to the latest WHO classification [21, 190] (Figure 1.4). Exceptions are the infantile tumours and the rare spermatocytic seminoma in elderly men which arises from late spermatogonia or spermatocytes [118, 196, 213, 264]. GCNIS was first described in 1972 [263] and is generally accepted to result from a delayed or blocked differentiation/maturation of PGCs, thus representing arrested PGCs with malignant transformation most likely initiated *in utero* [213, 267]. At puberty, GCNIS cells start to proliferate upon hormonal stimulation and gain invasive capacity resulting in the development of a seminoma, non-seminoma or mixed tumour [105, 224]. Premalignant GCNIS cells resemble fetal gonocytes morphologically [206, 264] and express genes that are associated with PGCs [8], specifically with their embryonic stem cell (ESC) -like features and pluripotency, such as *OCT3/4* [117, 166, 225], *NANOG* [93, 103], *TFAP2C* [104, 217] and *KIT* [228].

Seminomas are very similar to PGCs and GCNIS in respect of gene expression and histology [213]. In contrast, non-seminomas are initially present as undifferentiated embryonal carcinoma (EC). This stem cell population of the non-seminomas exhibits features of pluri- to totipotency with the capacity to further differentiate into teratoma (TER) (embryonic, composed of cells of all three germ layers), yolk sac tumour (YST) (extraembryonic) and choriocarcinoma (CHC) (extraembryonic) [213, 295] (Figure 1.4). Hence, ECs are regarded as the malignant counterpart of embryonic stem cells (ESCs) [213].

Type I TGCTs occur in infants and young children. They comprise teratoma and yolk sac tumours and are suggested to originate directly from PGCs during early PGC development. Type II TGCTs are tumours of adolescents and young adults comprising seminomas and non-seminomas. Both subtypes originate from a common precursor lesion, the GCNIS, which develops from PGCs arrested in late PGC development due to malignant transformation. Type III TGCTs, the spermatocytic tumours, are detected in elderly men (≥50 years) and originate from late spermatogonia or spermatocytes.

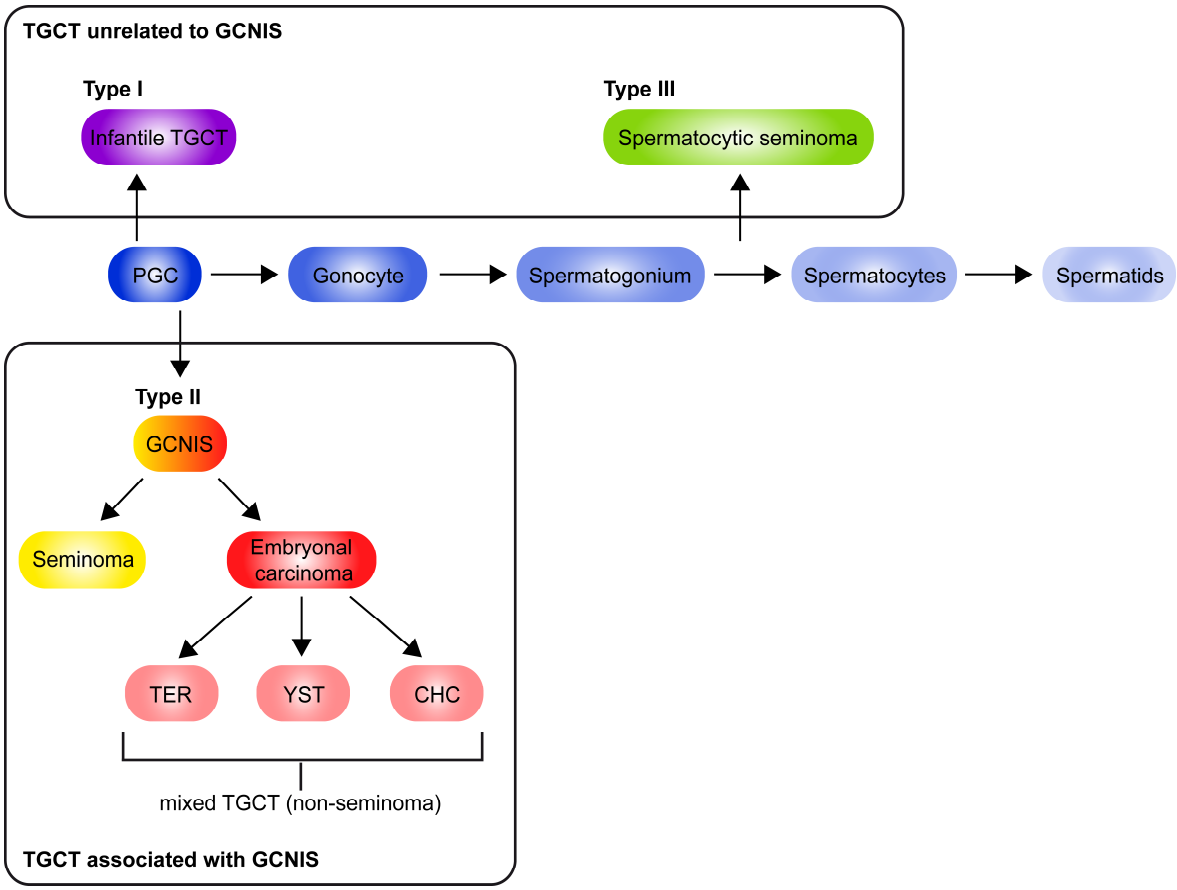

Figure 1.4 – Schematic representation of testicular germ cell tumour (TGCT) development
Type I TGCTs are assumed to arise early during PGC development in young children and infants. Type II TGCT arise from a so-called germ cell neoplasia in situ (GCNIS) which is a common precursor lesion developing from an error in late PGC maturation. They comprise of two subtypes: seminoma and non-seminoma. Non-seminomas initially exist as embryonal carcinomas which can differentiate into embryonic (teratoma (TER)) and extraembryonic tissues (yolk sac tumour (YST) and choriocarcinoma (CC)). Type III TGCTs comprise of spermatocytic seminomas which originate from late spermatogonia or spermatocytes and usually occur in older men. The figure is based on information from [36, 213, 226, 227].

1.3 *In vitro* cell system for the investigation of germ cell development

Clinically, it is of high interest to understand the molecular mechanisms that underlie the development of TGCT as well as sterility in men, both of which result from defects in germ cell development. However, research using the mouse surrogate system is limited by the low number of PGCs (40-100 cells) present during early embryonic development. Furthermore, in adult male mice the number of SSCs remains low accounting for only 0.03% of total germ cells [283]. In contrast, in the human testis undifferentiated SSCs constitute 22 % of all germ cells [68, 215]. Furthermore, until now PGCs could not be successfully cultured *in vitro* for a long-term without undergoing apoptosis or differentiating into pluripotent embryonic germ cells (EGCs), which resemble ESCs rather than PGCs [180]. Nowadays, PGC-like cells (PGCLCs) are generated by *in vitro* differentiation of ESCs or

induced pluripotent stem cells (iPSCs) via the induction of epiblast-like cells (EpiLCs) [96]. However, PGCLCs were only shown to persist robustly in culture up to 10 days [96]. In light of this, several cell lines derived from type II TGCTs still serve as well-established suitable model systems for *in vitro* studies (reviewed in [201]). Two of them are the seminoma-like cell line TCam-2 and the EC cell line NCCIT, which are described in more detail in the following sections.

1.3.1 The seminoma-like cell line TCam-2

The TCam-2 cell line has been derived from a seminoma of a 35-year-old man and is the only pure seminoma-like cell line that has been adapted to cell culture [64, 189]. TCam-2 cells show a polygonal and flat morphology with a large cytoplasm and round nucleus [64]. Noteworthy, TCam-2 cells feature a relative long doubling time (~58 h) which is similar to migratory PGCs [64, 189]. Furthermore, TCam-2 cells express the pluripotency markers as wells as PGC and TGCT markers OCT4, NANOG, LIN28, TFAP2C, BLIMP1 and KIT [63, 64, 201, 202]. Last but not least, TCam-2 cells display an aneuploid karyotype with the type II TGCT characteristic gain of the 12p chromosomal region [82, 189].

1.3.2 The EC cell line NCCIT

The NCCIT cell line is a pluripotent EC cell line that was established from a mediastinal mixed germ cell tumour [284]. The cells are hyperdiploid with chromosomes ranging from 54 to 64 [53]. Morphologically, NCCIT cells appear epithelial-like forming dense cell clusters upon *in vitro* culturing. NCCIT cells are negative for keratin but positive for vimentin, alkaline phosphatase and the pluripotent stem cell markers TRA-1-60 and TRA-1-81 [53]. In response to retinoic acid, NCCIT cells differentiate into cells of all three embryonic germ layers and extraembryonic lineage [53]. Upon xenotransplantation into nude mice, NCCIT cells differentiate into mixed non-seminoma showing foci of EC, YST, immature somatic tissue as well as extraembryonic cells [284].

1.4 The TRIM protein family

The TRIM/RBCC protein family is defined by the **tri**partite **m**otif consisting of a N-terminal RING finger domain, followed by one or two B-box motifs and a coiled-coil domain [236, 266, 289]. The order and spacing between these domains are conserved (Figure 1.5). At present the protein family comprises more than 70 members with diverse functionalities. These proteins are involved in various cellular processes, including transcriptional regulation, cell proliferation, apoptosis, development, viral response and tumorigenesis [95, 183].

1.4.1 The RING domain

The RING domain is named after the zinc finger motif that was first discovered in the Ring1 (really interesting new gene 1) protein by Freemont *et al.* [73]. It is characterised by a motif of cysteine and histidine residues binding two zinc cations in a 'cross-brace' conformation [16]. The coordination of zinc cations was described to be crucial for autonomous folding of the RING domain [24]. RING domain proteins possess a ubiquitin-protein ligase activity and act as E3 enzymes, thus are involved in the ubiquitin-mediated degradation of proteins [12, 116, 167]. In the first step of protein ubiquitination, an 8.5 kDa ubiquitin is activated by binding to an E1 ubiquitin-activating enzyme in an ATP-dependent manner. Following this, the ubiquitin is transferred to the E2 ubiquitin-conjugating enzyme. In the final step the E3 ubiquitin-ligase mediates the transfer of ubiquitin from the E2 enzyme to lysine residues on the target protein. E3 enzymes interact directly with both E2 enzyme and target protein, thereby functioning as the substrate recognition module. This labelling of proteins with Lysine-48 linked polyubiquitin chains, typically targets the protein for degradation by the 26S proteasomal pathway [129, 258]. However, ubiquitination has also been reported to be involved in regulating protein function, localisation as well as protein-protein interactions depending on the type of ubiquitin modification such as differential lysine linkage (e.g. Lysine-63) or mono- *versus* polyubiquitination (reviewed in [129, 255]).

1.4.2 The B-box domain

Besides the RING domain, the B-box domain is another zinc finger domain which is exclusively found in Trim proteins and always situated C-terminally of the RING domain [231]. The B-box domain is about 40 amino acids in length and binds one zinc cation with high affinity by its cysteine and histidine-rich motif [25, 26]. Two different B-box variants, B-box type 1 and B-box type 2, have been described, which differ slightly in their consensus sequence [232, 236]. In proteins containing only a single B-box domain, it is of type 2. If found together, the type 1 B-box usually precedes the type 2 [232, 236]. Until now little is known about the function of the B-box domains. Only in a more recent study, a structural similarity between the two B-boxes and the RING domain has been revealed with both domains binding two zinc cations in a 'cross-brace' conformation [178, 179]. Hence, the B-boxes may possible act as E3 ubiquitin-ligases *per se* or contribute to the E3-ligase activity of the RING domain [185, 282].

1.4.3 The Coiled-coil domain

The Coiled-coil (CC) domain is the last part of the tripartite motif and is located C-terminally of the RING and B-boxes. It is a common structural motif consisting of two to five parallel

or antiparallel α-helices forming a superhelix with a distinct packaging of amino acid sidechains in the core of the bundle (reviewed in [48, 169, 177]). In Trim proteins the CC domain is necessary for homo- or hetero-multimerization mediating the formation of high molecular weight complexes [236]. Furthermore, the Trim CC domain is predicted to be required for correct subcellular localisation of Trim proteins [236]. Indeed, recent studies of our group have shown that TRIM71's CC domain is required for its proper localization within processing bodies (P-bodies) [290].

1.4.4 The TRIM-NHL protein family

The TRIM protein family is further subdivided according to additional C-terminal domains. TRIM-NHL proteins represent one of the nine subfamilies based on the presence of two to six NHL repeats positioned C-terminally of the tripartite motif [266]. As seen in Figure 1.5 the TRIM-NHL protein family is comprised of four proteins encoded in *D. melanogaster* and *M. musculus* genomes and five in *C. elegans*. The orthologs of *C. elegans* LIN-41 are Wech (*D. melanogaster*) and TRIM71 (*M. musculus and H. sapiens*). All LIN-41 orthologs are highly conserved [309]. In conformity with this, an inhibition by the miRNA let-7 has been described for *C. elegans* LIN-41 [233, 265] as well as the orthologs in the fruit fly [211], zebrafish [127], chicken [120], mouse [120, 172, 246] and human [153]. The phylogenetic relatedness is also reflected by a 90 % identity in the amino acid sequence of the murine and human TRIM71.

Besides the tripartite motif and the NHL repeats, several of the TRIM-NHL protein family members feature a less conserved immunoglobin filamin-type domain situated immediately before the NHL. NHL stands for the three proteins in which the domain was first identified: *C. elegans* NCL-1 [72], *H. sapiens* HT2A (former name for TRIM32) [74] and *C. elegans* LIN-41. Each NHL-domain consist of 44 amino acids that form a multiblade β-propeller structure [66, 266]. The NHL repeats are known to mediate interactions with other proteins [66, 74, 268]. However, one of the propeller surfaces is positively charged, thus enabling interaction with the negatively charged RNA phosphate backbone [159, 266]. Yet, for the *D. melanogaster* TRIM-NHL protein Brat a consensus binding motif in the NHL domain has been defined [158]. More recently, the NHL domain of LIN-41 and its homologs were identified to specifically recognise a structural RNA motif consisting of a stem-loop element with specific nucleotides in conserved positions [137]. Similar RNA structural motifs have been found in several TRIM71 mRNA targets in mouse ESCs [305] and recent studies of our group have shown that the NHL domain of human TRIM71 also mediates direct RNA interaction with such structural motifs [290]. Interestingly, TRIM-NHL proteins have also been described to regulated miRNA expression [87, 203, 246, 257].

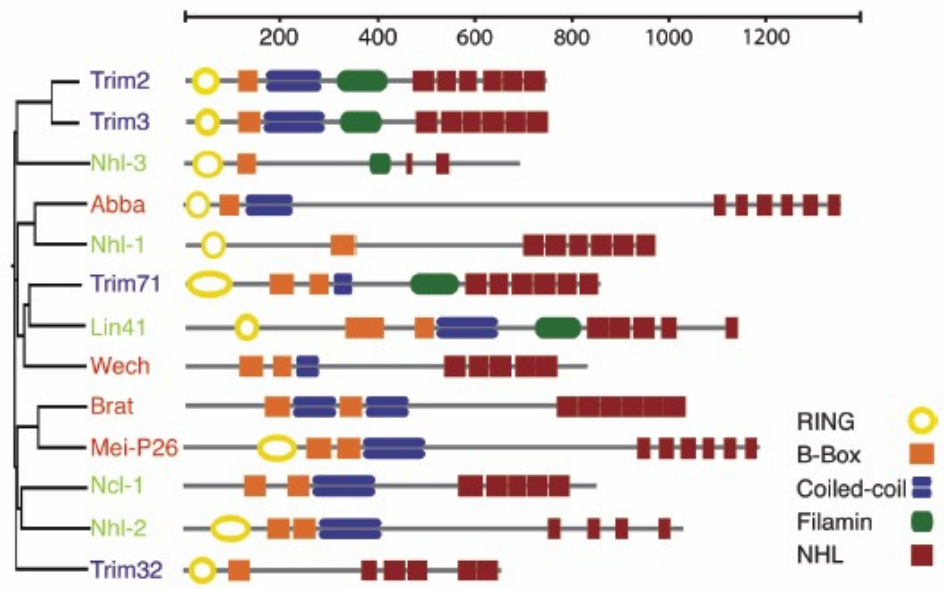

Figure 1.5 – Phylogenetic relatedness among members of the TRIM-NHL protein family
The TRIM-NHL protein family comprises a characteristic domain structure. An N-terminal RING domain is followed by one or two B-boxes and a coiled-coil (CC) domain. C-terminally a putative Filamin and an obligatory NHL domain consisting of two to six NHL repeats, is located. *C. elegans* proteins are depicted in green, *D. melanogaster* in red and *M. musculus* in blue. Reprinted by permission from Springer Nature: Springer, Wulczyn *et al.* [309], © Landes Bioscience and Springer Science+Business Media, LLC 2010, Licence: 4825810745048.

1.5 TRIM71 - a conserved regulator of embryonic development

The first studies of TRIM71 and its orthologs concentrated on their role in embryonic development. In *C. elegans* the TRIM71 ortholog named LIN-41 was described to be expressed in neurons, gonads and muscle [265]. In the same study, *lin-41* was identified as a heterochronic gene involved in developmental timing in *C. elegans* [265]. More precisely, LIN-41 mutant nematodes showed a precocious terminal differentiation of the seam cells [265]. Furthermore, a reciprocal expression pattern of LIN-41 protein and let-7 miRNA was described in the developing organism [233, 265]. Moreover, two partially complementary let-7 binding sites were found in the 3'UTR of *lin-41* mRNA [296, 297] which target *lin-41* for translational repression and mRNA degradation [13, 57]. This expression pattern and regulatory mechanism was discovered to be evolutionary conserved [120, 127, 145, 153, 211, 256].

In 2008, new insights in the role of TRIM71 in embryogenesis were gained due to the generation of a TRIM71 knockout mouse by Schulman et al. [172]. In mice, by E10.5, *Trim71* mRNA expression has been detected in neuroepithelium, dorsal root ganglia, branchial arches, limb buds and tail bud [172]. TRIM71 expression declines during development being absent from E12.5 onwards [172]. Postnatally, TRIM71 is only present in SSCs during postnatal testis development [246], in interfollicular epidermal stem cells

[246] and in ependymal cells of all four ventricles in the brain [51]. Mice with a homozygous knockout of TRIM71 are embryonically lethal dying around mid-gestation between E10.5 and E11.5 [41, 172]. Most strikingly, the mutant mice display a defect in the closure of the neural tube, the precursors of the central nervous system, at E9.5 which leads to exencephaly [172]. Hence, TRIM71 is essential for the morphogenesis of the central nervous system. The defective phenotype might be explained by a reduction of proliferation and premature differentiation in TRIM71-deficient neuroepithelial cells as reported by Chen and colleagues [41]. Intriguingly, it was described that merely the homozygous deletion of the C-terminal last 24 amino acids, was sufficient to cause the exencephaly defects and embryonic lethality in mice, phenocopying the complete loss of TRIM71 [172]. However, the neural tube closure defect is most likely not only responsible for the early embryonic death of the mutant mice as there exist examples of mice with a neural tube closure defect that survive until late embryogenesis or even until shortly after birth [50]. Accordingly, the exact cause of death is yet unexplained. Interestingly, two recurrent TRIM71 *de novo* mutations (R608H and R796H) located in the TRIM71 NHL domain have been recently identified in a cohort of congenital hydrocephalus patients [76] and predicted to disrupt RNA binding [305].

Independently, in other model organisms such as the fruit fly *D. melanogaster* or the zebrafish *D. rerio* the respective TRIM71 homologs have been identified to cause an embryonic muscle detachment [160] and retarded embryonic development [153], respectively. Eventually, this leaves TRIM71 expression restricted to undifferentiated cells (stem and progenitor cells) and essential for embryonic development [65].

1.6 Functional and molecular mechanisms of TRIM71

On the molecular level, multiple mechanisms on TRIM71 cellular functionality have been described until now. In general, the RING domain of TRIM71 features an E3 ligase activity whereas the NHL domain enables its function as a mRNA repressor [65, 287]. Albeit, in *C. elegans* LIN-41 silences mRNA post-transcriptionally either by translational repression or mRNA degradation through recognition of the 5’UTR or 3’UTR, respectively [3].

A regulation of miRNA expression by TRIM71 has been found by our group, as in TRIM71-deficient mouse ESCs the expression of ESC-specific miRNAs was reduced, which was accompanied by an increase in differentiation promoting miRNAs, such as brain- and gonad-specific miRNAs [188]. We showed that regulation of let-7 expression is achieved by TRIM71 in cooperation with the pluripotency factor LIN28 (abnormal cell lineage protein 28) [187]. Furthermore, TRIM71 has been found to colocalise and interact with AGO2 (Argonaute 2) as well as other AGO family members involved in mRNA synthesis and activity, in so-called P-bodies [39, 246]. P-bodies are organelles serving as sites for mRNA

surveillance where translational repression, mRNA decapping, nonsense-mediated decay (NMD) of mRNA as well as miRNA-mediated mRNA repression occurs [136, 262]. Rybak *et al.* showed that *TRIM71* is not only downregulated by let-7 but TRIM71 also reduces miRNA activity via ubiquitination of AGO2 through its E3 ubiquitin ligase activity, thereby targeting AGO2 for proteasomal degradation [246]. Importantly, we and several other groups failed to detect TRIM71-mediated degradation of AGO2 [39, 41, 157, 188]. Instead, our group has observed that TRIM71 can regulate let-7 activity in a LIN28-independent mechanism, which involves AGO2 binding, but not AGO2 degradation (Dr. Sibylle Mitschka and Dr. Lucia Torres Fernández unpublished data). Consequently, the activity of other miRNAs was not affected. Yet, TRIM71 is suggested to have a definite role in regulating miRNA biogenesis.

In 2012, Chen and colleagues identified another ubiquitination substrate of TRIM71, SHCBP1 (SHC SH2 domain-binding protein 1), in murine neuronal progenitor cells [41]. Recently, similar findings have been described in mouse ESCs [152]. However, here the ubiquitination leads to a stabilisation of the adapter protein SHCBP1 which is involved in FGF (fibroblast growth factor) signalling through phosphorylation of the effector proteins ERK and AKT [41, 152]. Consequently, these studies link TRIM71 to FGF signalling and describe TRIM71 as a positive regulator of FGF signalling. FGF signalling is known to be important for the development of the central nervous system (reviewed in [58, 71, 176]) by promoting proliferation and inhibiting premature neural differentiation of neuronal progenitor cells [56, 122]. Accordingly, this molecular mechanism might in part explain the neural tube closure defect observed TRIM71-deficient mice.

Furthermore, in 2017 Nguyen *et al.* described the tumour suppressor protein p53 to be ubiquitinated and inactivated by TRIM71 in mouse ESCs undergoing neural differentiation, thereby antagonising apoptosis (Caspase-3) and differentiation (Grhl3; Grainyhead-like 3) [204]. The transcription factor p53 is stabilised and activated (phosphorylated) upon cellular stress (e.g. DNA damage) to induce cell cycle arrest or apoptosis with Cdkn1a/p21 being a well-known transcriptional target [67, 155]. On the other hand, the transcription and pro-differentiation factor Grhl3 is a p53 target [31] which is linked to neural tube closure defects [125, 207, 286]. Thus, TRIM71 is necessary to limit differentiation and apoptosis during neural development, which both are putative causes of embryonic lethality and the neural tube closure defect of TRIM71-deficient mice [204].

In two independent studies in mouse ESCs, TRIM71 was reported to function as an RNA binding protein (RBP) repressing target mRNAs by translational inhibition and degradation, thus promoting ESC proliferation [39, 157]. Chang *et al.* described TRIM71 to cooperate with ESC-specific miRNAs, miRNA-290 and miR302 to bind and repress the mRNA of the cell cycle inhibitor and tumour suppressor *Cdkn1a/p21* [39]. Besides other proteins,

CDKN1A mediates the cell cycle arrest at the G1-S checkpoint [67]. Only after the degradation of CDKN1A, a cell is able to enter the S-phase of the cell cycle [320]. Hence, *Cdkn1a* repression leads to an increase in cell proliferation. Alternatively, as described, a siRNA-mediated knockdown of TRIM71 in mouse ESCs results in increased CDKN1A levels, and thus decreased proliferation [39]. Lately, a study of our group identified that TRIM71 specifically represses *CDKN1A* mRNA by cooperating with factors of the NMD pathway in humans cells [290]. Moreover, in humans only a stem/3-nucleotide-loop structure in the 3'UTR of *CDKN1A* mRNA is required for the recognition and interaction of *CDKN1A* mRNA by TRIM71 [290]. Loedige and colleagues reported that binding of TRIM71 to target mRNAs promotes translational repression and mRNA degradation [157]. By RIP-Chip analysis, two retinoblastoma-like transcription factors (*Rbl1* and *Rbl2*) were identified as further TRIM71 targets in mouse ESCs and *E2F7* was identified as a target in HEK293T cells [157]. E2F7, RBL1 and RBL2 are all inhibitors of the cell cycle whose downregulation is important for proper stem cell function [157]. Thus, similar to *CDKN1A*, their repression by TRIM71 might explain the increased proliferation observed in mouse ESCs.

Another study described a role of TRIM71 in cellular reprogramming by regulating developmental and differentiation genes [308]. When TRIM71 is expressed together with the stem cell factors OCT4, SOX2 and KLF4, it enhances the reprogramming efficiency of human dermal fibroblasts to iPSCs [308]. Specifically, the differentiation promoting transcription factor EGR1/LIN-29 was identified as a direct target gene whose repression by TRIM71 facilitates the transition to the pluripotency state [308]. This suggests a role of TRIM71 in regulating the balance between stemness and differentiation in ESCs.

Finally, TRIM71 has been linked to carcinogenesis being upregulated in different human cancers and correlating with advanced tumour stages and poor prognosis [38, 43, 290]. As such, in hepatocellular carcinoma cells TRIM71 has been reported to enhance proliferation [43, 290]. In contrast to Chen *et al.*, who claimed that TRIM71 promotes tumorigenesis by destabilisation of AGO1/2 [43], our group identified *CDKN1A* mRNA repression by TRIM71 to promote proliferation in HepG2 cells [290].

Altogether, TRIM71 functions via two distinct and possibly cooperating molecular mechanisms: on one hand by ubiquitination of target proteins and on the other hand by post-transcriptional repression of target mRNAs as an RBP. Furthermore, current literature points out TRIM71 as an important regulator of cell proliferation and differentiation in development and oncogenic processes.

1.7 CRISPR/Cas9 system

The CRISPR (clustered regularly interspaced short palindromic repeats)/Cas9 (CRISPR-associated protein 9) system was the method of choice for site specific genome editing within this study. In general, genome editing is the basis of modern research in molecular biology. The last breakthrough was the discovery of the CRISPR/Cas system as a method for RNA-based genome editing *in vitro* by the groups of Charpentier, Doudna and Siksnys in 2012 [78, 114]. In the next year, three independent studies successfully applied the system in mammalian cells and demonstrated the ease of programming and applying this technology [115, 148, 171].

Over 30 years ago, a CRSIPR array was described for the first time by the identification of a repetitive stretch of DNA in *E. coli* [113]. Today, it is known that CRISPR sequences are present in >40 % of characterised bacteria and 90 % of archaea [193] and confers an adaptive immune mechanism [17]. For genome editing, the type II CRISPR/Cas system from *S. pyogenes* has been primarily adapted due to its simplicity as it only requires one Cas protein (Cas9) and a single guide RNA (sgRNA). The sgRNA is an RNA chimera transcribed from one template and consisting of a palindromic scaffold sequence (tracRNA) directly downstream of the target/guide sequence (crRNA) [114] (Figure 1.6). Upon delivery of both, the Cas9 protein and sgRNA into the cell of interest, the sgRNA complexes with Cas9 endonuclease, recognises the target genomic loci through 20 bp base-pairing and mediates target cleavage (reviewed in [107, 251, 301]) (Figure 1.6). In addition, a direct interaction between the Cas9 and a short sequence in the invading genome, termed protospacer adjacent motif (PAM), is important for recruiting the Cas9-sgRNA complex and triggering DNA cleavage [301]. Cleavage of double-stranded DNA 3 bp upstream of the PAM results from the action of two different Cas9 nuclease domains (HNH and RuvC), which both nick one DNA strand thus, creating a double strand break (DSB) [78, 114].

The Cas9-inudced DSBs are repaired by one of two cell intrinsic DNA repair pathways: the non-homologous end joining (NHEJ) or the homology-directed repair (HDR) (reviewed in [310]) (Figure 1.7 A). NHEJ will combine the two DNA strands again, however this mechanism is error-prone and results in random insertion and deletion mutations (indels) of various lengths. These may disrupt the gene function and lead to a gene knockout by causing a shift in the target gene's translational reading frame or premature stop codons [60, 107, 154, 251]. Alternatively, DSBs can be repaired by exploiting the HDR mechanism by introducing a donor DNA template with two homologous sides flanking the desired insert. This will be inserted by homologous recombination resulting in targeted gene mutations or insertions [60, 107, 154, 251].

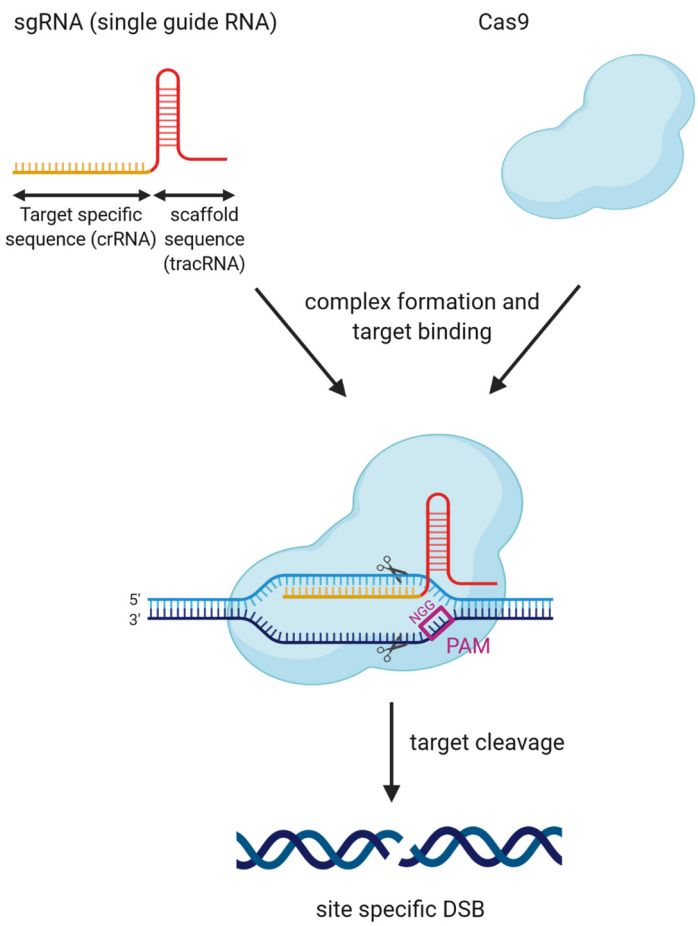

Figure 1.6 – Mechanism of engineered CRISPR/Cas9 system
(A) The engineered CRISPR/Cas9-system for genome editing comprises a Cas9 endonuclease and a single guide RNA (sgRNA). The sgRNA is a fusion between a target specific crRNA and a palindromic scaffold tracrRNA that is transcribed from one template. Cas9 and sgRNA form a complex with the sgRNA directing the complex to the target site which is complementary to the first (5') 20 nts of the sgRNA and lies next to a PAM sequence. The Cas9 cleaves the target genomic loci by generating a double strand break (DSB). Created with BioRender.com.

Eventually, the CRISPR/Cas9 system provides a powerful and versatile technology for advanced genome editing enabling sequence-specific gene knockout, gene deletion, gene knock-in as well as site-specific sequence mutagenesis and corrections [60, 107, 154, 251] (Figure 1.7 B). Compared to other genome editing technologies exploiting the endogenous DNA repair machinery, such as zinc finger nucleases (ZFNs) and transcription activator-like effector nucleases (TALENs), the CRISPR/Cas9 system displays remarkable advantages. These include foremost the simplicity of the method as only two components are required to perform genome editing: the Cas9 nuclease and a small RNA sequence (sgRNA) that needs to be designed [218]. Furthermore, the high target efficiency, assembly speed, low cost and potential to multiplex gene modifications let the CRISPR technology become the predominant approach for genetic engineering [161, 218].

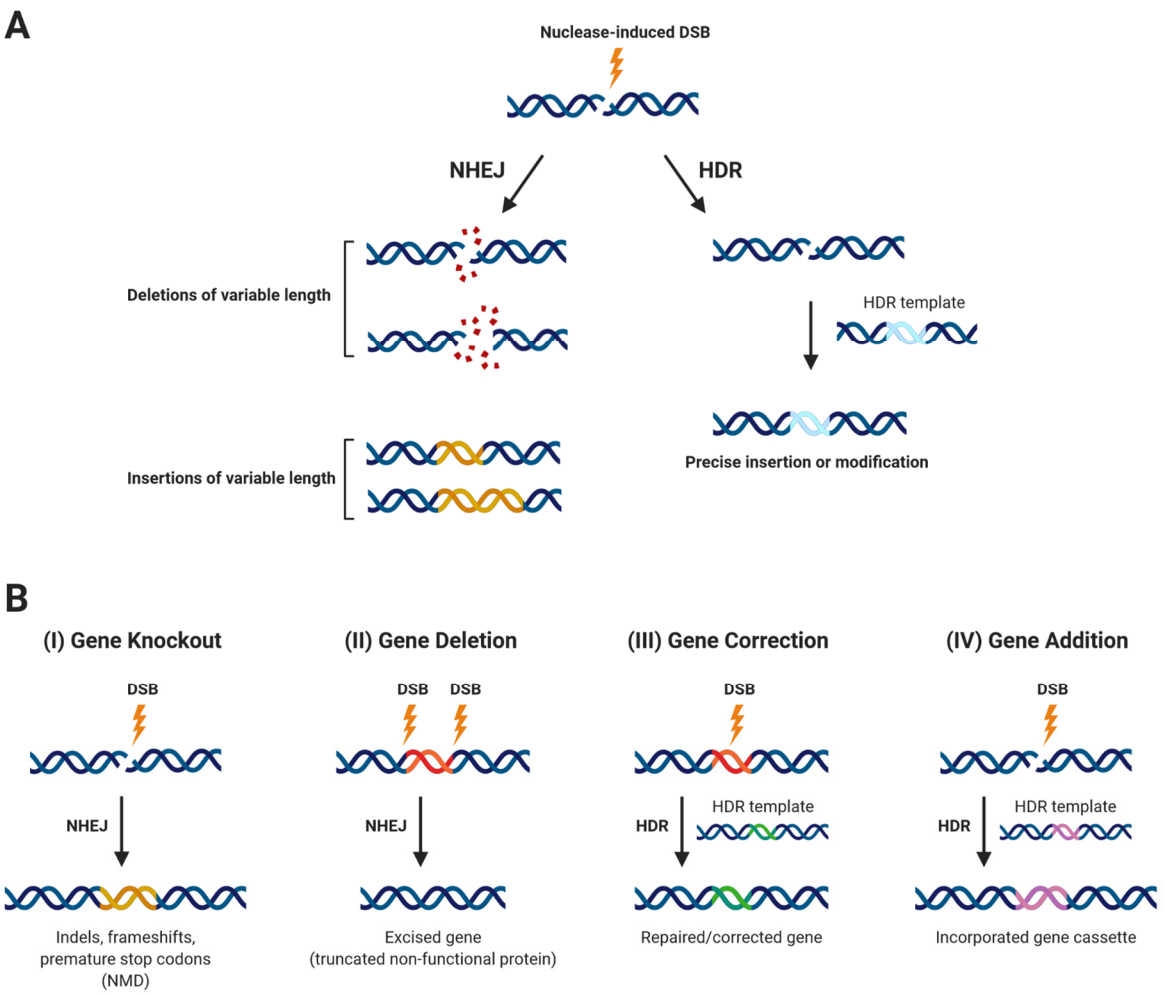

Figure 1.7 – Endogenous DNA repair mechanisms
(A) In eukaryotes double strand breaks (DSBs) can be repaired by both non-homologous end joining (NHEJ) or homology directed repair (HDR). In NHEJ the broken DNA strand is re-ligated, however resulting in random nucleotide insertions or deletions (indels). In HDR a homologous DNA template is used to precisely repair the DSB. **(B)** The error-prone NHEJ and the HDR can be exploited to generate: (I) gene knockouts by introducing indels and frameshifts into the coding region of a gene, thus resulting in the degradation of its mRNA via nonsense-mediated decay, (II) gene deletions by excision of a coding gene region by paired nucleases leading to premature truncation and knockout of the protein, (III) gene correction or mutation and (IV) gene addition. (III) and (IV) require an exogenous DNA template that contains homologous arms flanking the desired DNA region to be altered or added to. Figure 1.7 B is based on Lino *et al.* [154]. Created with BioRender.com.

1.8 Aim of the study

Even though mammalian germ cell development is well described, in 30-40 % of male infertility cases the associated factor is unknown [119]. Thus, it is of clinical relevance to investigate genetic defects and molecular mechanisms causing infertility.

In the somatic lineage, TRIM71 is known as a highly conserved protein involved in the regulation of embryonic development. Consistent with this, phenotypic analysis of different organisms including nematode, zebrafish, fruit fly and mouse, revealed severe defects in embryonic development upon TRIM71 ablation [153, 160, 172, 265]. Moreover, in the somatic compartment, TRIM71 expression is stem cell restricted being important for regulating stem and progenitor cell proliferation and differentiation [39, 41, 65, 157, 188, 246]. Despite TRIM71 expression being prominent in germ cells, little is known about TRIM71 function in the germ cell lineage until now. Yet, earlier studies described TRIM71 expression in the SSC population of the testis in adult mice [187] and in germ cells in testis of postnatal day 4 (P4) mice [246]. LIN-41 deficiency has also been shown to cause sterility in *C. elegans* [265, 270, 288] and previous studies of our group revealed that TRIM71 deficiency in mice causes a dramatic reduction of the testis size accompanied by sterility [187].

With regard to these findings and PGCs being closely related to ESCs, the present study aimed to investigate the role of TRIM71 in male germ cell development in more detail. It was first to elucidate whether the sterility causing defects are of embryonic or postnatal origin. Therefore, germ cell morphology, distribution and number were analysed histologically in testes of germline-specific TRIM71-deficient adult and neonatal P0.5 mice. Furthermore, it was to investigate the molecular functions of TRIM71 required for normal germ cell development. For this, proliferation, differentiation and apoptosis behaviour were analysed in CRISPR/Cas9-induced TRIM71 mutant NCCIT germ cell tumour cells either lacking the N-terminal RING domain or the C-terminal amino acids of the last NHL repeat of TRIM71. In addition, highly innovative analysis of the growth dynamics of a population of NCCIT cells with CRISPR/Cas9-induced truncations of TRIM71 *versus* wild type cells were used to gain new insights into the role of TRIM71 as a regulator of the balance between stemness and differentiation in the germ cell lineage

2 Material and Methods

2.1 Materials

2.1.1 Laboratory devices

Device	Model	Manufacturer (office)
Agarose gel documentation	Gel Max	Intas (Göttingen, D)
Autoclave	135T	H+P Medizintechnik (Oberschleißheim, D)
	DX-150	Systec (Linden, D)
	VX-150	Systec (Linden, D)
Blotting equipment	Mini Trans-Blot Cell	Bio-Rad (Munich, D)
Centrifuges	5810 R	Eppendorf (Hamburg, D)
	5415 R	Eppendorf (Hamburg, D)
	5424	Eppendorf (Hamburg, D)
	Avanti-J20 XP	Beckman Coulter (Krefeld, D)
	Optima LE-80K ultracentrifuge	Beckman Coulter (Krefeld, D)
CO_2 incubators	Model C150	Binder (Tuttlingen, D)
	C200	Labotect (Göttingen, D)
Cryostat	CM30505 S	Leica Biosystems (Wetzlar, D)
Dissecting set	Dumont	FST (Heidelberg, D)
Electrophoresis chamber (agarose gels)		Polymehr (Paderborn, D)
Electrophoresis chamber (SDS-PAGE)	Mini-PROTEAN Tetra Cell	Bio-Rad (Munich, D)
Flow cytometer	FACSCanto II	BD Biosciences (Heidelberg, D)
	FACSAria III	BD Biosciences (Heidelberg, D)
Heat block	Thermomixer compact	Eppendorf (Hamburg, D)
Hemocytometer	0.0025mm²	Paul Marienfeld (Lauda-Königshofen, D)
Incubator shaker	New Brunswick Innova 44	Eppendorf (Hamburg, D)
Laminar flow hood		BDK (Sonnenbühl, D)
	HeraSafe KS	Thermo Fisher Scientific (Waltham, USA)
Magnetic stirrer	Combimac RCT	IKA (Staufen, D)
	ARE heating magnetic stirrer	VELP scientica (Usmate, IT)
Microplate reader	Infinite M200	Tecan (Männedorf, CH)
Microscopes	Axio Lab.A1	Carl Zeiss (Jena, D)
	Axio Observer.Z1	Carl Zeiss (Jena, D)
	Eclipse TS100	Nikon (Tokyo, JP)

Microtome	RM2255	Leica Biosystems (Wetzlar, D)
PCR cyclers	Mastercycler pro Vapo.protect	Eppendorf (Hamburg, D)
	C1000 Touch Thermal Cycler	Bio-Rad (Munich, D)
	Biometra T3 Thermocycler	Analytik Jena (Jena, D)
pH meter	MP220	Mettler-Toledo (Greifensee, CH)
Pipette controller	Accu-jet pro	BRAND (Wertheim, D)
Pipettes	PIPETMAN	Gilson (Middleton, USA)
	ErgoOne	Starlab (Hamburg, D)
Power supplies	EV-234	Consort (Turnhout, B)
	Elite 300 Plus	Schütt Labortechnick (Göttingen, D)
Real-Time PCR cycler	CFX96	Bio-Rad (Munich, D)
Rotation wheel	NeoLab Rotator	NeoLab (Heidelberg, D)
Scales	JB2002-G/FACT	Mettler-Toledo (Greifensee, CH)
	AG285 (micro scale)	Mettler-Toledo (Greifensee, CH)
Scanner	CanoScan 9000F Mark II	Canon (Krefeld, D)
Stereomicroscope	M80	Leica Biosystems (Wetzlar, D)
Spectrophotometer	NanoDrop2000	Thermo Fisher Scientific (Waltham, USA)
Vacuum pump	AC 02	HLC BioTech (Bovenden, D)
Tilt shaker	WS-10	Edmund Bühler (Bodelshosen, D)
Tissue homogeniser	Precellys 24	Peqlab (Erlangen, D)
Tissue processor	TP1020	Leica Biosystems (Wetzlar, D)
Tube roller	RS-TR 05	Phoenix Instrument (Garbsen, D)
Vortex mixer	Unimag ZX3	VELP scientica (Usmate, IT)
	Vortex-Genie 2	Scientific Industries (New York, USA)
Waterbath	WNB 14	Memmert (Schwabach, D)
	HI1210	Leica Biosystems (Wetzlar, D)

2.1.2 Consumables

Consumable	Model	Manufacturer (office)
Aseptic gauze	Askina 10 cm x 10 m	Braun (Melsungen, D)
Blotting paper	Whatman 3 mm	GE Healthcare (Buckinghamshire, UK)
Cell culture dishes/ multiwell plates/ flasks	Cellstar	Greiner Bio-One (Kremsmünster, A)
Cell strainer	EASYstrainer 100 µm	Greiner Bio-One (Kremsmünster, A)
Coverslips	24 x 40 / 24 x 60 mm	Carl Roth (Karlsruhe, D)

Cryo embedding molds	15 x 15 x 5 mm	Sakura Finetek (Staufen, D)
	25 x 20 x 5 mm	Sakura Finetek (Staufen, D)
	7 x 7 x 5 mm	Klinipath, VWR (Darmstadt, D)
	22 (8) x 22 (8) x 20 mm	Polysciences (Warrington, USA)
Cryovials	1.6 ml	Sarstedt (Nümbrecht, D)
Falcon tubes	15 / 50 ml	Greiner Bio-One (Kremsmünster, A)
Filter tips	10 / 200 / 1000 µl	Sarstedt (Nümbrecht, D)
Flow cytometry tubes	5 ml	Sarstedt (Nümbrecht, D)
Freezing container	Mr. Frosty	Nalgene, Thermo Fisher Scientific (Waltham, USA)
Glass beads (acid-washed)		Sigma-Aldrich (Taufkirchen, D)
Glass ware		VWR (Darmstadt, D)
Hypodermic needles	Sterican	Braun (Melsungen, D)
Micro tubes	2 ml	Sarstedt (Nümbrecht, D)
Microscope slides (H&E)		Paul Marienfeld (Lauda-Königshofen, D)
Microscope slides (IF)	Superfrost Plus	Thermo Fisher Scientific (Waltham, USA)
Microtome blades	S-35	Feather (Osaka, JP)
Nitrocellulose membrane	BioTrace NT nitrocellulose membrane	Pall Corporation (Port Washington, USA)
Paraffin embedding cassettes	40.5 x 28.5 x 7 mm	Carl Roth (Karlsruhe, D)
Parafilm M		Bemis (Neenah, USA)
Pasteur pipettes	glass	BRAND (Wertheim, D)
PCR plate sealing film		Bio-Rad (Munich, D)
PCR reaction tubes/ stripes	0.2 ml Thin Wall	Axygen (Union-City, USA)
Pipette tips	10 / 200 / 1000 µl	Starlab (Hamburg, D)
Radiography film	Amersham Hyperfilm ECL	GE Healthcare (Buckinghamshire, UK)
Reaction tubes	0.5 / 1.5 / 2 ml	Starlab (Hamburg, D)
Real-Time PCR plates	96-well; hard shell	Bio-Rad (Munich, D)
Serological pipettes	5 / 10 / 25 ml	Greiner Bio-One (Kremsmünster, A)
Sterile filters	0.2 / 0.45 µm	Schleicher and Schuell (Dassel, D)
Syringes	Injekt 10 ml	Braun (Melsungen, D)
Tissue embedding sponges	32 x 26 x 2.5 mm	Carl Roth (Karlsruhe, D)
Ultracentrifuge tubes	Re-Seal Polyallomer	Seton (Petaluma, USA)

2.1.3 Chemicals

Chemical	Manufacturer (office)
1-Butanol	Carl Roth (Karlsruhe, D)
2-Propanol	VWR (Darmstadt, D)
Acetic acid	VWR (Darmstadt, D)
Acrylamide/ Bisacrylamide solution, Rotiphorese Gel 30 (37,5:1)	Carl Roth (Karlsruhe, D)
Agarose	VWR (Darmstadt, D)
Ammonium acetate	Carl Roth (Karlsruhe, D)
Ammonium persulfate (APS)	Serva (Heidelberg, D)
Ampicillin	Carl Roth (Karlsruhe, D)
Annexin V - APC	BioLegend (San Diego, USA)
Antipain	Carl Roth (Karlsruhe, D)
Aprotinin	Carl Roth (Karlsruhe, D)
Bacto Tryptone	Becton, Dickinson and Company (Franklin Lakes, USA)
Bacto Yeast extract	Becton, Dickinson and Company (Franklin Lakes, USA)
Benzamidine	Sigma-Aldrich (Taufkirchen, D)
Bovine serum albumin (BSA)	Carl Roth (Karlsruhe, D)
Bromophenol blue	Sigma-Aldrich (Taufkirchen, D)
Caesium chloride (CsCl)	Carl Roth (Karlsruhe, D)
Calcium chloride ($CaCl_2$)	Carl Roth (Karlsruhe, D)
Cell Proliferation Dye eFluor™670	eBiosciences (San Diego, USA)
Chloroform	Carl Roth (Karlsruhe, D)
DAPI Fluoromount-G	SouthernBiotech (Birmingham, USA)
Dimethyl sulfoxide (DMSO)	Carl Roth (Karlsruhe, D)
Dithiothreitol (DTT)	Carl Roth (Karlsruhe, D)
dNTPs	Thermo Fisher Scientific (Waltham, USA)
Donkey serum	Sigma-Aldrich (Taufkirchen, D)
DPX mountant for histology	Sigma-Aldrich (Taufkirchen, D)
Eosin Y solution 0.5 % aqueous	Merck (Darmstadt, D)
Ethanol	Werner Hofman Abteilung der Schnittmann GmbH (Düsseldorf, D)
Ethidium bromide (EtBr)	Carl Roth (Karlsruhe, D)
Ethylenediaminetetraacetic acid (EDTA)	Sigma-Aldrich (Taufkirchen, D)
Glucose	Carl Roth (Karlsruhe, D)
Glycerol	Grüssing (Filsum, D)
Glycerol phosphate	Sigma-Aldrich (Taufkirchen, D)
Glycine	Carl Roth (Karlsruhe, D)
Glycogen	Roche (Mannheim, D)

Hemalum solution acid according to Mayer	Carl Roth (Karlsruhe, D)
Hydrochloric acid (HCl)	Carl Roth (Karlsruhe, D)
Hydrogen peroxide (H_2O_2)	Merck (Darmstadt, D)
Hydroxyethylpiperazineethanesulfonic acid (HEPES)	Carl Roth (Karlsruhe, D)
Igepal CA-630	Sigma-Aldrich (Taufkirchen, D)
LB-Agar (Luria/Miller)	Carl Roth (Karlsruhe, D)
LB-Medium (Luria/Miller)	Carl Roth (Karlsruhe, D)
Leupeptin	Carl Roth (Karlsruhe, D)
Linear polyacrylamide (GenElute LPA)	Sigma-Aldrich (Taufkirchen, D)
Lithium chloride (LiCl)	Carl Roth (Karlsruhe, D)
Low melting agarose, peqGOLD	VWR (Darmstadt, D)
Magnesium chloride ($MgCl_2$)	Carl Roth (Karlsruhe, D)
Methanol	VWR (Darmstadt, D)
Milk powder	Carl Roth (Karlsruhe, D)
Paraffin (Pastilles)	Merck (Darmstadt, D)
Paraformaldehyde solution (16 %)	Thermo Fisher Scientific (Waltham, USA)
Phenol	Carl Roth (Karlsruhe, D)
Phenylmethanesulfonyl fluoride (PMSF)	Carl Roth (Karlsruhe, D)
PolyFreeze Tissue Freezing Medium	Polysciences (Warrington, USA)
Ponceau S	Carl Roth (Karlsruhe, D)
Potassium acetate	Carl Roth (Karlsruhe, D)
Potassium chloride (KCl)	Carl Roth (Karlsruhe, D)
Saccharose	Carl Roth (Karlsruhe, D)
Sodium azide (NaN_3)	Sigma-Aldrich (Taufkirchen, D)
Sodium chloride (NaCl)	Th. Geyer (Renningen, D)
Sodium deoxycholate	Sigma-Aldrich (Taufkirchen, D)
Sodium dodecyl sulphate (SDS)	Carl Roth (Karlsruhe, D)
Sodium fluoride (NaF)	Sigma-Aldrich (Taufkirchen, D)
Sodium hydrogen phosphate (Na_2HPO_4)	Carl Roth (Karlsruhe, D)
Sodium hydroxide (NaOH)	Grüssing (Filsum, D)
Sodium orthovanadate	Sigma-Aldrich (Taufkirchen, D)
Sodium pyrophosphate	Sigma-Aldrich (Taufkirchen, D)
Tetramethylethylenediamine (TEMED)	AppliChem (Darmstadt, D)
Tris(hydroxymethyl)aminomethane (Tris)	Carl Roth (Karlsruhe, D)
Triton X-100	Carl Roth (Karlsruhe, D)
TRIzol Reagent	Life Technologies, Thermo Fisher Scientific (Waltham, USA)
Trypan blue solution	Sigma-Aldrich (Taufkirchen, D)
Tween 20	Carl Roth (Karlsruhe, D)
Water, molecular biology reagent (RNase-free)	Sigma-Aldrich (Taufkirchen, D)

Xylene cyanol	Sigma-Aldrich (Taufkirchen, D)
Xylol	Carl Roth (Karlsruhe, D)

2.1.4 Enzymes

Enzyme	Manufacturer (office)
DNaseI (1 U/ µl)	Thermo Fisher Scientific (Waltham, USA)
DreamTaq DNA Polymerase (5 U/µl)	Thermo Fisher Scientific (Waltham, USA)
Fast Digest restriction endonucleases	Thermo Fisher Scientific (Waltham, USA)
FastAP (1 U/µl)	Thermo Fisher Scientific (Waltham, USA)
Phusion High-Fidelity DNA Polymerase (2 U/µl)	Thermo Fisher Scientific (Waltham, USA)
Proteinase K (20 mg/ml)	Thermo Fisher Scientific (Waltham, USA)
Q5 High-Fidelity DNA Polymerase (2 U/µl)	New England Biolabs (Ipswich, USA)
Restriction endonucleases	Thermo Fisher Scientific (Waltham, USA)
RNaseA (10 mg/ml)	Carl Roth (Karlsruhe, D)
T4 DNA Ligase (1 U/µl)	Thermo Fisher Scientific (Waltham, USA)
T4 DNA Ligase (2000 U/µl)	New England Biolabs (Ipswich, USA)
T4 Polynucleotide Kinase (10 U/µl)	New England Biolabs (Ipswich, USA)

2.1.5 Commercial kits

Kit	Manufacturer (office)
High-Capacity cDNA Reverse Transcription Kit	Applied Biosystems, Thermo Fisher Scientific (Waltham, USA)
iTaq Universal Probes Supermix	Bio-Rad (Munich, D)
iTaq Universal SYBR Green Supermix	Bio-Rad (Munich, D)
Lipofectamine RNAiMAX Transfection Reagent	Invitrogen, Thermo Fisher Scientific (Waltham, USA)
Lipofectamine Stem Transfection Reagent	Invitrogen, Thermo Fisher Scientific (Waltham, USA)
NucleoSpin Gel and PCR Clean-up Kit	Macherey-Nagel (Düren, D)
PE Annexin V Apoptosis Detection Kit I	BD Biosciences (Heidelberg, D)
Pierce BCA Protein Assay Kit	Thermo Fisher Scientific (Waltham, USA)
Pierce ECL Western Blotting Substrate	Thermo Fisher Scientific (Waltham, USA)
SuperSignal West Femto Maximum Sensitivity Substrate	Thermo Fisher Scientific (Waltham, USA)

2.1.6 Cell culture medium and additives

Product	Manufacturer (office)
0.05 % Trypsin/ 0.02 % EDTA	PAN-Biotech (Aidenbach, D)
Dulbecco's Modified Eagle's Medium (DMEM) with 4.5 g/l Glucose and 3.7 g/l $NaHCO_3$	PAN-Biotech (Aidenbach, D)
EDTA (0.5 M in H_2O)	Sigma-Aldrich (Taufkirchen, D)
Fetal calf serum (FCS)	Sigma-Aldrich (Taufkirchen, D)
Opti-MEM	Gibco, Gibco, Thermo Fisher Scientific (Waltham, USA)
Penicillin/Streptomycin (P/S)	PAN-Biotech (Aidenbach, D)
Phosphate Buffered Saline (PBS)	PAN-Biotech (Aidenbach, D)
Roswell Park Memorial Institute Medium (RPMI) 1640	PAN-Biotech (Aidenbach, D)

2.1.7 Solutions and buffers

If not noted differently, all solutions were prepared using double distilled water (ddH_2O).

2.1.7.1 Solutions for bacteria culture

Solution/ Buffer	Component	Final concentration
SOC-medium	Bacto Tryptone	2 % (w/v)
	Bacto Yeast Extract	0.5 % (w/v)
	NaCl	10 mM
	KCl	2.5 mM
	$MgCl_2$	20 mM
	Glucose (freshly added)	20 mM
LB-Medium	LB-Medium	25 g/l
	Ampicillin	100 µg/ml
LB-Agar	LB-Agar	40 g/l
	Ampicillin	100 µg/ml

2.1.7.2 Solutions and buffers for nucleic acid analysis and preparation

Solution/ Buffer	Component	Final concentration
1x TAE buffer	Tris	40 mM
	Acetic acid	40 mM
	EDTA pH 8.0	0.5 mM
6x loading dye	Bromphenol blue	0.25 % (w/v)
	Xylene cyanol	0.25 % (w/v)
	Glycerol	30 % (w/v)

Solution I (pH 8.0)	EDTA	10 mM
	Glucose	50 mM
	Tris-HCl	25 mM
Solution II (pH 13.0)	NaOH	200 mM
	SDS	1 % (w/v)
Solution III (pH 5.0)	Potassium acetate	5 M
	Acetic acid	2 M
Cell lysis buffer	Tris-HCl (pH 8.5)	100 mM
	EDTA	5 mM
	SDS	0.5 % (w/v)
	NaCl	200 mM
	Proteinase K (freshly added)	100 µg/ml

2.1.7.3 Solution and buffers for protein analysis

Solution/ Buffer	Component	Final concentration
RIPA lysis buffer	Sodium chloride	150 mM
	Triton X-100	1 %
	Sodium deoxycholate	0.5 %
	SDS	0.1 %
	Tris	50 mM
	Glycerol phosphate	10 mM
	Sodium fluoride	50 mM
	Sodium pyrophosphate	5 mM
	Sodium orthovanadate	1 mM
	Aprotinin (freshly added)	10 µg/ml
	Leupeptin (freshly added)	10 µg/ml
	Antipain (freshly added)	2 µg/ml
	Benzamidine (freshly added)	1 mM
	PMSF (saturated solution) (freshly added)	1:1000
5x sample buffer (pH 6.8)	Tris-HCl	100 mM
	SDS	4 % (w/v)
	Bromphenol blue	0.1 % (w/v)
	Glycerol	20 % (w/v)
	DTT	200 mM
10x Laemmli Running Buffer	Tris	250 mM
	Glycine	2.5 M
	SDS	1 % (w/v)
1x Transfer Buffer	Tris	25 mM
	Glycine	200 mM
	SDS	0.002 % (w/v)
	Methanol	20 % (v/v)

1x TBST (pH 7.9)	Tris	50 mM
	NaCl	140 mM
	Tween 20	0.05 % (w/v)
Ponceau Red	Acetic acid	5 % (v/v)
	Ponceau S	0.1 % (w/v)

2.1.7.4 Solutions for cell biological analysis

Solution/ Buffer	Component	Final concentration
Freezing medium	RPMI	40 % (v/v)
	FCS	50 % (v/v)
	DMSO	10 % (v/v)
2x HBS (pH 7.05)	HEPES	50 mM
	NaCl	274 mM
	KCl	10 mM
	Na_2HPO_4	1.5 mM
	D-Glucose	10 mM

2.1.7.5 Solutions for immunofluorescent staining

Solution/ Buffer	Component	Final concentration
Blocking solution (in PBS)	BSA	1 % (w/v)
	Donkey serum	2 % (v/v)
	Triton X-100	0.3 % (v/v)

2.1.8 Antibodies

2.1.8.1 Primary antibodies

Target	Clone	Host species	Dilution	Reference/Manufacturer
TRA98	-	rat	1:500 (IF)	ab82527; Abcam (Cambridge, UK)
WT-1	-	rabbit	1:50 (IF)	ab89901; Abcam (Cambridge, UK)
TRIM71 (human)	-	rabbit	1:1000 (WB)	HPA038142; Sigma-Aldrich (Taufkirchen, D)
TRIM71 (mouse)		rabbit	1:1000 (WB)	PAB19293; Abnova (Taipei, TW)
ACTIN	-	rabbit	1:1000 (WB)	A2066; Sigma-Aldrich (Taufkirchen, D)
FLAG	M2	mouse	1:2000 (WB)	F3165; Sigma-Aldrich (Taufkirchen, D)
CDKN1A/ p21	12D1	rabbit	1:1000 (WB)	#2947; Cell Signalling (Danvers, USA)

DDX4/ VASA	N-14	goat	1:400 (WB)	sc-48707; Santa Cruz, (Dallas, USA)
LIN28A	D1A1A	rabbit	1:1000 (WB)	#8641; Cell Signalling (Danvers, USA)
LIN28B	-	rabbit	1:500 (WB)	#5422; Cell Signalling (Danvers, USA)
GAPDH	6C5	mouse	1:5000 (WB)	ACR001PT; OriGene (Rockville, USA)
TUBULIN	DM1A	mouse	1:1000 (WB)	T9026; Sigma-Aldrich (Taufkirchen, D)
VINCULIN	hVIN-1	mouse	1:5000 (WB)	V9131; Sigma-Aldrich (Taufkirchen, D)

2.1.8.2 Secondary antibodies

Target	Conjugate	Host species	Dilution	Reference/Manufacturer
rat IgG	A488	donkey	1:250 (IF)	712-545-153; Jackson ImmunoResearch (West Grove, USA)
rabbit IgG	Cy3	donkey	1:400 (IF)	711-165-152; Jackson ImmunoResearch (West Grove, USA)
rabbit IgG	HRP	goat	1:5000 (WB)	sc-2004; Santa Cruz (Dallas, USA)
rabbit IgG	HRP	goat	1:3000 (WB)	#7074; Cell Signalling (Danvers, USA)
rabbit IgG	HRP	goat	1:50000 (WB)	111-035-114; Jackson ImmunoResearch (West Grove, USA)
mouse IgG	HRP	horse	1:5000 (WB)	#7076; Cell Signalling (Danvers, USA)
mouse IgG	HRP	goat	1:5000 (WB)	0300-0108P; Bio-Rad (Munich, D)
goat IgG	HRP	rabbit	1:5000 (WB)	sc-2768; Santa Cruz (Dallas, USA)

2.1.9 Plasmids

Vector	Resistance	Reference/ Manufacturer (office)
pRK5-Flag	Ampicillin	Prof. Dr. W. Kolanus lab*
pSpCas9(BB)-2A-GFP (PX458)	Ampicillin	# 48138; Addgene (Watertown; USA) [230]

*was originally obtained from Clontech (Mountain View, USA) and the cloning site was modified by Prof. Dr. W. Kolanus enabling a cloning using the restriction endonucleases *MluI* and *NotI*.

2.1.10 Oligonucleotides

If not noted differently, all oligonucleotides were synthesised by MWG Eurofins (Ebersberg, D) or Biolegio (Nijmegen, NL).

2.1.10.1 Primer for cloning

Primer for cloning were designed to contain the *MluI* and *NotI* restriction sites for ligation into the vector. Upstream of the restriction site a so-called GC-clamp was inserted, which is facilitating the restriction digest.

Primer	Sequence (5‘->3‘)	T_m
hTRIM71_Mlu_f	GGGGCGACGCGTATGGCTTCGTTCCCCGAGACC	58 °C
hTRIM71_Not_r	GGGGCGGCGGCCGCTTAGAAGACGAGGATTCGATTGTTGCC	58 °C

2.1.10.2 Primer for Sanger sequencing

Primer	Sequence (5‘->3‘)	Application
PX458_U6_f	GAGGGCCTATTTCCCATGATTCC	sgRNA cloning into PX458
pRK5-Flag_T7_f	TAATACGACTCACTATAGGG	Inserts cloned into pRK5-Flag
pRK5-Flag_r	GTAACCATTATAAGCTGCAATAAAC	
hTRIM71_f	ATGGCTTCGTTCCCCGAGACC	TRIM71ΔRING clones generated with sgRNA#1
hTRIM71_seq_r_3	GCACTACTTTCTGGTCGCAC	
hTRIM71_gRNA4_f	CGGATTCCAGGAACCATCGGGTAC	TRIM71Δ6NHL clones generated with sgRNA#2
hTRIM71_gRNA4_r_2	GAGACGATTTCTTCTTTGAAATTC	

2.1.10.3 Primer for genotyping

Primer	Sequence (5‘->3‘)	T_m	Amplicon size
TG206-Trim71	GAAAGGAGGCTAGCCAAAGG	59 °C	WT=242 bp
TG207-Trim71	ATGCTGTACGGTAGGAGTCTTCC	59 °C	fl=361 bp
TG209-Trim71	CACACAAAAAACCAACACACAG	59 °C	KO=322 bp
nos3-F1	CCAGCCATGGGGACTTTC	59 °C	WT=220 bp
nos3-R1	GGGACTGATAGATGGCAC	59 °C	tg=270 bp
PGK-neo-R2a	CAGAGGCCACTTGTGTAGCG	59 °C	

2.1.10.4 Primer for qRT-PCR

Primer	Sequence (5‘->3‘)	T_m	Amplicon size
q_Hs_EGR1	f: CCTGACCGCAGAGTCTTTTC r: AGCGGCCAGTATAGGTGATG	60 °C	113 bp
q_Hs_HPRT1	f: AGCCCTGGCGTCGTGATTAG r: GTAATCCAGCAGGTCAGCAA	60 °C	231 bp
q_Hs_KLF4	f: TCTCAAGGCACACCTGCGAA r: TAGTGCCTGGTCAGTTCATC	60 °C	105 bp
q_Hs_MYC	f: ACTCTGAGGAGGAACAAGAA r: TGGAGACGTGGCACCTCTT	60 °C	159 bp
q_Hs_OCT4	f: AGCGAACCAGTATCGAGAAC r: TTACAGAACCACACTCGGAC	60 °C	142 bp
q_Hs_SOX2	f: AGCTACAGCATGATGCAGGA r: GGTCATGGAGTTGTACTGCA	60 °C	126 bp
q_Hs_TRIM71	f: GTGCTGCACCTGTACTGTGA r: GCTCGATGCTCAGCTGGATT	60 °C	181 bp
q_Mm_Hprt	f: GCTGGTGAAAAGGACCTCT r: CACAGGACTAGAACACCTGC	55 °C	249 bp
q_Mm_Trim71NHL	f: CACCCTGATTGCCAATCTG r: CAAAGTCCACCACGACGA	55 °C	259 bp

2.1.10.5 TaqMan Probes

If not stated differently, all TaqMan probes were obtained from Applied Biosystems, Thermo Fisher Scientific (Waltham, USA).

Gene	ID number	Fluorophore	Amplicon size
CDKN1A	Hs00355782_m1	FAM	66 bp
INHBB	Hs00173582_m1	FAM	90 bp
PLXNB2	Hs01019888_m1	FAM	56 bp
HPRT1	Hs01003267_m1	FAM	72 bp
TRIM71*	f: CCCTTCTCCATCCTCTCAGTGTT r: CAGATGGGTACAGAGCAAGTGTCA Probe: CCTCGGCTTCTGCCAGCACCACGACG	FAM	104 bp
let-7a	000377	FAM	22 bp
U6 snRNA	001973	FAM	106 bp
Hprt	Mm03024075_m1	FAM	131 bp
Sall4	Mm00453037_s1	FAM	93 bp
Lin28a	Mm00524077_m1	FAM	79 bp
Lin28b	Mm01190673_m1	FAM	106 bp
Oct4	Mm03053917_g1	FAM	139 bp
Cdkn1a	Mm04205640_g1	FAM	80 bp

*Individual primers were synthesised by MWG Eurofins (Ebersberg, D)

2.1.10.6 siRNAs

siRNA	Target sequence (5‘->3‘)	Targeted TRIM71 region	Supplier
siRenilla	AAACAUGCAGAAAAUGCUG	-	Dharmacon (Lafayette, USA)
siTRIM71 #1	CGUGUGCGACCAGAAAGUA	end of RING domain	MWG Eurofins (Ebersberg. D)
siTRIM71 #2	AGAAAGUAGUGCUAGCCGA	immediately after RING domain	Dharmacon (Lafayette, USA)
siTRIM71 #3	GGAGGAGGGUAGAGCGCUA	end of coiled-coiled domain	Dharmacon (Lafayette, USA)
siTRIM71 #4	CUUGGGAUGUGGCGGUGAA	3rd NHL repeat	Dharmacon (Lafayette, USA)
siTRIM71 #5	CACCAAGGCCACAGGCGAU	start of Filamin domain	Dharmacon (Lafayette, USA)

2.1.10.7 sgRNA oligonucleotides

Primer	Sequence (5‘->3‘)	Targeted TRIM71 region
TRIM71 gRNA#1	s: CACCGCTCGCAGACGTCCACGTCGT as: AAACACGACGTGGACGTCTGCGAGC	start of RING domain
TRIM71 gRNA#2	s: CACCGCACAACGATCATTCCGTCGG as: AAACCCGACGGAATGATCGTTGTGC	6th NHL repeat

2.1.10.8 Primer for MiSeq

Amplification primer	Sequence (5‘->3‘)	T_m	Amplicon size
TRIM71_NGS_gRNA#1	f: ACACTCTTTCCCTACACGACGCTCTTCCG ATCTCTCCTCCGGGCTGGGTTGCAAATG r: TGACTGGAGTTCAGACGTGTGCTCTTCC GATCTCAGCGCAGCTTGAGCGGCTCTCCC	62 °C	359 bp
TRIM71_NGS_gRNA#2	f: ACACTCTTTCCCTACACGACGCTCTTCCG ATCTCGGATTCCAGGAACCATCGGGTAC r: TGACTGGAGTTCAGACGTGTGCTCTTCC GATCTGAGACGATTTCTTCTTTGAAATTC	55 °C	348 bp

All Index primers had an annealing temperature of 65 °C and added an additional 70 bp to the amplicon size. Hence for TRIM71 gRNA#1 and TRIM71 gRNA#2 the amplicon size was 429 bp and 418 bp, respectively.

Index primer	Sequence (5‘->3‘)
D501_long (#732)	AATGATACGGCGACCACCGAGATCTACACTATAGCCTACACTCT TTCCCTACACGACGCT
D502_long (#733)	AATGATACGGCGACCACCGAGATCTACACATAGAGGCACACTCT TTCCCTACACGACGCT

D503_long (#734)	AATGATACGGCGACCACCGAGATCTACACCCTATCCTACACTCT TTCCCTACACGACGCT
D504_long (#735)	AATGATACGGCGACCACCGAGATCTACACGGCTCTGAACACTCT TTCCCTACACGACGCT
D505_long (#736)	AATGATACGGCGACCACCGAGATCTACACAGGCGAAGACACTC TTTCCCTACACGACGCT
D506_long (#737)	AATGATACGGCGACCACCGAGATCTACACTAATCTTAACACTCTT TCCCTACACGACGCT
D507_long (#738)	AATGATACGGCGACCACCGAGATCTACACCAGGACGTACACTCT TTCCCTACACGACGCT
D508_long (#739)	AATGATACGGCGACCACCGAGATCTACACGTACTGACACACTCT TTCCCTACACGACGCT
D701_long (#740)	CAAGCAGAAGACGGCATACGAGATCGAGTAATGTGACTGGAGT TCAGACGTGTGCT
D702_long (#741)	CAAGCAGAAGACGGCATACGAGATTCTCCGGAGTGACTGGAGT TCAGACGTGTGCT
D703_long (#742)	CAAGCAGAAGACGGCATACGAGATAATGAGCGGTGACTGGAGT TCAGACGTGTGCT
D704_long (#743)	CAAGCAGAAGACGGCATACGAGATGGAATCTCGTGACTGGAGT TCAGACGTGTGCT
D705_long (#744)	CAAGCAGAAGACGGCATACGAGATTTCTGAATGTGACTGGAGTT CAGACGTGTGCT
D706_long (#745)	CAAGCAGAAGACGGCATACGAGATACGAATTCGTGACTGGAGTT CAGACGTGTGCT
D707_long (#746)	CAAGCAGAAGACGGCATACGAGATAGCTTCAGGTGACTGGAGT TCAGACGTGTGCT
D708_long (#747)	CAAGCAGAAGACGGCATACGAGATGCGCATTAGTGACTGGAGT TCAGACGTGTGCT
D709_long (#748)	CAAGCAGAAGACGGCATACGAGATCATAGCCGGTGACTGGAGT TCAGACGTGTGCT
D710_long (#749)	CAAGCAGAAGACGGCATACGAGATTTCGCGGAGTGACTGGAGT TCAGACGTGTGCT
D711_long (#750)	CAAGCAGAAGACGGCATACGAGATGCGCGAGAGTGACTGGAGT TCAGACGTGTGCT
D712_long (#751)	CAAGCAGAAGACGGCATACGAGATCTATCGCTGTGACTGGAGTT CAGACGTGTGCT

2.1.11 DNA and protein standards

Product	Manufacturer (office)
GeneRuler 1 kb DNA Ladder	Thermo Fisher Scientific (Waltham, USA)
GeneRuler 100 bp DNA Ladder	Thermo Fisher Scientific (Waltham, USA)
Precision Plus Protein™ All Blue Standard	Bio-Rad (Munich, D)

2.1.12 Organisms

2.1.12.1 Bacterial strains

Escherichia coli (*E. coli*)	Genotype
DH5α	F- endA1 deoR (ϕ80lacZΔM15) recA1 gyrA (Nalr) thi-1 hsdR17 (rK-, mK +) supE44 relA1 Δ(lacZYA-argF) U169
Stbl3	F- mcrB mrr hsdS20 (rB-, mB-) recA13 supE44 ara-14 galK2 lacY1 proA2 rpsL20 (Str) xyl-5 λ- leu mtl-1r

2.1.12.2 Eukaryotic cell lines

Cell line	Type	Donor
HEK293T	Embryonic kidney cells	Human
NCCIT	Embryonal carcinoma cell line	Human
TCam-2	Seminoma cell line	Human

2.1.12.3 Mice

Strain	Background	Description	Abbreviation	Reference
Trim71^{tm1695Arte}	C57BL/6J	Generated by Taconic Biosciences (Cologne, Germany). Derived from an ES cell clone in which exon 4 of one *Trim71* allele was floxed.	*Trim71*$^{+/fl}$	[188]
Nanos3-Cre-PGKneo-pA	unknown	Received from Prof. Dr. Hubert Schorle, Department of Developmental Pathology, University Hospital Bonn, Germany Originally derived from an ES cell clone in which the *Cre* gene was knocked in at the *Nanos3* locus.	*Nanos3*$^{Cre/+}$	[276]

2.1.13 Software and databases

Application	Software	Manufacturer/Reference
Image processing	Adobe Illustrator CS4	Adobe (San José; USA)
Image processing	Adobe Photoshop CS4	Adobe (San José; USA)
Sequence viewer	ApE Plasmid editor	M. Wayne Davis
Sequence analysis	BLAST	NCBI (USA)
qRT-PCR analysis	CFX Manager	Bio-Rad (Munich, D)
Chromatogram viewer and editor	Chromas	Technelysium (Brisbane, AUS)

sgRNA design	CRISPOR	[84]
MiSeq data analysis	CRISPResso2	[46, 222]
FACS measurement	FACSDiva	BD Biosciences (Heidelberg, D)
FACS analysis	FlowJo	BD Biosciences (Heidelberg, D)
Cancer database	GEPIA2 web server	[281]
Statistical analysis	GraphPad Prism	GraphPad Software (San Diego, USA)
Western blot quantification	Image Studio Lite	LI-COR Biosciences (Lincoln, USA)
Image processing	ImageJ (Fiji)	[253]
Documentation	Microsoft Office	Microsoft (USA)
Plagiarism analysis	PlagScan	PlagScan GmbH (Cologne, D)
Primer design	Primer BLAST	NCBI (USA)
Primer design	Primer3	University of Massachusetts (USA)
Cancer database	R2: Genomics Analysis and Visualization Platform	Koster, J.; Academic Medical Center (AMC) (Amsterdam, NL) (http://r2.amc.nl)
Plasmid design	SnapGene Viewer	GSL Biotech LLC (Chicago; USA)
Sequence analysis	StarORF	Massachusetts Institute of Technology (Cambridge, USA) (http://star.mit.edu/orf/)
Imaging and Image processing	ZEN 2012 (blue edition)	Carl Zeiss (Jena, D)

2.2 Methods

2.2.1 Molecular biological methods

2.2.1.1 Agarose gel electrophoresis

Agarose gel electrophoresis was used to separate DNA fragments according to their size by applying an electrical field. For this, 1 - 4 % (w/v) agarose (depending on the size of the nucleic acids to be separated) was added to 1x TAE buffer heated in the microwave until it was dissolved completely. The agarose was cooled down slightly before adding ethidium bromide (0.2 µg/ml). Then, the agarose was poured into a special agarose gel cast tray with a comb inserted for form loading pockets for the samples. After complete polymerisation of the gel, it was transferred into the gel electrophoresis chamber and covered with 1x TAE buffer (chapter 2.1.7.2). The comb was removed and the samples, previously mixed with 6x loading dye (chapter 2.1.7.2), were loaded into the gel pockets. Additionally, as a reference a DNA ladder was loaded into one pocket enabling the determination of the size of the DNA fragments in the sample. Electrophoretic separation was performed by applying a voltage of 80-120 V for 30 - 60 min depending on the gel size. Afterwards, the DNA fragments were visualised at a wavelength of 230 nm in a UV transilluminator.

In general, 1 % gels were used for separation of preparative restriction digest (~1000 bp) and analytical restriction digest. Small DNA amplicons generated by genotyping PCR (<500 bp) were separated using 2 % agarose gels. Even smaller DNA fragments generated by the amplification and indexing PCR for MiSeq analysis were separated on a 2.5 % agarose gels.

2.2.1.2 Determination of nucleic acid concentrations

The concentration of nucleic acids (DNA and RNA) was determined using a NanoDrop spectrophotometer (Thermo Fisher Scientific). For this, absorbance measurements at 230 nm, 260 nm and 280 nm were performed using 1 µl of DNA or RNA. The nucleic acid concentration as calculates based on the generally accepted extinction coefficient for double-stranded DNA (50 ng/µl) and RNA (40 µg/µl). In order to determine the sample quality, the absorbance at 280 nm was measured. The ratio of the absorbance at 260 nm and 280 nm was used to access the sample quality. DNA and RNA were accepted as pure with a ratio of ~1.8 and ~2.0, respectively. If the ratio was lower, it indicated the contamination with proteins or phenol.

2.2.1.3 DNA precipitation and purification

Depending on the specificity of the PCR amplification, the DNA was directly purified from the reaction mix or extracted from an agarose gel.

In case of a single amplicon, this was purified by phenol extraction to remove the DNA polymerase, primers and nucleotides and then precipitated. First, the PCR reaction mix was filled up with distilled water to a final volume of 400 µl. Then, 300 µl of Phenol:Chloroform (1:1) was added to the sample and vortexed. After centrifugation (13,000 rpm, 5 min, room temperature), the upper aqueous phase was transferred into a new 1.5 ml reaction tube. The DNA was precipitated by the addition of 40 µl lithium chloride, 1 µl glycogen and 1 ml ice-cold 100 % ethanol and incubation at -20 °C overnight. The next day, the precipitated DNA was pelleted by centrifugation (13,000 rpm, 15 min, 4 °C) and the pellet washed with 70 % ethanol twice. Finally, the pellet was air-dried and dissolved in 15 µl RNase-free water.

Alternatively, for subsequent sanger sequencing, the DNA from a PCR reaction yielding a single amplicon, was purified using the NucleoSpin Gel and PCR Clean-up Kit (Macherey-Nagel) according to manufacturer's instructions.

For the purification of DNA from a single band in an agarose gel, the desired band was cut out from the agarose gel with a scalpel applying attenuated UV-light. The DNA extraction from the gel piece was performed using the NucleoSpin Gel and PCR Clean-up Kit (Macherey-Nagel) according to manufacturer's instructions.

Independent of the DNA purification method, concentration and purity were measured using a NanoDrop spectrophotometer (chapter 2.2.1.2).

2.2.1.4 PCR amplification of DNA fragments for subsequent cloning

For cloning of new DNA sequences into eukaryotic expression vectors, the desired DNA fragments were amplified by polymerase chain reaction (PCR) using previously reverse transcribed cDNA (chapter 2.2.1.16) as template. The amplification was performed using Phusion High-Fidelity DNA Polymerase (Thermo Fisher Scientific). Besides being able to generate long templates with high speed, this polymerase possesses a very low error rate (4.4×10^{-7}) due to a proofreading (3´→5´ exonuclease) activity. Primers used for amplification are listed in chapter 2.1.10.1. Importantly, the 5' and 3' primers were designed to carry a *MluI* and *NotI* restriction site, respectively, for subsequent cloning. The PCR reaction was set up using the following components and thermal cycler conditions:

PCR reaction	Component	Volume for 1x reaction
	cDNA	100 ng
	5x Phusion GC Buffer	10 µl
	dNTPs (10 mM)	1 µl
	Forward Primer (10 µM)	2.5 µl
	Reverse Primer (10 µM)	2.5 µl
	DMSO	2.5 µl
	Phusion DNA Polymerase (2 U/µL)	0.5 µl
	ddH_2O	ad 50 µl

PCR programme	Step	Temperature	Time	Cycles
	Initial denaturation	98 °C	1 min	1
	Denaturation	98 °C	30 s	35
	Primer annealing	58 °C	20 s	
	Elongation	72 °C	30 s/kb	
	Final elongation	72 °C	5 min	1
	Hold	4 °C	∞	

In order to verify the amplification, 5 µl of PCR reaction were separated by agarose gel electrophoresis (chapter 2.2.1.1). The remaining PCR reaction was purified by DNA precipitation (chapter 2.2.1.3) followed by restriction digest (chapter 2.2.1.5) and subsequent ligation (chapter 2.2.1.7).

2.2.1.5 Restriction digest of DNA by restriction endonucleases

For most of the vectors, the restriction sites *MluI* (5' end) and *NotI* (3' end) were used for cloning. The double digest was performed using the buffer recommended by Thermo Fisher Scientific. For the preparative restriction digest of vector or purified PCR product, the following components were used and the reaction mix was incubated at 37 °C for 2 h:

Restriction digest reaction	Component	Volume for 1x reaction	
		Vector	PCR product (insert)
	DNA	4-5 µg	Complete volume
	10x Restriction Buffer	5 µl	2 µl
	Enzyme 1 (10 U/µl)	1-2 µl	1-2 µl
	Enzyme 2 (10 U/µl)	1-2 µl	1-2 µl
	ddH_2O	ad 50 µl	ad 20 µl

Afterwards, solely the vector was dephosphorylated (chapter 2.2.1.6). Then, the complete reaction mix was loaded on an agarose gel prepared with low-melting agarose. After agarose gel electrophoresis (chapter 2.2.1.1) the DNA bands of desired size were cut out using a scalpel and utilised in the subsequent ligation (chapter 2.2.1.7).

2.2.1.6 Vector dephosphorylation

In order to inhibit re-ligation of the vector, the 5' overhangs of the vector were dephosphorylated using thermosensitive alkaline phosphatase (Thermo Fisher Scientific). The enzyme catalyses the hydrolysis of the 5'-phosphate residue of DNA and RNA. The reaction mixture was set up with the following components and was incubated at 37 °C for 30 min with subsequent heat-inactivation of the enzyme at 75 °C for 5 min:

Dephosphorylation reaction	Component	Volume for 1x reaction
	Vector (post restriction digest)	complete volume
	FastAP (1 U/µl)	1 µl

2.2.1.7 Ligation of DNA fragments

In general, the restriction digested PCR products were inserted in a vector cut with the identical restriction enzymes with the cohesive ends being joined by a T4 DNA ligase (Thermo Fisher Scientific). For this, the gel pieces containing the digested vector and insert, were melted at 68 °C for 3-5 min. The ligation reaction was set up with a 1:2 (vector:insert) ration as followed and was incubated at 16 °C overnight:

Ligation reaction	Component	Volume for 1x reaction
	Vector (dephosphorylated)	1 µl
	Insert	2 µl
	10x T4 DNA Ligase Buffer	5 µl
	T4 DNA Ligase (1 U/µl)	2 µl
	ddH_2O	ad 50 µl

2.2.1.8 Bacterial transformation

For transformation of plasmid DNA, chemically competent *E. coli* bacteria of the strains DH5α and Stbl3 were used. First, the bacteria were thawed on ice. Then, 5-7 µl of ligation reaction were added to 50-70 µl bacterial suspension, respectively, and incubated for 15 min on ice to allow the DNA to accumulate around the bacterial cell wall. Thereafter, by incubation at 37 °C for 5 min (heat-shock), the DNA entered the cell. The suspension was cooled down at room temperature before adding 250 µl of SOC-medium (chapter 2.1.7.1) and incubating at 37 °C in a shaker incubator (250 rpm) for 1-1.5 h. Then, 50-150 µl of bacterial suspension was plated on LB agar plates containing the selective antibiotics corresponding to the resistance cassette on the plasmid (100 µg/ml ampicillin). The plated bacteria were grown at 37 °C in the incubator overnight.

2.2.1.9 Preparation of plasmid DNA in small scale ('mini-preparation')

DNA mini-preparation was used for the fast isolation of small amounts of plasmid DNA in order to verify newly constructed plasmids. For this, 4 ml of LB-medium supplemented with relevant selection antibiotic (Ampicillin 100 µg/ml) was inoculated with one transformed bacterial colony. Bacteria were grown at 37 °C in a shaker incubator (220 rpm) overnight (12-16 h). Next day, the isolation of plasmid DNA was performed via alkaline lysis, phenol-chloroform extraction and subsequent precipitation. First, the 2 ml of overnight bacterial culture was pelleted by centrifugation (13,000 rpm, 2 min, room temperature). The supernatant was discarded and the pellet was resuspended in 200 µl Solution I (chapter 2.1.7.2). In the following cell disruption was performed by alkaline lysis adding 400 µl Solution II (chapter 2.1.7.2). The solution was carefully mixed by inversion. After a maximum 5 min of incubation at room temperature, 300 µl Solution III (chapter 2.1.7.2) were added for neutralisation resulting in the precipitation of bacterial proteins and genomic DNA. The cell lysate was centrifuged (13,000 rpm, 5 min, room temperature) and the supernatant containing the plasmid DNA was transferred into a new 1.5 ml reaction tube. To remove remaining proteins, the supernatant was mixed with 300 ml Phenol:Chloroform (1:1) and centrifuged (13,000 rpm, 5 min, room temperature). The upper aqueous phase containing the plasmid DNA was again transferred into a new 1.5 ml reaction tube and 600 µl 2-propanol was added for precipitation. The precipitated plasmid DNA was pelleted by centrifugation (13,000 rpm, 10 min, 4 °C). Then, the DNA pellet was washed once with 70 % ethanol (1 ml) before drying the pellet at 37 °C. Finally, the dried plasmid DNA was dissolved in 30-50 µL distilled water containing 0.1 µg/µl RNaseA and incubated at 37 °C for 5 min.

By subsequent restriction digest (chapter 2.2.1.5) and agarose gel electrophoresis (chapter 2.2.1.1) the newly constructed plasmids were verified. The remaining volume of overnight bacterial culture of a positive bacterial colony was utilised for the inoculation of LB-medium for maxi-preparation (chapter 2.2.1.10).

2.2.1.10 Preparation of plasmid DNA in large scale ('maxi-preparation')

After identification of the correct bacterial colony, plasmid DNA was prepared in large scale. In principle. the maxi-preparation equals the mini-preparation except that the DNA is isolated via a caesium chloride (CsCl) density gradient [184]. First, 1 l of LB-medium supplemented with the required selection antibiotic (Ampicillin 100 µg/ml) was inoculated and incubated at 37 °C in a shaker incubator (180 rpm) overnight (12-16 h). The next day, the overnight bacterial culture was centrifuged (4200 rpm, 15 min, room temperature). Afterwards, the supernatant was discarded and the bacteria pellet was resuspended thoroughly in 40 ml Solution I (chapter 2.1.7.2). In the following, alkaline lysis was performed

by the addition of 80 ml Solution II (chapter 2.1.7.2) and carefully mixing. After a maximum 5 min of incubation at room temperature, lysis was stopped by adding 40 ml Solution III (chapter 2.1.7.2) for neutralisation which causes the precipitation of bacterial proteins and genomic DNA. The cell lysate was centrifuged (4200 rpm, 10 min, 4 °C) and the supernatant containing the plasmid DNA was filtered through gauze into a new 250 ml tube and mixed with 100 ml 2-propanol for precipitation. The precipitated plasmid DNA was pelleted by centrifugation (6000 rpm, 10 min, 4 °C). Then, the DNA pellet was dried at room temperature before resuspending in a 3.7 ml Solution I (chapter 2.1.7.2). Subsequently, 5.5 g caesium chloride was dissolved completely in the solution and 100 µl 10 % Igepal and 500 µl ethidium bromide was added. The solution was centrifuged (5300 rpm, 5 min, room temperature) and the clear supernatant was filled into ultra-centrifugation tubes using a Pasteur glass pipette. The ultra-centrifugation tubes were sealed properly before ultra-centrifugation (3.5 h, 80,000 rpm, room temperature or overnight, 55,000 rpm, room temperature). During the centrifugation, a continuous caesium-chloride density gradient is formed with the plasmid DNA accumulating at their specific isopycnic position. Due to the intercalation of ethidium bromide into double-stranded DNA, the plasmid DNA becomes visible as a pink band. After centrifugation, this visible ethidium bromide containing DNA layer was collected using a syringe. Subsequently, the ethidium bromide was removed by washing three times with 10 ml 1-butanol. Finally, the plasmid DNA was precipitated by adding 1 volume of ammonium acetate and 3 volumes of 96 % ethanol. The precipitate was pelleted by centrifugation (5300 rpm, 10 min, 4 °C) and the resulting DNA pellet was washed with 70 % ethanol once. Then, the pellet was dried overnight at room temperature before being dissolved in 150-1000 µl RNase-free water depending on the pellet size. Concentration and purity were measured using a NanoDrop spectrophotometer (chapter 2.2.1.2). In addition, the newly constructed plasmids were verified by Sanger sequencing (chapter 2.2.1.11). Plasmid DNA was stored at -20 °C (long-term) or 4 °C (short-term).

2.2.1.11 Sanger sequencing

Sanger sequencing was carried out by GATC Biotech AG, Cologne, Germany. Primers used for sequencing are listed in chapter 2.1.10.2.

2.2.1.12 Cloning of CRISPR/Cas9 plasmid PX458

Gene editing using the CRISPR/Cas9 system was carried out using the plasmid pSpCas9(BB)-2A-GFP (PX458) which was obtained as a gift from Feng Zhang (Addgene plasmid # 48138). The plasmid carries the cloning backbone for the single guide RNA (sgRNA) together with the Cas9 from *S. pyogenes* and eGFP as a selection maker separated by the self-cleaving peptide T2A (Supplementary Figure S1). sgRNAs were

designed using the guide RNA selection web tool CRISPOR available at http://crispor.org [84] and are listed in chapter 2.1.10.7. Cloning of sgRNAs into the PX458 vector was performed as described in the Zhang Lab cloning protocol [230] inserting the phosphorylated and annealed sgRNA into the PX458 plasmid via *BbsI* restriction site.

First, the PX458 vector was digested with the *BbsI* restriction endonuclease at 37 °C for 1 h followed by heat-inactivation of the enzyme at 70 °C for 5 min. The reaction mixture was set up with the following components:

Restriction digest reaction	Component	Volume for 1x reaction
	PX458 vector	1 µg
	10x FastDigest Buffer	2 µl
	FastDigest *BbsI*	1 µl
	FastAP (1 U/µl)	1 µl
	ddH_2O	ad 20 µl

The complete reaction mix was loaded on an agarose gel. After agarose gel electrophoresis (chapter 2.2.1.1) the DNA band of desired size was cut out using a scalpel and gel purified using the NucleoSpin Gel and PCR Clean-up Kit (Macherey-Nagel) according to manufacturer's instructions (chapter 2.2.1.3). Concentration and purity were measured using a NanoDrop spectrophotometer (chapter 2.2.1.2).

Simultaneously, the sgRNA was prepared by phosphorylation and annealing of the pair of oligos using the following components and thermal cycler conditions:

Phosphorylation/Annealing reaction	Component	Volume for 1x reaction
	Oligo 1 (stock 100 µM)	1 µl (10 µM)
	Oligo 2 (stock 100 µM)	1 µl (10 µM)
	10x T4 Ligation Buffer (NEB)	1 µl
	T4 Polynucleotide Kinase (10 U/µl) (NEB)	0.5 µl
	ddH_2O	ad 10 µl

Thermal cycler programme	Step	Temperature	Time	Cycles
	1	37 °C	30 min	1
	2	95 °C	5 min	1
	3	95-25 °C (-5 °C increments)	1 min/step	1
	Hold	4 °C	∞	

Thereafter, the annealed oligo duplex (10 µM) was diluted 1:20 in RNase-free water to get a 500 nM stock, of which 5 µl were analysed on a 4 % agarose gel (chapter 2.2.1.1). For subsequent ligation, the 500 nM stock was further diluted 1:10 to get a 50 nM oligo duplex.

The ligation reaction was performed with the following components and incubated at 22 °C for 15 min:

Ligation reaction	Component	Volume for 1x reaction
	BbsI digested PX458 vector	50 ng
	Phosphorylated and annealed oligo duplex (1:200 dilution)	1.5 µl
	10x T4 Ligation Buffer (NEB)	1 µl
	T4 DNA Ligase (2000 U/µl) (NEB)	0.5 µl
	ddH_2O	ad 10 µl

After ligation, the cloned plasmid was transformed into chemically competent *E.coli* bacteria of the strain Stbl3 (chapter 2.2.1.8). This was followed by mini preparation of the plasmid DNA (chapter 2.2.1.9) and subsequent restriction digest (chapter 2.2.1.5) and agarose gel electrophoresis (chapter 2.2.1.1) to verify the newly constructed plasmids. Finally, large amounts of plasmid DNA were isolated by maxi preparation (chapter 2.2.1.10) and the insert (sgRNA) was confirmed by Sanger sequencing (chapter 2.2.1.11).

2.2.1.13 RNA isolation and DNaseI digestion

Total RNA was isolated using TRIzol reagent (Life Technologies) according to manufacturer's instructions. Firstly, the cells of interest were harvested (chapter 2.2.3.3) and the cell pellet was resuspended in 500 µl (for 0.5 – $1x10^7$ cells) or 300 µl (for ≤ $0.5x10^7$ cells) TRIzol reagent and incubated for 2 min at room temperature. Next, 200 µl of chloroform per 1 ml of TRIzol reagent were added and the solution was vortexed thoroughly for approximately 15 seconds. After centrifugation (12,000 rpm, 10 min, room temperature), the RNA containing aqueous phase (upper phase) was transferred into a new 1.5 ml reaction tube and mixed with 500 µL 2-propanol per 1 ml of TRIzol reagent. The samples were stored overnight at -20 °C or immediately processed by centrifugation of the precipitate (13,000 rpm, 30 min, 4 °C). The supernatant was discarded and the pellet was washed once with 1 ml of 70 % (v/v) ethanol. After centrifugation (13,000 rpm, 5 min, 4 °C), the supernatant was discarded again and the RNA pellet was air dried. Finally, the RNA pellet was resuspended in 20 – 80 µl RNase-free water containing DNaseI (1 U/25 µl) and 1x DNaseI buffer depending on the pellet size. The samples were incubated at 37 °C for 30 min to remove contaminating genomic DNA before the enzyme was heat-inactivated at 75 °C for 15 min. The RNA concentration and purity were measured using a NanoDrop spectrophotometer (chapter 2.2.1.2). Isolated RNA samples were stored at -80 °C.

2.2.1.14 RNA isolation from <1x10^6 cells and DNaseI digestion

The isolation of RNA from a small number of available cells (<1x10^6) was performed according to a slightly modified protocol by Baugh *et al.* [19]. For this, the cells of interest were harvested (chapter 2.2.3.3) and the cell pellet was resuspended in 300 µl of TRIzol reagent. In order to enhance the RNA yield, 5 µg of linear polyacrylamide (GenElute LPA) was added to the sample. After the addition of 60 µl chlorophorm, the solution was vortexed thoroughly for approximately 30 seconds followed by centrifugation (13,000 rpm, 5 min, room temperature). The RNA containing aqueous phase (upper phase) was transferred into a new 1.5 ml reaction tube and mixed with 180 µL 2-propanol. The RNA was precipitated at -20 °C overnight. The next day, RNA was pelleted by centrifugation (13,000 rpm, 30 min, 4 °C) and washed with 1 ml of 70 % (v/v) ethanol. Finally, the RNA pellet was resuspended in 12 - 15 µl RNase-free water containing DNaseI (1 U/25 µl) and 1x DNaseI buffer. The samples were incubated at 37 °C for 30 min to remove contaminating genomic DNA before the enzyme was heat-inactivated at 75 °C for 15 min. The RNA concentration and purity were measured using a NanoDrop spectrophotometer (chapter 2.2.1.2). Isolated RNA samples were stored at -80 °C.

2.2.1.15 RNA isolation from tissue

To extract RNA from tissue, freshly isolated or frozen samples were transferred into a 2 ml micro tube with screw cap containing 0.4 g of acidic washed glass beads. Per 20 - 50 mg tissue 1 ml TRIzol reagent was added and the samples homogenised using a Precellys tissue homogenizer (Peqlab) with the following programme: 3x15 s with 5000 rpm. All subsequent steps were performed according to the protocol described in detail in chapter 2.2.1.13.

2.2.1.16 cDNA synthesis

Up to 2 µg of isolated RNA were transcribed into cDNA using the High-Capacity cDNA Reverse Transcription Kit (Applied Biosystems). As described in the manufacturer's instructions, the following components and thermal cycler conditions were used:

cDNA reaction	Component	Volume for 1x reaction
	RNA	≤2 µg
	10x RT Buffer	2 µl
	25x dNTP Mix (100 mM)	0.8 µl
	10x RT Random Primers	2 µl
	MultiScribe Reverse Transcriptase (50 U/µl)	1 µl
	ddH_2O (RNase-free)	ad 20 µl

cDNA synthesis programme	Step	Temperature	Time
	1	25 °C	10 min
	2	37 °C	120 min
	3	85 °C	5 min
	4 (Hold)	4 °C	∞

The cDNA was stored at -20 °C.

2.2.1.17 cDNA synthesis for miRNA analysis

For miRNA analysis, 250 ng of isolated total RNA were reverse transcribed into cDNA using the miRNA-specific stem-looped primers provided in the TaqMan miRNA Assays (Applied Biosystems) and the High-Capacity cDNA Reverse Transcription Kit (Applied Biosystems). The following components and thermal cycler conditions were used:

cDNA reaction	Component	Volume for 1x reaction
	RNA	250 ng
	10x Reverse Transcription Buffer	1 µl
	25x dNTP Mix (100 mM)	0.4 µl
	5x TaqMan miRNA Primer	2 µl
	MultiScribe Reverse Transcriptase (50 U/µl)	0.5 µl
	ddH_2O (RNase-free)	ad 10 µl

cDNA synthesis programme	Step	Temperature	Time
	1	16 °C	30 min
	2	42 °C	30 min
	3	85 °C	5 min
	4 (Hold)	4 °C	∞

The cDNA was stored at -20 °C.

2.2.1.18 Quantitative Real-Time PCR (qRT-PCR) with SYBR Green and TaqMan Probes

Quantitative Real-Time (qRT-PCR) was used to analyse the relative gene (mRNA) and miRNA expression. Two different methods were used for real-time analysis: Either TaqMan based quantification in combination with gene/miRNA-specific TaqMan assays (Applied Biosystems) or SYBR Green based quantification together with conventional primers. The sequences of all primers and the TaqMan probes are listed in chapter 2.1.10.4 and 2.1.10.5, respectively. All reactions were performed in technical duplicates or triplicates in sealed 98-well plates in the CFX96 Touch Real-Time PCR cycler (Bio-Rad).

For TaqMan based qRT-PCR analysis the iTaq Universal Probes Supermix (Bio-Rad) was used according to manufacturer's instructions. The 2x master mix contained all essential

components for qRT-PCR except for the cDNA and the gene/miRNA-specific TaqMan probes. One qRT-PCR reaction was set up as followed using the following thermal cycler conditions:

qRT-PCR reaction setup	Component	Volume for 1x reaction
	cDNA	60 -10 ng
	2x iTaq Universal Probes Supermix	7.5 µl
	20x TaqMan Probe	0.75 µl
	ddH_2O (RNase-free)	ad 15 µl

PCR programme	Step	Temperature	Time	Cycles
	Initial denaturation	95 °C	10 min	1
	Denaturation	95 °C	15 s	50
	Primer annealing and elongation*	60 °C	30 s	
	Hold	25 °C	∞	

*Plate read at the end of the elongation.

SYBR Green based gene expression quantification were performed using the iTaq Universal SYBR Green Supermix (Bio-Rad) according to manufacturer's instructions. The 2x master mix also included all essential components for qRT-PCR except for the cDNA and the target gene specific conventional primers. One reaction mix contained the following components and qRT-PCR was performed with the following thermal cycler conditions:

qRT-PCR reaction setup	Component	Volume for 1x reaction
	cDNA	60 -10 ng
	2x iTaq Universal SYBR Green Supermix	7.5 µl
	Forward Primer (10 µM)	0.3 µl
	Reverse Primer (10 µM)	0.3 µl
	ddH_2O (RNase-free)	ad 15 µl

PCR programme	Step	Temperature	Time	Cycles
	Initial denaturation	95 °C	30 s	1
	Denaturation	95 °C	5 s	50
	Primer annealing and elongation*	60 °C	40 s	
	Melting Curve	65-95 °C (+0.5 °C increments)	5 s/step	1
	Hold	4 °C	∞	

*Plate read at the end of the elongation. In case of a different annealing temperature, primer annealing and elongation was performed in two separate steps.

Specifically, for the SYBR Green based gene expression analysis, a melting curve analysis was performed at the end of the qRT-PCR run in order to detect unspecific amplicons, which might have formed and distort gene expression measurements. In addition, the PCR amplicons were analysed by agarose gel electrophoresis (chapter 2.2.1.1) for their expected size to verify specificity of the qRT-PCR.

For both, TaqMan and SYBR Green based gene expression analysis, the relative gene expression was calculated in relation to the expression of the housekeeping gene HPRT using the comparative C_T method (ΔC_T method). The $\Delta\Delta C_T$ method [156] was used to show the level of gene expression as the fold change compared to the control sample.

2.2.1.19 Establishment of a standard curve for qRT-PCR assay

The principle of the standard curve method is based on the linear dependency of the number of cycles required for a PCR product to reach a defined threshold, on the logarithm of the applied cDNA template amount. The cycle number at which the PCR product exceeds the defined threshold is termed the Ct value. A standard curve must be generated separately for each gene of interest using defined concentrations of the target sequence. This was achieved by PCR amplification of the target sequence and subsequent purification of the PCR product using the NucleoSpin Gel and PCR Clean-up Kit (Macherey-Nagel) (chapter 2.2.1.3). The concentration was calculated based on the optical density at 260 nm using the following formula:

$$concentration\ [mol/\mu l] = \frac{OD_{260nm} * d * F}{M_w * L * 10^9}$$

OD_{260nm} = total number of counted cells

d = dilution factor

F = conversion factor (50 ng/µl for dsDNA)

M_w = molecular weight per base pair (660 g/mol)

L = length of the PCR product in base pairs

Subsequently, the copy number per µl is determined according to the following formula:

$$copies/\mu l = concentration\ mol/\mu l * Avogadro\ constant$$

Avogadro constant = 6.02214076 x 10^{23} molecules/mol

The Ct value is plotted *versus* the logarithm of applied copy numbers and the data is fitted to a straight line applying linear regression. This plot is then used as the standard curve to determine the quantity of the gene of interest in an unknown experimental sample based on the Ct value.

2.2.1.20 Isolation of genomic DNA from eukaryotic cells

To isolate genomic DNA from eukaryotic cells, the cell were harvested (chapter 2.2.3.3) and the cell pellet was resuspended in 200 µl cell lysis buffer supplemented with freshly added 1 µl Proteinase K (stock: 20 mg/ml) (chapter 2.1.7.2). The samples were incubated at 37 °C for 10 min under mild agitation. After the cells were completely lysed, samples were centrifuged (13,000 rpm, 10 min, room temperature). The supernatant was decanted into a new 1.5 ml reaction tube and the DNA was precipitated by the addition of 500 µl 2-propanol. The tubes were inverted several times followed by centrifugation (13,000 rpm, 30 min, 4 °C). Then, the supernatant was discarded and the DNA pellet was washed once with 1 ml 70 % ethanol. After a final centrifugation (13,000 rpm, 10 min, 4 °C), the supernatant was discarded and the pellet was air-dried. Finally, the DNA pellet was dissolved in 50-200 µl RNase-free water depending on the pellet size and stored at 4 °C. Concentration and purity were measured using a NanoDrop spectrophotometer (chapter 2.2.1.2).

2.2.1.21 Illumina MiSeq analysis

Cells that have been gene-edited using the CRISPR/Cas9 system, were screened for modifications by Illumina MiSeq. This next-generation sequencing approach allows for the high-throughput identification of CRISPR/Cas9-induced mutations and the quantification of insertions or deletions generated by NHEJ. The samples were prepared for MiSeq analysis as followed. First, genomic DNA was isolated from edited cell (chapter 2.2.1.20). The subsequent preparation of a barcoded DNA library is achieved by initial amplification around the CRISPR/Cas9 target site (1st PCR) followed by the addition of barcodes and the appropriate P5/P7 adaptors (making the template compatible with the flow cell) to the PCR product during the second amplification process (2nd PCR) as both are incorporated into PCR primers (Figure 2.1). The barcodes allowed to identify separate samples in the sequencing results.

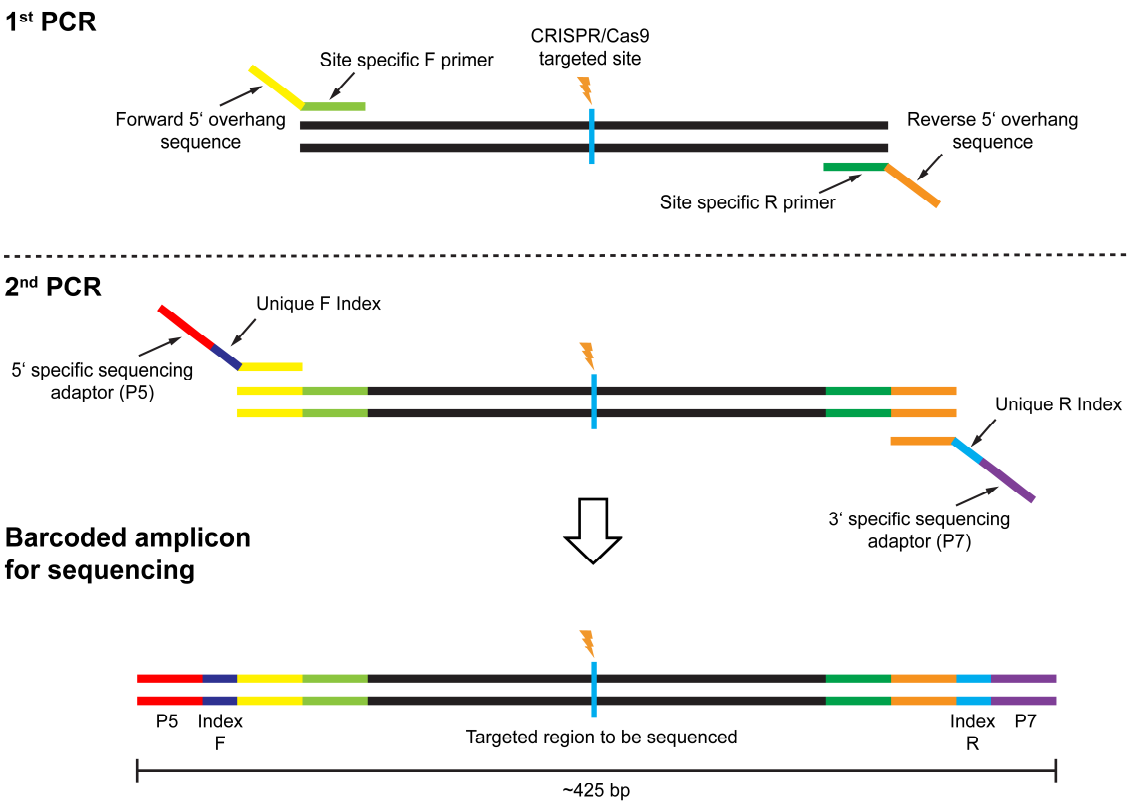

Figure 2.1 – Strategy for preparation of barcoded amplicon
In the first PCR reaction, the region around the CRISPR/Cas9-targeted site is amplified using site specific forward and reverse primers with a common 5' overhang. In the second PCR, Illumina index primers, which contain unique barcode/index sequences and appropriate 5' (P5) or 3' (P7) specific adaptor sequences, bind to the common 5' overhangs of the first primers and are amplified along with the targeted region.

In more detail, to amplify around the CRISPR/Cas9-targeted site, primers with a common 5' overhang (listed in chapter 2.1.10.8) were designed for the amplification of a PCR-amplicon of ≤ 300 bp. This first PCR was performed using the following components and thermal cycler conditions:

1st PCR reaction (amplification)	Component	Volume for 1x reaction
	Genomic DNA	25 ng
	5x Q5 Reaction Buffer	3 µl
	dNTPs (10 mM)	0.3 µl
	Forward Primer (10 µM)	0.75 µl
	Reverse Primer (10 µM)	0.75 µl
	5x Q5 High GC Enhancer	3 µl
	Q5 High-Fidelity DNA Polymerase (2U/µL)	0.15 µl
	ddH_2O	ad 15 µl

PCR programme	Step	Temperature	Time	Cycles
	Initial denaturation	98 °C	5 min	1
	Denaturation Primer annealing Elongation	98 °C 62 or 55 °C 72 °C	10 s 30 s 30 s	30
	Final elongation	72 °C	5 min	1
	Hold	4 °C	∞	

5-7 µl of PCR product was analysed on a 2 % agarose gel (chapter 2.2.1.1). Another 2 µl of PCR product was subjected to a second PCR, this time using Illumina index primers (listed in chapter 2.1.10.8) which contain unique barcode and P5/P7 adaptor sequences and bind to the common 5'-extension of the first primers. For this second PCR reaction, the following components and thermal cycler conditions were used:

2nd PCR reaction (indexing)	Component	Volume for 1x reaction
	PCR product (from 1st PCR reaction)	2 µl
	5x Q5 Reaction Buffer	4 µl
	dNTPs (10 mM)	0.4 µl
	Forward Index Primer (10 µM)	0.5 µl
	Reverse Index Primer (10 µM)	0.5 µl
	5x Q5 High GC Enhancer	4 µl
	Q5 High-Fidelity DNA Polymerase (2U/µL)	0.2 µl
	ddH_2O	ad 20 µl

PCR programme	Step	Temperature	Time	Cycles
	Initial denaturation	98 °C	5 min	1
	Denaturation Primer annealing Elongation	98 °C 65 °C 72 °C	10 s 30 s 30 s	30
	Final elongation	72 °C	5 min	1
	Hold	4 °C	∞	

Again 5-7 µl PCR product was analysed on a 2.5 % agarose gel (chapter 2.2.1.1). For all samples of the same amplicon 10 µl of indexed PCR sample was pooled. The pooled samples were loaded on an agarose gel (chapter 2.2.1.1) and PCR bands were cut out and purified using NucleoSpin Gel and PCR-Clean-up Kit (Macherey-Nagel) according to manufacturer's instructions (chapter 2.2.1.3). Gel purified samples were sequencing on an Illumina MiSeq-sequencing platform. Data analysis was performed using CRISPResso2 [46, 222] with the quality cut of set at 30 and the minimum identity score for the alignment being adjusted to 50.

2.2.2 Protein biochemical methods

2.2.2.1 Protein extraction

Cells were harvested (chapter 2.2.3.3) and centrifuged (300 g, 5 min, 4 °C). The supernatant was discarded and the cells washed once by resuspending in ice-cold PBS followed by centrifugation (300 g, 5 min, 4 °C). Again, the supernatant was discarded before the cell pellet was resuspended in ice-cold RIPA lysis buffer supplemented with pre-added phosphatase inhibitors and freshly added protease inhibitors (chapter 2.1.7.3) (50-100 µl per 2 x 10^6 cells). The cell suspension was incubated on ice for 20 min. After cell lysis, the samples were centrifuged (13,000 rpm, 5 min, 4 °C) in order to separate the lysate from insoluble cell debris. The lysate was transferred into a new 1.5 ml reaction tube and kept at 4 °C in case of immediate determination of the protein concentration (chapter 2.2.2.2) or stored at -80 °C.

For protein isolation from tissue, RIPA lysis buffer supplemented with pre-added phosphatase inhibitors and freshly added protease inhibitors was added to the freshly isolated or frozen samples which were minced using a small pre-cooled pestle. All other steps were performed as described above.

2.2.2.2 Determination of protein concentration by BCA Assay

The protein concentration of cell lysates was determined using the Pierce BCA Protein Assay Kit (Thermo Fisher Scientific) according to manufacturer's instructions. Briefly, a small aliquot (3 µl) of each sample was added to a well of a 96-well plate. Additionally, 3 µl of a serial dilution (0-4 µg/µl) of bovine serum albumin (BSA) serving as a standard curve was transferred to a well of the 96-well plate. Both, samples and standards, were mixed with 200 µl of BCA reagent (1:50 Solution A:Solution B). Then, the plate was incubated for 10 min at 65 °C and the absorbance at 562 nm was measured using a Tecan plate reader. By applying linear regression to the entire set of standards a standard curve was determined. According to this BSA standard curve the protein concentration was calculated. In order to minimise differences due to pipetting errors, the BCA assay was performed in duplicates.

2.2.2.3 Protein lysate preparation for SDS-PAGE

After determination of the protein concentration (chapter 2.2.2.2), the respective volume for 15-25 µg protein was transferred into a new 1.5 ml reaction tube and adjusted to a final concentration of 1µg/ml using an adequate amount of 5x sample buffer (chapter 2.1.7.3) and RIPA lysis buffer supplemented with pre-added phosphatase inhibitors and freshly

added protease inhibitors (chapter 2.1.7.3). Then, the samples were boiled at 95 °C for 5 min to denature the proteins. Following a short spin of the samples to collect the protein lysates at the bottom of the reaction tube, the samples were subjected to SDS-PAGE.

2.2.2.4 SDS-PAGE

SDS-PAGE (Sodium Dodecyl Sulfate Polyacrylamide Gel Electrophoresis) is a method by which proteins are separate according to their molecular weight by applying electrical current to discontinuous SDS-gels [143]. These polyacrylamide gels are comprised of an upper gel (stacking gel) with low pH (6.8) and acrylamide concentration (5 %) and a lower gel (resolving gel) with a higher pH (8.8) and acrylamide concentration (8-15 %). In the stacking gel the proteins are concentrated and collected in a sharp band, which are subsequently separated according to their molecular weight in the resolving gel. The higher the acrylamide concentration in the resolving gel, the lower the molecular weight of the separated proteins.

The SDS-gels with different acrylamide concentrations were prepared according the scheme below. At first the dissolving gel was poured and covered with 2-propanol. After polymerisation the stacking gel was poured on top and a comb with the appropriated number of loading pockets was inserted. For short-term storage at 4 °C, the gels were wrapped in paper towels soaked in ddH_2O.

	Resolving gel (8-15 %)	**5 % stacking gel**
ddH_2O	4.6 – 2.3 ml	2.1 ml
30 % Acrylamide/ Bisacrylamide mix	2.7 – 5.0 ml	0.5 ml
1.5 M Tris (pH 8.8)	2.5 ml	----
1 M Tris (pH 6.8)	----	380 µl
10 % SDS	100 µl	30 µl
10 % APS	100 µl	30 µl
TEMED	4 µl	3 µl
∑	10 ml	3 ml

(the amount is sufficient for two polyacrylamide gels)

SDS-gels were inserted into the electrophoresis apparatus (Bio-Rad) and covered with 1x Laemmli running buffer (chapter 2.1.7.3). The prepared protein samples (chapter 2.2.2.3) and marker (Precision Plus Protein All Blue Standard, Bio-Rad) were loaded on the SDS-gel. Electrophoresis was initially conducted at 80 V until the samples reached the resolving gel. Then the voltage was increased to 120 V for approximately 1-1.5 h until the dye front leaked into the running buffer. Afterwards, the separated proteins were transferred onto a nitrocellulose membrane (chapter 2.2.2.5).

2.2.2.5 Protein transfer (Western blot)

Separated proteins were immobilised by transfer from the SDS-gel to a nitrocellulose membrane in a process called Western blotting. For this, the Mini Trans-Blot system (Bio-Rad) was used. A blot sandwich was assembled in a mini gel holder cassette according to the scheme below while drenched in cooled 1x Transfer buffer (chapter 2.1.7.3).

Cathode

Sponge

3x Whatman paper

SDS-gel

Nitrocellulose membrane

3x Whatman paper

Sponge

Anode

The cassette with the blot sandwich was placed together with a cooling package into a blotting chamber, which was filled with cooled 1x Transfer buffer. The transfer was performed for 2 h at 80 V and 4 °C. The successful transfer was confirmed by Ponceau S staining. For this, the membrane was incubated in Ponceau Red solution (chapter 2.1.7.3) for 1-2 min and rinsed with VE-H_2O until well-defined protein band were visible.

2.2.2.6 Immunodetection of proteins

The detection of single proteins was performed via a two-stage antibody staining with a subsequent chemiluminescent detection reaction. At first, after Ponceau S staining (chapter 2.2.2.5), the nitrocellulose membrane was rinsed with 1x TBST (chapter 2.1.7.3) and incubated with 5 % milk powder dissolved in 1x TBST for 2 h at room temperature to block unspecific binding sites. Afterwards, the blocked membrane was incubated with the primary antibody diluted in 5 % milk powder in 1x TBST (antibody dilutions see chapter 2.1.8.1) overnight at 4 °C. On the next day, the membrane was washed three times in 1x TBST for 10 min before being incubated with the respective HRP-conjugated secondary antibody directed against the host species of the primary antibody diluted in 5 % milk powder in 1x TBST (antibody dilutions see chapter 2.1.8.2) for 1 h at room temperature. Next, the membrane was washed again three times in 1x TBST for 10 min. Finally, an immune-reactive signal was detected using Pierce ECL Western Blotting Substrate (Thermo Fisher Scientific). The freshly prepared ECL reagent (1:1 mixture of solution A and solution B) was equally distributed by pipetting on the membrane. Then the membrane was placed in an X-ray film cassette and emitting chemiluminescent signals were detected using photosensitive

X-ray films. For each protein and membrane, the exposure time was adjusted to the signal intensity. If after 30 min exposure time no or only a very weak signal was detectable, the membrane was washed and the developing was repeated mixing 20-40 % of SuperSignal West Femto Maximum Sensitivity Substrate (Thermo Fisher Scientific) to the standard ECL reagent. All films were developed manually and digitalised using a transmitted light scanner.

2.2.3 Cell biological methods

All here cultured cells are adherent cell lines. Cells were cultivated in an incubator at 37 °C and 7.5 % CO_2 in a water-saturated atmosphere. All work was performed on a sterile bench with laminar air flow. If not mentioned differently, the PBS used was Mg^{2+}- and Ca^{2+} free.

2.2.3.1 Thawing of cells

Thawing of cells should be conducted fairly quickly as the DMSO included in the freezing media as a frost protection is toxic and should be removed immediately. First, cells were removed from liquid nitrogen and thawed in the water bath at 37 °C. Before thawing completely, the cells were resuspended in 5 ml of prewarmed medium and centrifuged (280 g, 5 min, room temperature). The supernatant was aspirated and the pellet resuspended in fresh medium and plated on cell culture dishes or in flasks.

2.2.3.2 Freezing of cells

For long-term storage of cells, they were frozen in liquid nitrogen. First, adherent cell were harvested (chapter 2.2.3.3) and the cell number determined (chapter 2.2.3.4). Then, the cells were centrifuged (280 g, 5 min, room temperature) and the supernatant was discarded. The cell pellet was resuspended in freezing medium (chapter 2.1.7.4) at a concentration of $2x10^6$ cells/ml. In each cryovial 1 ml of cell suspension was transferred. The cryovials were then collected in a special freezing container (Mr. Frosty, Nalgene) and frozen at -80 °C overnight. On the next day, the cells were then transferred into the liquid nitrogen.

2.2.3.3 Harvesting and passaging of cells

Adherent cells were passaged at 70-90 % confluency using Trypsin/EDTA. Before trypsinisation, cells were washed with PBS once. Cells were detached from cell culture dishes by incubation with 0.05 % Trypsin/0.02 % EDTA in PBS for 1-3 min at 37 °C in the incubator. Trypsin was inactivated by the addition of double the volume of standard growth medium. Cells were singularised by pipetting before collecting the cell suspension in a 15 ml or 50 ml falcon tube. Next, the cell number was determined (chapter 2.2.3.4) and an

adequate number of cells was transferred into a new cell culture dish or flask containing fresh standard growth medium.

2.2.3.4 Determination of cell number

Cells were counted using a hemocytometer (Neubauer chamber). For determining the cell number 10 µl were applied to the hemocytometer. With a microscope, all cells within four big squares were counted. By mixing an aliquot of the cell suspension 1:1 with Trypan blue live cells can be discriminated from dead cells as Trypan blue only traverses the membrane of dead cells. The number of (live) cells per ml in the original cell suspension was calculated according to the following formula:

$$Cell\ number\ [cells/ml] = \frac{n}{Sq} \cdot \frac{1}{V_{Sq}} \cdot d = \frac{n}{Sq} \cdot \frac{1}{10^{-4}} \cdot d = \frac{n}{Sq} \cdot 10^4 \cdot d$$

n = total number of counted cells

Sq = number of counted big squares

V_{Sq} = volume of one big square (0.1 mm^3=10^{-4} ml)

d = dilution factor

2.2.3.5 Transient transfection of HEK293T cells using calcium phosphate

The calcium phosphate method is well established for the transfection of cells based on the formation of DNA-salt precipitates which enter the cells via endocytosis [40]. One day before transfection, HEK293T cell from an exponentially growing culture were seeded so they reach approximately 50 % confluence the next day. The transfection was carried out with a calcium phosphate solution containing 25 µg/ml plasmid DNA. For transfection of cells in a 6-well, 5 µg plasmid DNA was diluted in 100 µl of 0.25 M $CaCl_2$ solution. While vortexing, this DNA dilution was added dropwise to 100 µl 2x HBS (chapter 2.1.7.4). The mixture was incubated for 1 min at 37 °C and then added dropwise to the cells. After 6 h incubation at 37 °C, the cells were washed twice with PBS and fresh medium was added. 48 h after transfection, the cells were harvested (chapter 2.2.3.3) for further analysis.

2.2.3.6 Transient transfection of NCCIT cells using Lipofectamine® Stem Transfection Reagent

One day prior transfection, $1.5x10^6$ NCCIT cells from an exponentially growing culture were seeded on a 10 cm cell culture dish in 10 ml standard growth medium. The next day, just before transfection, the medium was changed to medium without antibiotics. DNA transfection was conducted using Lipofectamine® Stem Transfection Reagent (Invitrogen) at a 1 µg:4 µl (DNA:Lipofectamine) ratio. For transfection, two separate reaction tubes were prepared. In one of them, 14 µg plasmid DNA were diluted in 700 µl Opti-MEM. In the second reaction tube, 56 µl Lipofectamine® Stem Transfection Reagent were diluted in 700 µl Opti-MEM. Subsequently, the diluted DNA was added to the diluted Lipofectamine® Stem Transfection Reagent in a 1:1 ratio. The mixture was incubated for 10 min at room temperature. Then, the DNA-lipid complex was added dropwise to the cells, which were incubated at 37 °C in the incubated. The next day, the medium was changed to standard growth medium supplemented with antibiotics. The cells were cultivated for 48 h after transfection and then harvested (chapter 2.2.3.3) for FACS using a FACSAria III (BD Biosciences) (chapter 2.2.3.9).

2.2.3.7 siRNA transfection using Lipofectamine® RNAiMAX Transfection Reagent

One day before transfection, $1.5x10^5$ (TCam-2) or $3x10^5$ (NCCIT) cells from an exponentially growing culture were seeded per 6-well in 2 ml standard growth medium. The siRNA transfection of all cell lines was performed using Lipofectamine® RNAiMAX Transfection Reagent (Invitrogen) at a ratio of 10 pmol:3 µl (siRNA:Lipofectamine). Two separate reaction tubes were prepared. In one reaction tube, 25 pmol siRNA or siRenilla (siRNA control) were diluted in 125 µl Opti-MEM. In the second reaction tube, 7.5 µl Lipofectamine® RNAiMAX Transfection Reagent were diluted in 125 µl Opti-MEM. In the following, the diluted siRNA was added to the diluted Lipofectamine® RNAiMAX Transfection Reagent in a 1:1 ratio. The mixture was incubated for 10 min at room temperature before the DNA-lipid complex was added dropwise to the cells. After 6 h incubation at 37 °C, the medium was changed. Depending on the cell line, the cells were cultivated 60 h (TCam-2) or 72 h (NCCIT) after transfection and then harvested (chapter 2.2.3.3) for further analysis.

2.2.3.8 Generation of (stable) knockout cells using CRISPR/Cas9 system

Knockout cells were generated by the use of the powerful CRISPR/Cas9 system inducing double-strand breaks at specific genomic locations which are repaired via the cellular non-homologous end joining (NHEJ) DNA repair mechanism. Knockout mutations are obtained

as NHEJ is error-prone resulting in random insertions or deletions (INDELs) which can lead to frame-shift mutations and disrupt gene function.

Gene editing using the CRISPR/Cas9 system was carried out using the plasmid pSpCas9(BB)-2A-GFP (PX458) which was a gift from Feng Zhang (Addgene plasmid # 48138). After plasmid preparation including the insertion of specific gRNAs into the PX458 vector (chapter 2.2.1.12), cells were transfected using lipofectamine Stem Transfection Reagent (chapter 2.2.3.6). For wild type control, cells were transfected with empty PX458 vector (PX458 EV) which has no specific sgRNA inserted. 48 hours post transfection cells were sorted by FACS for GFP positive cells (chapter 2.2.3.9) and plated as a bulk population. A few days after sorting, cells were seeded into 96-well plates with serial dilutions (0.5 and 1 cell per well) or the growth assay (chapter 2.2.3.10) was started. For enhanced growth of the single cells, 20 % conditioned medium from wild type cells was added to the wells. The single cells were grown until a stable cell line was established. In order to analyse if gene editing had been successful and to confirm that the cell line was derived from a single clone, genomic DNA was isolated from edited cell lines (chapter 2.2.1.20). The edited region was amplified using primers designed for the amplification of a PCR-amplicon containing the sgRNA-complementary site (chapter 2.2.1.21). A small PCR sample was analysed on a 2 % agarose gel (chapter 2.2.1.1). The remaining PCR sample was purified using NucleoSpin Gel and PCR-Clean-up Kit (Macherey-Nagel) according to manufacturer's instructions (chapter 2.2.1.3). Gel purified samples were sequenced (Sanger sequencing) (chapter 2.2.1.11) with cell lines derived from a single cell showing clean defined peaks on the chromatogram.

2.2.3.9 Flow cytometry and fluorescence activated cell sorting (FACS)

Flow cytometry is a method by which thousands of single cells can be quickly examined and counted based on scattered light and fluorescence. Simultaneously, various parameters (e.g. size, granularity or (surface) expression of proteins) are analysed. Basically, cells become precisely positioned by a technique called hydrodynamic focusing, so that one cell at a time passes the laser beam. Depending on the size and granularity, the light is differentially scattered. This is measured by two detection systems: the forwards scatter (FSC) detector giving information about the cell size and the sideward scatter (SSC) detector giving information about the internal complexity (granularity) of the cell. In addition, cells are often labelled with fluorochrome-conjugated antibodies. The lasers are able to excite multiple fluorochromes at the same time. The emitted light in a band of wavelengths is separated from each other by specific band pass filters and finally measured by an additional set of detectors. Here, flow cytometry analysis was performed on a FACSCanto II (BD Biosciences) flow cytometer. Cells stained with eFluor670 (chapter 2.2.3.10) or APC

AnnexinV/7-AAD (chapter 2.2.3.12) were measured at an event rate of maximum 1500 events/s.

Fluorescence activated cell sorting (FACS) is a specialised type of flow cytometry enabling the sorting of a heterogenous mixture of cells according to cell size, granularity and protein expression. Thereby, single cells are encapsulated into small liquid droplets by a vibrating mechanism. These droplets are given an electric charge depending on the previously user-defined parameters (size, granularity, fluorescence) for the cells to be sorted. When the charged droplets fall through an electrostatic deflection system, they are diverted into collection tubes based on their charge. Here, FACS was performed on a FACSAria III (BD Biosciences) system. Cells transfected with SpCas9(BB)-2A-GFP (PX458) expressing or lacking sgRNA, were sorted based on the GFP fluorescence. For this, the cells were resuspended in PBS allowing a detection of ~800 cells/s with the flow rate set to 1. GFP positive cells were sorted as a bulk population into a collection tube containing standard growth medium. Sorted cells were centrifuged and cultivated in standard growth medium for several days before being used for proliferation assays (chapter 2.2.3.10) or generating stable knockout cells (chapter 2.2.3.8).

In general, for flow cytometry setup and data acquisition the FACSDiva software (BD Biosciences) was applied. Subsequent flow cytometric analysis was performed using FlowJo (BD Biosciences).

2.2.3.10 Growth assay of CRISPR/Cas9 knockout cells

With this growth assay including Illumina MiSeq analysis, not only proliferation, but the complete population dynamic was investigated over the given time period. In order to analyse the growth behaviour of CRISPR/Cas9 knockout (KO) *versus* wild type (WT) cells, GFP-positive bulk sorted PX458 EV and PX458 sgRNA transfected cells (chapter 2.2.3.8 and 2.2.3.9) were mixed in a 1:1 (WT:KO) ratio. Pure WT and KO cells were served as controls. In total, for each condition $2x10^5$ cells were seeded per 6-well in standard growth medium. Every 2 to 3 days over a time period of 21 days the cells were harvested (chapter 2.2.3.3), the cell number was determined (chapter 2.2.3.4), samples ($2x10^5$ cells) were taken for the isolation of genomic DNA and $1x10^5$ or $2x10^5$ cells were re-plated in standard growth medium, respectively. Genomic DNA was isolated from samples on day 0, 3, 7, 14 and 21 (chapter 2.2.1.20). These samples were subjected to Illumina MiSeq analysis (chapter 2.2.1.21). After analysis of the sequencing data, with the single reads categorised according to their sequence as wild type, frame-shift mutations (resulting in KO) and in-frame mutations, they were displayed as percentages in a pie chart. By comparing changes in the distribution of single reads for wild type and with frame-shift mutations over time, this gave insights int the dynamics of the cell population.

2.2.3.11 eFlour670 cell proliferation assay

Cell proliferation assays were performed with CRISPR/Cas9 knockout (KO) and corresponding wild type (WT) stable cells (chapter 2.2.3.8). Firstly, cells were harvested (chapter 2.2.3.3) and the cell number determined (chapter 2.2.3.4). $1.5x10^6$ cells were transferred into a new 15 ml falcon tube, centrifuged (280 g, 5 min, room temperature) and washed once with PBS to remove any serum. Following this, the cells ($1.5x10^6$) were resuspended in 1 ml of a 5 µM solution of Cell Proliferation Dye eFluor™ 670 (eBioscience) in PBS and stained for 10 min at 37 °C in the dark. The labelling was stopped by adding 4-5 volumes of cold FCS and incubating for 5 min on ice. Next, the cells were centrifuged (280 g, 5 min, 4 °C) and washed once with complete growth medium. The cell number was determined again and $5x10^4$ (day 1)/ $3.5x10^4$ (day 2)/ $2.5x10^4$ (day 3)/ $1.5x10^4$ (day 4) cells were seeded in triplicates on a 24-well plate in a final volume of 500 µl. The initial fluorescence intensity (day 0) was determined as well as the fluorescence intensity was monitored every 24 h for the next 4 days by FACS analysis on a FACSCanto II (BD Biosciences) flow cytometer. The dye eFluor™ 670 binds to any cellular proteins containing primary amines and as the cell divides, it is distributed equally between the two daughter cells. Hence, the median fluorescence intensity (MedFI) of the dye was assumed to half with every cell division. Accordingly, the number of cell divisions was calculated applying the following formula:

$$Number\ of\ divisions = log_2 \left| \frac{\left(MedFI_{day0} - MedFI_{unstained}\right)}{\left(MedFI_{dayX} - MedFI_{unstained}\right)} \right|$$

At the end of the experiment, the average cell cycle duration was estimated based on the number of cell division in the given time period.

2.2.3.12 Annexin V/7-AAD apoptosis assay

In CRISPR/Cas9 knockout (KO) and corresponding wild type (WT) stable cells (chapter 2.2.3.8), cells actively undergoing apoptosis were determined by Annexin V/7-AAD FACS using PE Annexin V Apoptosis Detection Kit I (BD Biosciences), however substituting PE Annexin V for APC Annexin V (BioLegend). In apoptotic cells the membrane phospholipid phosphatidylserine is translocated from the inner layer of the membrane to the outer layer. Thus, phosphatidylserine is exposed to the external environment and can be bound by Annexin V in a calcium-dependent manner. 7-Amino-Actinomycin (7-AAD) is a standard flow cytometry viability dye allowing for the discrimination between viable and dead cells as only in dead cells the membrane is permeable to 7-AAD. Cells staining positive for both Annexin V and 7-AAD are either in late stages of apoptosis, are undergoing necrosis or are

already dead. In contrast, cells that stain positive for only Annexin V are in early apoptotic stages and cells staining negative for both Annexin V and 7-AAD are alive.

Three days prior, per 6-well $1.5x10^5$ NCCIT EV, $2x10^5$ NCCIT ΔRING and $2.5x10^5$ NCCIT Δ6NHL cells from an exponentially growing culture were seeded. One day before the assay, medium was exchanged in order to remove false dead cells that resulted from the plating. For Annexin V/7-AAD FACS the medium was collected in falcon tubes. The cells were washed once with PBS which was also collected in the respective tubes. Subsequently, the cells were harvested by incubation with 2 mM EDTA in PBS for 3-5 min at 37 °C in the incubator. Then, the cells were collected in the respective tubes and centrifuged (1200 rpm, 5 min, room temperature). The supernatant was discarded and the cell pellet resuspended in PBS followed by determination of the cell number (chapter 2.2.3.4). $2x10^5$ cells each were transferred into a FACS tube and again centrifuged (1200 rpm, 5 min, room temperature). Next, the supernatant was discarded and the cells stained with 2.5 µl APC Annexin V and 2.5 µl 7-AAD diluted in 50 µl 1x Annexin V Binding Buffer. After an incubation for 15 min at room temperature in the dark, 200 µl of 1x Annexin V Binding Buffer was added to each sample. Immediately after this, the samples were measured in a FACSCanto II (BD Biosciences) flow cytometer. As a positive control, cells were treated with 0.5 mM H_2O_2 for 3-4 h. Single stainings of H_2O_2 treated cells were also performed which served as compensation controls.

2.2.4 Histological methods

2.2.4.1 Fixation, embedding and generation of histological sections

Testes were dissected from adult (> 10 weeks) and P0 male mice and fixed by immersion in 4 % paraformaldehyde (PFA) at 4 °C for 2 h (P0) or overnight (adult). Following fixation, testes were washed in 1x PBS at 4 °C overnight (adult) or three times for 15-30 min (P0). Then, for paraffin sections, using the semi-closed benchtop tissue processor TP1020 (Leica Biosystems), testes were dehydrated in an ascending ethanol series (70 % (2x), 80 % (2x), 90 %, 96 %, 100 % (2x)) for 1 h each followed by incubation in xylol twice for 1 h and embedding in paraffin. In case of cryosections, testes were incubated in 30 % sucrose in 1x PBS at 4 °C overnight before being embedded in PolyFreeze Tissue Freezing Medium on dry ice and frozen at -80 °C.

Using the rotary microtome Leica RM2255 (Leica Biosystems), 7 µm paraffin cross-sections were cut, which were flattened in 42 °C warm water prior to mounting on positively-charged microscopy slides and drying at 50 °C. The paraffin sections were stored at room temperature until used for staining. Cryosections (cross-sections) were cut at 7 µm (P0) or

10 µm (adult) thickness using the cryostat Leica CM30505 S (Leica Biosystems). The cut tissue sections were immediately transferred to a room temperature positively-charged microscopy slide and stored at -20 °C until staining.

2.2.4.2 Haematoxylin and Eosin staining (H&E staining)

The haematoxylin and eosin (H&E) staining is a common staining method in histology to view cellular and tissue structures. It combines two histological dyes: haematoxylin and eosin. The natural dye haematoxylin is used to stain acidic structures (nucleus, ribosomes) in a dark purple to blue. Eosin is used as a counterstain and stains basic structures (cytoplasm, muscle, collagen) red to pink. For H&E staining paraffin-embedded sections were used as they have the advantage that cellular morphology is well-maintained.

First, before staining, the paraffin-embedded murine testis sections were deparaffinised. For this, the paraffin sections were incubated at 65 °C for 15-20 min until the paraffin wax had melted, then placed in xylol twice for 10 min. Next, the sections were rehydrated by passing through a descending alcohol series (100 % (2x), 95 %, 90 %, 80 %, 70 %) for 30 sec each and were kept in distilled water until staining. The paraffin sections were stained in haematoxylin for 3 min and blued by washing in cold running tap water for 3-5 min. Afterwards, the sections were counterstained with 0.5 % eosin for 3 min. As eosin is highly water-soluble, excess dye was removed by rinsing in cold running tap water for 30-60 seconds until the water was clear. Subsequently, the paraffin sections were again dehydrated in an ascending ethanol series (70 %, 80 %, 90 %, 95 %, 100 % (2x)) and cleared by incubating in xylol twice for 1-2 min. Paraffin sections were kept in xylol until mounting with the xylene based DPX mountant for histology (Sigma-Aldrich). H&E stained sections were stored under the fume hood for at least 24 h before imaging by bright-field microscopy.

2.2.4.3 Immunofluorescent staining of cryosections

For the indirect immunofluorescent staining of proteins of germ and somatic cells, PFA-fixed murine testis cryosections were used because they feature a better epitope retention compared to paraffin sections. In order to prevent evaporation of the working solutions along with dehydration of the tissue sections as this impairs the staining quality and enhances background signal, all staining steps were conducted in a humid chamber. Furthermore, all washing steps were performed with PBST (1x PBS + 0.3 % Triton X-100) in a copling jar by gentle rocking on a shaking platform.

Firstly, the microscopy slides were removed from the -20 °C freezer and allowed to defrost and dry at room temperature for 15 min. Afterwards, the murine testis cryosections were

rehydrated and the tissue freezing medium removed by dipping the slides in 1x PBS until the tissue freezing medium was completely washed away followed by a short rinse dipping the slides in distilled water. Then, the slides were dried at room temperature for 10-15 min. In the next step, 70-100 µl blocking solution (chapter 2.1.7.5) was added to the slides, which were covered with a parafilm to prevent evaporation After incubation at room temperature for 30-60 min, the blocking solution was removed by carefully tilting the slide so that the liquid runs down on a tissue paper as the sections often do not adhere strongly to the glass slide. Next, primary antibodies diluted in PBST supplemented with 1 % BSA (70-100 µl per slide) was added and incubated at 4 °C overnight. For secondary antibody controls (omitting primary antibody), only PBST supplemented with 1 % BSA was added. The primary antibodies used and their respective dilutions are listed in chapter 2.1.8.1. On the next day, sections were washed three times for 5 min with PBST. Then, 70-100 µl secondary antibody solution was applied which contained fluorescently conjugated donkey antibodies directed against the different host species of the primary antibodies (listed in chapter 2.1.8.2) diluted in PBST supplemented with 1 % BSA. The incubation with the secondary antibody solution at room temperature for 1-2 h as well as all subsequent steps were performed in the dark to prevent photobleaching of the coupled fluorophores. Following incubation with the secondary antibodies, the sections were washed three times for 5 min with PBST. Finally, excess liquid around the sample was removed and the sections were mounted with the aqueous mounting medium Fluoromount-G containing DAPI (4′,6-diamidino-2-phenylindole) and photobleaching inhibitors (SouthernBiotech). DAPI labels nuclei [123], thereby allowing the determination of size, shape and position of the nucleus. The slides were stored at 4 °C for at least 24 h prior to imaging by immunofluorescent microscopy.

2.2.4.4 Microscopic imaging

H&E staining were imaged by bright-field microscopy (DIC) using the Zeiss Axio Lab.A1 microscope (Carl Zeiss). Images were taken using the ZEN 2012 (blue edition) software (Carl Zeiss). Standard settings were applied and the exposure time was adjusted to get the best image quality.

Immunofluorescent stainings were imaged with the Zeiss Observer.Z1 epifluorescence microscope (Carl Zeiss) equipped with a Plan-Apochromat 20x/0.8 M27 or LD Plan - Neofluar 40x/0.6 Korr M27 objective and an ORCA-Flash4.0 LT PLUS camera (Hamamatsu). The light source was a Polychrome V 150 W xenon lamp (Till Photonics). Images and tile scans were taken by also using the ZEN 2012 (blue edition) software (Carl Zeiss). Again, standard settings were used which were adjusted to obtain excellent image quality. In order to avoid cross-excitation of fluorophores, the stained tissue section was sequentially scanned using a separate fluorescent track for every fluorophore including

DAPI. For tile scans an image overlap of 15 % was chosen allowing an accurate stitching of the image tiles.

All images were processed employing the ZEN 2012 (blue edition) (Carl Zeiss) and ImageJ software. Figures were designed using Adobe Illustrator CS4 and Adobe Photoshop CS4.

2.2.5 Animal experimental methods

2.2.5.1 Mouse breeding and husbandry

The breeding and husbandry of all mice was conducted according to the guidelines of the German animal welfare act. In general, the mouse strains were bred in IVCs (individually ventilated cages) under SPF (specific-pathogen free)-conditions in the animal facility of the LIMES Institute (LIMES-GRC (genomic resource centre)) of the University of Bonn.

Originally, the *Trim71* conditional knockout mouse was generated by Taconic Artemis (Cologne) in a C57BL/6JCrl genetic background and was first described by Mitschka *et al.* [188]. In order to generate a germline-specific *Trim71* knockout mouse, *Trim71*$^{fl/fl}$ females were bred with *Nanos3*$^{Cre/+}$ male mice which expressed the *Cre* recombinase under the control of the endogenous *Nanos3* promotor. The *Nanos3*$^{Cre/+}$ mouse strain was first described in 2008 by Suzuki *et al.* [276] and has the coding sequence of the *Cre* recombinase introduced into the endogenous *Nanos3* locus by homologous recombination, thus substituting one *Nanos3* allele and resulting in heterozygous expression of *Nanos3*. The heterozygous *Trim71*$^{-/+}$*; Nanos3*$^{Cre/+}$ male offspring was then crossed with *Trim71*$^{fl/fl}$ or *Trim71*$^{+/+}$ (wild type) females to produce *Trim71*$^{-/fl}$*; Nanos3*$^{Cre/+}$ (germline-specific *Trim71* knockout), *Trim71*$^{-/+}$*; Nanos3*$^{Cre/+}$ (heterozygous *Trim71*), *Trim71*$^{+/fl}$*; Nanos3*$^{Cre/+}$ (germline-specific heterozygous *Trim71*) and *Trim71*$^{+/+}$*; Nanos3*$^{Cre/+}$ (wild type *Trim71*) mice for experiments and analyses.

2.2.5.2 Alkaline DNA isolation from ear biopsies and genotyping

To determine the genotype of the mice, PCR on genomic DNA from ear biopsies was performed. The genomic DNA was isolated by boiling the ear biopsies in 200 µl 50 mM Sodium hydroxide (NaOH) at 95 °C for 20 min. Afterwards, the solution was neutralised by the addition of 70 µl Tris-HCl pH 8.0 followed by centrifugation (4000 rpm, 1 min, 4 °C). The samples were stored at 4 °C.

All primers used for genotyping are listed in chapter 2.1.10.3. Mice from the *Trim71* strain were genotyped by applying a three-primer strategy which resulted in a 242 bp amplicon for the wild type allele, a 322 bp amplicon for the knockout allele and a 361 bp amplicon for

the conditional allele. The PCR reaction was performed using the DreamTaq DNA Polymerase (Thermo Fisher Scientific) according to manufacturer's instructions using the following components and thermal cycler conditions:

PCR reaction	Component	Volume for 1x reaction
	Genomic DNA	2 µl
	10x DreamTaq Buffer	2 µl
	dNTPs (10 mM)	0.4 µl
	Primer 1 (20 µM)	0.8 µl
	Primer 2 (20 µM)	0.8 µl
	Primer 3 (20 µM)	0.8 µl
	DreamTaq DNA Polymerase (5U/µL)	0.2 µl
	ddH_2O	ad 20 µl

PCR programme	Step	Temperature	Time	Cycles
	Initial denaturation	95 °C	3 min	1
	Denaturation	95 °C	30 s	
	Primer annealing	59 °C	30 s	30
	Elongation	72 °C	30 s	
	Final elongation	72 °C	5 min	1
	Hold	4 °C	∞	

For genotyping of mice from the *Nanos3* mouse strain, also a three-primer strategy was applied which generated a 220 bp amplicon for the wild type allele and an additional 270 bp amplicon in all transgenic animals. The PCR reaction was set up as for Trim71 genotyping applying the identical thermal cycler conditions.

After the PCR reaction was completed, amplicons were separated by agarose gel electrophoresis (chapter 2.2.1.1) using 2 % agarose to determine the genotype of the animals.

3 Results

3.1 Role of TRIM71 in male germ cell development *in vivo*

Until now, the function of TRIM71 has been mainly investigated in relation to embryonic development with various studies describing endogenous expression of TRIM71 in mouse ESCs [39, 141, 157, 188, 204, 246]. Yet, not much is known about the role of TRIM71 in adult tissues and organs. Notably, in an RNA-seq experiment performed by Dr. Sibylle Mitschka, factors involved in fertility as well as proliferation were found to be differently expressed in TRIM71-deficient mouse ESCs compared to the wild type control cells [187]. In addition, TRIM71 is expressed in testes of neonatal, prepubertal and adult mice [246] and previous studies of our group showed that Trim71 deficiency results in infertility in mice [187]. Furthermore, TRIM71 expression in the testes has been restricted to spermatogonial stem cells (SSCs) – the stem cell niche in mouse testes [187]. As proteins important for pluripotency and early germ cell development such as OCT4, NANOG and TNAP are expressed in both, ESCs and germline stem cells [59, 325], we analysed the role of TRIM71 in the germ cell compartment hypothesising that infertility in TRIM71-deficient mice has its origin already in early germ cell development.

3.1.1 TRIM71 expression is essential for normal testis development

Germline-specific TRIM71-deficient mice were generated by crossing homozygously floxed *Trim71* females (*Trim71*$^{fl/fl}$) with males heterozygous for *Trim71* and additionally expressing the Cre recombinase under the control of the endogenous *Nanos3* promotor (*Trim71*$^{-/+}$; *Nanos3*$^{Cre/+}$) (Figure 3.1 A). Endogenous *Nanos3* is expressed in primordial stem cells (PGCs) shortly after their formation, as early as E7.25, until their settlement in the gonads when almost all male germ cells have entered mitotic arrest at E14.5 [275, 291, 314]. Re-expression of *Nanos3* only occurs in testes of neonatal mice (P1.5) [291, 314]. By this mating strategy 25 % of the offspring carried a germline-specific *Trim71* knockout whilst being heterozygous for *Trim71* in all other tissues (*Trim71*$^{-/fl}$; *Nanos3*$^{Cre/+}$). For the generation of appropriate control animals expressing *Nanos3*-Cre, *Trim71*$^{-/+}$; *Nanos3*$^{Cre/+}$ male mice were crossed with wild type females (Figure 3.1 B).

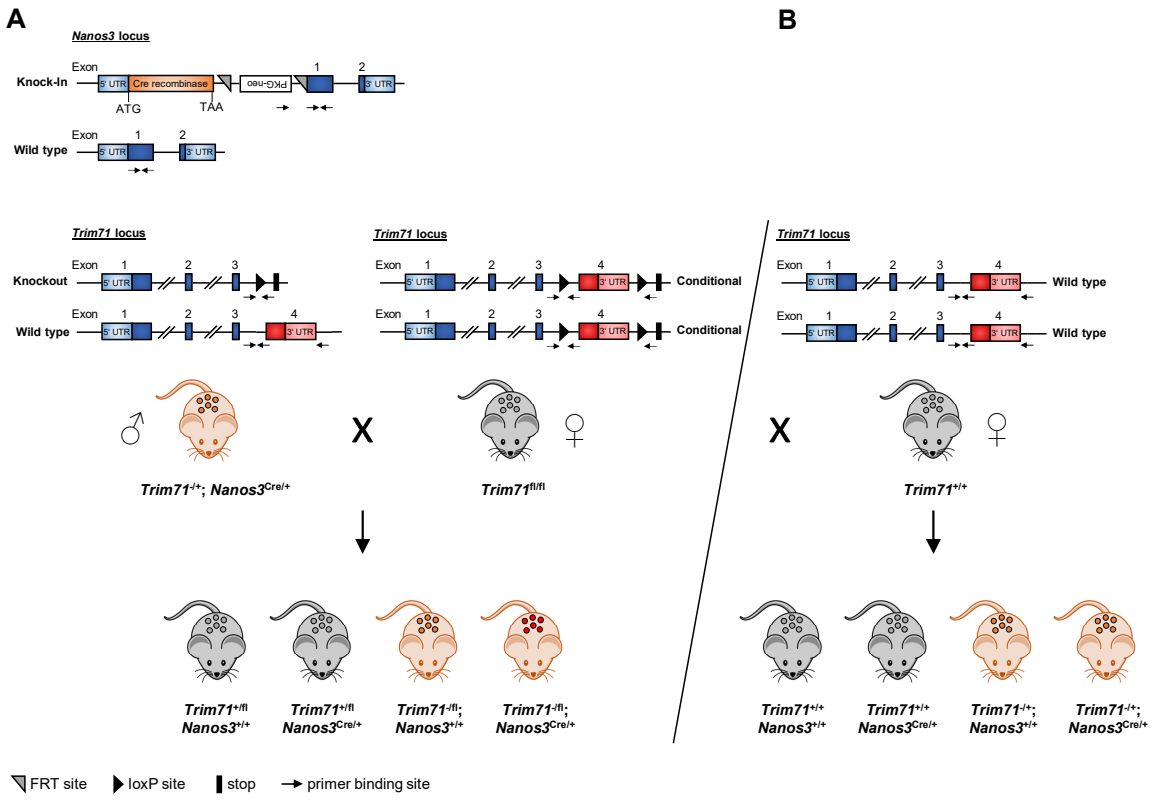

C

***Trim71*$^{+/+}$; *Nanos3*$^{Cre/+}$**	***Trim71* wild type**
***Trim71*$^{+/fl}$; *Nanos3*$^{Cre/+}$**	**germline-specific *Trim71* heterozygous**
***Trim71*$^{-/+}$; *Nanos3*$^{Cre/+}$**	**heterozygous *Trim71***
***Trim71*$^{-/fl}$; *Nanos3*$^{Cre/+}$**	**germline-specific *Trim71* knockout**

Figure 3.1 – Mouse breeding scheme for the generation of germline-specific TRIM71-deficient mice

Exon 4 of the conditional *Trim71* knockout mouse is flanked by loxP sites and can be excised by crossing with a *Nanos3*-Cre mouse line to generate a germline-specific *Trim71* knockout (*Trim71*$^{-/fl}$; *Nanos3*$^{Cre/+}$). **(A)** Specifically, males heterozygous for *Trim71* carrying the *Nanos*-Cre allele (*Trim71*$^{-/+}$; *Nanos3*$^{Cre/+}$) were mated with homozygously floxed *Trim71* females (*Trim71*$^{fl/fl}$). **(B)** For the generation of control animals, *Trim71*$^{-/+}$; *Nanos3*$^{Cre/+}$ males were crossed with wild type females (*Trim71*$^{+/+}$). Grey = wild type and floxed *Trim71*; orange = heterozygous *Trim71*; red = homozygous *Trim71* deletion. The round symbols represent the germline (ovary and testis) in adult females and males. **(C)** TRIM71 mice used within this study: wild type *Trim71*$^{+/+}$; *Nanos3*$^{Cre/+}$ (black), germline-specific heterozygous *Trim71*$^{+/fl}$; *Nanos3*$^{Cre/+}$ (dark orange), heterozygous *Trim71*$^{-/+}$; *Nanos3*$^{Cre/+}$ (light orange) and germline-specific knockout *Trim71*$^{-/fl}$; *Nanos3*$^{Cre/+}$ (red).

In a first analysis, testes of adult male *Trim71*$^{-/fl}$; *Nanos3*$^{Cre/+}$ as well as control mice (Figure 3.1 C) were examined macroscopically. Through this, a reduction in size (Figure 3.2 A and B) and weight of the testes (Figure 3.2 C) in germline-specific TRIM71-deficient mice, as described by Dr. Sibylle Mitschka [187], was confirmed. Remarkably, all *Nanos3*-Cre expressing mice tended towards smaller testes when comparing mice with a similar TRIM71 expression (Figure 3.2 C). This most likely underlies the fact that the *Cre*

recombinase coding sequence has been introduced into the endogenous *Nanos3* locus by homologous recombination, thereby substituting one *Nanos3* allele and resulting in *Nanos3* heterozygosity in all *Nanos3*-Cre expressing mice. Nevertheless, TRIM71-deficiency in a *Nanos3* heterozygous background had an even more drastic effect concerning the testis weight of *Trim71*$^{-/fl}$; *Nanos3*$^{Cre/+}$ mice, being only about 25 % of that of the wild type (Figure 3.2 C). Overall, in this investigation TRIM71 was pointed out to be crucial for a normal testis development in mice.

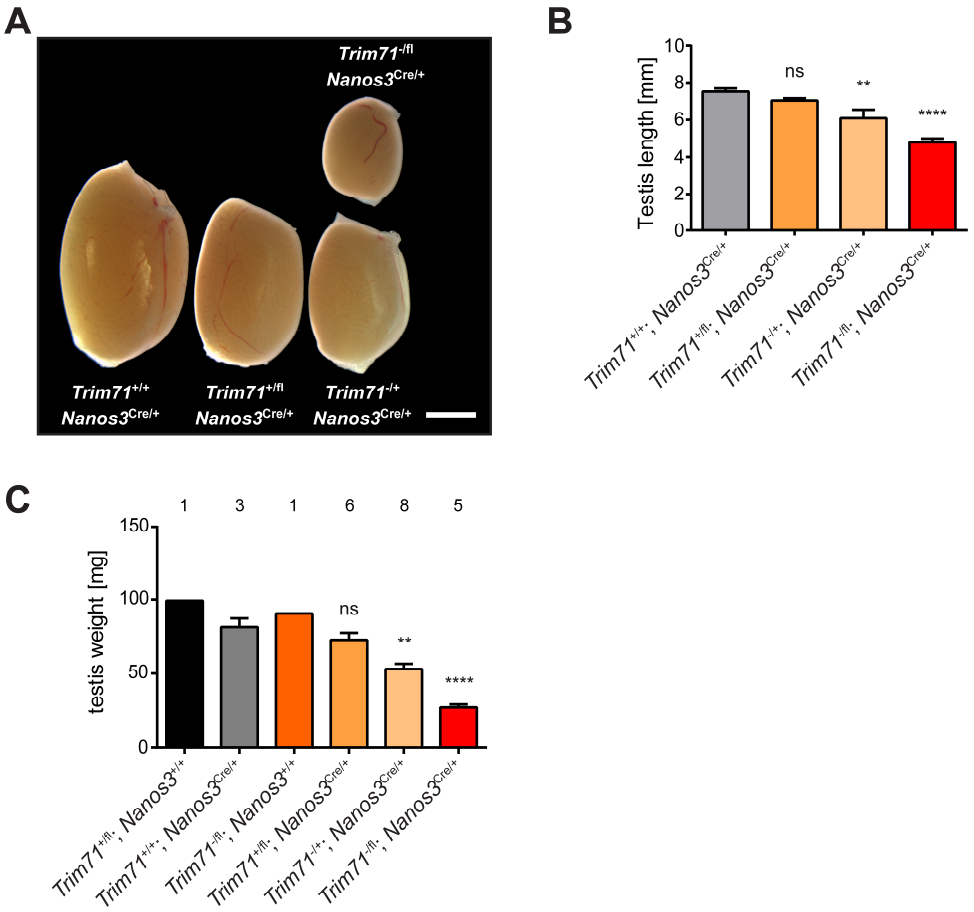

Figure 3.2 – Germline-specific TRIM71 deficiency results in reduced testis size and weight
(A) Representative images of testes of adult *Trim71*$^{+/+}$; *Nanos3*$^{Cre/+}$ (wild type), *Trim71*$^{+/fl}$; *Nanos3*$^{Cre/+}$ (germline-specific heterozygous), *Trim71*$^{-/+}$; *Nanos3*$^{Cre/+}$ (heterozygous) and *Trim71*$^{-/fl}$; *Nanos3*$^{Cre/+}$ (germline-specific knockout) mice. Scale bar represents 2 mm. **(B)** Testis length and **(C)** testis weight of adult mice (≥ 10 weeks) of different *Trim71*/*Nanos3*-Cre genotypes. *Trim71* wild type = black and grey; *Trim71* heterozygous = orange, germline-specific *Trim71* knockout = red. n≥3 for testis length and n=1-8 for testis weight as indicated by the number above each bar. Error bars indicate mean ± SEM. Statistical analysis was performed by one-way ANOVA with Dunnetts multiple comparisons post hoc test setting *Trim71*$^{+/+}$; *Nanos3*$^{Cre/+}$ (wild type) mice as control. ns=non-significant (p>0.05); **p<0.01; ****p<0.0001.

3.1.2 TRIM71-deficient adult testes lack SSCs showing a partial Sertoli-cell-only syndrome

To further analyse the male germ cell compartment, a histological investigation of the testis tissue was performed. Cross-sections of testes of minimum 10-week old males were stained with H&E as described in chapter 2.2.4.2. Testis sections show drastic differences in the histological appearance revealing a major degeneration of germ cells in germline-specific *Trim71* KO (*Trim71*$^{-/fl}$; *Nanos3*$^{Cre/+}$) male mice compared to *Trim71* wild type controls (*Trim71*$^{+/+}$; *Nanos3*$^{Cre/+}$) (Figure 3.3 A-A'''' and D-D''''). A normal tubule morphology with SSCs undergoing spermatogenesis to form spermatozoa towards the lumen of the tubule was observed only in a minority of seminiferous tubules in germline-specific *Trim71* KO mice (Figure 3.3 D-D'''). Most of the seminiferous tubules in germline-specific *Trim71* KO mice appeared 'empty' (Figure 3.3 D''''). Compared to the germline-specific *Trim71* KO mice, in the heterozygous controls (*Trim71*$^{+/fl}$; *Nanos3*$^{Cre/+}$ and *Trim71*$^{-/+}$; *Nanos3*$^{Cre/+}$) less tubules with an abnormal histology were visible (Figure 3.3 B-B'''' and C-C''''). Surprisingly, also seminiferous tubules with abnormal spermatogenic phenotype were apparent in *Trim71* wild type control mice (Figure 3.3 A-A''''). Again, this can be explained by the *Nanos3* heterogeneity in these mice and the fact that NANOS3-deficient mice are infertile [291].

In order to clearly examine the spermatogenesis phenotypes in *Trim71*$^{-/fl}$; *Nanos3*$^{Cre/+}$ and control male mice, testis cross-sections were immunofluorescently stained for TRA98, a well-established nuclear marker for germ cells from gonocytes to adult differentiating spermatogonia [131, 280]. Additionally, Sertoli cells were stained with an antibody against the nuclear marker WT1. Sertoli cells are a kind of somatic cell lining the inside of the seminiferous tubules and are often referred to as 'nurse' cells as they provide the microenvironment for spermatogenesis by nourishing the developing sperm [260]. Stained testis sections revealed that the seminiferous tubules of germline-specific *Trim71* KO male mice, which were regarded as 'empty' by H&E staining, were lacking spermatogonia completely and were only comprised of the Sertoli cell layer (Figure 3.4 D and DI). This phenotype has been described in humans known as the so called Sertoli-cell-only (SCO) syndrome or germ cell aplasia. As already seen by H&E staining of testis sections from *Trim71* heterozygous mice (Figure 3.3 B-B'''' and C-C''''), seminiferous tubules with a SCO syndrome were observed by immunofluorescent staining of testis sections from these animals, although less than in the testes of germline-specific knockout *Trim71*$^{-/fl}$; *Nanos3*$^{Cre/+}$ mice (Figure 3.4 B, BI, C and CI). This was in congruence with the already reduced testis size in *Trim71* heterozygous males. Also, the few 'empty' tubules present in *Trim71* wild type control animals showed a germ cell aplasia (Figure 3.4 A and AI).

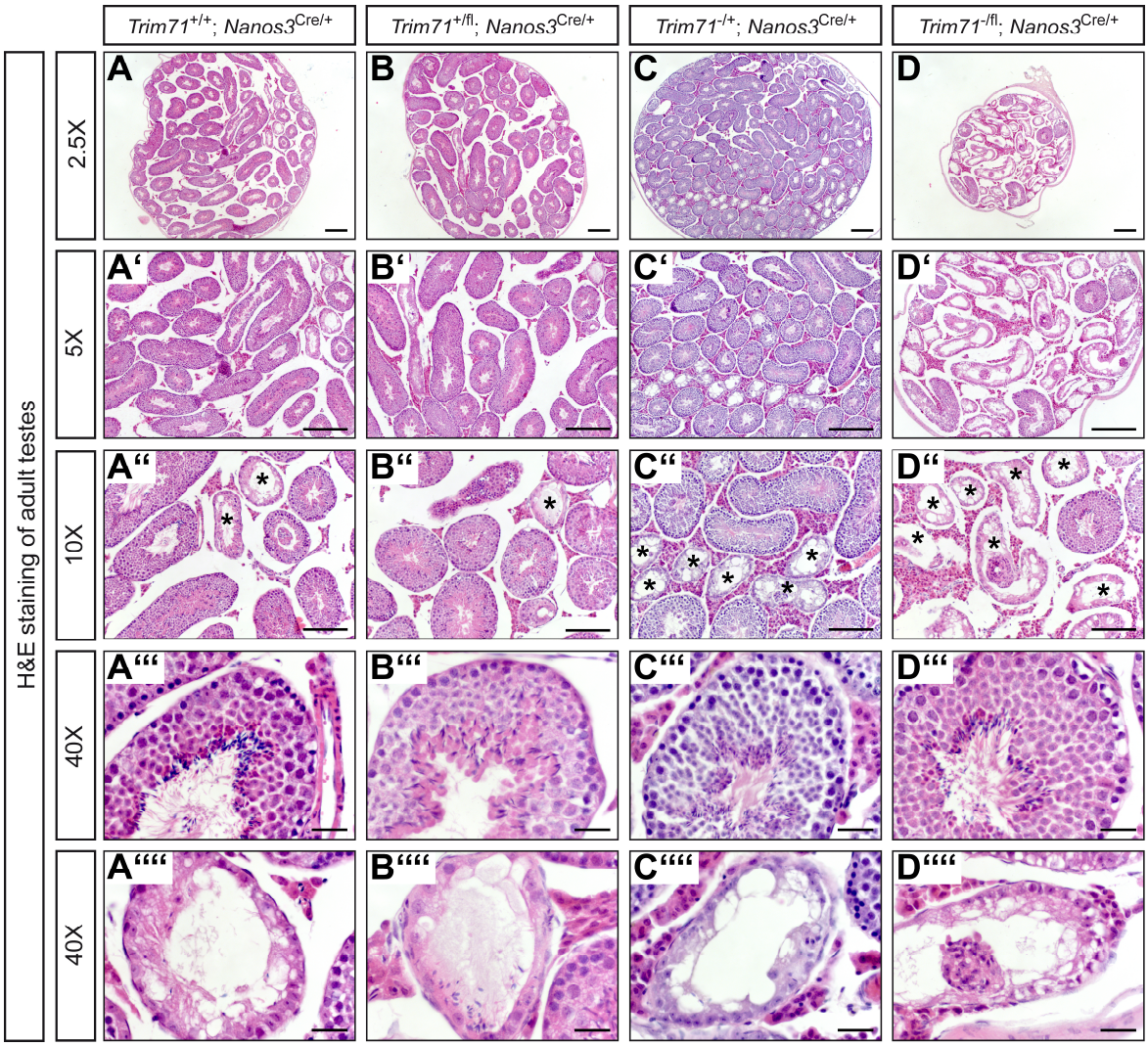

Figure 3.3 – Morphological differences in testes from adult germline-specific TRIM71-deficient mice

Representative images of H&E stainings on paraffin sections (cross-sections) of testes from adult wild type *Trim71*$^{+/+}$; *Nanos3*$^{Cre/+}$ **(A – A’’’)**, germline-specific heterozygous *Trim71*$^{+/fl}$; *Nanos3*$^{Cre/+}$ **(B – B’’’)**, heterozygous *Trim71*$^{-/+}$; *Nanos3*$^{Cre/+}$ **(C – C’’’)** and germline-specific knockout *Trim71*$^{-/fl}$; *Nanos3*$^{Cre/+}$ **(D – D’’’)** mice. Images were taken in four different magnifications (2.5x, 5x, 10x and 40x). To give an overview of the testis size and morphology, images were taken with 2.5x magnification **(A – D)** and 5x magnification **(A’ – D’)**. In images taken with 10x magnification **(A’’ – D’’)** seminiferous tubules with a defective morphology are marked with an asterisk (*). One seminiferous tubule with normal **(A’’ – D’’)** and defective **(A’’’ – D’’’)** morphology are represented in images taken with 40x magnification. Scale bars represent 200 µm (2.5x and 5x magnification), 100 µm (10x magnification) and 20 µm (40x magnification).

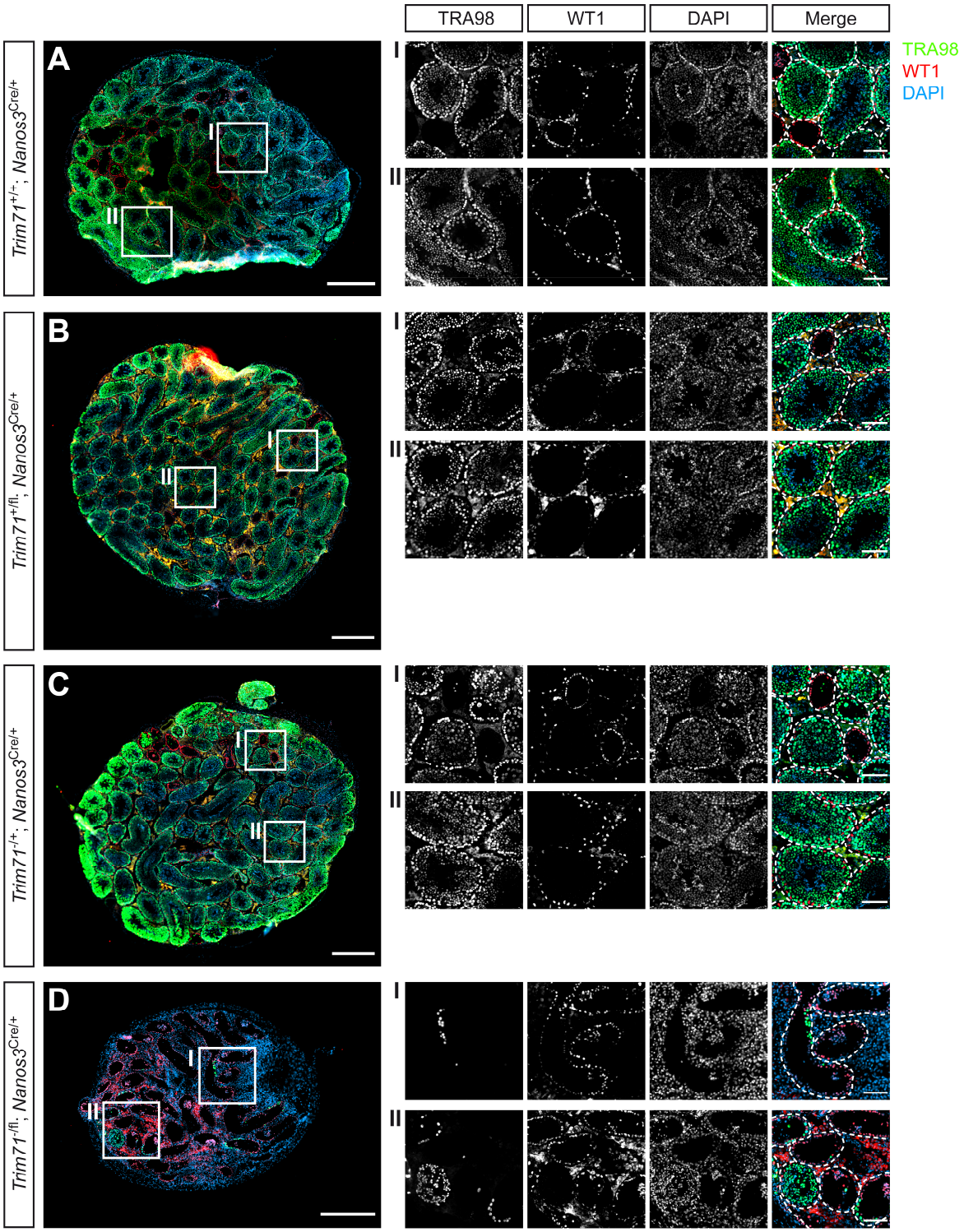

Figure 3.4 – Testes of adult germline-specific TRIM71-deficient mice show a partial SCO syndrome

Representative immunofluorescent stainings on cryosections (cross-sections) of testes from adult **(A)** wild type *Trim71*$^{+/+}$; *Nanos3*$^{Cre/+}$, **(B)** germline-specific heterozygous *Trim71*$^{+/fl}$; *Nanos3*$^{Cre/+}$, **(C)** heterozygous *Trim71*$^{-/+}$; *Nanos3*$^{Cre/+}$ and **(D)** germline-specific knockout *Trim71*$^{-/fl}$; *Nanos3*$^{Cre/+}$ mice. For each genotype two regions are depicted in higher magnification and are indicated as (I) and (II). Images show co-staining with TRA98 (green), WT1 (red) and DAPI (blue) labelling spermatogenic cells including SSCs, Sertoli cells and nuclei in the seminiferous tubules, respectively. For the magnifications, single channel images of TRA98, WT1 and DAPI stainings are depicted in greyscale. TRA98 stains SSCs undergoing spermatogenesis towards the lumen of the seminiferous tubules with Sertoli cells (WT1-postive) lining the inside of the seminiferous tubules. In seminiferous

tubules with a SCO syndrome, TRA98 staining is absent and tubules are marked with an asterisk (*). Scale bars represent 500 µm for complete testes cross-section and 100 µm for the magnification images.

A quantification of seminiferous tubules containing differentiating SSCs *versus* tubules lacking SSCs in testis from adult germline-specific *Trim71* KO, heterozygous and wild type male mice is depicted in Figure 3.5. In general, the results were corresponding to the testes weight. In *Trim71* wild type control mice, >90 % of seminiferous tubules per testis cross-section contained a normal number of germ cells undergoing spermatogenesis. Thus, *Nanos3* heterozygosity has only a minor effect on the fertility. Strikingly, for germline-specific TRIM71-deficient adult male mice, in only 30 to 40 % of the seminiferous tubules per testis cross-section spermatogenic cells were observed with more than half (60 to 70 %) of the tubules per cross-section lacking SSCs and showing a SCO syndrome. Interestingly, in testes of germline-specific heterozygous *Trim71*$^{+/fl}$; *Nanos3*$^{Cre/+}$ mice a similar number of tubules as in wild type testes contained spermatogenic cells, whereas in heterozygous *Trim71*$^{-/+}$; *Nanos3*$^{Cre/+}$ animals this number was reduced with a significant increase in the percentage of seminiferous tubules displaying a SCO syndrome (~15 % per cross-section). This can be explained by the *Nanos3*-Cre activity as *Trim71*$^{+/fl}$; *Nanos3*$^{Cre/+}$ mice are only heterozygous for *Trim71* in the germ cells in which the Cre recombinase has been active. In contrast, *Trim71*$^{-/+}$; *Nanos3*$^{Cre/+}$ mice are heterozygous for *Trim71* in all tissues, including the germ cells.

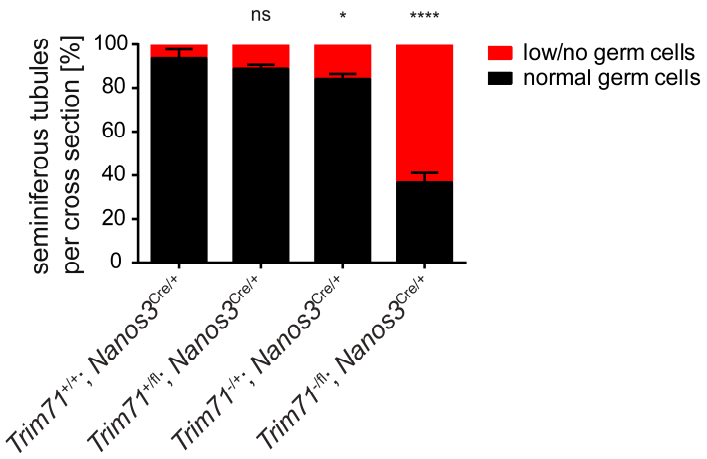

Figure 3.5 – Quantification of germ cell containing seminiferous tubules per testis cross-section in adult mice

The number of seminiferous tubules containing germ cells *versus* without or low number of germ cells was counted per testis cross-section for adult wild type *Trim71*$^{+/+}$; *Nanos3*$^{Cre/+}$, germline-specific heterozygous *Trim71*$^{+/fl}$; *Nanos3*$^{Cre/+}$, heterozygous *Trim71*$^{-/+}$; *Nanos3*$^{Cre/+}$ and germline-specific knockout *Trim71*$^{-/fl}$; *Nanos3*$^{Cre/+}$ mice. All seminiferous tubules in immunofluorescently stained testis cross-sections were counted for every condition and counts are depicted as percentages. n=3 for each genotype with each biological replicate containing technical triplicates. Error bars indicate mean ± SD. Statistical analysis was performed by applying one-way ANOVA with Dunnetts multiple comparisons post hoc test setting *Trim71*$^{+/+}$; *Nanos3*$^{Cre/+}$ (wild type) mice as control: ns=non-significant (p>0.05); *p<0.05; ****p<0.0001.

To further validate that TRIM71-deficiency in the male germline results in the absence of SSCs, the expression of SSC markers in adult testes tissue was analysed by qRT-PCR and Western blot (Figure 3.6). Similar to previous experiments in our group [187], germline-specific knockout *Trim71*$^{-/fl}$; *Nanos3*$^{Cre/+}$ adult male mice had a reduced *Trim71* mRNA expression (Figure 3.6 A) along with an almost complete absence of TRIM71 on protein level (Figure 3.6 B). Hence, the recombination rate of *Nanos3*-Cre was always high, however never complete. Yet, the analysed established SSC markers *Sall4* (mRNA) [79], *Lin28a*/LIN28A (mRNA and protein) [80, 322], *Oct4* (mRNA) [219, 277] and DDX4 (protein) [75] were strongly downregulated in testes of germline-specific *Trim71* KO mice (Figure 3.6 A and B), in agreement with previous findings [187]. Already in adult heterozygous *Trim71* males these SSC genes tended to be downregulated, which is in line with the slightly reduced testis weight in these animals (Figure 3.6 A and B). Similar to the SCC marker genes, LIN28B, which is expressed in postmeiotic spermatids during the nuclear elongation phase as well as in interstitial Leydig cells [80], was strongly downregulated in germline-specific *Trim71* KO testes and by tendency in testes of *Trim71* heterozygous animals on both RNA and protein level (Figure 3.6 A and B). Therefore, spermatogenesis is strongly inhibited in adult testis of *Trim71*$^{-/fl}$; *Nanos3*$^{Cre/+}$ with partial abolishment in *Trim71* heterozygous mice. This is highly congruent with the quantifications of the immunofluorescently stained testis cross-sections in these animals. Moreover, the expression of the cell cycle inhibitor *Cdkn1a* (*p21*) was downregulated on mRNA level in germline-specific *Trim71* KO testes and by tendency in testes of *Trim71* heterozygous animals (Figure 3.6 A). CDKN1A protein expression has been shown in spermatocytes and spermatids but not in spermatogonia, implying an important function in meiosis [22]. Thus, reduced *Cdkn1a* mRNA levels in *Trim71*$^{-/fl}$; *Nanos3*$^{Cre/+}$ testes suggests less spermatogenic activity very likely due to SSC deficiency in these males. Overall, these results indicate that the absence of TRIM71 in the male germ cell compartment leads to a lack of SSCs with a consequent partial SCO syndrome in adult mice.

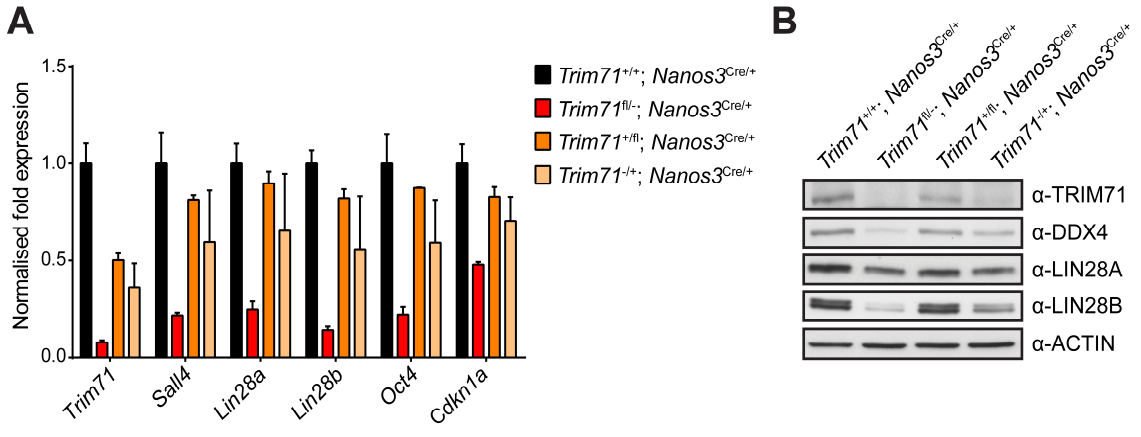

Figure 3.6

Figure 3.6 – Testes of adult germline-specific TRIM71-deficient mice lack SSCs
(A) qRT-PCR analysis of *Trim71*, SSC markers (*Sall4*, *Lin28a*, *Oct4*), spermatid marker *Lin28b* and cell cycle inhibitor *Cdkn1a* mRNA expression in testes from adult *Trim71*$^{+/+}$; *Nanos3*$^{Cre/+}$ (wild type), *Trim71*$^{+/fl}$; *Nanos3*$^{Cre/+}$ (germline-specific heterozygous), *Trim71*$^{-/+}$; *Nanos3*$^{Cre/+}$ (heterozygous) and *Trim71*$^{-/fl}$; *Nanos3*$^{Cre/+}$ (germline-specific knockout) mice (n≥2). Relative mRNA expression was normalised to the housekeeping gene *Hprt*. Values are depicted as fold changes with the respective wild-type expression set to 1. Error bars indicate mean ± SEM. **(B)** Corresponding representative Western blot analysing the expression of Trim71, the SSC markers (DDX4 and LIN28A) and the spermatid marker LIN28B in testis lysates from *Trim71*$^{+/+}$; *Nanos3*$^{Cre/+}$ (wild type), *Trim71*$^{+/fl}$; *Nanos3*$^{Cre/+}$ (germline-specific heterozygous), *Trim71*$^{-/+}$; *Nanos3*$^{Cre/+}$ (heterozygous) and *Trim71*$^{-/fl}$; *Nanos3*$^{Cre/+}$ (germline-specific knockout) adult mice. Equal loading was verified by ACTIN expression.

3.1.3 Absence of TRIM71 during germ cell development causes SSCs deficiency already in testes of neonatal mice

Besides being active during embryogenesis, a distinctive increase in TRIM71 expression level has been described in male mice 1 to 2 weeks after birth [187]. Previously, PGCs of germline-specific knockout *Trim71*$^{-/fl}$; *Nanos3*$^{Cre/+}$ mice have been shown to be successfully specified (E7.5) and migrating along the hindgut into the genital ridge (E10.5) [187]. Until this timepoint, no differences in development in germline-specific knockout *Trim71*$^{-/fl}$; *Nanos3*$^{Cre/+}$ compared to *Trim71* wild type mice were observed. However, in the germline-specific *Trim71* KO adult male mice we observed the number of germ cells to be reduced drastically (chapter 3.1.2). Importantly, in males, PGCs proliferate after generation (E7.5) until going in mitotic arrest at E13.5 [279, 321]. The PGCs remain quiescent until re-entering the cell cycle 1 or 2 days after birth and establishing the adult SSC pool [9, 321]. In order to investigate whether the lack of SSCs in adult males originates from embryogenesis or early postnatal development, we examined germ cell development in neonatal mice at postnatal day 0.5 (P0.5).

Histological investigations of the early testis tissue were performed. Cross-sections of testes of P0.5 mice were stained with H&E (Figure 3.7) as well as immunofluorescently stained for the germ cell marker (TRA98) and the Sertoli cell marker (WT1) (Figure 3.8). Independent of the genotype, the gonocytes were located in the centre of the lumen-less seminiferous tubules and presented a distinctive morphology of round shaped cells with pale-staining nuclei surrounded by a ring-like cytosol as described by Baillie *et al*. [14]. In contrast, Sertoli cells could be easily distinguished by smaller, ovoid nuclei and being anchored to the basement membrane [52, 314]. In general, not many gonocytes were visible in any of the investigated genotypes including the testes of the wild type control mice (Figure 3.7 and Figure 3.8). By H&E staining less to no gonocytes were apparent in germline-specific TRIM71-deficient (*Trim71*$^{-/fl}$; *Nanos3*$^{Cre/+}$) and heterozygous *Trim71*$^{-/+}$; *Nanos3*$^{Cre/+}$ testes compared to the *Trim71* wild type control (Figure 3.7 A-A', C-C' and D-D'). This was

confirmed by immunofluorescent staining of TRA98 (Figure 3.8 A, C and D). The gonocyte-deficient seminiferous tubules were only comprised of Sertoli cells being positively stained for WT1 (Figure 3.8). Accordingly, a SCO syndrome is already existing in testes of germline-specific *Trim71* KO neonatal mice as early as P0.5 with its origin most likely in embryogenesis after reaching the genital ridges at E10.5.

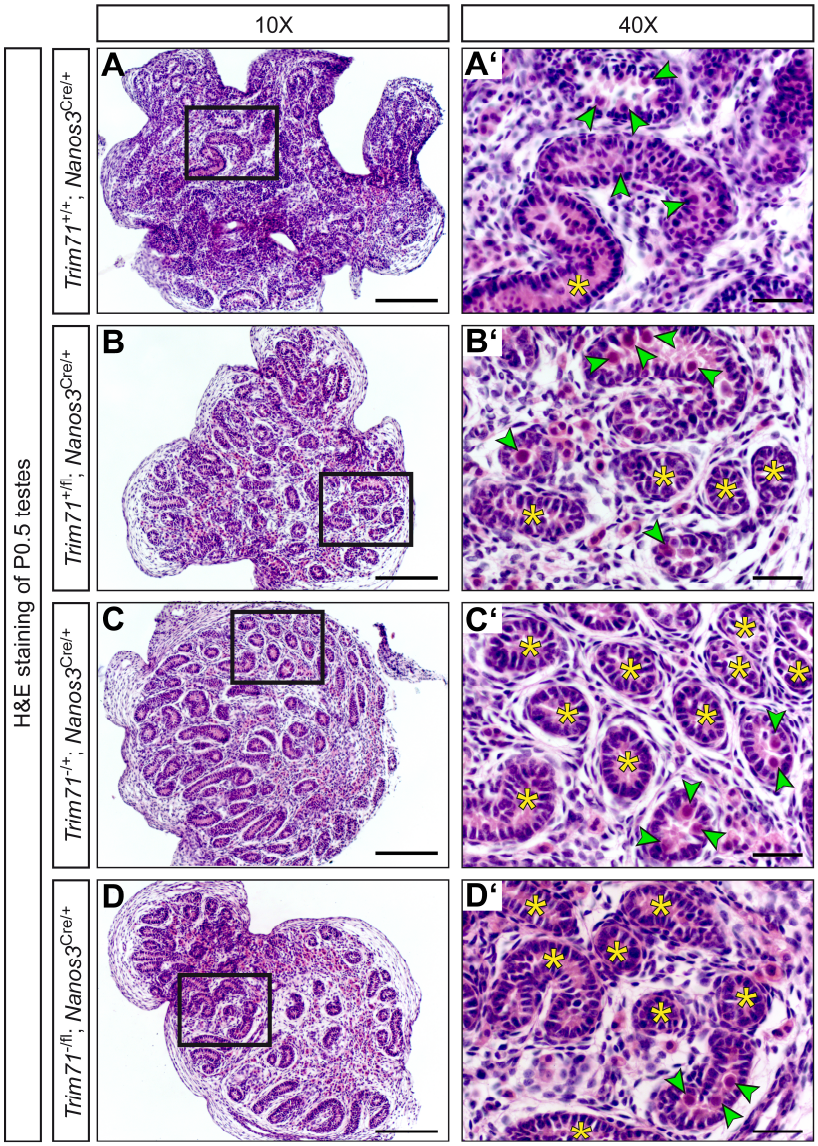

Figure 3.7 – Testes of neonatal (P0.5) germline-specific TRIM71-deficient mice have a reduced number of gonocytes

Representative images of H&E stainings on paraffin sections of testes from neonatal (P0.5) wild type *Trim71*$^{+/+}$; *Nanos3*$^{Cre/+}$ **(A – A'''),** germline-specific heterozygous *Trim71*$^{+/fl}$; *Nanos3*$^{Cre/+}$ **(B – B''')**, heterozygous *Trim71*$^{-/+}$; *Nanos3*$^{Cre/+}$ **(C – C''')** and germline-specific knockout *Trim71*$^{-/fl}$; *Nanos3*$^{Cre/+}$ **(D – D''')** mice. Images were taken in two different magnifications (10x and 40x). To give an overview of the testis size and morphology, images were taken with 10x magnification **(A – D)**. For each genotype one region (black frame) is shown in 40x magnification **(A'' – D'')**. Seminiferous tubules lacking gonocytes are marked with a yellow asterisk (*). Gonocytes within the seminiferous tubules are marked with a green arrow head. Scale bars represent 100 µm (10x magnification) and 20 µm (40x magnification).

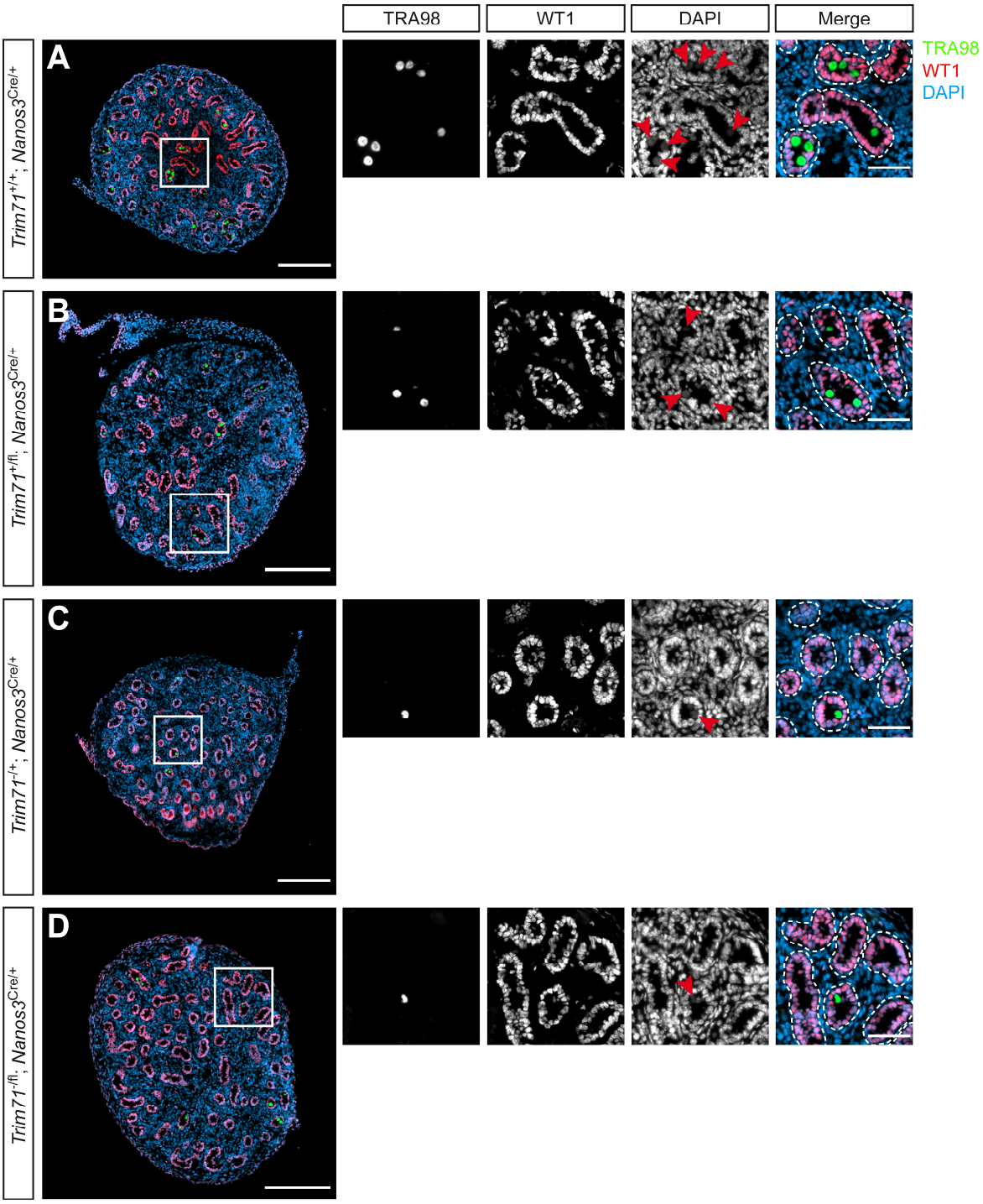

Figure 3.8 – Testes of neonatal (P0.5) germline-specific TRIM71-deficient mice show a partial SCO syndrome

Representative immunofluorescent stainings on cryosections (cross-sections) of testes from neonatal (P0.5) **(A)** wild type *Trim71*$^{+/+}$; *Nanos3*$^{Cre/+}$, **(B)** germline-specific heterozygous *Trim71*$^{+/fl}$; *Nanos3*$^{Cre/+}$, **(C)** heterozygous *Trim71*$^{-/+}$; *Nanos3*$^{Cre/+}$ and **(D)** germline-specific knockout *Trim71*$^{-/fl}$; *Nanos3*$^{Cre/+}$ mice. For each genotype one region (white frame) is shown in a higher magnification on the right. In all images co-staining of germ cells (TRA98, green), Sertoli cells (WT1, red) and nuclei (DAPI, blue) is depicted. For the magnifications, single channel images of TRA98, WT1 and DAPI stainings are depicted in greyscale. In P0.5 testes, TRA98 stains the gonocytes located in the centre of the lumen-less seminiferous tubules with Sertoli cells (WT1 positive) lining the inside of the seminiferous tubules. The pale-stained nuclei of gonocytes are marked with a red arrow head in the DAPI staining. Scale bars represent 200 µm for complete testes cross-sections and 50 µm for the magnification images.

Quantifications of seminiferous tubules in the cross-sections of immunofluorescently stained P0.5 testes from germline-specific *Trim71* KO, heterozygous and wild type mice revealed that even in the wild type, gonocytes were only present in 30 % of the tubules on average (Figure 3.9). This most probably is due to the fact that less than 25,000 gonocytes are present in the whole testis at P0.5 [81, 321] and the sections represent only a very thin part of the tissue. As for adult testes, no difference in gonocyte number was observed in germline-specific heterozygous *Trim71*$^{+/fl}$; *Nanos3*$^{Cre/+}$ in comparison with *Trim71* wild type males (Figure 3.9). Strikingly, in both, germline-specific knockout *Trim71*$^{-/fl}$; *Nanos3*$^{Cre/+}$ and heterozygous *Trim71*$^{-/+}$; *Nanos3*$^{Cre/+}$ testes, the number of gonocyte containing seminiferous tubules was reduced to below 10 % on average (Figure 3.9). This is not in line with the only slight reduction in germ cell number in adult testes of heterozygous *Trim71*$^{-/+}$; *Nanos3*$^{Cre/+}$ mice described above (chapter 3.1.2). Yet, it is of note that *Nanos3* is re-expressed in testes of neonatal mice (P1.5) [291]. Thus, both, embryonic (after E10.5) as well as postnatal TRIM71 expression seems to be important for the successful establishment of an adult SCC pool.

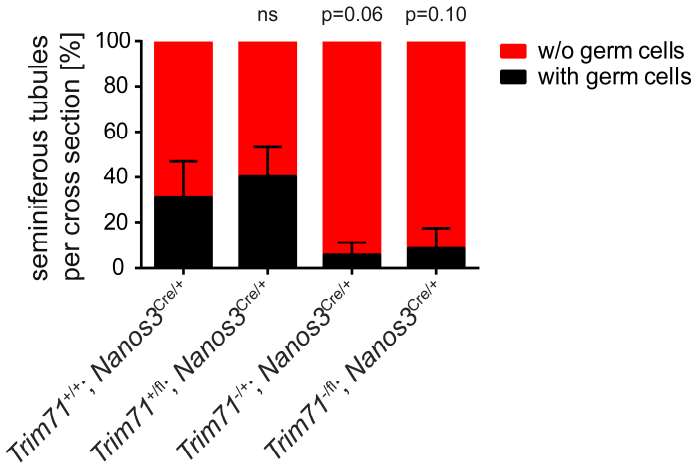

Figure 3.9 – Quantification of germ cell containing seminiferous tubules per testis cross-section in neonatal (P0.5) mice

The number of seminiferous tubules containing germ cells *versus* without germ cells was counted per testis cross-section for neonatal (P0.5) wild type *Trim71*$^{+/+}$; *Nanos3*$^{Cre/+}$, germline-specific heterozygous *Trim71*$^{+/fl}$; *Nanos3*$^{Cre/+}$, heterozygous *Trim71*$^{-/+}$; *Nanos3*$^{Cre/+}$ and germline-specific knockout *Trim71*$^{-/fl}$; *Nanos3*$^{Cre/+}$ mice. All seminiferous tubules in immunofluorescently stained testis cross-sections were counted for every condition and counts are depicted as percentages. n=3 for each genotype with each biological replicate containing technical triplicates. Error bars indicate mean ± SD. Statistical analysis was performed by applying one-way ANOVA with Dunnetts multiple comparisons post hoc test setting *Trim71*$^{+/+}$; *Nanos3*$^{Cre/+}$ (wild type) mice as control: ns=non-significant (p>0.05).

3.2 Germ cell tumour cell line as an *in vitro* model

As described in chapter 3.1.3, a reduction in germ cell number in germline-specific TRIM71-deficient testes of mice at P0.5 was detected, which most likely originates from late embryonic development although TRIM71 may also be important in early postnatal testis development. Apart from proliferation being vital for PGC development, many PGCs undergo apoptosis between mitotic arrest (E14.5) and 1 to 2 days after birth [321]. As TRIM71 has been described previously as a critical regulator of stem cell fate, hence promoting proliferation, impairing differentiation and reducing apoptosis, we wanted to investigate this specific aspect in more detail. However, the isolation and cultivation of PGCs is complicated, especially as the number of germline stem cell is very limited in germline-specific TRIM71-deficient animals, making an *in vivo* assessment difficult. Therefore, an *in vitro* model was used to analyse the impact of TRIM71 deficiency on proliferation and apoptosis.

3.2.1 Endogenous TRIM71 expression is highest in the germ cell tumour cell lines NCCIT, TCam-2 and 2012EP

Besides being essential for embryonic development, previous analysis by our group of online available cancer RNA-sequencing datasets found *TRIM71* expression upregulated in a variety of human cancers such as acute myeloid leukaemia, neuroblastoma, hepatocellular carcinoma and most importantly testicular germ cell tumours (TGCT) [281, 290] (Figure 3.10). Moreover, high *TRIM71* expression has been correlated to advanced cancer progression and poor prognosis [38, 43]. With TRIM71 linked to TGCT, cell lines established from these tumours were regarded as a suitable *in vitro* system to study the role of TRIM71. In culture, pluripotent stem cells derived from murine embryonic primordial germ cells [180, 234] or adult germ cells [83, 121] retained similarities with ESCs. Furthermore, germ cell tumours have long been used as a surrogate model for ESCs to investigate stemness and differentiation [126].

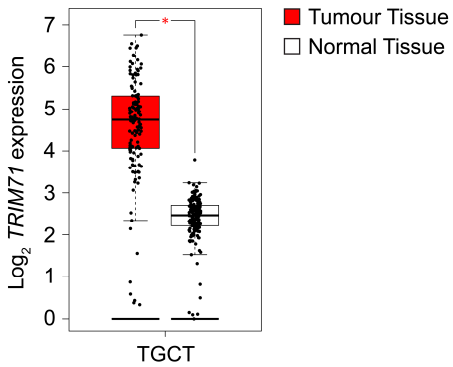

Figure 3.10

Figure 3.10 – *TRIM71* mRNA expression is increased in testicular germ cell tumours
Significant upregulation of *TRIM71* mRNA expression in testicular germ cell tumours (TGCT) according to the GEPIA2 web server [281]. The graph and statistics are depicted as provided by the web server.

First, the endogenous TRIM71 expression was examined across several available germ cell tumour cell lines (JKT-1, NCCIT, NTera2, TCam-2 and 2102EP) (Figure 3.11). All of these cell lines resemble a mixed germ cell tumour *in vitro* except for TCam-2, which is a pure human seminoma cell line. In order to compare the endogenous *TRIM71* mRNA expression across different cell lines none of the standard housekeeping genes was suitable for normalisation (data not shown). Therefore, a standard curve was established using 10^1 to 10^6 copies of *TRIM71* as template for amplification in qRT-PCR (chapter 2.2.1.19). In order to generate the standard curve, the PCR cycle number, at which the sample crosses a defined threshold (threshold cycle or Ct value), was plotted against the logarithm of the applied copy number with a subsequent linear regression analysis being performed (Figure 3.11 A). The standard curve showed that the applied copy number of the target sequence was proportional to the Ct value. Hence, the higher the number of applied copies the earlier the PCR reached a certain product threshold. Based on the linear equation, the copy numbers of *TRIM71* in the different germ cell tumour cell lines were calculated (Figure 3.11 B). HepG2 cells were used as positive control as a TRIM71 expression has been described in several hepatocellular carcinoma cell lines [43]. In general, the *TRIM71* mRNA expression level varied across the different germ cell tumour cell lines. *TRIM71* mRNA expression was observed highest in NCCIT, TCam-2 and 2102EP cells (Figure 3.11 B). These results were highly congruent with the protein analysis in these germ cell tumour cell lines which revealed the highest expression of TRIM71 in NCCIT cells followed by 2102EP and TCam-2 cells (Figure 3.11 C and D). Taken together, these results indicate the NCCIT cell line as the best *in vitro* model system to study the molecular functions of TRIM71 in the germ cell lineage. Nonetheless, TCam-2 cells are also of interest as it is the only available seminoma cell line and seminoma being one of the most common testicular germ cell tumours caused by delayed or blocked differentiation of PGCs.

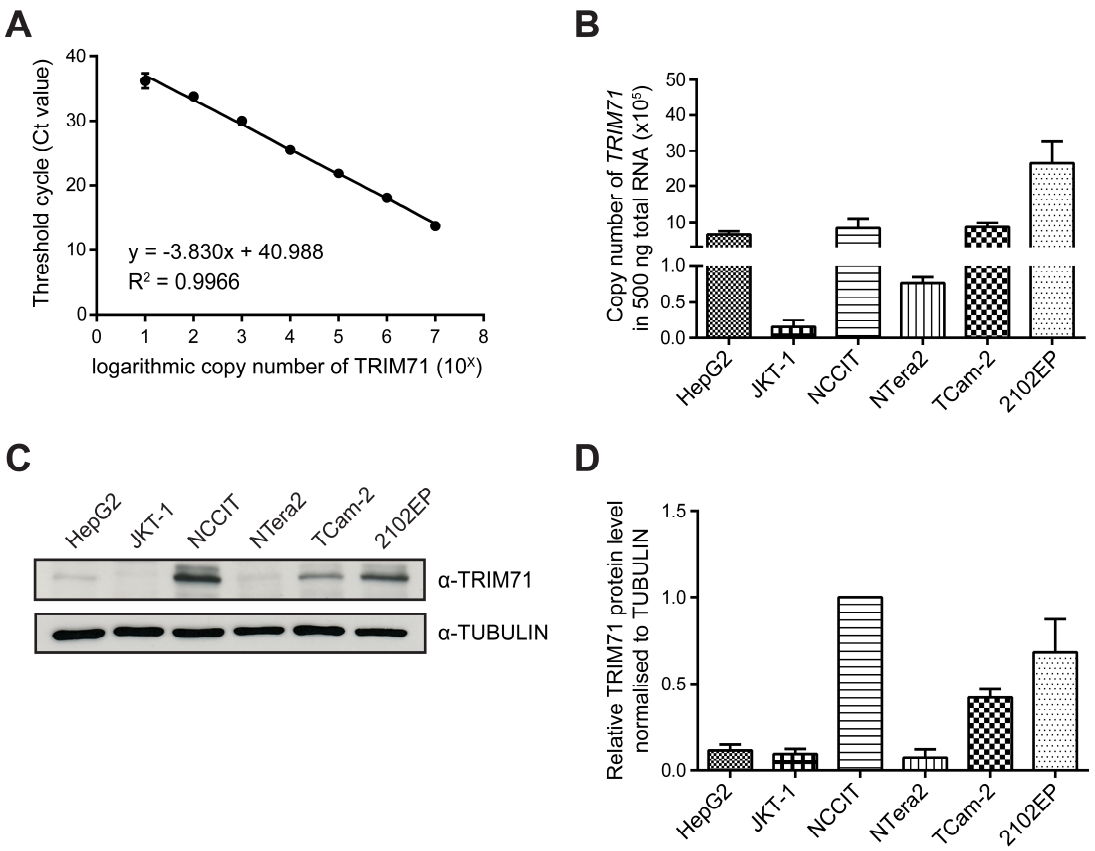

Figure 3.11 – Highest endogenous TRIM71 expression is detectable in NCCIT, TCam-2 and 2102EP cells
(A) Standard curve of *TRIM71* with 10^1 to 10^6 copies of *TRIM71* used for amplification by qRT-PCR (n=4 (technical)). The logarithm of the applied copy number was plotted against the respective Ct value, which is defined as the point where a specific amount of PCR product crosses a defined threshold. Error bars indicate mean ± SD. **(B)** qRT-PCR analysis of *TRIM71* mRNA expression in HepG2 and several germ cell tumour cell lines (n≥4). The expression was quantified using the standard curve. Error bars indicate mean ± SEM. **(C)** Representative Western blot and **(D)** Quantification of TRIM71 protein expression in HepG2 and different germ cell tumour cell lines (n=3). TRIM71 expression was normalised to TUBULIN and is depicted in relation to the expression in NCCIT cells which is set to 1. Error bars indicate mean ± SEM.

3.2.2 Knockdown of TRIM71 in TCam-2 and NCCIT cells using various siRNA oligos shows no effect on TRIM71 target gene expression

In a first approach to analyse the molecular functions of TRIM71 in germ cell development, siRNA-mediated knockdown of TRIM71 was performed in the germ cell tumour cell lines TCam-2 and NCCIT which exhibited a high endogenous TRIM71 expression. Several siRNAs targeting TRIM71 at different regions (chapter 2.1.10.6) were used.

With all siRNAs except for siTRIM71 #5 a successful downregulation of TRIM71 was achieved in both germ cell tumour cell lines (Figure 3.12): In TCam-2 cells *TRIM71* mRNA levels were reduced by at least 66 % (Figure 3.12 A) with less than 10 % of TRIM71 protein remaining (Figure 3.12 B) as observed by qRT-PCR and Western blot analysis,

respectively. A less strong reduction of TRIM71 was present in NCCIT cells. Yet, a reduction of *TRIM71* mRNA level by minimum 57 % was apparent (Figure 3.12 C) with at most 27 % TRIM71 protein remaining (Figure 3.12 D).

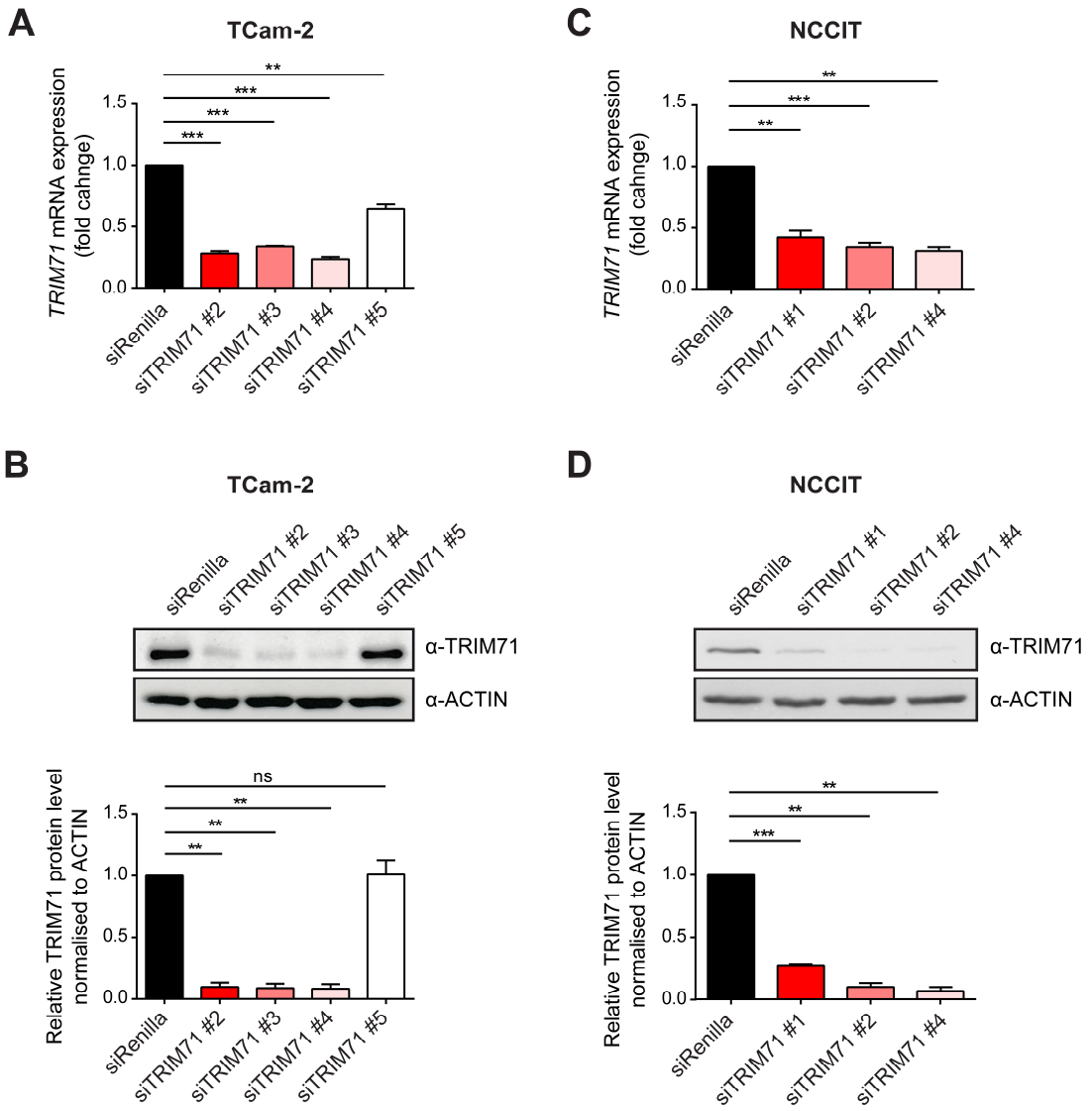

Figure 3.12 – siRNA-mediated knockdown of TRIM71 in TCam-2 and NCCIT cells
Knockdown of TRIM71 in TCam-2 and NCCIT cells was verified by qRT-PCR **(A and C)** and on protein level by Western blot analysis **(B and D)**. **(A)** *TRIM71* mRNA levels measured in control (siRenilla) and TRIM71 knockdown (siTRIM71 #2, #3, #4 and #5) TCam-2 cells 60 hpt normalised to the housekeeping gene *HPRT1* (n=3). **(B)** Representative Western blot showing TRIM71 protein levels in TCam-2 cells upon TRIM71 knockdown corresponding to mRNA levels, and quantification of 3 independent experiments. **(C)** *TRIM71* mRNA levels measured in control (siRenilla) and TRIM71 knockdown (siTRIM71 #1, #2 and #4) NCCIT cells 72 hpt normalised to the housekeeping gene *HPRT1* (n≥3). **(D)** Representative Western blot showing TRIM71 protein levels in NCCIT cells upon TRIM71 knockdown corresponding to mRNA levels, and quantification of 3 independent experiments. Error bars indicate mean ± SEM. Statistical significance was tested using two-tailed paired t-test: ns=non-significant ($p>0.05$); **$p<0.01$; ***$p<0.001$.

In order to validate this siRNA-mediated downregulation of TRIM71 as an adequate *in vitro* system, the expression of known TRIM71 targets (*CDKN1A*, *EGR1*, *INHBB*, *PLXNB2*, *HMGA2* and let-7a) was analysed on mRNA level by qRT-PCR in both TCam-2 and NCCIT cells (Figure 3.13).

The cyclin-dependent kinase inhibitor CDKN1A is a negative regulator of cell proliferation inhibiting G1 – S transition signals [92, 168]. In 2012, Chang *et al.* reported that TRIM71 promotes the proliferation in mouse ESCs by post-transcriptional repression of the cell-cycle regulator *Cdkn1a* [39]. Latest investigations by our group have identified *CDKN1A* as a direct mRNA target of TRIM71 with a hairpin motif in the TRIM71 NHL domain binding to CDKN1A 3' UTR, thereby targeting it for mRNA degradation by NMD [290]. Consequently, in the absence of TRIM71 an upregulation of *CDKN1A* mRNA was expected. However, neither in TCam-2 nor in NCCIT cells *CDKN1A* mRNA was upregulated upon TRIM71 silencing (Figure 3.13 A and B). In TCam-2 cells TRIM71 knockdown rather resulted in *CDKN1A* mRNA downregulation. Though, this result is questionable as the strongest *CDKN1A* downregulation was observed with siTRIM71 #5 which did not display a reduction in TRIM71 protein in TCam-2 cells.

EGR1 (LIN-29) is a transcription factor regulating differentiation and mitogenesis in various animals and cell types [135, 146, 186, 205]. Together with let-7 and TRIM71, EGR1 was shown to be important in reprogramming mammalian epidermal fibroblasts into induced pluripotent stem cells [308]. Previously, *EGR1* mRNA has been reported to co-immunoprecipitate with TRIM71 in human ESCs [308]. Furthermore, in 2017 *lin-29a* has been described as a direct target of *C. elegans* LIN-41 with the LIN41 NHL domain binding its 5' UTR and thereby mediating LIN41-dependent translational repression [3]. Here, in TCam-2 and NCCIT cells no difference in *EGR1* mRNA level upon TRIM71 downregulation was observed (Figure 3.13 A and B). Hence, similar to *C. elegans*, no mRNA degradation of *EGR1* by TRIM71 was present in germ cell tumour cells. However, a post-transcriptional regulation of *EGR1* by TRIM71 through translational repression could be still possible.

Both, *Inhbb* and *Plxnb2* have been described as TRIM71 targets in mouse ESCs by our group [187]. TRIM71-mediated repression of these target mRNAs was demonstrated to occur via TRIM71 responsive elements in the 3' UTR [187]. INHBB is a protein subunit of the dimeric activin and inhibin protein complexes and present predominantly in spermatogonia, spermatocytes, Sertoli cells, and Leydig cells of immature testis [15]. Regulatory functions of inhibins and activins acting as hormones as well as growth and differentiation factors have been described during testicular development [133, 134]. The transmembrane receptor PLXNB2 is implicated in brain corticogenesis and normal mouse embryonic brain development being required for differentiation and migration of neuronal cells [54, 102]. As germ cell tumours arise from PGCs, which are selected embryonic stem

cells, a similar repression of *INHBB* and *PLXNB2* mRNA by TRIM71 was expected in both germ cell tumour cell lines as in mouse ESCs. Yet, siRNA-mediated downregulation of TRIM71 did not affect *INHBB* mRNA level in neither TCam-2 nor NCCIT cells (Figure 3.13 A and B). Only by tendency *PLXNB2* mRNA was upregulated in NCCIT cells upon TRIM71 knockdown with two of the three siRNAs (Figure 3.13 B). Thus, no definite TRIM71-mediated regulation of these described target mRNAs could be validated in the two germ cell tumour cell lines.

TRIM71 (and orthologs) and let-7 miRNA display evolutionary conserved reciprocal expression patterns, temporally and spatially, in the developing embryo as well as in adult tissue [120, 145, 153, 211, 256, 265]. During differentiation *TRIM71* is translationally repressed by let-7 which binds to the 3' UTR of *TRIM71* targeting it for mRNA decay [13, 172, 233, 296]. On the other hand, TRIM71 has also been demonstrated to regulate let-7 activity. The study by Rybak *et al.* proposed TRIM71 to ubiquitinate AGO2, the major mediator of miRNA biogenesis and function, for proteasomal degradation [246]. However, several groups failed to detect a downregulation of steady-state AGO2 levels by TRIM71 [39, 41, 157]. In contrast, another publication identified the pluripotency factor LIN28B to be bound and ubiquitylated by TRIM71, thereby inducing let-7 expression [150]. LIN28-mediated let-7 miRNA repression is a well-studied process in miRNA research [85, 98, 200, 285, 300, 302, 323]. Previous investigations of our group have found a partial de-repression of mature let-7 miRNA upon TRIM71 deficiency in mouse ESCs. Moreover, TRIM71 was identified to fine-tune the let-7-LIN28 bistable switch for the regulation of the balance between stemness and differentiation [187]. As both germ cell tumour cell lines were shown to express the paralogs LIN28A and LIN28B (data not shown), this proposed mechanism of TRIM71 was to be proven in these cells. Furthermore, an increase in let-7a miRNA level could also hint towards an induced differentiation in these cells. However, no differences in mature let-7a miRNA levels were observed upon TRIM71 knockdown in neither TCam-2 nor NCCIT cells (Figure 3.13 A and B).

Altogether, for none of the investigated TRIM71 targets, except *EGR1*, a distinct post-transcriptional regulation as described in previous studies was observed. Concluding from this, a minimal amount of TRIM71, which is remaining by siRNA-mediated knockdown, may be sufficient to maintain the complete molecular function. Moreover, this methodology can produce undesired off-target effects which might not reflect the molecular functions of TRIM71 in a normal cellular environment.

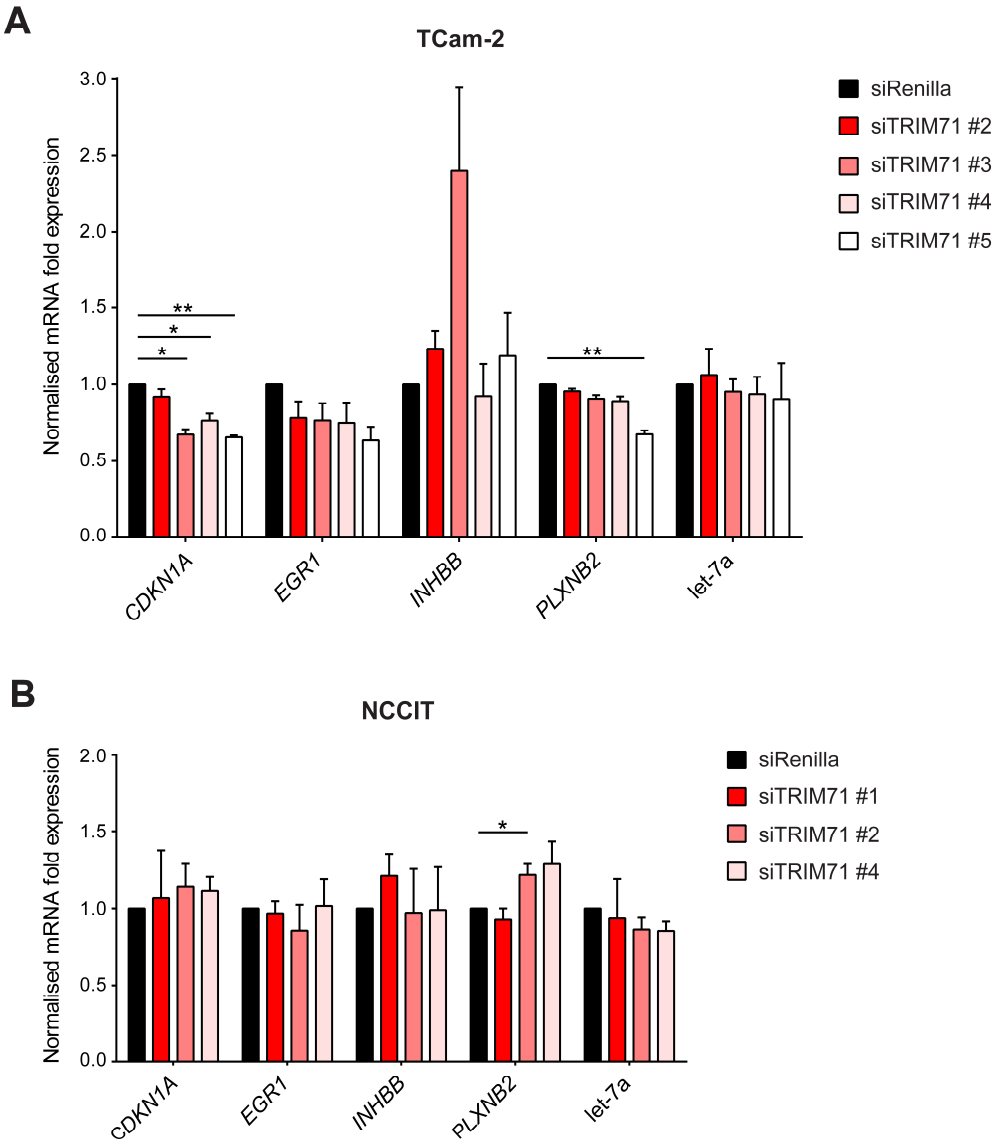

Figure 3.13 – TRIM71 target gene expression is not altered upon TRIM71 knockdown in TCam-2 and NCCIT cells

The expression of described TRIM71 target genes (*CDKN1A, EGR1, INHBB, PLXNB2*) and miRNA let-7a was measured in control (siRenilla) and TRIM71 knockdown (siTRIM71 #1, #2, #3, #4 and #5) **(A)** TCam-2 (n=3) and **(B)** NCCIT cells (n≥3) 60 and 72 hpt, respectively. TCam-2 cells 60 hpt. Relative mRNA expression was normalised to the housekeeping gene *HPRT*. Values are depicted as fold changes with the respective expression of control (siRenilla) cells set to 1. Error bars indicate mean ± SEM. Statistical analysis was performed by applying two-tailed paired t-test: *p<0.05; **p<0.01. All other data was non-significant (p>0.05).

3.3 Deletion of TRIM71 in NCCIT cells using CRISPR/Cas9 system

Assuming that the presence of a little amount of TRIM71 is sufficient to maintain its regulatory function, only a full irreversible gene knockout of *TRIM71* allows the investigation of protein function in the germ cell compartment. For the generation of *TRIM71* knockout cell lines, we made use of the powerful CRISPR/Cas9 genome-editing system targeting two different sites of the *TRIM71* gene in NCCIT cells: KO#1 located in the RING domain shortly after the ATG start codon and KO#2 located in the last NHL repeat (Figure 3.14 A). The respective sgRNA sequences are listed in chapter 2.1.10.7. *TRIM71* was targeted on the one hand by sgRNA#1 very close to the N-terminus in order to disrupt protein expression as early as possible predicting a complete protein deletion without functional truncations of the TRIM71 protein. On the other hand, in mice the same developmental defects have been described in a 24 amino acid C-terminal truncation and the full deletion of TRIM71 [172]. Therefore, gene editing using sgRNA#2 was carried out, predicted to generate a protein product with a short C-terminal truncation.

Gene editing was conducted by transfection of NCCIT cells with the plasmid pSpCas9(BB)-2A-GFP (PX458) carrying the specific sgRNA targeting *TRIM71*, the Cas9 from *S. pyogenes* and eGFP as a selection maker separated by the self-cleaving peptide T2A (chapter 2.2.1.12). As a control the PX458 plasmid without a specific sgRNA inserted was transfected (EV control). Generally, a transfection efficiency of 50 % to 68 % was achieved as determined by FACS for GFP positive cells 48 hpt (Figure 3.14 B and C). Following transfection, the TRIM71 protein expression was controlled by Western blot analysis (Figure 3.14 B and C). In the sorted GFP positive fractions of targeted NCCIT cells a reduced TRIM71 protein level was apparent in *TRIM71* KO#1 cells with nearly no TRIM71 detectable in *TRIM71* KO#2 cells compared to EV transfected control cells. The remaining TRIM71 protein levels varied between each FACS depending on the sorting efficiency (data not shown) with a higher TRIM71 protein level indicating a less efficient cell sorting. Furthermore, also the targeting efficiency of the Cas9 has an influence on the TRIM71 protein level. Hence, a lower Cas9 cutting efficiency results in a higher TRIM71 protein expression. Besides, not in every positively transfected cell the gene editing results in a knock-out mutation as the NHEJ repair mechanism repairs DNA damages randomly. Nevertheless, for all further analysis the GFP positive cells obtained by FACS were used and CRISPR/Cas9-induced NCCIT *TRIM71* KO cells were compared to NCCIT EV cells.

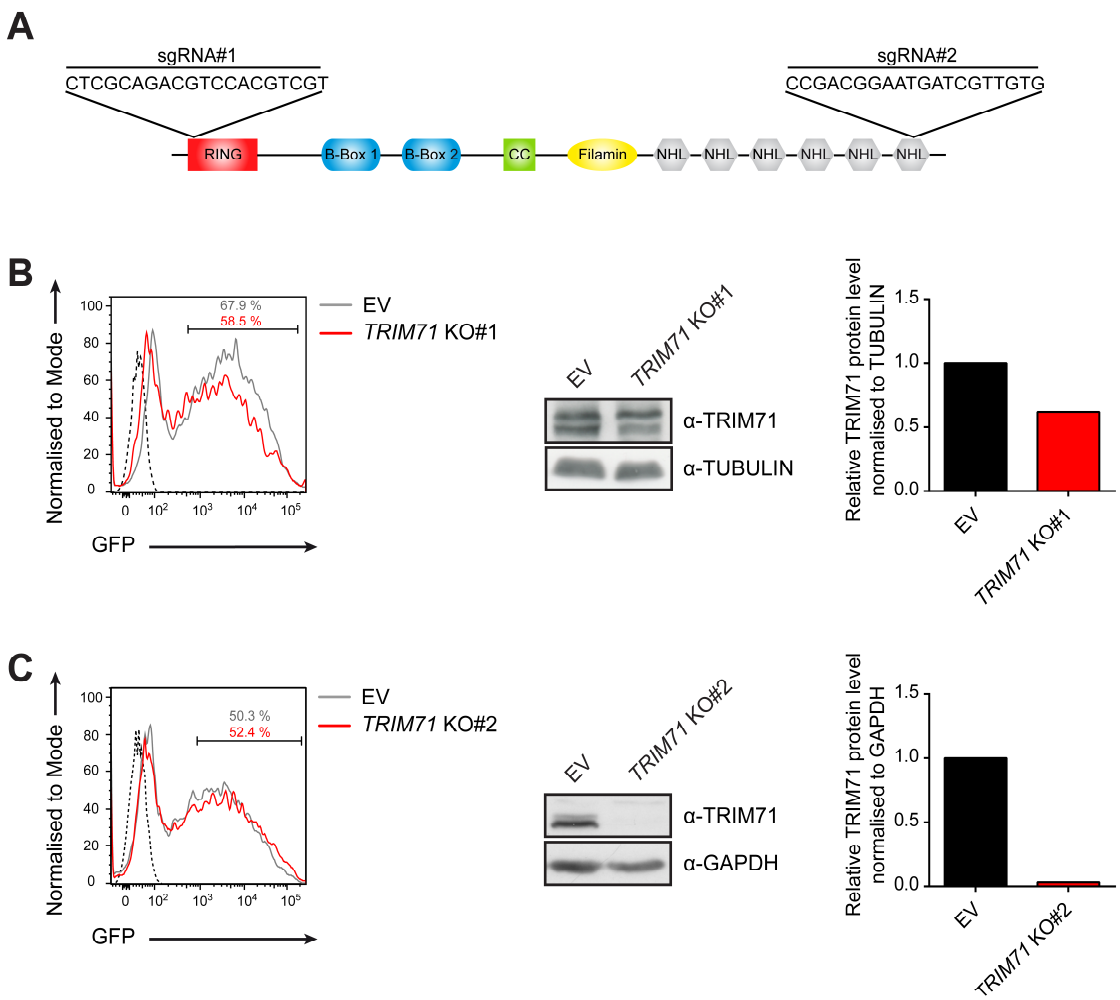

Figure 3.14 – Generation and verification of CRISPR/Cas9-mediated NCCIT *TRIM71* KO cells
(A) Scheme representation depicting the respective binding site of the two sgRNAs with sgRNA#1 targeting *TRIM71* in the RING domain shortly after ATG start codon and sgRNA#2 in the last NHL repeat. Transfection and sorting efficiency of **(B)** *TRIM71* KO#1 and **(C)** *TRIM71* KO#2 NCCIT cells. The histograms (left) show the percentage of NCCIT cells positively transfected with PX458 sgRNA#1 (58.5 %) / PX458 sgRNA#2 (52.4 %) and PX458 EV control (50.3 - 67.9 %) cells which were sorted by FACS based on the expression of the GFP reporter. Western blot (middle) and quantification (right) of TRIM71 protein level in GFP-positive sorted *TRIM71* KO#1 / *TRIM71* KO#2 and control (EV) cells. Equal loading was verified by TUBULIN or GAPDH expression.

3.3.1 *TRIM71* KO#1 single cell clones express a truncated TRIM71 protein lacking the RING domain (ΔRING)

In order to analyse the molecular functions of TRIM71 in germ cells, two single cell clones were derived from the CRISPR/Cas9-edited NCCIT *TRIM71* KO#1 bulk cell population and further characterised. CRISPR/Cas9-mediated editing of the *TRIM71* gene using sgRNA#1 was predicted to interfere with TRIM71 protein expression very early by disrupting the reading frame, thus resulting in an aberrant, mostly non-functional protein that is degraded by NMD. Sanger sequencing as well as MiSeq of the single cell clones *TRIM71* KO#1 C4 and *TRIM71* KO#1 G5 revealed a 16 bp and 19 bp deletion compared to the wild type gene,

respectively (Figure 3.15 A and Supplementary Figure S2). Both deletions caused a +1/-2 bp frameshift mutation in *TRIM71*. Against the expectation that these mutations result in a full deletion of the TRIM71 protein, Western blot analysis of the single cell clones *TRIM71* KO#1 C4 and *TRIM71* KO#1 G5 revealed the expression of a truncated TRIM71 protein (Figure 3.15 C). Using the online application StarORF provided by the Massachusetts Institute of Technology (http://star.mit.edu/orf/), it was observed that the frameshift mutation in the single cell clones *TRIM71* KO#1 C4 and *TRIM71* KO#1 G5 induced a premature stop codon shortly after the sequence coding for the RING domain (Figure 3.15 B). However, only a few amino acids downstream an in-frame ATG start codon was present. This ATG was predicted to serve as an alternative start codon generating a TRIM71 protein lacking the RING domain (TRIM71 ΔRING). According to StarORF, this truncated TRIM71 protein has a molecular weight of 83 kDa, hence being 10 kDa smaller than the full-length protein (93 kDa). This was highly consistent with the size difference observed by Western blot analysis (Figure 3.15 C). To validate these truncated TRIM71 protein variants, the DNA sequence with the 16 or 19 bp deletion was overexpressed in HEK 293 cells lacking endogenous TRIM71. Western blot analysis of these cells confirmed the presence of a truncated TRIM71 protein using anti-TRIM71 antibody (Figure 3.15 D). In addition, as the *TRIM71* sequences were cloned downstream of the sequence coding for a N-terminal FLAG-tag, FLAG-TRIM71 fusion proteins could be detected using an anti-FLAG antibody. For the *TRIM71* wild type controls EV E10 and EV G1, FLAG-TRIM71 was detected in Western blot analysis by the anti-FLAG antibody (Figure 3.15 C). However, for both *TRIM71* KO#1 C4 (Δ-16 bp) and *TRIM71* KO#1 G5 (Δ-19 bp) overexpressed sequences no FLAG-TRIM71 protein was detectable using anti-FLAG antibody. Consequently, as the FLAG-tag is N-terminal, the truncated TRIM71 protein lacked the N-terminus as predicted by StarORF and was only detectable by the anti-TRIM71 antibody. Taken together, these results confirmed the two NCCIT single cell clones *TRIM71* KO#1 C4 (Δ-16 bp) and *TRIM71* KO#1 G5 (Δ-19 bp) derived from the CRISPR/Cas9-edited bulk cell population to express a truncated TRIM71 protein lacking the N-terminal RING domain and thus, will be referred to as TRIM71 ΔRING from now on.

A

Clone	PCR-product	Δ
WT/ EV	CCTCCTCGCAGACGTCCACGTCGTCGGGGGGCGGCGGCGGGGGCCC	
***T71* KO#1 C4**	CCTCCTCGCAGACG----------GCGGCGGCGGGGGCCC	-16 bp
***T71* KO#1 G5**	CCTCCTCGCAGACGTCCACG----------GGGGCCC	-19 bp

B

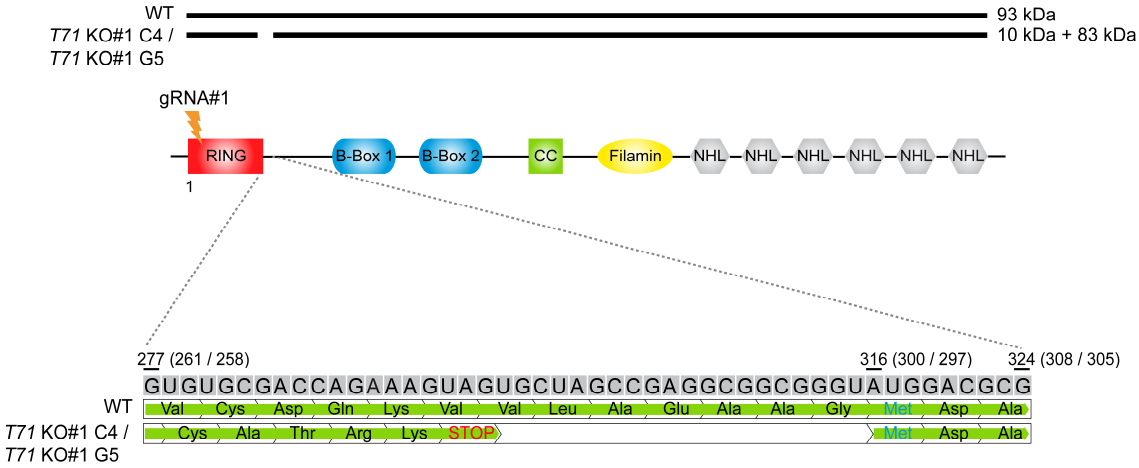

C

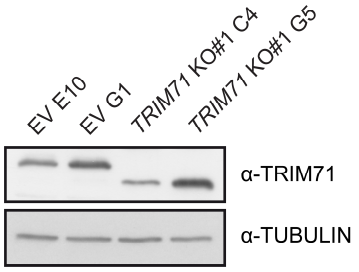

D

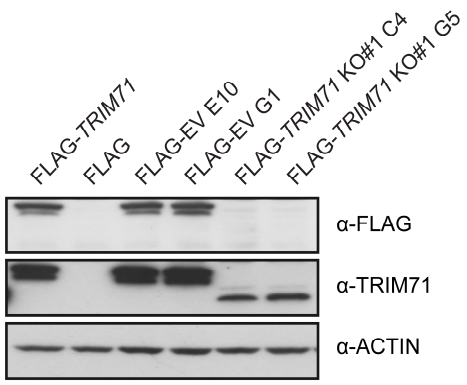

Figure 3.15 – NCCIT *TRIM71* KO#1 single cell clones are lacking the N-terminal RING domain **(A)** Alignment of wild type sequence of sgRNA#1 target locus with the sequence of edited single cell clones *TRIM71* KO#1 C4 and *TRIM71* KO#1 G5 as identified by Sanger sequencing. The sgRNA#1 target site is marked in red and deletions in the edited alleles are depicted as blue dashes. The column marked with "Δ" gives the number of deleted base pairs. **(B)** Detailed schematic representation of the sgRNA#1 target locus highlighting the frame-shift induced premature STOP codon (red) and the distance to the next alternative in-frame start codon ATG (blue) predicted by the online tool StarORF (http://star.mit.edu/orf/). The corresponding protein sizes are depicted as black lines on the top. **(C)** Representative Western blot showing the endogenous TRIM71 protein level in the NCCIT *TRIM71* KO#1 C4 and *TRIM71* KO#1 G5 single cell clones and the wild type control singe cell clones EV E10 and EV G1. **(D)** Western blot showing TRIM71 protein levels detected with antibodies against the N-terminal Flag tag and TRIM71 itself upon transient overexpression of FLAG-ctrl, *TRIM71* wild type controls (FLAG-*TRIM71*, FLAG-EV E10 and FLAG-EV G1), FLAG-*TRIM71* KO#1 C4 and FLAG-*TRIM71* KO#1 G5 in HEK293T cells. Equal loading was verified by ACTIN expression. *T71*=*TRIM71*; WT=wild type.

3.3.2 *TRIM71* KO#2 single cell clones express a TRIM71 protein with a functional deletion of the last NHL repeat (Δ6NHL)

Equally to the NCCIT *TRIM71* KO#1 single cell clones, two single cell clones were derived from the CRISPR/Cas9-edited NCCIT *TRIM71* KO#2 bulk cell population. Gene editing using the sgRNA#2 was expected to result in a TRIM71 protein with a short C-terminal truncation similar to the gene-trap mice generated by Schulman *et al.* [172]. By Sanger sequencing a 19 bp and 1 bp deletion was observed for the *TRIM71* KO#2 C5 and *TRIM71* KO#2 C8.2 single cell clone, respectively (Figure 3.16 A and Supplementary Figure S3). The online application StarORF (http://star.mit.edu/orf/) revealed that both deletions induced a shift in the ribosomal reading frame of +1/-2 bp and a premature stop codon (Figure 3.16 A). Thus, the resulting truncated TRIM71 protein was lacking the C-terminal 15 amino acids in addition to the CRISPR/Cas9-deleted codons and substituted amino acids due to the frameshift mutation. Accordingly, in the single cell clones *TRIM71* KO#2 C5 and *TRIM71* KO#2 C8.2 the C-terminal 24 or 18 amino acids were missing and/or altered, respectively. By Western blot analysis the expression of TRIM71 protein was confirmed (Figure 3.16 B). A difference in the molecular weight of the C-terminal truncated TRIM71 protein in the clones *TRIM71* KO#2 C5 and *TRIM71* KO#2 C8.2 compared to the *TRIM71* wild type controls (EV E10 and EV G1) was not apparent. This can be explained by the minor size difference of approximately 1 kDa between the full-length TRIM71 protein and the C-terminal truncations which is indistinguishable by Western blot analysis. Notably, for the *TRIM71* KO#2 C5 clone, the TRIM71 protein expression was very low to absent. Altogether, the C-terminal deletion and/or alteration of 24 or 18 amino acids in the two *TRIM71* KO#2 clones resembled the *Trim71* mutant mouse model merely lacking the C-terminal 24 amino acids by Schulman *et al.* [172]. As these mice phenocopied the complete loss of TRIM71, in both *TRIM71* KO#2 single cell clones the C-terminal truncation of the TRIM71 protein was regarded as a functional deletion of the last NHL repeat being referred to as TRIM71 Δ6NHL from now on. This nomenclature is not to be confused with the a very similar nomenclature ΔNHL6 used by Torres-Fernández *et al.* [290] which describes the complete deletion of the sixth NHL of the TRIM71 protein. In sum, these single cell clones are a powerful tool for studying the role of TRIM71 in germ cell development.

A

Clone	PCR-product	Δ
WT/ EV	TTCCGGCATCGCCATCACCCCCGACGGAATGATCGTTGTGGTGGACTTT	
***T71* KO#2 C5**	TTCC----------ACGGAATGATCGTTGTGGTGGACTTT	-19 bp
***T71* KO#2 C8.2**	TTCCGGCATCGCCATCACCCCC-ACGGAATGATCGTTGTGGTGGACTTT	-1 bp

B

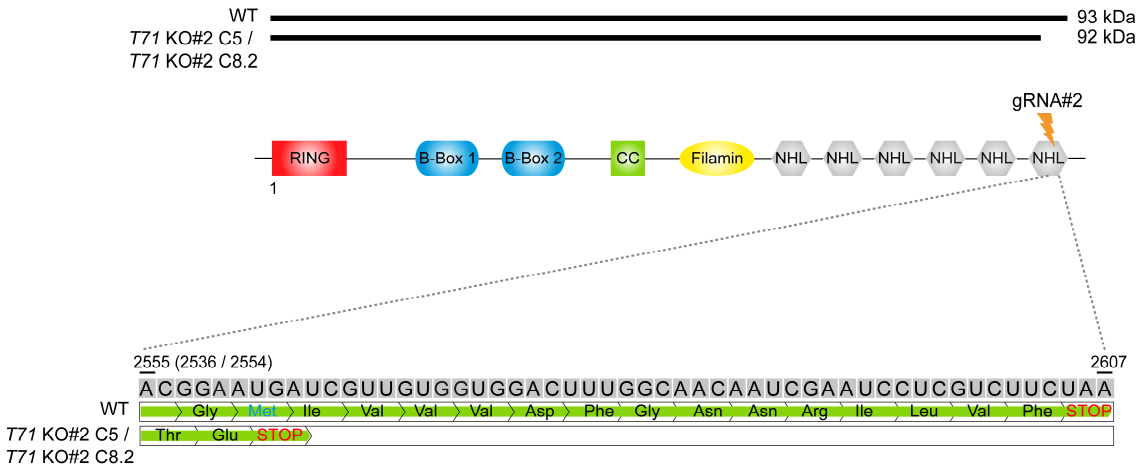

C

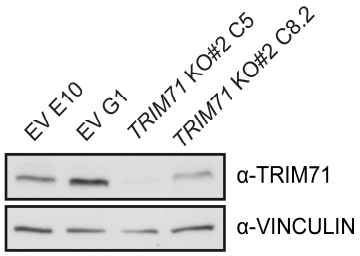

Figure 3.16 – NCCIT *TRIM71* KO#2 single cell clones are lacking the C-terminal last NHL repeat
(A) Alignment of wild type sequence of sgRNA#2 target locus with the sequence of edited single cell clones *TRIM71* KO#2 C5 and *TRIM71* KO#1 C8.2 as identified by Sanger sequencing. The sgRNA#2 target site is marked in red and deletions in the edited alleles are depicted as blue dashes. The number of deleted base pairs is given in the column marked with "Δ". **(B)** Detailed schematic representation of the sgRNA#2 target locus showing the C-terminally deleted amino acids as predicted by the online tool StarORF (http://star.mit.edu/orf/). The wild type STOP codon as well as the premature STOP codon induced by frame-shift mutation is highlighted in red. Corresponding protein sizes are depicted as black lines on the top. **(C)** Representative Western blot showing the endogenous TRIM71 protein level in the NCCIT *TRIM71* KO#2 C5 and *TRIM71* KO#2 C8.2 single cell clones and the wild type control single cell clones EV E10 and EV G1. *T71*=*TRIM71*; WT=wild type.

3.3.3 Stem cell state of NCCIT TRIM71 ΔRING and TRIM71 Δ6NHL cells is not altered

During early embryonic development Trim71 expression is restricted to undifferentiated cells, such as stem and progenitor cells [65, 246]. Trim71 is temporally and spatially regulated and is important for the stem cell maintenance, thus promoting proliferation and inhibiting premature differentiation [65]. Accordingly, decreasing Trim71 levels have been described in differentiating in mouse ESCs [39]. To investigate if premature differentiation

is induced in the NCCIT TRIM71 ΔRING and TRIM71 Δ6NHL single cell clones, the mRNA expression of classical stem cell markers *OCT4*, *SOX2*, *KLF4* and *MYC*, also known as the Yamanaka factors [278], was determined by qRT-PCR. None of the single cell mutant clones showed a significant difference in the expression level of any of the markers tested compared to wild type control cells (EV E10 and EV G1) (Figure 3.17 A-D). Consequently, all TRIM71 KO clones maintained their stem cell identity. Neither NCCIT cells lacking the N-terminal RING domain nor with a deletion in the terminal NHL repeat were prone to premature differentiation in the absence of differentiation stimuli. This was in line with Trim71-deficient mouse ESCs showing a preserved expression of typical stem cell markers [204].

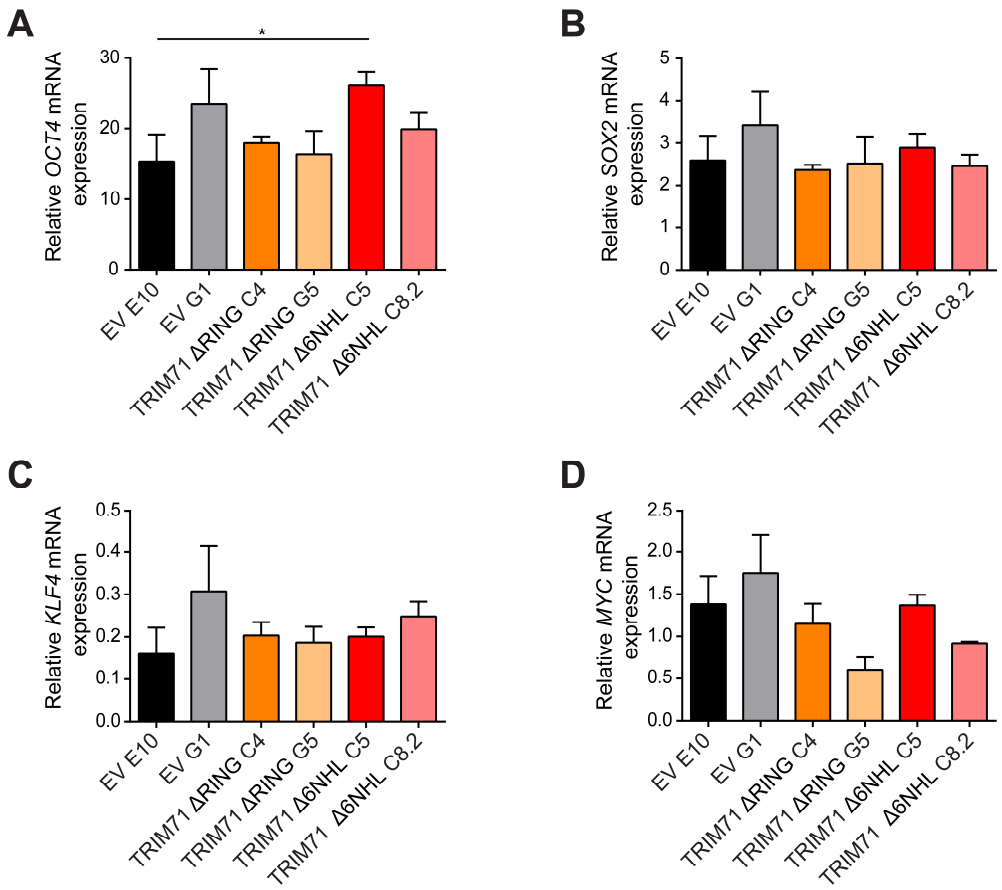

Figure 3.17 – Stem cell marker expression is not altered in NCCIT TRIM71 ΔRING and TRIM71 Δ6NHL single cell clones

Quantification of mRNA expression of the Yamanaka stem cell markers **(A)** *OCT4* (n=4), **(B)** *SOX2* (n=4), **(C)** *KLF4* (n=3) and **(D)** *MYC* (n=3) in the NCCIT TRIM71 ΔRING C4, TRIM71 ΔRING G5, TRIM71 Δ6NHL C5 and TRIM71 Δ6NHL C8.2 single cell clones as well as the respective NCCIT EV E10 and EV G1 control single cell clones by qRT-PCR. Relative mRNA expression was normalised to the housekeeping gene *HPRT1*. Error bars indicate mean ± SEM. Statistical analysis was performed by applying two-tailed unpaired t-test: *p<0.05. All other data was non-significant (p>0.05).

3.3.4 TRIM71 is a positive regulator of proliferation in the TGCT cell line NCCIT

As described in chapter 3.1, the absence of TRIM71 *in vivo* leads to a loss of gonocytes in embryonic development after E10.5 resulting in reduced testis size and infertility in adult mice. Yet, proliferation is known to be important in germ cell development both in embryogenesis and postnatal generating the foetal PGC and adult SSC pool, respectively. Here, TRIM71 might be involved as it is known to be important in stem cell maintenance by promoting proliferation and inhibiting premature differentiation [39, 41, 65]. Previously, TRIM71 has been described to repress the cell cycle inhibitor *Cdkn1a* in mouse ESC, thus promoting proliferation [39]. However, in germ cells a regulatory function of TRIM71 on proliferation has not been described and attributed to particular molecular targets, yet. Therefore, we aimed to investigate the molecular role of TRIM71 in germ cell proliferation *in vitro* using the CRISPR/Cas9-edited NCCIT TRIM71 ΔRING and NCCIT TRIM71 Δ6NHL single cell clones cells characterised in chapters 3.3.1 and 3.3.2.

3.3.4.1 Absence of the RING domain partially reduces proliferation

In order to evaluate whether the RING domain of TRIM71 contributes to the regulation of proliferation in NCCIT cells, a well-established *in vitro* proliferation assay was performed with the two NCCIT TRIM71 ΔRING C4 and TRIM71 ΔRING G5 single cell clones characterised to lack the N-terminal RING domain of TRIM71 (chapter 3.3.1). The fluorescent intensity of these cells stained with the proliferation dye eFluor670 was monitored by FACS every 24 h for 4 days. In general, a progressive loss of fluorescence intensity was observed overtime as a result of cell proliferation as depicted in Figure 3.18 A and B. Strikingly, the loss of fluorescence intensity was significantly delayed at day 4 for the single cell clone TRIM71 ΔRING C4. Consequently, also the number of cell divisions calculated as described in chapter 2.2.3.11 by assuming that the MFI is halved with every cell division, was significantly decreased in this single cell clone with a significant prolongation of the cell cycle of approximately 2.5 h which is equal to a 16 % reduction in proliferation (Figure 3.18 C and D). For the single cell clone TRIM71 ΔRING G5 a decreased proliferation was only observed by tendency.

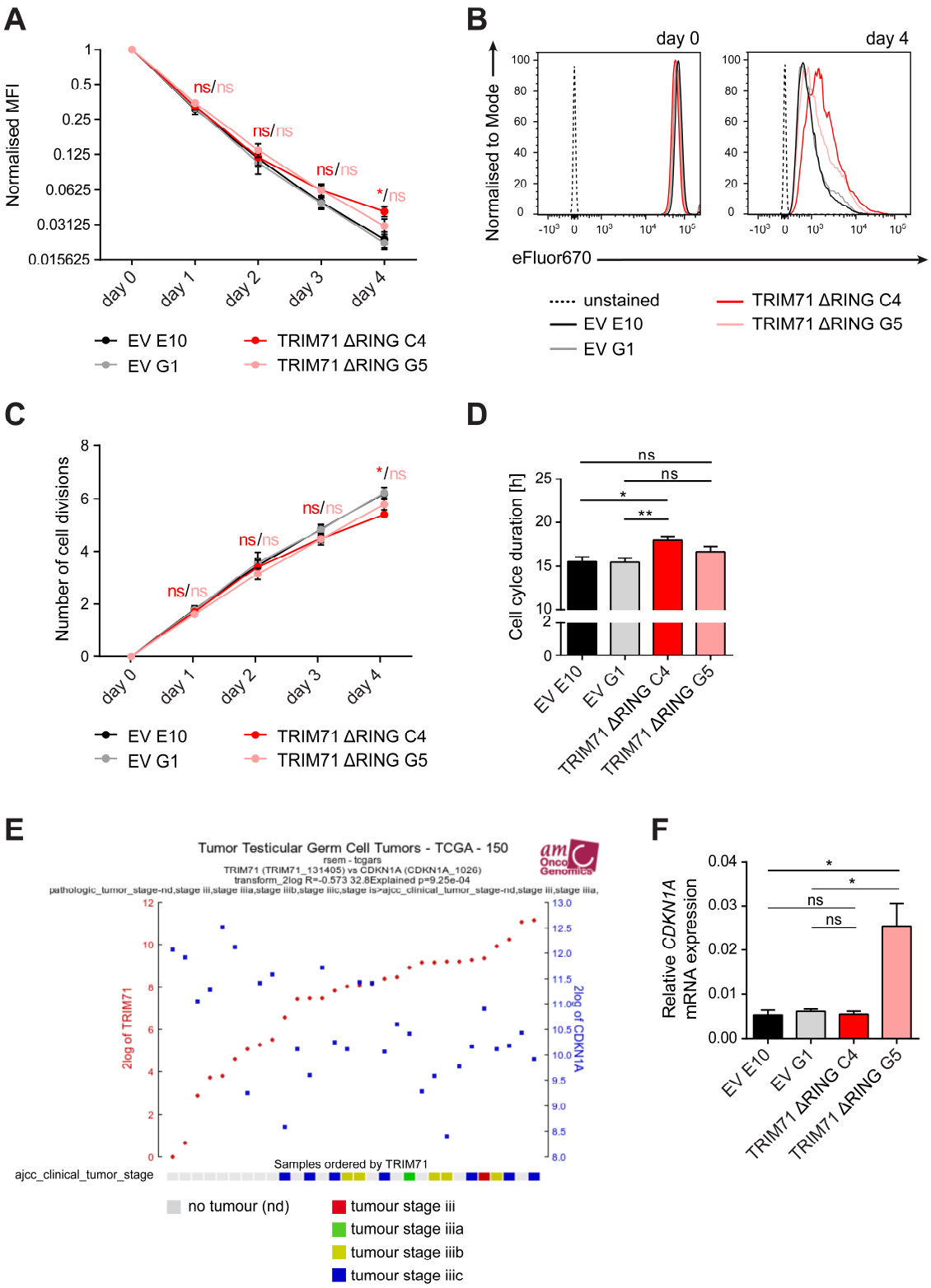

Figure 3.18 – NCCIT TRIM71 ΔRING single cell clones show a mild proliferation defect
(A) eFluor670 dye fluorescence intensity decline upon proliferation of NCCIT TRIM71 ΔRING and EV control single cell clones (n=4). MFI = mean fluorescence intensity of eFluor670. **(B)** Representative overlap of eFluor670 histograms of NCCIT TRIM71 ΔRING and EV control single cell clones with similar staining for the different single cell clones at the start of the experiment (day 0: left panel) and stronger fluorescence staining of the NCCIT TRIM71 ΔRING single cell clones at the end of the proliferation assay (day 4; right panel) due to reduced proliferation. **(C)** Number of cell divisions NCCIT TRIM71 ΔRING and EV control single cell clones have passed through over the

given time period (n=4). The number of cell divisions was calculated as described in chapter 2.2.3.11 assuming that the MedFI is halved with each cell division. **(D)** Average cell cycle duration in hours (h) calculated from the number of cell divisions at the end of the proliferation experiment (day 4) for the NCCIT TRIM71 ΔRING and EV control single cell clones (n=4). **(E)** Negative correlation between *TRIM71* and *CDKN1A* mRNA expression in samples of patients with advanced stage testicular germ cell tumours (Source: R2 Genomics Analysis and Visualization Platform (http://r2.amc.nl); The Cancer Genome Atlas (TCGA) dataset). **(F)** Relative *CDKN1A* mRNA expression measured by qRT-PCR in NCCIT TRIM71 ΔRING and EV control single cell clones (n=3). The housekeeping gene *HPRT1* was used for normalisation. In A, C, D and F the error bars indicate mean ± SEM and statistical analysis was performed using two-tailed unpaired t-test: ns=non-significant (p>0.05); *p<0.05**; p<0.01. In A and C statistics are only shown for the comparison of the NCCIT TRIM71 ΔRING single cell clones with the NCCIT EV E10 wild type control single cell clone as the two control single cell clones behave very similar.

TRIM71 has been described as a mRNA binding protein [141]. Previously, Chang et al. [39] reported the cell cycle inhibitor Cdkn1a to be repressed by Trim71 at mRNA level in mouse ESCs, thereby promoting proliferation. Later studies of our group extended these findings to several human cells and suggested that TRIM71-mediated CDKN1A regulation is involved in controlling proliferation of hepatocellular carcinoma cells [290]. Confirming this, a negative correlation of *CDKN1A* mRNA with highly expressed TRIM71 in advanced TGCT stages was identified using the R2 Genomics Analysis and Visualization platform (http://r2.amc.nl) (Figure 3.18 E). As of yet an E3 ligase activity has been assigned to the RING domain whereas the NHL domain functions as a mRNA repressor [65]. Nevertheless, regulation of *CDKN1A* mRNA by the NHL domain may also require the presence of the RING domain in regard to TRIM71's 3D protein structure and folding or the recruitment of other proteins. Therefore, *CDKN1A* mRNA levels were determined by qRT-PCR in the two NCCIT TRIM71 ΔRING single cell clones (Figure 3.18 F). Controversially, a strong upregulation of *CDKN1A* was only apparent for the NCCIT TRIM71 ΔRING G5 single cell clone for which the cell cycle was not prolonged significantly. No change in *CDKN1A* expression was present in TRIM71 ΔRING C4 cells with a reduced proliferation. In sum, these results suggest that the RING domain has only a mild contribution to TRIM71's function controlling the proliferation of NCCIT cells. This supporting function by the RING domain is presumably not via *CDKN1A* repression confirming the finding by Loedige *et al.* [157] that the RING domain of TRIM71 is not required for target mRNA repression.

3.3.4.2 Last C-terminal NHL repeat of TRIM71 is important for cell proliferation

As evaluated in the previous experiment, the RING domain of TRIM71 is only partially involved in the proliferation control in germ cells. Thus, the role of the other TRIM71 domains is of importance in the context of proliferation regulation in germ cells. Especially the NHL domain of TRIM71 is of high interest as in *C. elegans* the vast majority of loss of function mutations in TRIM71 reside in the NHL domain [265]. Moreover, in mice the deletion of the

last NHL repeat phenocopies the complete loss of TRIM71 [172]. Therefore, the two NCCIT TRIM71 Δ6NHL clones, characterised with a functional deletion of the last NHL repeat (chapter 3.3.2), were analysed in more detail. In *in vitro* eFluor670 proliferation assays the continuous loss of fluorescence intensity due to cell proliferation was significantly less for both TRIM71 Δ6NHL clones (Figure 3.19 A and B). Hence, these clones also displayed a reduced number of cell divisions associated with a prolonged cell cycle by 2 h (TRIM71 Δ6NHL C4) to 4 h (TRIM71 Δ6NHL C8.2) (Figure 3.19 C and D). This corresponded to a decrease in proliferation of up to 27 % and thus, being more prominent than in the TRIM71 ΔRING NCCIT single cell clones.

In mammalian TRIM71 as well as in the ortholog proteins LIN-41 (*C. elegans*), Brat (*D. melanogaster*) and Trim71 (*D. rerio*) the NHL domain has been described to directly interact with RNAs [3, 137, 141, 158, 159, 290]. More specifically, a direct interaction of the TRIM71 NHL domain with *CDKN1A* requiring a stem-loop structural motif within the *CDKN1A* 3'UTR has been reported [290]. In mouse ESCs as well as hepatocellular carcinoma cells, a recognition of the *CDKN1A* 3'UTR by TRIM71 was shown to repress *CDKN1A* mRNA, thereby promoting proliferation [39, 290]. To investigate whether the recognition of *CDKN1A* mRNA by the TRIM71 NHL domain and its repression is conserved in germ cells, CDKN1A mRNA and protein levels were determined by qRT-PCR and Western blot, respectively, in the two NCCIT TRIM71 Δ6NHL single cell clones. Corresponding to the reduction on proliferation, a significant upregulation of CDKN1A was observed for both TRIM71 Δ6NHL clones (Figure 3.19 E and F). The NCCIT TRIM71 Δ6NHL C8.2 single cell clone with the slowest proliferation showed the highest CDKN1A expression. Taken together, these results imply that also in germ cells the last NHL repeat of TRIM71 is important in controlling proliferation with CDKN1A possibly being the molecular switch.

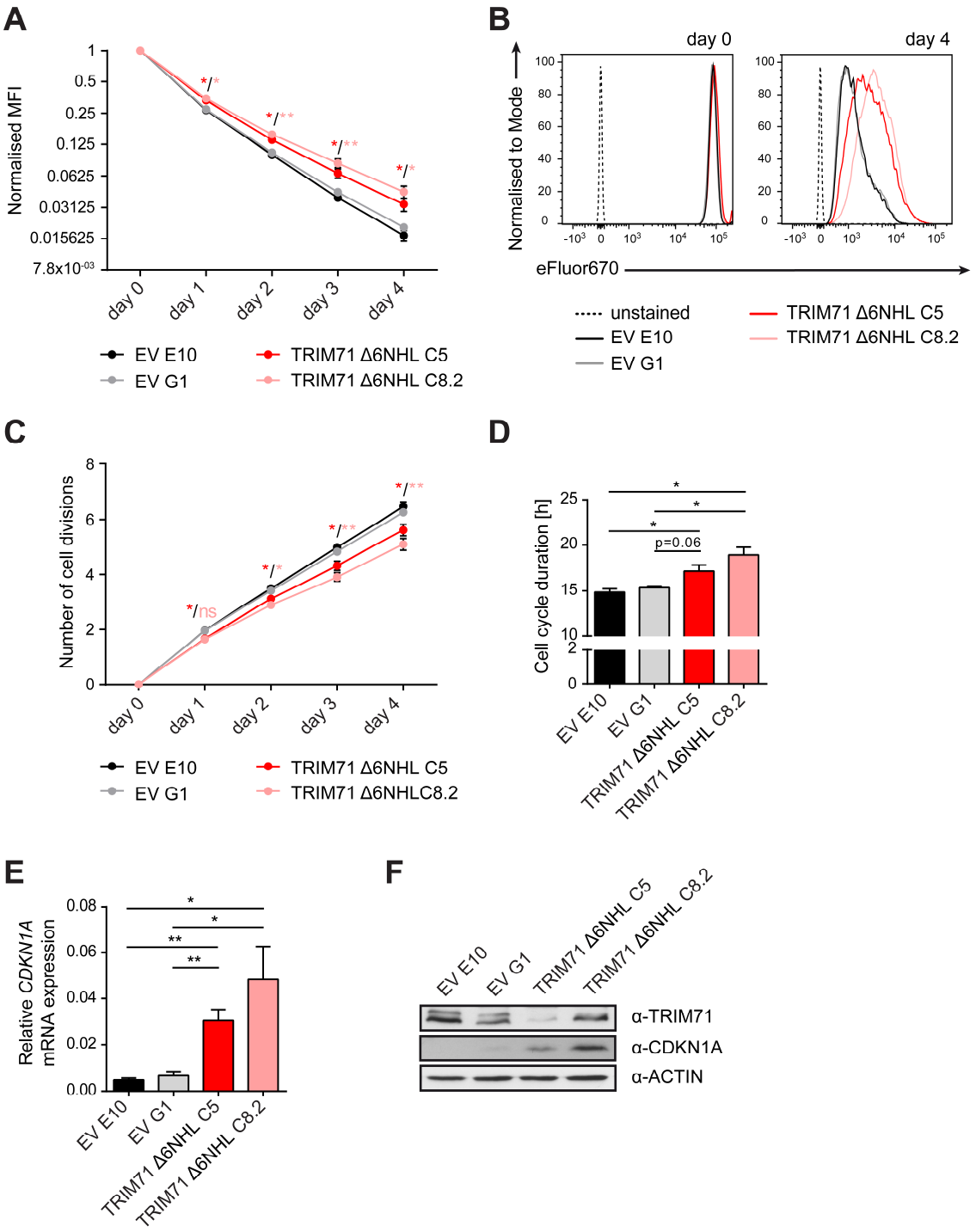

Figure 3.19 – The last NHL repeat is important for proliferation in NCCIT cells
(A) eFluor670 dye fluorescence intensity decline upon proliferation of NCCIT TRIM71 Δ6NHL and EV control single cell clones (n=3). MFI = mean fluorescence intensity of eFluor670. **(B)** Representative overlap of eFluor670 histograms of NCCIT TRIM71 Δ6NHL and EV control single cell clones with similar staining for the different single cell clones at the start of the experiment (day 0: left panel) and stronger fluorescence staining of the NCCIT TRIM71 Δ6NHL single cell clones at the end of the proliferation assay (day 4; right panel) due to decreased proliferation. **(C)** Number of cell divisions NCCIT TRIM71 Δ6NHL and EV control single cell clones have passed through over the given time period (n=3). The number of cell divisions was calculated as described in chapter 2.2.3.11 assuming that the MedFI is halved with each cell division. **(D)** Average cell cycle duration in hours (h) calculated from the number of cell divisions at the end of the proliferation experiment (day 4) for the NCCIT TRIM71 Δ6NHL and EV control single cell clones (n=3). **(E)** Relative *CDKN1A* mRNA

expression measured by qRT-PCR in NCCIT TRIM71 Δ6NHL and EV control single cell clones (n=3). The housekeeping gene *HPRT1* was used for normalisation. **(F)** Western blot showing CDKN1A protein level in TRIM71 Δ6NHL and EV wild type control single cell clones. Equal loading was verified by ACTIN expression. In A, C, D and E the error bars indicate mean ± SEM and statistical analysis was performed by applying two-tailed unpaired t-test: ns=non-significant ($p>0.05$); *$p<0.05$; **$p<0.01$. In A and C statistics are only shown for the comparison of the NCCIT TRIM71 ΔRING single cell clones with the NCCIT EV E10 wild type control single cell clone as both control single cell clones behaved very similar.

3.3.5 TRIM71 Δ6NHL mutation results in increased sensitivity for apoptosis in NCCIT cells

Cell cycle arrest is known to not only result in reduced proliferation but also to induce controlled cell death. As of yet, in NCCIT TRIM71 ΔRING and NCCIT TRIM71 Δ6NHL single cell clones a retarded proliferation has been discovered (chapter 3.3.4). However, up to this point, it cannot be excluded that the proliferation defect observed in these single cell clones results from an enhanced apoptosis. Therefore, to investigate whether the reduced proliferation in the absence of the RING domain and/or the C-terminal 18 or 24 amino acids of the TRIM71 protein is accompanied by an increased cell death, the well-established Annexin V/7-AAD apoptosis assay was performed on the NCCIT TRIM71 ΔRING and NCCIT TRIM71 Δ6NHL single cell clones. For neither the two NCCIT TRIM71 ΔRING nor the two NCCIT TRIM71 Δ6NHL single cell clones a difference in the amount of late apoptotic or necrotic (Annexin V^+/7-AAD^+) cells compared to the EV wild type control (NCCIT EV E10 and NCCIT EV G1) was observed (Figure 3.20 A and B). Though, a significantly increased percentage of NCCIT TRIM71 Δ6NHL C5 and NCCIT TRIM71 Δ6NHL C8.2 cells were early apoptotic (Annexin V^+/7-AAD^-) (Figure 3.20 A and B). In NCCIT TRIM71 ΔRING C4 and NCCIT TRIM71 ΔRING G5 cells the percentage of early apoptotic cells was only increased by tendency congruent with the only mild decrease in NCCIT *TRIM71* KO#1 (ΔRING) cells (chapter 3.3.6) and the partial reduction of proliferation (chapter 3.3.4) observed.

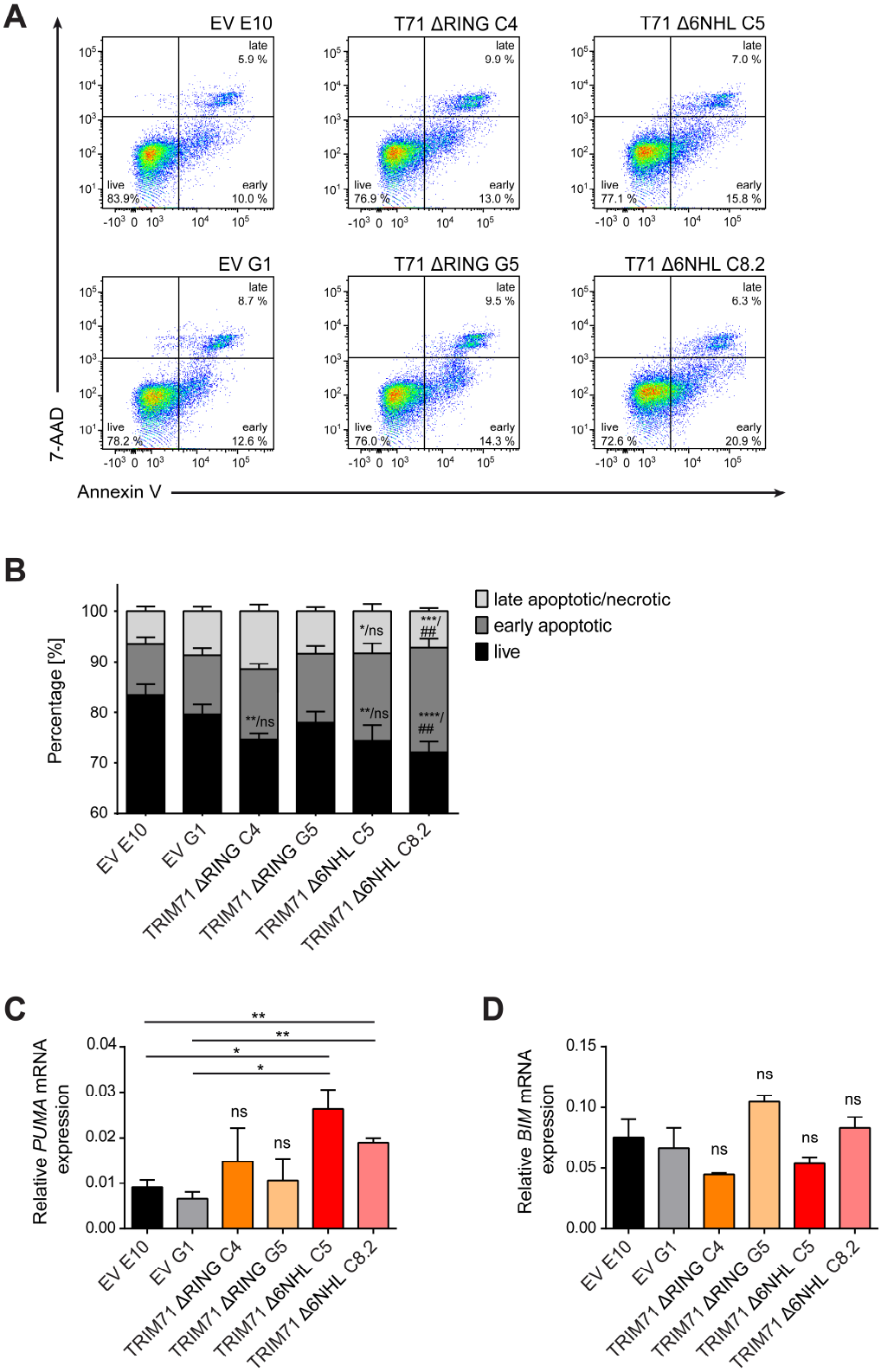

Figure 3.20 – NCCIT TRIM71 Δ6NHL single cell clones are prone towards apoptosis
(A) Representative pictures of flow cytometric identification of live (Annexin V$^-$/7-AAD$^-$), early apoptotic (Annexin V$^+$/7-AAD^{--}) and late apoptotic/necrotic (Annexin V$^+$/7-AAD^{-+}) cells in the NCCIT TRIM71 ΔRING, TRIM71 Δ6NHL and wild type control NCCIT EV single cell clones. Indicated percentages of the subpopulations are within the parental populations. T71=TRIM71. **(B)** Percentages of live, early apoptotic and late apoptotic/necrotic cells within NCCIT TRIM71 ΔRING, TRIM71 Δ6NHL and wild type control NCCIT EV single cell clones investigated by

flow cytometric analysis of Annexin V and 7-AAD$^-$ staining exemplary depicted in A (n≥4). Error bars indicate mean ± SEM. Statistical analysis was performed by applying two-way ANOVA with Dunnetts multiple comparisons post hoc test setting NCCIT EV E10 (*) or EV G1 (#) single cell clone as control: ns=non-significant (p>0.05); */#p<0.05; **/##p<0.01; ***/###p<0.001; ****/####p<0.0001. (C and D) Relative **(C)** *PUMA* and **(D)** *BIM* mRNA expression measured by qRT-PCR in NCCIT TRIM71 ΔRING, TRIM71 Δ6NHL and wild type control NCCIT EV single cell clones (n=3). Relative mRNA expression was normalised to the housekeeping gene *HPRT1*. Error bars indicate mean ± SEM. Statistical significance was testes by two-tailed unpaired t-test: ns=non-significant (p>0.05); *p<0.05; **p<0.01.

Previous studies have shown that TRIM71 targets p53 for degradation via ubiquitination, thereby dampening p53-dependent apoptosis [204]. p53 induces cell death in part by direct transcriptional activation of the pro-apoptotic factor *Puma*. In our experiments, the level of *PUMA* mRNA was significantly enhanced in both NCCIT TRIM71 Δ6NHL single cell clones while being unchanged in the two NCCIT TRIM71 ΔRING single cell clones (Figure 3.20 C). Yet, the expression of *BIM* mRNA, a p53 non-transcriptional pro-apoptotic target, was not altered in any of the NCCIT TRIM71 ΔRING and NCCIT TRIM71 Δ6NHL single cell clones (Figure 3.20 D). Noteworthy, NCCIT cells have been described to be hemizygous for p53 and encoding a truncated p53 protein of 347 amino acids [33]. Thus, the upregulation of *PUMA* mRNA and the induction of apoptosis might not be p53-dependent similar to what has been described when applying a variety of apoptotic stimuli to TGCT cell lines [34, 35]. Overall, these results suggest that NCCIT cells lacking the C-terminal 18 amino acids of the TRIM71 protein are more sensitive for apoptosis. Hence, the last NHL repeat is important for the inhibition of apoptosis.

3.3.6 TRIM71 is a regulator of cell population maintenance in the TGCT cell line NCCIT

Maintenance of a cell population is relying on the balance between cell proliferation and apoptosis. The previous results described TRIM71 to be involved in both of these cellular processes (chapters 3.3.4 and 3.3.5). However, the results were obtained using CRISPR/Cas9-edited NCCIT single cell clones which have been unintentionally pre-selected based on their proliferation and survival behaviour. Due to this fact, they might falsify the actual molecular functions of TRIM71 in germ cells. Therefore, so called growth assays were performed with the two NCCIT bulk cell populations, *TRIM71* KO#1 (ΔRING) and *TRIM71* KO#2 (Δ6NHL), over a period of 21 days. A highly innovative method including Illumina MiSeq analysis was used as a read out of the assay. By this, not only proliferation, but the complete population dynamic is investigated over the given time period. A further advantage of this assay is the unbiased analysis of a whole cell population, not relying on

pre-selected single cell clones. Moreover, also mild effects on cell populations are visible. In general, the analysis is based on the presence of single reads obtained by MiSeq at certain time points. These are categorised according to their sequence as wild type, frame-shift mutations (resulting in *TRIM71* KO) and in-frame mutations. The latter are comprising mutations that can result in the expression of a mutated as well as wild type protein, however indistinguishable on genomic level. Therefore, they were not considered in the analysis of the population dynamics. Comparing changes in the distribution of single reads for wild type and with frame-shift mutations over time, gives some indication of the growth behaviour of the cell population. Hence, the cell population with a growth advantage displays a percental increase in the respective single cell reads and *vice versa*. If neither of the cell populations have a growth advantage, the distribution of the allele frequencies remains constant over the given time period.

First, it was tested whether PCR amplification as a part of the sample preparation, might have an influence on the allele frequencies obtained by MiSeq. For this purpose, the isolated genomic DNA of the FACS sorted *TRIM71* KO cell population and EV cell population was mixed in three different ratios: 1:1, 4:1, and 1:4 (Figure 3.21 A). This was performed for both TRIM71 ΔRING and TRIM71 Δ6NHL cell population. Sample preparation and MiSeq analysis was carried out with these DNA mixtures and the corresponding unmixed samples as described in chapter 2.2.1.21. The obtained allele frequencies for the mixed samples are illustrated in Figure 3.21 C and for the unmixed samples as respective day 0 samples in Figure 3.22 A and Figure 3.23 A. Remarkably, for both *TRIM71* KO cell populations the percentage of alleles with frame-shift mutations was not 100 % (Figure 3.22 A and Figure 3.23 A). Instead, they contained a significant amount of non-edited wild type alleles which was highly congruent with the TRIM71 protein expression observed in these samples. Consequently, when mixing the DNA of these *TRIM71* KO cell populations with EV cells, the expected theoretical distribution of allele frequencies needed to be adjusted based on the percentage of CRISPR/Cas9-edited and wild type alleles present in the respective starting populations (Figure 3.21 B). When comparing the single reads for wild type and with mutations (frameshift and in-frame) obtained by MiSeq analysis for the DNA mixtures (Figure 3.21 C) with the corrected theoretical distribution of allele frequencies (Figure 3.21 B), the difference for all three *TRIM71* KO cell populations was mostly below 10 %. Thus, concluding that PCR amplification of none of the two *TRIM71* KO loci influences the allele frequencies in MiSeq analysis.

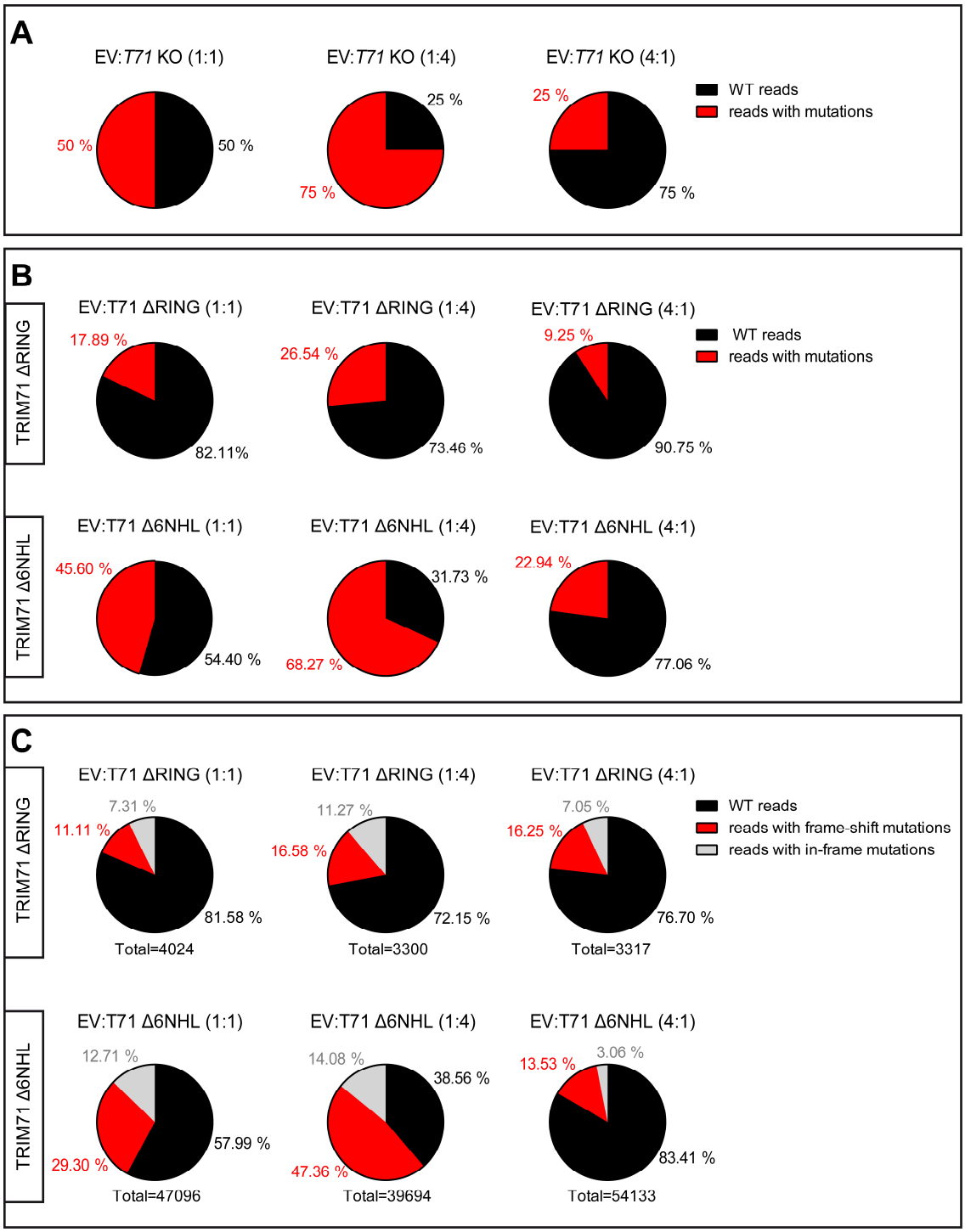

Figure 3.21 – Allele frequencies in MiSeq analysis is not influenced by PCR amplification of neither *TRIM71* KO loci

(A) Pie charts illustrating the three different mixing ratios (1:1 (left), 1:4 (middle), 4:1 (right)) of the GFP-positive FACSed *TRIM71* KO cell (red) and EV (black) control cell population. **(B)** Expected theoretical distribution of allele frequencies (wild type (black) *versus* mutation (red)) adjusted based on the percentage of CRISPR-edited and wild type alleles actually present in the respective unmixed populations of TRIM71 ΔRING (top) / TRIM71 Δ6NHL (bottom) and EV control cells. **(C)** Allele frequencies for wild type (black) and mutations (frameshift (red) and in-frame(grey)) obtained by MiSeq analysis of NCCIT TRIM71 ΔRING (top) / NCCIT TRIM71 Δ6NHL (bottom) and NCCIT EV control cells mixed in the ratios mentioned in A.

Next, as the system was proven to be robust, the effect of Trim71 deficiency on the growth behaviour of a cell population was analysed by MiSeq. This was performed by evaluating changes in the distribution of single reads for wild type and frame-shift mutations (*TRIM71* KO) over a time period of three weeks. In order to investigate the growth difference of Trim71-deficient compared to wild type cells, NCCIT *TRIM71* KO and EV cells were mixed in a 1:1 ratio: Thus, generating a growth competition between the two cell populations. The MiSeq results of samples on day 0, 3, 7, 14 and 21 are depicted for TRIM71 ΔRING and TRIM71 Δ6NHL in Figure 3.22 and Figure 3.23, respectively.

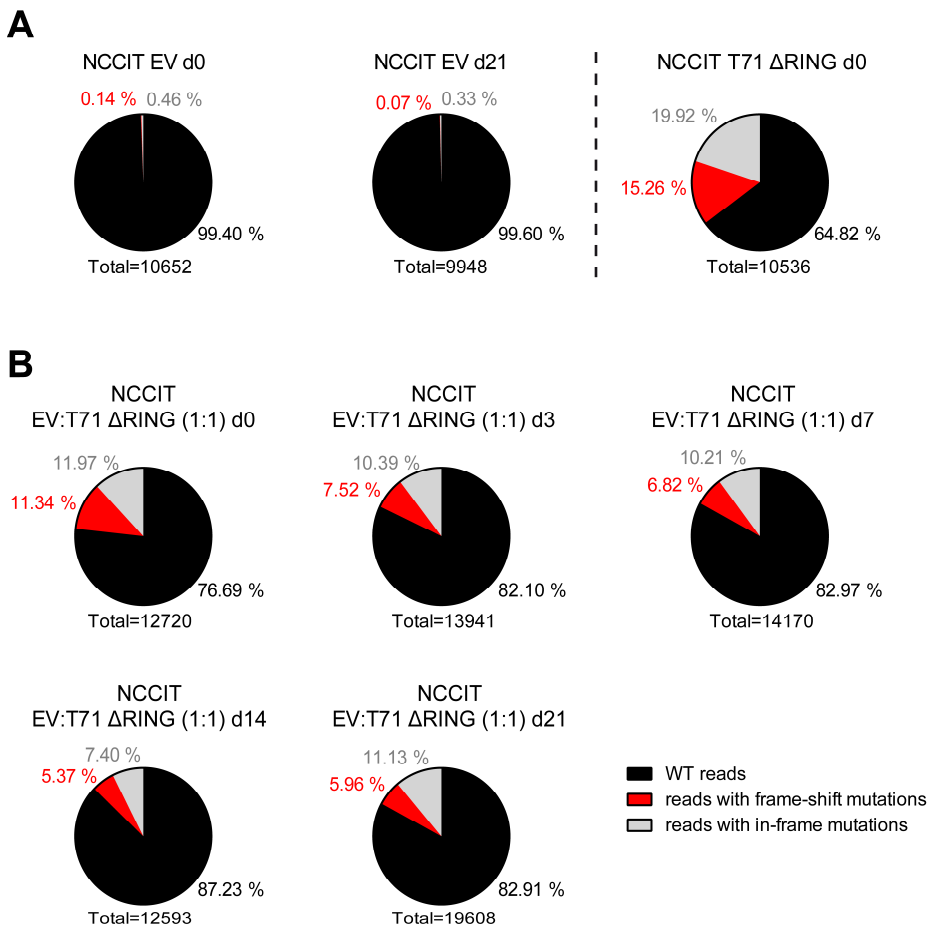

Figure 3.22 – Minor decline of the NCCIT TRIM71 ΔRING cell population upon competition with wild type cells
(A) Internal control of the growth assay displaying the percentage of wild type (black) and CRISPR-edited (frameshift (red) and in-frame (grey)) alleles present in the unmixed TRIM71 ΔRING (right) and EV control (left) cell starting population at d0 and d21 (EV only; middle). **(B)** Allele frequencies for wild type (black), TRIM71 ΔRING (frame-shift mutations; red) and in-frame mutations (grey) obtained at d0, d3, d7, d14 and d21 of the growth assay by MiSeq analysis. For the assay, NCCIT TRIM71 ΔRING and EV control cells from A were mixed in a 1:1 ratio.

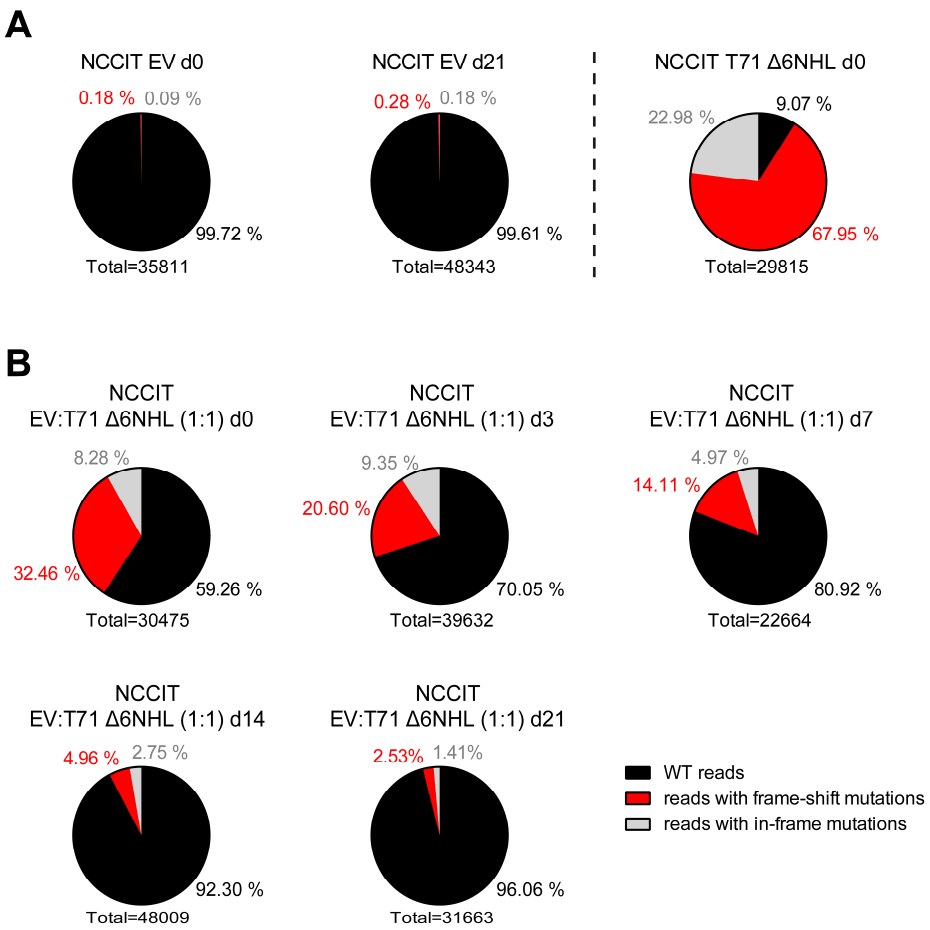

Figure 3.23 – Large decline of the NCCIT TRIM71 Δ6NHL cell population upon competition with wild type cells
(A) Internal control of the growth assay depicting the percentage of wild type (black) and CRISPR-edited (frameshift (red) and in-frame (grey)) alleles present in the unmixed TRIM71 Δ6NHL (right) and EV control (left) cell starting population at d0 and d21 (EV only; middle). **(B)** Allele frequencies for wild type (black), TRIM71 Δ6NHL (frame-shift mutations; red) and in-frame mutations (grey) obtained at d0, d3, d7, d14 and d21 of the growth assay by MiSeq analysis. For the assay, NCCIT TRIM71 Δ6NHL and EV control cells from A were mixed in a 1:1 ratio.

As an internal control, in both experiments a respective pure NCCIT EV cell population was cultivated and analysed at day 0 and day 21 (Figure 3.22 A and Figure 3.23 A). For this population, no change in the distribution of wild type and *TRIM71* KO reads was observed over the 21 days, confirming the assay reliability. Notably, in both experiments the percentage of CRISPR/Cas9-edited TRIM71 alleles present in the starting population was not as expected 50 % when mixing NCCIT *TRIM71* KO and EV cells in a 1:1 ratio. As before, this can be explained primarily by the FACS purity and to a minor extent by the Cas9 efficiency. Nevertheless, a mild change in allele distribution was observed in NCCIT TRIM71 ΔRING *versus* EV cells (Figure 3.22 B). The percentage of NCCIT TRIM71 ΔRING cells present in the population was halved (11.34 % to 5.96 %) within 21 days. A starting decrease in NCCIT TRIM71 ΔRING cells was already apparent at day 3 of analysis. In contrast, a much stronger change in population dynamic was observed for NCCIT

TRIM71 Δ6NHL *versus* EV cells (Figure 3.23 B). After 21 days TRIM71 Δ6NHL cells accounted for only 2.53 % of the cell population. This corresponded to less than a tenth of the starting population (32.46 %). Already at day 3 of analysis, the percentage of NCCIT TRIM71 Δ6NHL cells present in the population decreased by a third (32.46 % to 20.60 %). As this assay is analysing a population dynamic, the decrease observed in the *TRIM71* KO cell population can be resulting from a proliferation defect, differentiation, apoptosis or even a combination of these. However, by microscopic analysis (data not shown) no distinctive morphological changes or increase in floating dead cells was observed in NCCIT *TRIM71* KO compared to EV cells which would hint at differentiation or apoptosis, respectively. This is affirming the observations for the NCCIT TRIM71 ΔRING and TRIM71 Δ6NHL single cell clones which displayed no difference in stemness (chapter 3.3.3) but a decreased proliferation (chapter 3.3.4) combined with an enhanced sensitivity towards apoptosis (chapter 3.3.5). Finally, these results indicate that TRIM71 is predominantly important for germ cell maintenance by *in vitro* promoting proliferation and inhibiting apoptosis in both RING and 6NHL mutant NCCIT cells, with the NHL mutant effects being much stronger

4 Discussion

Over the last years, TRIM71 has attracted increasing attention in scientific research especially in regard to cancer and neurological disorders. So far, in adult tissues and organs, TRIM71 expression has only been described in ependymal cells of the brain [51] and in the testes [246] of mice. Whereas *Trim71* homozygous knockout mice are embryonically lethal and show a neural tube closure defect [41, 172], the germline specific knockout of *Trim71* causes sterility [187]. Yet, the molecular functions of TRIM71 in these tissues are still mostly unknown as investigations have been conducted primarily with regard to pluripotency regulation in mouse ESCs [39, 157].

In the context of this study, it is of importance that PGCs, the precursors of sperm and oocytes, share many characteristics with pluripotent cells such as ESCs. These features comprise indefinite proliferation as well as contribution to every cell type in the chimeric embryo, inclusively the germline, after re-transplantation into blastocyst [62, 142, 180, 234, 273]. Moreover, *in vivo* PGCs are able to spontaneously form teratomas, tumours containing multiple differentiated cell types from all three primary germ layers, – a hallmark of pluripotent cells [175]. In the present study we therefore asked whether TRIM71 is involved similarly in germ cell development as in somatic lineage development. By histological analysis of germline-specific TRIM71-deficient mice, we could observe that the absence of TRIM71 results in a lack of gonocytes with only Sertoli cells (somatic cells nourishing the immature sperm) lining the seminiferous tubules - a deficiency in humans termed Sertoli-cell-only (SCO) syndrome. This phenotype we found to be apparent in neonatal mice as early as P0.5. Using the germ cell tumour cell line NCCIT as a surrogate model, the CRISPR/Cas9-mediated specific deletion of the RING domain or the last C-terminal 18-24 amino acids of the TRIM71 protein reduced proliferation and increased the sensitivity towards apoptosis with more dramatic effects in the latter. Based on these findings, we conclude that TRIM71 is required in germ cell development by regulating the balance of proliferation and apoptosis, and thus maintaining the stem cell pool.

4.1 TRIM71 is critical for germ cell development

The expression of TRIM71 in adult testes of mice was first discovered by Rybak *et al.* [246]. Previous studies have detected a TRIM71 expression in the small population of spermatogonial stem cells (SSCs), the stem cell niche of the male reproductive organ where self-renewal and differentiation is tightly regulated spatially and temporally [187]. As homozygous *Trim71* knockout mice have been described to be embryonic lethal with embryos dying between E9.5 and E11.5 [41, 172], germline-specific TRIM71-deficient mice were generated by crossing *Trim71*$^{fl/fl}$ females with heterozygous *Trim71*$^{-/+}$*; Nanos3*$^{Cre/+}$

male mice expressing the *Cre* recombinase under the control of the endogenous germ cell-specific *Nanos3* promotor (Figure 3.1). NANOS3 is an RBP expressed in PGCs after their specification (~E7.75) until shortly after their settlement in the genital ridges at E14.5. Only in males it is re-expressed postnatally (P1.5) in the testes [291] with the *Nanos3*-Cre mouse line exhibiting almost 100 % recombination in male gonocytes after birth [276]. Previously, our group has found that germline-specific deletion of TRIM71 leads to infertility in mice [187]. This was validated as part of this study by the drastically reduced testis weight and size (Figure 3.2) as well as by the absence of SSC marker genes expression observed in *Trim71*$^{-/fl}$; *Nanos3*$^{Cre/+}$ mice (Figure 3.6). Histological observations in adult mice further confirmed this phenotype by the almost complete absence of germ cells associated with a SCO syndrome in germline-specific TRIM71-deficient mice (Figure 3.3, Figure 3.4 and Figure 3.5). The fact that we already observed a lack of germ cells in testes of neonatal *Trim71*$^{-/fl}$; *Nanos3*$^{Cre/+}$ mice at P0.5 (Figure 3.7, Figure 3.8 and Figure 3.9), suggests TRIM71-induced defects to be of embryonic origin. Hence, the expression of TRIM71 seems to be crucial for embryonic germ cell development.

Similar to our findings in *Trim71*$^{-/fl}$; *Nanos3*$^{Cre/+}$ mice, a loss of PGCs has been described in BLIMP1 [212, 249, 299] and PRDM14 [313] -deficient mice during embryonic development. With both Blimp1 and Prdm14 being essential for PGC specification as early as E6.25/E6.5 [212, 299, 313], TRIM71 function could also be important in such an early developmental step. However, it has been shown by our group that TRIM71-deficient PGCs are specified in the embryo and start migrating along the hindgut to the genital ridges [187]. Although the PGCs are predicted to reach the genital ridges, it is known that the survival of migrating PGCs depends on Steel/c-Kit signalling and PGCs are lost by apoptosis upon the absence of Steel expression [244, 272]. On the one hand, as male germ cells become mitotically arrested at E13.5 [100, 307] and do not undergo meiosis until after birth [182, 197, 245], the loss of PGCs is assumed between E10.5 and E13.5. Shortly before and after settlement in the genital ridges, PGCs proliferate enormously with the population increasing from 350 to 25,000 cells [279]. TRIM71-deficient PGCs might therefore be unable to expand because of proliferation defects as they have been described upon downregulation of TRIM71 in mouse ESCs resulting in the upregulation of the cell cycle inhibitor *Cdkn1a* mRNA [39]. Contrarily, it is also known that a considerable number of germ cells die after successfully reaching the gonads as mitotically arrested male PGCs undergo several massive apoptotic waves: the first one between E13.5 and E17.0 followed by a second one around birth and a third during the first wave of spermatogenesis around P10 to P13 [303]. Accordingly, the loss of PGCs upon TRIM71 deficiency can also be presumed to be due to enhanced apoptosis during or even after mitotic arrest.

Despite the lack of germ cells in the testes of germline-specific TRIM71-deficient mice at P0.5, this was more prominent in adult mice suggesting a secondary role of TRIM71 in postnatal germ cell development. In particular, in male mice, gonocytes resume proliferation at 1 or 2 days after birth [197]. Even though TRIM71 and its ortholog LIN-41 are known to be downregulated upon differentiation along with the rise of let-7 miRNA level [120, 145, 233, 256, 265], in mouse testis it has been observed that TRIM71 expression levels increase again between P7 and P14 [187]. Consequently, TRIM71 is certainly important postnatally for the establishment of the spermatogonial stem cell niche.

Additionally, it should be noted that the phenotype we observed in mice with germline-specific TRIM71 deficiency resembles that of NANOS3-deficient mice. Previous studies described a reduced testis size and infertility in *Nanos3* null mice [291]. As a consequence of apoptosis, a progressive loss of the migrating PGC population has been observed along with sterility in these mice [276]. Similar to *Trim71*, the *Nanos* genes are evolutionary conserved and important for germ cell development in many organisms [130, 140, 192, 195, 221, 274, 291]. Notably, the transgenic *Nanos3*-Cre mouse line used in this study for germline specific targeting of *Trim71*, is heterozygous for *Nanos3* as the coding sequence of one *Nanos3* allele is replaced by the *Cre* recombinase. Thus, the *Nanos3* heterozygosity by itself is responsible for the slightly reduced testis size observed in *Nanos3*-Cre expressing compared to respective *Nanos3* wild type mice (Figure 3.2 C). Upon simultaneous absence of TRIM71 and one *Nanos3* allele, the phenotype, however, was much more pronounced (Figure 3.2 C), letting presume a synergistic effect.

Data previously generated by our group has also found alterations in the miRNA profiles of TRIM71-deficient mouse ESCs, with gonad-specific differentiation promoting miRNAs being increased [188]. This suggests that TRIM71-mediated miRNA regulation may play a role in proper germ cell development. One of the miRNAs we know to be regulated by TRIM71 is let-7. Moreover, the let-7 miRNA processing regulator, LIN28, is known to be involved in germ cell development as LIN28-deficiency causes a loss of germ cells [306], albeit not as drastic as observed in the absence of TRIM71. This indicates TRIM71 targets other than let-7 (either miRNAs or mRNAs) may as well be involved in germ cell development.

Importantly, studies in *C. elegans* demonstrated that the nematode homolog of TRIM71, LIN-41, is required for normal oocyte growth and meiotic maturation [265, 270, 271, 288, 292]. In *lin-41* null mutants, oocytes cellularise prematurely, fail to grow and prematurely start embryonic-like differentiation, causing sterility [270, 288]. In stark contrast to our observation of male infertility in germline-specific TRIM71-deficient mice, spermatogenesis was normal in *lin-41* mutant nematodes [265, 270].

Taken together, by showing the loss of germ cells in the testes of germline-specific knockout *Trim71*$^{-/fl}$; *Nanos3*$^{Cre/+}$ mice, we demonstrate the importance of TRIM71 in mammalian germ cell development and the cause of infertility in these mice. This is independent from the newest study by Du *et al.* which describes a similar phenotype for germline-specific knockout *Trim71*$^{-/fl}$; *Ddx4*$^{Cre/+}$ mice from P10 onwards [61]. Besides the recent publication revealing TRIM71 to be required for the expansion of the undifferentiated SSC population and transition to the differentiating stage [61], we independently demonstrate an important role of TRIM71 in the postnatal establishment of the SSC pool. Moreover, we observed a lack of germ cells in mouse testes as early as P0.5. This is in contradiction to the very recent study by Du *et al.* describing a germ cell loss from P10 onwards in mice, with no difference in germ cell number detectable at P1 [61]. However, the study by Du *et al.* is generating germline-specific TRIM71-deficient mice by crossing *Trim71* conditional mice with a *Ddx4* promotor-driven transgenic Cre mice [77] since DDX4 expression is confined to the germ cell lineage in mouse and human [37, 75]. In contrast to the *Nanos3*-Cre mouse line used as part of the present study, the *Ddx4*-Cre line exhibits recombination activity rather late in germ cell development starting at approximately E15.0 when germ cells are in mitotic (male) or meiotic (female) arrest [77]. Thus, this comparably late transgenic Cre activity in germline-specific knockout *Trim71*$^{-/fl}$; *Ddx4*$^{Cre/+}$ mice might be the reason why Du and colleagues did not observe a difference in germ cell number in these mice at P1 [61] whereas the amount of gonocytes was significantly reduced in *Trim71*$^{-/fl}$; *Nanos3*$^{Cre/+}$ mice at P0.5 as part of our study. It is noteworthy that despite early Cre activity in germ cell development, the recombination capacity in the *Nanos3*-Cre line is at low efficiency in PGCs with ~11 – 25 % at E12.5 [276]. This low recombination activity might still be sufficiently responsible for the reduced number of gonocytes present in *Trim71*$^{-/fl}$; *Nanos3*$^{Cre/+}$ mice at P0.5. Irrespective of that, a major drawback of both Cre mouse lines is their global *Cre* expression at a relatively high rate (~20 % for *Ddx4*-Cre and ~12 % *Nanos3*-Cre) [77, 276].

Finally, for the first time our study shows that the lack of germ cells is of embryonic origin but can be enhanced during postnatal development since PGCs were absent in testes of germline-specific TRIM71-deficient mice at P0.5. The elucidation of the exact time window of germ cell loss would require further investigations involving time-lapse histological analysis of embryos from E10.5 until birth.

4.2 TRIM71 as a new regulator of germ cell maintenance

In embryonic development, TRIM71 and its orthologs have been described as important regulators of the proliferation *versus* differentiation balance [65]. As our phenotypic analysis of the testis of germline-specific TRIM71-deficient mice identified a drastic loss of germ cells

already in neonatal mice (Figure 3.7, Figure 3.8 and Figure 3.9), we hypothesise a molecular role of TRIM71 in embryonic germ cells. By unbiased miSeq analysis in the germ cell tumour cell line NCCIT used as a surrogate model, we observed a reduced growth upon the absence of both the N-terminal RING (ΔRING) (Figure 3.22) and the C-terminal 18 or 24 amino acids of the last NHL repeat (Δ6NHL) of TRIM71 (Figure 3.23). Yet, the growth defect was more pronounced in the functional deletion of the last NHL repeat. Consistent with this, proliferation was found more strongly reduced in NCCIT TRIM71 Δ6NHL than NCCIT TRIM71 ΔRING single cell clones (Figure 3.18 and Figure 3.19). This was accompanied by an increased sensitivity towards apoptosis, with more dramatic effects again in NCCIT TRIM71 Δ6NHL single cell clones (Figure 3.20). Therefore, the NHL domain is assumed to be more important for germ cell maintenance which is in line with the mouse model, in which a truncation of the C-terminal 24 amino acids phenocopies the complete loss of TRIM71 and causes embryonic lethality [172].

Cell or tissue homeostasis is regulated by cell proliferation, differentiation and death. In the centre of attention is the timing and order of cell cycle events, which is monitored by cell cycle checkpoints [170]. By sequential activation and deactivation of cyclin-dependent kinases (CDKs), eukaryotic cells progress through the four phases (G1, S, G2 and M phase) of the cell cycle [223]. An impact of TRIM71 on proliferation is known in ESCs [39], neural progenitor cells [41], in the hepatocellular carcinoma cell lines Huh7, Hep3B and HepG2 [43, 290]. As part of this study, we additionally observed a reduced proliferation together with a prolonged cell cycle by 1.5 - 4 h in both NCCIT TRIM71 Δ6NHL and NCCIT TRIM71 ΔRING single cell clones (Figure 3.18 and Figure 3.19). Thus, TRIM71 is also involved in the regulation of germ cell proliferation.

Specifically in mouse ESCs and HepG2 cells, TRIM71 promotes proliferation by inhibition of the cell cycle regulator *CDKN1A* [39, 290]. CDKN1A is a CDK inhibitor which restrains cell cycle progression by binding and inactivating G1- and S-phase CDKs in response to intra- and extracellular signals [92, 168]. Accordingly, we showed that the proliferation defect in NCCIT cells in the absence of the last 18 or 24 amino acids of the C-terminal NHL repeat was accompanied by an increase in CDKN1A expression and an assumed arrest in G1 phase of the cell cycle (Figure 3.19 E and F). One of Trim71 known functions is the repression of target mRNAs as an RBP which involves its NHL domain [65]. Moreover, our group recently identified TRIM71 responsive elements in the human *CDKN1A* 3'UTR which allows direct RNA interaction with the TRIM71's NHL domain [290]. Such elements are RNA structural motifs that were also identified in other TRIM71 mRNA targets in mouse [305] and *C. elegans* [137]. Furthermore, other cell cycle inhibitors including *E2F7*, *Rbl1* and *Rbl2* have been identified as mRNA targets being repressed by TRIM71 in HEK293Tcells and mouse ESCs [157]. It would be of high interest to elucidate whether these mRNA targets

are repressed likewise by TRIM71 in germ cells. So far, our findings uncovered a role of TRIM71 in the regulation of proliferation and self-renewal of germ cells most likely via the repression of cell cycle specific mRNAs, including *CDKN1A*.

On the other hand, a differentiating cell exits the cell cycle at G1 phase and enters a quiescent state of proliferation referred to as G0 [223]. Upon differentiation, the RBP TRIM71 is also known to be downregulated [39, 41, 172]. Congruently, in *Trim71* knockout mice it was shown that TRIM71 deficiency causes premature differentiation of neural progenitor cells which is accompanied by a decreased proliferation [41]. In the present study it is remarkable that neither the absence of the RING domain nor the C-terminal 18/24 amino acids of the last NHL repeat resulted in spontaneous differentiation of the NCCIT cells (Figure 3.17). As a result, stemness was not affected by the absence of TRIM71's RING domain or the functional deletion of the last NHL repeat during steady state. This leads to the assumption that in germ cells similar to ESCs, TRIM71 most likely acts as a wall against differentiation. Consequently, in the absence of TRIM71, this wall would be weaker so that cells would be more sensitive to differentiation in the presence of differentiation stimuli, and hence primed towards premature differentiation. In order to prove this, the differentiation behaviour of NCCIT TRIM71 Δ6NHL than NCCIT TRIM71 ΔRING single cell clones would need to be monitored upon application of differentiation stimuli such as retinoic acid.

Several lines of evidence link apoptosis to proliferation. Especially as in normal tissue homeostasis, uncontrolled proliferation is associated with enhanced apoptosis [223]. Thus, an imbalance of proliferation and apoptosis results in cancers as well as degenerative diseases. While defects in apoptosis cause cancer, enhanced apoptosis leads to degenerative diseases. Our results in NCCIT single cell clones show that the last C-terminal NHL repeat of TRIM71 is important for apoptosis inhibition as cells with a functional deletion of this repeat were more prone towards apoptosis (Figure 3.20 A and B). As described before, apoptosis occurs as part of normal germ cell development in mice: first between E13.5 and E17.0, a second time around birth and a third time during the first wave of spermatogenesis around P10 to P13 [303]. Therefore, in the absence of TRIM71 as in the case of the germline-specific TRIM71-deficient mice, an increased amount of germ cells might be lost during all three apoptotic waves due to their higher susceptibility.

On the molecular level, a previous study identified p53 as a target of TRIM71, being ubiquitinated and targeted for proteasomal degradation by TRIM71 during neural stem cell differentiation [204]. Thereby p53-induced apoptosis is dampened in order to control the balance between self-renewal, differentiation and cell death [204]. In line with an increased apoptosis observed in differentiating TRIM71-deficient mouse ESCs [204], in the present study, NCCIT cells with a functional deletion of the last NHL repeat were revealed to be more prone towards apoptosis (Figure 3.20 A and B). Similar to earlier findings in TRIM71-

deficient pluripotent mouse ESCs [204], we showed an increase in the mRNA expression of the p53 direct transcriptional target *PUMA* in NCCIT cells with a functional deletion of the last NHL repeat while the mRNA level of the p53-independent pro-apoptotic gene *BIM* was unaltered (Figure 3.20 C and D). Generally, the tumour suppressor p53 has a key role in cell cycle regulation by acting as 'the guardian of the genome' inducing cell cycle arrest, apoptosis and senescence in response to cellular stress (eg. DNA damage) [23]. More recent studies have identified a role of p53 in regulating stem cell maintenance by demonstrating that p53 is capable to suppress the reprogramming of somatic cells to iPSCs by either a restrained cell cycle, via *Cdkn1a* induction, or the induction of apoptosis [90, 106, 124, 174, 317]. A regulatory role of p53 in germ cell surveillance and reproduction in mice [94, 242], which is conserved in invertebrates including *D. melanogaster* [312] and *C. elegans* [55], has been described in other studies. Accordingly, the deletion of p53 in the testis of mice harbouring dysfunctional telomeres was demonstrated to rescue apoptosis and spermatogenesis [45].

Most importantly, it has been shown by co-immunoprecipitation assays that the NHL domain of TRIM71 is necessary and sufficient for binding of p53 [204]. Thus, the pro-apoptotic effects we observed upon the deletion of the C-terminal 18/24 amino acids of the last NHL repeat of TRIM71 (Figure 3.20) might be due to abrogated binding of p53 by TRIM71 which goes along with the prevention of ubiquitination and proteasomal degradation of p53. It therefore needs to be proven whether the C-terminal 18 amino acids of the last TRIM71 NHL repeat are necessary for p53 binding. Additionally, the p53 protein level would need to be determined in NCCIT TRIM71 Δ6NHL cells in comparison to wild type cells. In this context, it should be highlighted that the NCCIT germ cell tumour cell line is hemizygous for *TP53* encoding a truncated p53 protein of 347 amino acids [33]. The sites, however, mostly ubiquitinated within p53 are the lysine residues K313-315 [204] which are still present in the truncated p53 in NCCIT cells. In fact, in ovarian cancer a specific binding of the N-terminal transactivation (TA) domain of point mutated p53 by TRIM71's NHL domain has been described recently [42]. Strikingly, in the last-mentioned publication, the ubiquitination of mutated p53 by TRIM71 resulted in reduced proliferation associated with increased patient survival.

Arguing against TRIM71 controlling apoptosis via p53 ubiquitylation and proteasomal degradation, we identified the RING domain with an attributed E3 ubiquitin ligase activity [150, 246] to be dispensable for apoptosis inhibition, since deletion of the RING domain in NCCIT cells did not result in an enhanced sensitivity towards apoptosis (Figure 3.20). In accordance with this, RNA levels of the p53 direct transcriptional target *PUMA* were consistently unaltered (Figure 3.20 C). These results indicate apoptosis to be induced rather in a p53-independent than dependent manner in NCCIT cells. This has been

suggested for TGCT cell lines previously as they showed p53-independent differential sensitivity to diverse therapeutic apoptosis inducing agents [33–35]. In addition, *PUMA* has been described to be induced by other transcription factors initiating cellular apoptosis independently of p53 in response to nongenotoxic stimuli, including growth factor/cytokine deprivation, kinase inhibition, endoplasmic reticulum stress, altered redox status, oncogenic stress, ischemia/reperfusion, immune modulation and infection [261, 319]. Further investigations are, however, required to determine whether in NCCIT TRIM71 ΔRING cells apoptosis regulation might still be p53-dependent. For p53 ubiquitination and degradation in the absence of the RING domain, TRIM71 may cooperate with other E3 and E4 ubiquitin ligases or involves the B-boxes also known to act as E3 ligases [282].

Despite the exact molecular mechanisms leading to enhanced sensitivity towards apoptosis upon the functional deletion of the C-terminal NHL repeat being unknown, an increase in apoptosis remains a putative cause for the germ cell loss observed in germline-specific TRIM71-deficient mice.

Altogether, we identified both proliferation and apoptosis, as two possibly cooperating processes regulated by TRIM71 in germ cell development and maintenance using the germ cell tumour cell line NCCIT. In agreement with our data, a recently published, independent study by Du and colleagues [61] describes an impaired proliferation together with an increased level of apoptosis in primary murine undifferentiated spermatogonial cells subjected to knockdown of TRIM71 [61]. Beyond that, on the molecular level we observed TRIM71 to promote proliferation v*ia* repression of *CDKN1A* mRNA while antagonising apoptosis possibly by p53 regulation in NCCIT cells, even though a definitive proof of p53 levels and activity is missing. Such effects are very likely to play a role in the initial establishment and the subsequent maintenance of the spermatogonial stem cell niche *in vivo*. Conversely, upon loss of TRIM71 during germ cell development, the proliferation and self-renewal of PGCs, gonocytes and SSCs may be diminished accompanied by enhanced apoptosis (Figure 4.1). In the future, further unravelling of the molecular mechanisms by which TRIM71 governs germ cell biology will certainly help to understand the causes of male infertility and will contribute to the identification of new therapeutic targets and strategies for cancer treatment as well as reproductive medicine.

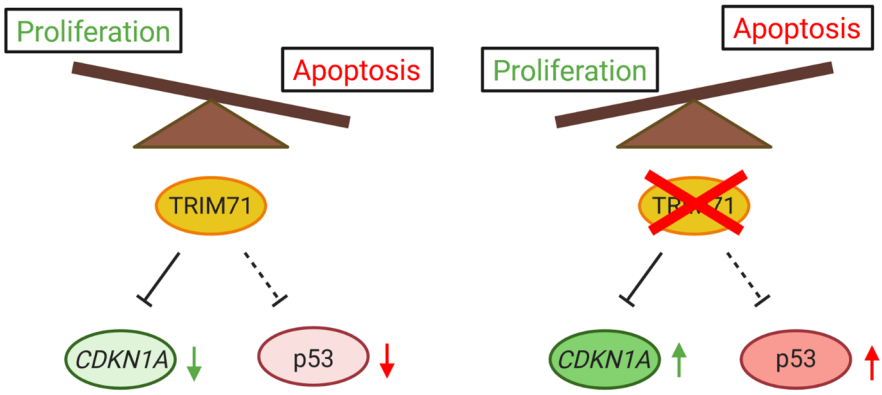

Figure 4.1 – TRIM71 regulates the balance between proliferation and apoptosis for germ cell development and maintenance
In germ cells TRIM71 is highly expressed and promotes proliferation via mRNA repression of the cell cycle inhibitor *CDKN1A* while antagonising apoptosis possibly by p53 regulation (dashed line), although a definitive proof of p53 levels and activity is missing. Upon the absence of TRIM71, this regulatory balance is disrupted enhancing apoptosis sensitivity and diminishing proliferation in germ cells. Created with BioRender.com.

4.3 TRIM71 is a factor of clinical relevance

With ageing of the world population, there is an increasing demand for new therapeutic applications for cancer treatment and reproductive medicine. Cancer is certainly not restricted to the older population but is also frequently occurring in young people. According to the WHO global cancer observatory, in 2018 testicular cancer was estimated to have the largest number of new cases among all cancers in males aged between 20 and 39 years worldwide [70]. The incidences of TGCT in young men are steadily rising with a predicted increase of 19 % within the next 20 years [70]. Despite the successful treatment of testicular cancers, TGCT patients treated with cisplatin-based therapy suffer from life-long side effects including infertility, hypogonadism, cardiovascular diseases, decreased pulmonary and renal function, neurotoxicity and a greater risk of developing secondary malignancies [1]. Therefore, there is a clinical need for new treatment strategies. In this study, TRIM71 was found expressed in various germ cell derived embryonic carcinoma and seminoma cell lines (Figure 3.11). As these cell lines have been isolated from germ cell tumours of patients, it is with a great likelihood that TRIM71 is expressed to a comparable extent in the tumours of patients *in vivo*. By targeting *TRIM71* in the NCCIT germ cell tumour cell line, proliferation was reduced accompanied by enhanced apoptosis sensitivity. Hence, TRIM71 might be a potential target for the treatment of TGCTs. A benefit of targeting TRIM71 would be its restricted expression in the adult organism which would minimise side effects upon treatment. This is still a major disadvantage of many currently applied chemotherapies which are targeting crucial factors of the proliferation pathways.

As TRIM71 expression is restricted to stem and progenitor cells [65], it would be of additional therapeutic interest to investigate whether TRIM71 is also highly expressed in cancer stem cells of other tumour types. These cells are assumed to be the reason for cancer relapse and therapy resistance [235]. Until now, cancer stem cells have been identified in numerous solid tumours including breast cancer [6, 30], colon cancer [243, 294], head and neck cancer [88, 173], pancreatic cancer [151], liver cancer [315, 316], lung cancer [5] *etc*. Thus, TRIM71 might as well be a therapeutic target in cancers resistant to traditional chemo- and radiotherapy.

Yet, in a recent study in ovarian cancer, ectopic TRIM71 was found to suppress tumorigenesis [42]. In this case, rather applying a drug delivering TRIM71 to the tumour would be of therapeutic value. Eventually, it is important to understand the molecular functions of TRIM71 within the different cancer types to ensure an adequate treatment.

Besides testicular cancer, infertility is a major problem affecting 15 % of couples worldwide [4, 119]. With males contributing to 50 % across all infertility cases, they are estimated to be solely responsible in 20-30 % [4]. But up to now, in many of the infertility cases the associated factor is unknown, also referred to as idiopathic male infertility [119]. As we found the absence of germ cells in germline-specific TRIM71-deficient mice to be of embryonic origin, loss of TRIM71 may be considered as a genetic factor causing infertility. Moreover, a reduction in testis size and germ cell number had already been detected in *Trim71* heterozygous mice which suggests humans with a heterozygous mutation of *TRIM71* to be possibly categorised as subfertile. In particular, predominantly in the Western civilisation, modern lifestyle has led to delayed family planning which is accompanied by reduced fertility due to increasing age. Therefore, it is of high interest to find effective treatments to counteract (age-related) infertility and at the same time improve assisted reproductive technologies. This requires in the first line the identification of genes affecting fertility and secondly, the understanding of the molecular mechanisms regulating germ cell maintenance and differentiation.

4.4 Conclusion and outlook

Taken together, the results of this study identify TRIM1 as a crucial factor in germ cell maintenance. We have been able to elucidate that the almost complete germ cell loss associated with a partial SCO syndrome in TRIM71-deficient mice primarily results from errors during embryonic germ cell development and becomes more pronounced after birth upon reinitiating of germ cell proliferation. In this context, TRIM71 acts as a key player by regulating the balance between proliferation and apoptosis. Both, the N-terminal RING domain and in particular a functional C-terminal last NHL repeat of TRIM71 are required to

ensure the development of the germ cell population. For normal germ cell proliferation to some extent post-transcriptional repression of the known TRIM71 target and cell cycle inhibitor *CDKN1A* by TRIM71's NHL domain was found to be necessary. In contrast, inhibition of apoptosis in germ cells presumably involves the downregulation of the tumour suppressor p53 by TRIM71. Finally, by simply promoting germ cell proliferation and inhibiting apoptosis, TRIM71 might enable the proper development of the germ cell niche.

In the future, the exact molecular mechanisms underlying TRIM71-dependent germ cell maintenance need to be clarified. By RNA sequencing on TRIM71-deficient and wild type control PGCs or PGCLCs useful hints on the cellular pathways and genes necessary for maintaining the germ cell pool could be obtained. Moreover, interaction studies (e.g. co-immunoprecipitation) and ubiquitination assays are essential to confirm the conserved targeting mechanisms of TRIM71 in germ cells. *In vivo*, further studies on embryonic gonads E10.5 until birth are needed to identify the time point and cause of germ cell loss. Possible methods include TUNEL assays as well as the immunofluorescent staining of proliferation (e.g. Phospho-Histone 3 or Ki67) and apoptosis (Cleaved Caspase-3) markers.

Albeit we have not been able to elucidate the molecular mechanisms by which TRIM71 builds and maintains the germ cell pool, further experiments – *in vivo* and *in vitro* – will determine if TRIM71 is a new therapeutic target for testicular cancer treatment and reproductive medicine.

5 Summary

Germ cells are the key to continuation of life as they are the unique cell lineage capable to transfer the complete genetic information to the next generation. Both, infertility and testicular cancers are usually originating from errors during embryonic germ cell development. Germ cell development is a very precisely regulated process – spatially and temporally – with cell proliferation, differentiation and apoptosis being involved.

An evolutionary conserved role in the regulation of embryonic development has been described for TRIM71 and its orthologs. In the somatic lineage, TRIM71 is restrictively expressed in stem and progenitor cells and regulates the balance between stem cell renewal and differentiation. Besides the expression of TRIM71 being validated in gonocytes and spermatogonial stem cells (SSCs) in mouse testes, the function of TRIM71 in the germ cell lineage is only poorly understood. Therefore, this study aimed at elucidating the role of TRIM71 in male germ cell development.

In mice, TRIM71 deficiency causes infertility which is associated with reduced testis size and weight. By histological analysis of testes from germline-specific TRIM71-deficient adult mice, an almost complete lack of germ cells was observed with the testes resembling symptoms of a Sertoli-cell-only (SCO) syndrome. This loss of germ cells was found to be predominantly of embryonic origin and becoming more pronounced after birth, when mitosis is reinitiated in germ cells. To better understand the molecular functions of TRIM71 in germ cell maintenance, we used the germ cell tumour cell line NCCIT as an *in vitro* surrogate model to analyse the growth behaviour of NCCIT cell populations with CRISPR/Cas9-mediated deletion of the N-terminal TRIM71 RING domain (ΔRING) or functional deletion of the C-terminal amino acids within the last NHL repeat (Δ6NHL). Highly innovative growth competition analysis revealed that the RING domain and particularly the last NHL repeat are necessary for proper growth behaviour. For both TRIM71 truncations a decline in the respective NCCIT cell population was present, though being more pronounced in the NCCIT TRIM71 Δ6NHL population. Moreover, while stemness markers were unaltered, proliferation was decreased and sensitivity towards apoptosis was enhanced in NCCIT TRIM71 ΔRING and again more strongly in NCCIT TRIM71 Δ6NHL cells. In this context, two factors and known TRIM71 targets, namely the cell cycle inhibitor CDKN1A as well as the tumour suppressor and ‘guardian of the genome’ p53, were found to be involved in regulating proliferation and apoptosis in NCCIT cells, respectively.

Overall, our findings strongly indicate that TRIM71 is indispensable for sustaining and building the germ cell niche by promoting proliferation combined with the inhibition of apoptosis. Thus, we advance the understanding on genetic factors that cause testicular cancer and male infertility. Consequently, TRIM71 might be a putative pharmacological target paving the way for improved testicular cancer treatment and reproductive medicine.

References

[1] Abouassaly, R., Fossa, S. D., Giwercman, A., Kollmannsberger, C., Motzer, R. J., Schmoll, H.-J., and Sternberg, C. N. (2011). Sequelae of treatment in long-term survivors of testis cancer. *Eur Urol* 60(3):516–526.

[2] Adami, H. O., Bergström, R., Möhner, M., Zatoński, W., Storm, H., Ekbom, A., Tretli, S., Teppo, L., Ziegler, H., and Rahu, M. (1994). Testicular cancer in nine northern European countries. *Int J Cancer* 59(1):33–38.

[3] Aeschimann, F., Kumari, P., Bartake, H., Gaidatzis, D., Xu, L., Ciosk, R., and Großhans, H. (2017). LIN41 Post-transcriptionally Silences mRNAs by Two Distinct and Position-Dependent Mechanisms. *Mol Cell* 65(3):476-489.e4.

[4] Agarwal, A., Mulgund, A., Hamada, A., and Chyatte, M. R. (2015). A unique view on male infertility around the globe. *Reprod Biol Endocrinol* 13:37.

[5] Alamgeer, M., Peacock, C. D., Matsui, W., Ganju, V., and Watkins, D. N. (2013). Cancer stem cells in lung cancer: Evidence and controversies. *Respirology* 18(5):757–764.

[6] Al-Hajj, M., Wicha, M. S., Benito-Hernandez, A., Morrison, S. J., and Clarke, M. F. (2003). Prospective identification of tumorigenic breast cancer cells. *Proc Natl Acad Sci U S A* 100(7):3983–3988.

[7] Allegrucci, C., Thurston, A., Lucas, E., and Young, L. (2005). Epigenetics and the germline. *Reproduction* 129(2):137–149.

[8] Almstrup, K., Hoei-Hansen, C. E., Wirkner, U., Blake, J., Schwager, C., Ansorge, W., Nielsen, J. E., Skakkebaek, N. E., Rajpert-De Meyts, E., and Leffers, H. (2004). Embryonic stem cell-like features of testicular carcinoma in situ revealed by genome-wide gene expression profiling. *Cancer Res* 64(14):4736–4743.

[9] Ancelin, K., Lange, U. C., Hajkova, P., Schneider, R., Bannister, A. J., Kouzarides, T., and Surani, M. A. (2006). Blimp1 associates with Prmt5 and directs histone arginine methylation in mouse germ cells. *Nat Cell Biol* 8(6):623–630.

[10] Anderson, R., Copeland, T. K., Schöler, H., Heasman, J., and Wylie, C. (2000). The onset of germ cell migration in the mouse embryo. *Mech Dev* 91(1-2):61–68.

[11] Aponte, P. M., van Bragt, M. P. A., Rooij, D. G. de, and van Pelt, A. M. M. (2005). Spermatogonial stem cells: characteristics and experimental possibilities. *APMIS* 113(11-12):727–742.

[12] Ardley, H. C. and Robinson, P. A. (2005). E3 ubiquitin ligases. *Essays Biochem* 41:15–30.

[13] Bagga, S., Bracht, J., Hunter, S., Massirer, K., Holtz, J., Eachus, R., and Pasquinelli, A. E. (2005). Regulation by let-7 and lin-4 miRNAs results in target mRNA degradation. *Cell* 122(4):553–563.

[14] Baillie, A. H. (1964). The histochemistry and ultrastructure of the gonocyte. *J Anat* 98(Pt 4):641–645.

[15] Barakat, B., O'Connor, A. E., Gold, E., Kretser, D. M. de, and Loveland, K. L. (2008). Inhibin, activin, follistatin and FSH serum levels and testicular production are highly modulated during the first spermatogenic wave in mice. *Reproduction* 136(3):345–359.

[16] Barlow, P. N., Luisi, B., Milner, A., Elliott, M., and Everett, R. (1994). Structure of the C3HC4 domain by 1H-nuclear magnetic resonance spectroscopy. A new structural class of zinc-finger. *J Mol Biol* 237(2):201–211.

[17] Barrangou, R., Fremaux, C., Deveau, H., Richards, M., Boyaval, P., Moineau, S., Romero, D. A., and Horvath, P. (2007). CRISPR provides acquired resistance against viruses in prokaryotes. *Science* 315(5819):1709–1712.

[18] Barrios, F., Irie, N., and Surani, M. A. (2013). Perceiving signals, building networks, reprogramming germ cell fate. *Int J Dev Biol* 57(2-4):123–132.

[19] Baugh, L. R., Hill, A. A., Brown, E. L., and Hunter, C. P. (2001). Quantitative analysis of mRNA amplification by in vitro transcription. *Nucleic Acids Res* 29(5):E29.

[20] Bellvé, A. R., Cavicchia, J. C., Millette, C. F., O'Brien, D. A., Bhatnagar, Y. M., and Dym, M. (1977). Spermatogenic cells of the prepuberal mouse. Isolation and morphological characterization. *J Cell Biol* 74(1):68–85.

[21] Berney, D. M., Looijenga, L. H. J., Idrees, M., Oosterhuis, J. W., Rajpert-De Meyts, E., Ulbright, T. M., and Skakkebaek, N. E. (2016). Germ cell neoplasia in situ (GCNIS): evolution of the current nomenclature for testicular pre-invasive germ cell malignancy. *Histopathology* 69(1):7–10.

[22] Beumer, T. L., Roepers-Gajadien, H. L., Gademan, I. S., Rutgers, D. H., and Rooij, D. G. de. (1997). P21(Cip1/WAF1) expression in the mouse testis before and after X irradiation. *Mol. Reprod. Dev.* 47(3):240–247.

[23] Bieging, K. T., Mello, S. S., and Attardi, L. D. (2014). Unravelling mechanisms of p53-mediated tumour suppression. *Nat Rev Cancer* 14(5):359–370.

[24] Borden, K. L., Boddy, M. N., Lally, J., O'Reilly, N. J., Martin, S., Howe, K., Solomon, E., and Freemont, P. S. (1995). The solution structure of the RING finger domain from the acute promyelocytic leukaemia proto-oncoprotein PML. *EMBO J* 14(7):1532–1541.

[25] Borden, K. L., Lally, J. M., Martin, S. R., O'Reilly, N. J., Etkin, L. D., and Freemont, P. S. (1995). Novel topology of a zinc-binding domain from a protein involved in regulating early Xenopus development. *EMBO J* 14(23):5947–5956.

[26] Borden, K. L., Martin, S. R., O'Reilly, N. J., Lally, J. M., Reddy, B. A., Etkin, L. D., and Freemont, P. S. (1993). Characterisation of a novel cysteine/histidine-rich metal binding domain from Xenopus nuclear factor XNF7. *FEBS Lett* 335(2):255–260.

[27] Bosl, G. J. and Motzer, R. J. (1997). Testicular germ-cell cancer. *N Engl J Med* 337(4):242–253.

[28] Bray, F., Ferlay, J., Soerjomataram, I., Siegel, R. L., Torre, L. A., and Jemal, A. (2018). Global cancer statistics 2018: GLOBOCAN estimates of incidence and mortality worldwide for 36 cancers in 185 countries. *CA Cancer J Clin* 68(6):394–424.

[29] Bray F., Colombet M., Mery L., Piñeros M., Znaor A., Zanetti R., Ferlay J., and editors. (2017). *Cancer Incidence in Five Continents, Vol. XI* (electronic version), Lyon, France: International Agency for Research on Cancer. Available from http://ci5.iarc.fr. Accessed 5 February 2020.

[30] Britton, K. M., Kirby, J. A., Lennard, T. W. J., and Meeson, A. P. (2011). Cancer stem cells and side population cells in breast cancer and metastasis. *Cancers (Basel)* 3(2):2106–2130.

[31] Brynczka, C., Labhart, P., and Merrick, B. A. (2007). NGF-mediated transcriptional targets of p53 in PC12 neuronal differentiation. *BMC Genomics* 8:139.

[32] Buljubašić, R., Buljubašić, M., Bojanac, A. K., Ulamec, M., Vlahović, M., Ježek, D., Bulić-Jakuš, F., and Sinčić, N. (2018). Epigenetics and testicular germ cell tumors. *Gene* 661:22–33.

[33] Burger, H., Nooter, K., Boersma, A. W., Kortland, C. J., and Stoter, G. (1997). Lack of correlation between cisplatin-induced apoptosis, p53 status and expression of Bcl-2 family proteins in testicular germ cell tumour cell lines. *Int J Cancer* 73(4):592–599.

[34] Burger, H., Nooter, K., Boersma, A. W., Kortland, C. J., and Stoter, G. (1998). Expression of p53, Bcl-2 and Bax in cisplatin-induced apoptosis in testicular germ cell tumour cell lines. *Br J Cancer* 77(10):1562–1567.

[35] Burger, H., Nooter, K., Boersma, A. W., van Wingerden, K. E., Looijenga, L. H., Jochemsen, A. G., and Stoter, G. (1999). Distinct p53-independent apoptotic cell death signalling pathways in testicular germ cell tumour cell lines. *Int J Cancer* 81(4):620–628.

[36] Bustamante-Marín, X., Garness, J. A., and Capel, B. (2013). Testicular teratomas: an intersection of pluripotency, differentiation and cancer biology. *Int J Dev Biol* 57(2-4):201–210.

[37] Castrillon, D. H., Quade, B. J., Wang, T. Y., Quigley, C., and Crum, C. P. (2000). The human VASA gene is specifically expressed in the germ cell lineage. *Proc Natl Acad Sci U S A* 97(17):9585–9590.

[38] Cecco, L. de, Negri, T., Brich, S., Mauro, V., Bozzi, F., Dagrada, G., Disciglio, V., Sanfilippo, R., Gronchi, A., D'Incalci, M., Casali, P. G., Canevari, S., Pierotti, M. A., and Pilotti, S. (2014). Identification of a gene expression driven progression pathway in myxoid liposarcoma. *Oncotarget* 5(15):5965–5977.

[39] Chang, H.-M., Martinez, N. J., Thornton, J. E., Hagan, J. P., Nguyen, K. D., and Gregory, R. I. (2012). Trim71 cooperates with microRNAs to repress Cdkn1a expression and promote embryonic stem cell proliferation. *Nat Commun* 3:923.

[40] Chen, C. and Okayama, H. (1987). High-efficiency transformation of mammalian cells by plasmid DNA. *Mol Cell Biol* 7(8):2745–2752.

[41] Chen, J., Lai, F., and Niswander, L. (2012). The ubiquitin ligase mLin41 temporally promotes neural progenitor cell maintenance through FGF signaling. *Genes Dev* 26(8):803–815.

[42] Chen, Y., Hao, Q., Wang, J., Li, J., Huang, C., Zhang, Y., Wu, X., Lu, H., and Zhou, X. (2019). Ubiquitin ligase TRIM71 suppresses ovarian tumorigenesis by degrading mutant p53. *Cell Death Dis* 10(10):737.

[43] Chen, Y.-L., Yuan, R.-H., Yang, W.-C., Hsu, H.-C., and Jeng, Y.-M. (2013). The stem cell E3-ligase Lin-41 promotes liver cancer progression through inhibition of microRNA-mediated gene silencing. *J Pathol* 229(3):486–496.

[44] Chia, V. M., Quraishi, S. M., Devesa, S. S., Purdue, M. P., Cook, M. B., and McGlynn, K. A. (2010). International trends in the incidence of testicular cancer, 1973-2002. *Cancer Epidemiol Biomarkers Prev* 19(5):1151–1159.

[45] Chin, L., Artandi, S. E., Shen, Q., Tam, A., Lee, S. L., Gottlieb, G. J., Greider, C. W., and DePinho, R. A. (1999). p53 deficiency rescues the adverse effects of telomere loss and cooperates with telomere dysfunction to accelerate carcinogenesis. *Cell* 97(4):527–538.

[46] Clement, K., Rees, H., Canver, M. C., Gehrke, J. M., Farouni, R., Hsu, J. Y., Cole, M. A., Liu, D. R., Joung, J. K., Bauer, D. E., and Pinello, L. (2019). CRISPResso2 provides accurate and rapid genome editing sequence analysis. *Nat Biotechnol* 37(3):224–226.

[47] Clermont, Y. and PEREY, B. (1957). Quantitative study of the cell population of the seminiferous tubules in immature rats. *Am J Anat* 100(2):241–267.

[48] Conway, J. F. and Parry, D. A. (1990). Structural features in the heptad substructure and longer range repeats of two-stranded alpha-fibrous proteins. *Int J Biol Macromol* 12(5):328–334.

[49] Cools, M., Wolffenbuttel, K. P., Drop, S. L. S., Oosterhuis, J. W., and Looijenga, L. H. J. (2011). Gonadal development and tumor formation at the crossroads of male and female sex determination. *Sex Dev* 5(4):167–180.

[50] Copp, A. J., Greene, N. D. E., and Murdoch, J. N. (2003). The genetic basis of mammalian neurulation. *Nat Rev Genet* 4(10):784–793.

[51] Cuevas, E., Rybak-Wolf, A., Rohde, A. M., Nguyen, D. T. T., and Wulczyn, F. G. (2015). Lin41/Trim71 is essential for mouse development and specifically expressed in postnatal ependymal cells of the brain. *Front Cell Dev Biol* 3:20.

[52] Culty, M. (2009). Gonocytes, the forgotten cells of the germ cell lineage. *Birth Defects Res C Embryo Today* 87(1):1–26.

[53] Damjanov, I., Horvat, B., and Gibas, Z. (1993). Retinoic acid-induced differentiation of the developmentally pluripotent human germ cell tumor-derived cell line, NCCIT. *Lab Invest* 68(2):220–232.

[54] Deng, S., Hirschberg, A., Worzfeld, T., Penachioni, J. Y., Korostylev, A., Swiercz, J. M., Vodrazka, P., Mauti, O., Stoeckli, E. T., Tamagnone, L., Offermanns, S., and Kuner, R. (2007). Plexin-B2, but not Plexin-B1, critically modulates neuronal migration and patterning of the developing nervous system in vivo. *J Neurosci* 27(23):6333–6347.

[55] Derry, W. B., Putzke, A. P., and Rothman, J. H. (2001). Caenorhabditis elegans p53: role in apoptosis, meiosis, and stress resistance. *Science* 294(5542):591–595.

[56] Diez del Corral, R., Breitkreuz, D. N., and Storey, K. G. (2002). Onset of neuronal differentiation is regulated by paraxial mesoderm and requires attenuation of FGF signalling. *Development* 129(7):1681–1691.

[57] Ding, X. C. and Grosshans, H. (2009). Repression of C. elegans microRNA targets at the initiation level of translation requires GW182 proteins. *EMBO J* 28(3):213–222.

[58] Dono, R. (2003). Fibroblast growth factors as regulators of central nervous system development and function. *Am J Physiol Regul Integr Comp Physiol* 284(4):R867-81.

[59] Donovan, P. J. and Miguel, M. P. de. (2003). Turning germ cells into stem cells. *Curr Opin Genet Dev* 13(5):463–471.

[60] Doudna, J. A. and Charpentier, E. (2014). Genome editing. The new frontier of genome engineering with CRISPR-Cas9. *Science* 346(6213):1258096.

[61] Du, G., Wang, X., Luo, M., Xu, W., Zhou, T., Wang, M., Yu, L., Li, L., Cai, L.'e., Wang, P. J., Li, J. Z., Oatley, J. M., and Wu, X. (2020). mRBPome capture identifies the RNA binding protein TRIM71, an essential regulator of spermatogonial differentiation. *Development*.

[62] Durcova-Hills, G., Ainscough, J., and McLaren, A. (2001). Pluripotential stem cells derived from migrating primordial germ cells. *Differentiation* 68(4-5):220–226.

[63] Eckert, D., Biermann, K., Nettersheim, D., Gillis, A. J. M., Steger, K., Jäck, H.-M., Müller, A. M., Looijenga, L. H. J., and Schorle, H. (2008). Expression of BLIMP1/PRMT5 and concurrent histone H2A/H4 arginine 3 dimethylation in fetal germ cells, CIS/IGCNU and germ cell tumors. *BMC Dev Biol* 8:106.

[64] Eckert, D., Nettersheim, D., Heukamp, L. C., Kitazawa, S., Biermann, K., and Schorle, H. (2008). TCam-2 but not JKT-1 cells resemble seminoma in cell culture. *Cell Tissue Res* 331(2):529–538.

[65] Ecsedi, M. and Grosshans, H. (2013). LIN-41/TRIM71: emancipation of a miRNA target. *Genes Dev* 27(6):581–589.

[66] Edwards, T. A., Wilkinson, B. D., Wharton, R. P., and Aggarwal, A. K. (2003). Model of the brain tumor-Pumilio translation repressor complex. *Genes Dev* 17(20):2508–2513.

[67] Elledge, S. J. (1996). Cell cycle checkpoints: preventing an identity crisis. *Science* 274(5293):1664–1672.

[68] Fayomi, A. P. and Orwig, K. E. (2018). Spermatogonial stem cells and spermatogenesis in mice, monkeys and men. *Stem Cell Res* 29:207–214.

[69] Felici, M. de. (2009). Primordial germ cell biology at the beginning of the XXI century. *Int J Dev Biol* 53(7):891–894.

[70] Ferlay, J., Ervik, M., Lam, F., Colombet, M., Mery, L., Piñeros, M., Znaor, A., Soerjomataram, I., and Bray, F. (2018). *Global Cancer Observatory: Cancer Today*, Lyon, France: International Agency for Research on Cancer. Available from https://gco.iarc.fr/today. Accessed 1 February 2020.

[71] Ford-Perriss, M., Abud, H., and Murphy, M. (2001). Fibroblast growth factors in the developing central nervous system. *Clin Exp Pharmacol Physiol* 28(7):493–503.

[72] Frank, D. J. and Roth, M. B. (1998). ncl-1 is required for the regulation of cell size and ribosomal RNA synthesis in Caenorhabditis elegans. *J Cell Biol* 140(6):1321–1329.

[73] Freemont, P. S., Hanson, I. M., and Trowsdale, J. (1991). A novel cysteine-rich sequence motif. *Cell* 64(3):483–484.

[74] Fridell, R. A., Harding, L. S., Bogerd, H. P., and Cullen, B. R. (1995). Identification of a novel human zinc finger protein that specifically interacts with the activation domain of lentiviral Tat proteins. *Virology* 209(2):347–357.

[75] Fujiwara, Y., Komiya, T., Kawabata, H., Sato, M., Fujimoto, H., Furusawa, M., and Noce, T. (1994). Isolation of a DEAD-family protein gene that encodes a murine homolog of Drosophila vasa and its specific expression in germ cell lineage. *Proc Natl Acad Sci U S A* 91(25):12258–12262.

[76] Furey, C. G., Choi, J., Jin, S. C., Zeng, X., Timberlake, A. T., Nelson-Williams, C., Mansuri, M. S., Lu, Q., Duran, D., Panchagnula, S., Allocco, A., Karimy, J. K., Khanna, A., Gaillard, J. R., DeSpenza, T., Antwi, P., Loring, E., Butler, W. E., Smith, E. R., Warf, B. C., Strahle, J. M., Limbrick, D. D., Storm, P. B., Heuer, G., Jackson, E. M., Iskandar, B. J., Johnston, J. M., Tikhonova, I., Castaldi, C., López-Giráldez, F., Bjornson, R. D., Knight, J. R., Bilguvar, K., Mane, S., Alper, S. L., Haider, S., Guclu, B., Bayri, Y., Sahin, Y., Apuzzo, M. L. J., Duncan, C. C., DiLuna, M. L., Günel, M., Lifton, R. P., and Kahle, K. T. (2018). De Novo Mutation in Genes Regulating Neural Stem Cell Fate in Human Congenital Hydrocephalus. *Neuron* 99(2):302-314.e4.

[77] Gallardo, T., Shirley, L., John, G. B., and Castrillon, D. H. (2007). Generation of a germ cell-specific mouse transgenic Cre line, Vasa-Cre. *Genesis* 45(6):413–417.

[78] Gasiunas, G., Barrangou, R., Horvath, P., and Siksnys, V. (2012). Cas9-crRNA ribonucleoprotein complex mediates specific DNA cleavage for adaptive immunity in bacteria. *Proc Natl Acad Sci U S A* 109(39):E2579-86.

[79] Gassei, K. and Orwig, K. E. (2013). SALL4 expression in gonocytes and spermatogonial clones of postnatal mouse testes. *PLoS ONE* 8(1):e53976.

[80] Gaytan, F., Sangiao-Alvarellos, S., Manfredi-Lozano, M., García-Galiano, D., Ruiz-Pino, F., Romero-Ruiz, A., León, S., Morales, C., Cordido, F., Pinilla, L., and Tena-Sempere, M. (2013). Distinct expression patterns predict differential roles of the miRNA-binding proteins, Lin28 and Lin28b, in the mouse testis: studies during postnatal development and in a model of hypogonadotropic hypogonadism. *Endocrinology* 154(3):1321–1336.

[81] Ginsburg, M., Snow, M. H., and McLaren, A. (1990). Primordial germ cells in the mouse embryo during gastrulation. *Development* 110(2):521–528.

[82] Goddard, N. C., McIntyre, A., Summersgill, B., Gilbert, D., Kitazawa, S., and Shipley, J. (2007). KIT and RAS signalling pathways in testicular germ cell tumours: new data and a review of the literature. *Int J Androl* 30(4):337-48; discussion 349.

[83] Guan, K., Nayernia, K., Maier, L. S., Wagner, S., Dressel, R., Lee, J. H., Nolte, J., Wolf, F., Li, M., Engel, W., and Hasenfuss, G. (2006). Pluripotency of spermatogonial stem cells from adult mouse testis. *Nature* 440(7088):1199–1203.

[84] Haeussler, M., Schönig, K., Eckert, H., Eschstruth, A., Mianné, J., Renaud, J.-B., Schneider-Maunoury, S., Shkumatava, A., Teboul, L., Kent, J., Joly, J.-S., and Concordet, J.-P. (2016). Evaluation of off-target and on-target scoring algorithms and integration into the guide RNA selection tool CRISPOR. *Genome Biol* 17(1):148.

[85] Hagan, J. P., Piskounova, E., and Gregory, R. I. (2009). Lin28 recruits the TUTase Zcchc11 to inhibit let-7 maturation in mouse embryonic stem cells. *Nat Struct Mol Biol* 16(10):1021–1025.

[86] Hajkova, P., Erhardt, S., Lane, N., Haaf, T., El-Maarri, O., Reik, W., Walter, J., and Surani, M. A. (2002). Epigenetic reprogramming in mouse primordial germ cells. *Mech Dev* 117(1-2):15–23.

[87] Hammell, C. M., Lubin, I., Boag, P. R., Blackwell, T. K., and Ambros, V. (2009). nhl-2 Modulates microRNA activity in Caenorhabditis elegans. *Cell* 136(5):926–938.

[88] Han, J., Fujisawa, T., Husain, S. R., and Puri, R. K. (2014). Identification and characterization of cancer stem cells in human head and neck squamous cell carcinoma. *BMC Cancer* 14:173.

[89] Handel, M. A. and Schimenti, J. C. (2010). Genetics of mammalian meiosis: regulation, dynamics and impact on fertility. *Nat Rev Genet* 11(2):124–136.

[90] Hanna, J., Saha, K., Pando, B., van Zon, J., Lengner, C. J., Creyghton, M. P., van Oudenaarden, A., and Jaenisch, R. (2009). Direct cell reprogramming is a stochastic process amenable to acceleration. *Nature* 462(7273):595–601.

[91] Hara, K., Nakagawa, T., Enomoto, H., Suzuki, M., Yamamoto, M., Simons, B. D., and Yoshida, S. (2014). Mouse spermatogenic stem cells continually interconvert between equipotent singly isolated and syncytial states. *Cell Stem Cell* 14(5):658–672.

[92] Harper, J. W. and Elledge, S. J. (1996). Cdk inhibitors in development and cancer. *Curr Opin Genet Dev* 6(1):56–64.

[93] Hart, A. H., Hartley, L., Parker, K., Ibrahim, M., Looijenga, L. H. J., Pauchnik, M., Chow, C. W., and Robb, L. (2005). The pluripotency homeobox gene NANOG is expressed in human germ cell tumors. *Cancer* 104(10):2092–2098.

[94] Hasegawa, M., Zhang, Y., Niibe, H., Terry, N. H., and Meistrich, M. L. (1998). Resistance of differentiating spermatogonia to radiation-induced apoptosis and loss in p53-deficient mice. *Radiat Res* 149(3):263–270.

[95] Hatakeyama, S. (2011). TRIM proteins and cancer. *Nat Rev Cancer* 11(11):792–804.

[96] Hayashi, K., Ohta, H., Kurimoto, K., Aramaki, S., and Saitou, M. (2011). Reconstitution of the mouse germ cell specification pathway in culture by pluripotent stem cells. *Cell* 146(4):519–532.

[97] Hayashi, K., Sousa Lopes, S. M. C. de, and Surani, M. A. (2007). Germ cell specification in mice. *Science* 316(5823):394–396.

[98] Heo, I., Joo, C., Cho, J., Ha, M., Han, J., and Kim, V. N. (2008). Lin28 mediates the terminal uridylation of let-7 precursor MicroRNA. *Mol Cell* 32(2):276–284.

[99] Hersmus, R., Leeuw, B. H. C. G. M. de, Wolffenbuttel, K. P., Drop, S. L. S., Oosterhuis, J. W., Cools, M., and Looijenga, L. H. J. (2008). New insights into type II germ cell tumor pathogenesis based on studies of patients with various forms of disorders of sex development (DSD). *Mol Cell Endocrinol* 291(1-2):1–10.

[100] Hilscher, B., Hilscher, W., Bülthoff-Ohnolz, B., Krämer, U., Birke, A., Pelzer, H., and Gauss, G. (1974). Kinetics of gametogenesis. I. Comparative histological and autoradiographic studies of oocytes and transitional prospermatogonia during oogenesis and prespermatogenesis. *Cell Tissue Res* 154(4):443–470.

[101] Hinton, B. T. and Turner, T. T. (1993). The seminiferous tubular microenvironment. In: Cell and molecular biology of the testis, Desjardins, C. and Ewing, L. L. (Eds.), 238–265. Oxford Univ. Press, New York, NY.

[102] Hirschberg, A., Deng, S., Korostylev, A., Paldy, E., Costa, M. R., Worzfeld, T., Vodrazka, P., Wizenmann, A., Götz, M., Offermanns, S., and Kuner, R. (2010). Gene deletion mutants reveal a role for semaphorin receptors of the plexin-B family in mechanisms underlying corticogenesis. *Mol Cell Biol* 30(3):764–780.

[103] Hoei-Hansen, C. E., Almstrup, K., Nielsen, J. E., Brask Sonne, S., Graem, N., Skakkebaek, N. E., Leffers, H., and Rajpert-De Meyts, E. (2005). Stem cell pluripotency factor NANOG is expressed in human fetal gonocytes, testicular carcinoma in situ and germ cell tumours. *Histopathology* 47(1):48–56.

[104] Hoei-Hansen, C. E., Nielsen, J. E., Almstrup, K., Sonne, S. B., Graem, N., Skakkebaek, N. E., Leffers, H., and Rajpert-De Meyts, E. (2004). Transcription factor AP-2gamma is a developmentally regulated marker of testicular carcinoma in situ and germ cell tumors. *Clin Cancer Res* 10(24):8521–8530.

[105] Hoei-Hansen, C. E., Rajpert-De Meyts, E., Daugaard, G., and Skakkebaek, N. E. (2005). Carcinoma in situ testis, the progenitor of testicular germ cell tumours: a clinical review. *Ann Oncol* 16(6):863–868.

[106] Hong, H., Takahashi, K., Ichisaka, T., Aoi, T., Kanagawa, O., Nakagawa, M., Okita, K., and Yamanaka, S. (2009). Suppression of induced pluripotent stem cell generation by the p53-p21 pathway. *Nature* 460(7259):1132–1135.

[107] Hsu, P. D., Lander, E. S., and Zhang, F. (2014). Development and applications of CRISPR-Cas9 for genome engineering. *Cell* 157(6):1262–1278.

[108] Huckins, C. (1971). The spermatogonial stem cell population in adult rats. I. Their morphology, proliferation and maturation. *Anat Rec* 169(3):533–557.

[109] Huckins, C. (1971). The spermatogonial stem cell population in adult rats. II. A radioautographic analysis of their cell cycle properties. *Cell Tissue Kinet* 4(4):313–334.

[110] Huckins, C. and Clermont, Y. (1968). Evolution of gonocytes in the rat testis during late embryonic and early post-natal life. *Arch Anat Histol Embryol* 51(1):341–354.

[111] Huckins, C. and Oakberg, E. F. (1978). Morphological and quantitative analysis of spermatogonia in mouse testes using whole mounted seminiferous tubules, I. The normal testes. *Anat Rec* 192(4):519–528.

[112] Huyghe, E., Matsuda, T., and Thonneau, P. (2003). Increasing incidence of testicular cancer worldwide: a review. *J Urol* 170(1):5–11.

[113] Ishino, Y., Shinagawa, H., Makino, K., Amemura, M., and Nakata, A. (1987). Nucleotide sequence of the iap gene, responsible for alkaline phosphatase isozyme conversion in Escherichia coli, and identification of the gene product. *J Bacteriol* 169(12):5429–5433.

[114] Jinek, M., Chylinski, K., Fonfara, I., Hauer, M., Doudna, J. A., and Charpentier, E. (2012). A programmable dual-RNA-guided DNA endonuclease in adaptive bacterial immunity. *Science* 337(6096):816–821.

[115] Jinek, M., East, A., Cheng, A., Lin, S., Ma, E., and Doudna, J. (2013). RNA-programmed genome editing in human cells. *Elife* 2:e00471.

[116] Joazeiro, C. A. and Weissman, A. M. (2000). RING finger proteins: mediators of ubiquitin ligase activity. *Cell* 102(5):549–552.

[117] Jones, T. D., Ulbright, T. M., Eble, J. N., and Cheng, L. (2004). OCT4: A sensitive and specific biomarker for intratubular germ cell neoplasia of the testis. *Clin Cancer Res* 10(24):8544–8547.

[118] Jørgensen, N., Müller, J., Giwercman, A., Visfeldt, J., Møller, H., and Skakkebaek, N. E. (1995). DNA content and expression of tumour markers in germ cells adjacent to germ cell tumours in childhood: probably a different origin for infantile and adolescent germ cell tumours. *J Pathol* 176(3):269–278.

[119] Jungwirth, T., Diemer, T., Kopa, Z.: Krausz, C., Minhas, S., and Tournaye, H. (2019). *EAU Guidelines on Male Infertility.* EAU Guidelines, Ed. presented at the EAU Annual Congress Barcelona 2019, EAU Guidelines Office, Arnhem, The Netherlands. http://uroweb.org/guidelines/compilations-of-all-guidelines/.

[120] Kanamoto, T., Terada, K., Yoshikawa, H., and Furukawa, T. (2006). Cloning and regulation of the vertebrate homologue of lin-41 that functions as a heterochronic gene in Caenorhabditis elegans. *Dev Dyn* 235(4):1142–1149.

[121] Kanatsu-Shinohara, M., Ogonuki, N., Iwano, T., Lee, J., Kazuki, Y., Inoue, K., Miki, H., Takehashi, M., Toyokuni, S., Shinkai, Y., Oshimura, M., Ishino, F., Ogura, A., and Shinohara, T. (2005). Genetic and epigenetic properties of mouse male germline stem cells during long-term culture. *Development* 132(18):4155–4163.

[122] Kang, W., Wong, L. C., Shi, S.-H., and Hébert, J. M. (2009). The transition from radial glial to intermediate progenitor cell is inhibited by FGF signaling during corticogenesis. *J Neurosci* 29(46):14571–14580.

[123] Kapuściński, J. and Szer, W. (1979). Interactions of 4', 6-diamidine-2-phenylindole with synthetic polynucleotides. *Nucleic Acids Res* 6(11):3519–3534.

[124] Kawamura, T., Suzuki, J., Wang, Y. V., Menendez, S., Morera, L. B., Raya, A., Wahl, G. M., and Izpisúa Belmonte, J. C. (2009). Linking the p53 tumour suppressor pathway to somatic cell reprogramming. *Nature* 460(7259):1140–1144.

[125] Kimura-Yoshida, C., Mochida, K., Ellwanger, K., Niehrs, C., and Matsuo, I. (2015). Fate Specification of Neural Plate Border by Canonical Wnt Signaling and Grhl3 is Crucial for Neural Tube Closure. *EBioMedicine* 2(6):513–527.

[126] Kleinsmith, L. J. and Pierce, G. B. (1964). Multipotentiality of single embryonal carcinoma cells. *Cancer Res* 24:1544–1551.

[127] Kloosterman, W. P., Wienholds, E., Ketting, R. F., and Plasterk, R. H. A. (2004). Substrate requirements for let-7 function in the developing zebrafish embryo. *Nucleic Acids Res* 32(21):6284–6291.

[128] Kluin, P. M. and Rooij, D. G. de. (1981). A comparison between the morphology and cell kinetics of gonocytes and adult type undifferentiated spermatogonia in the mouse. *Int J Androl* 4(4):475–493.

[129] Komander, D. and Rape, M. (2012). The ubiquitin code. *Annu Rev Biochem* 81:203–229.

[130] Köprunner, M., Thisse, C., Thisse, B., and Raz, E. (2001). A zebrafish nanos-related gene is essential for the development of primordial germ cells. *Genes Dev* 15(21):2877–2885.

[131] Koshimizu, U., Nishioka, H., Watanabe, D., Dohmae, K., and Nishimune, Y. (1995). Characterization of a novel spermatogenic cell antigen specific for early stages of germ cells in mouse testis. *Mol. Reprod. Dev.* 40(2):221–227.

[132] Koubova, J., Menke, D. B., Zhou, Q., Capel, B., Griswold, M. D., and Page, D. C. (2006). Retinoic acid regulates sex-specific timing of meiotic initiation in mice. *Proc Natl Acad Sci U S A* 103(8):2474–2479.

[133] Kretser, D. M. de, Buzzard, J. J., Okuma, Y., O'Connor, A. E., Hayashi, T., Lin, S.-Y., Morrison, J. R., Loveland, K. L., and Hedger, M. P. (2004). The role of activin, follistatin and inhibin in testicular physiology. *Mol Cell Endocrinol* 225(1-2):57–64.

[134] Kretser, D. M. de, Hedger, M. P., Loveland, K. L., and Phillips, D. J. (2002). Inhibins, activins and follistatin in reproduction. *Hum Reprod Update* 8(6):529–541.

[135] Krishnaraju, K., Nguyen, H. Q., Liebermann, D. A., and Hoffman, B. (1995). The zinc finger transcription factor Egr-1 potentiates macrophage differentiation of hematopoietic cells. *Mol Cell Biol* 15(10):5499–5507.

[136] Kulkarni, M., Ozgur, S., and Stoecklin, G. (2010). On track with P-bodies. *Biochem Soc Trans* 38(Pt 1):242–251.

[137] Kumari, P., Aeschimann, F., Gaidatzis, D., Keusch, J. J., Ghosh, P., Neagu, A., Pachulska-Wieczorek, K., Bujnicki, J. M., Gut, H., Großhans, H., and Ciosk, R. (2018). Evolutionary plasticity of the NHL domain underlies distinct solutions to RNA recognition. *Nat Commun* 9(1):1549.

[138] Kurimoto, K., Yabuta, Y., Ohinata, Y., Shigeta, M., Yamanaka, K., and Saitou, M. (2008). Complex genome-wide transcription dynamics orchestrated by Blimp1 for the specification of the germ cell lineage in mice. *Genes Dev* 22(12):1617–1635.

[139] Kurimoto, K., Yamaji, M., Seki, Y., and Saitou, M. (2008). Specification of the germ cell lineage in mice: a process orchestrated by the PR-domain proteins, Blimp1 and Prdm14. *Cell Cycle* 7(22):3514–3518.

[140] Kurokawa, H., Aoki, Y., Nakamura, S., Ebe, Y., Kobayashi, D., and Tanaka, M. (2006). Time-lapse analysis reveals different modes of primordial germ cell migration in the medaka Oryzias latipes. *Dev Growth Differ* 48(3):209–221.

[141] Kwon, S. C., Yi, H., Eichelbaum, K., Föhr, S., Fischer, B., You, K. T., Castello, A., Krijgsveld, J., Hentze, M. W., and Kim, V. N. (2013). The RNA-binding protein repertoire of embryonic stem cells. *Nat Struct Mol Biol* 20(9):1122–1130.

[142] Labosky, P. A., Barlow, D. P., and Hogan, B. L. (1994). Embryonic germ cell lines and their derivation from mouse primordial germ cells. *Ciba Found Symp* 182:157-68; discussion 168-78.

[143] Laemmli, U. K. (1970). Cleavage of structural proteins during the assembly of the head of bacteriophage T4. *Nature* 227(5259):680–685.

[144] Lagarrigue, M., Becker, M., Lavigne, R., Deininger, S.-O., Walch, A., Aubry, F., Suckau, D., and Pineau, C. (2011). Revisiting rat spermatogenesis with MALDI imaging at 20-microm resolution. *Mol Cell Proteomics* 10(3):M110.005991.

[145] Lancman, J. J., Caruccio, N. C., Harfe, B. D., Pasquinelli, A. E., Schageman, J. J., Pertsemlidis, A., and Fallon, J. F. (2005). Analysis of the regulation of lin-41 during chick and mouse limb development. *Dev Dyn* 234(4):948–960.

[146] Laslo, P., Spooner, C. J., Warmflash, A., Lancki, D. W., Lee, H.-J., Sciammas, R., Gantner, B. N., Dinner, A. R., and Singh, H. (2006). Multilineage transcriptional priming and determination of alternate hematopoietic cell fates. *Cell* 126(4):755–766.

[147] Lawson, K. A. and Hage, W. J. (1994). Clonal analysis of the origin of primordial germ cells in the mouse. *Ciba Found Symp* 182:68-84; discussion 84-91.

[148] Le Cong, Ran, F. A., Cox, D., Lin, S., Barretto, R., Habib, N., Hsu, P. D., Wu, X., Jiang, W., Marraffini, L. A., and Zhang, F. (2013). Multiplex genome engineering using CRISPR/Cas systems. *Science* 339(6121):819–823.

[149] Lee, J., Inoue, K., Ono, R., Ogonuki, N., Kohda, T., Kaneko-Ishino, T., Ogura, A., and Ishino, F. (2002). Erasing genomic imprinting memory in mouse clone embryos produced from day 11.5 primordial germ cells. *Development* 129(8):1807–1817.

[150] Lee, S. H., Cho, S., Kim, M. S., Choi, K., Cho, J. Y., Gwak, H.-S., Kim, Y.-J., Yoo, H., Lee, S.-H., Park, J. B., and Kim, J. H. (2014). The ubiquitin ligase human TRIM71 regulates let-7 microRNA biogenesis via modulation of Lin28B protein. *Biochim Biophys Acta* 1839(5):374–386.

[151] Li, C., Heidt, D. G., Dalerba, P., Burant, C. F., Zhang, L., Adsay, V., Wicha, M., Clarke, M. F., and Simeone, D. M. (2007). Identification of pancreatic cancer stem cells. *Cancer Res* 67(3):1030–1037.

[152] Li, Y.-P., Duan, F.-F., Zhao, Y.-T., Gu, K.-L., Liao, L.-Q., Su, H.-B., Hao, J., Zhang, K., Yang, N., and Wang, Y. (2019). A TRIM71 binding long noncoding RNA Trincr1 represses FGF/ERK signaling in embryonic stem cells. *Nat Commun* 10(1):1368.

[153] Lin, Y.-C., Hsieh, L.-C., Kuo, M.-W., Yu, J., Kuo, H.-H., Lo, W.-L., Lin, R.-J., Yu, A. L., and Li, W.-H. (2007). Human TRIM71 and its nematode homologue are targets of let-7 microRNA and its zebrafish orthologue is essential for development. *Mol Biol Evol* 24(11):2525–2534.

[154] Lino, C. A., Harper, J. C., Carney, J. P., and Timlin, J. A. (2018). Delivering CRISPR: a review of the challenges and approaches. *Drug Deliv* 25(1):1234–1257.

[155] Liu, D. and Xu, Y. (2011). p53, oxidative stress, and aging. *Antioxid Redox Signal* 15(6):1669–1678.

[156] Livak, K. J. and Schmittgen, T. D. (2001). Analysis of relative gene expression data using real-time quantitative PCR and the 2(-Delta Delta C(T)) Method. *Methods* 25(4):402–408.

[157] Loedige, I., Gaidatzis, D., Sack, R., Meister, G., and Filipowicz, W. (2013). The mammalian TRIM-NHL protein TRIM71/LIN-41 is a repressor of mRNA function. *Nucleic Acids Res* 41(1):518–532.

[158] Loedige, I., Jakob, L., Treiber, T., Ray, D., Stotz, M., Treiber, N., Hennig, J., Cook, K. B., Morris, Q., Hughes, T. R., Engelmann, J. C., Krahn, M. P., and Meister, G. (2015). The Crystal Structure of the NHL Domain in Complex with RNA Reveals the Molecular Basis of Drosophila Brain-Tumor-Mediated Gene Regulation. *Cell Rep* 13(6):1206–1220.

[159] Loedige, I., Stotz, M., Qamar, S., Kramer, K., Hennig, J., Schubert, T., Löffler, P., Längst, G., Merkl, R., Urlaub, H., and Meister, G. (2014). The NHL domain of BRAT is an RNA-binding domain that directly contacts the hunchback mRNA for regulation. *Genes Dev* 28(7):749–764.

[160] Löer, B., Bauer, R., Bornheim, R., Grell, J., Kremmer, E., Kolanus, W., and Hoch, M. (2008). The NHL-domain protein Wech is crucial for the integrin-cytoskeleton link. *Nat Cell Biol* 10(4):422–428.

[161] Lohrasbi, V., Shirmohammadlou, N., Jahanshahi, A., and Razavi, S. (2019). Overview development and applications of CRISPR-Cas systems after a decade of research with a glance at anti-CRISPR proteins. *Reviews in Medical Microbiology* 30(1):47–55.

[162] Lok, D., Jansen, M. T., and Rooij, D. G. de. (1983). Spermatogonial multiplication in the Chinese hamster. II. Cell cycle properties of undifferentiated spermatogonia. *Cell Tissue Kinet* 16(1):19–29.

[163] Lok, D. and Rooij, D. G. de. (1983). Spermatogonial multiplication in the Chinese hamster. III. Labelling indices of undifferentiated spermatogonia throughout the cycle of the seminiferous epithelium. *Cell Tissue Kinet* 16(1):31–40.

[164] Lok, D., Weenk, D., and Rooij, D. G. de. (1982). Morphology, proliferation, and differentiation of undifferentiated spermatogonia in the Chinese hamster and the ram. *Anat Rec* 203(1):83–99.

[165] Looijenga, L. H. J., Hersmus, R., Leeuw, B. H. C. G. M. de, Stoop, H., Cools, M., Oosterhuis, J. W., Drop, S. L. S., and Wolffenbuttel, K. P. (2010). Gonadal tumours and DSD. *Best Pract Res Clin Endocrinol Metab* 24(2):291–310.

[166] Looijenga, L. H. J., Stoop, H., Leeuw, H. P. J. C. de, Gouveia Brazao, C. A. de, Gillis, A. J. M., van Roozendaal, K. E. P., van Zoelen, E. J. J., Weber, R. F. A., Wolffenbuttel, K. P., van Dekken, H., Honecker, F., Bokemeyer, C., Perlman, E. J., Schneider, D. T., Kononen, J., Sauter, G., and Oosterhuis, J. W. (2003). POU5F1 (OCT3/4) identifies cells with pluripotent potential in human germ cell tumors. *Cancer Res* 63(9):2244–2250.

[167] Lorick, K. L., Jensen, J. P., Fang, S., Ong, A. M., Hatakeyama, S., and Weissman, A. M. (1999). RING fingers mediate ubiquitin-conjugating enzyme (E2)-dependent ubiquitination. *Proc Natl Acad Sci U S A* 96(20):11364–11369.

[168] Luo, Y., Hurwitz, J., and Massagué, J. (1995). Cell-cycle inhibition by independent CDK and PCNA binding domains in p21Cip1. *Nature* 375(6527):159–161.

[169] Lupas, A. (1996). Coiled coils: new structures and new functions. *Trends Biochem Sci* 21(10):375–382.

[170] MacLachlan, T. K., Sang, N., and Giordano, A. (1995). Cyclins, cyclin-dependent kinases and cdk inhibitors: implications in cell cycle control and cancer. *Crit Rev Eukaryot Gene Expr* 5(2):127–156.

[171] Mali, P., Yang, L., Esvelt, K. M., Aach, J., Guell, M., DiCarlo, J. E., Norville, J. E., and Church, G. M. (2013). RNA-guided human genome engineering via Cas9. *Science* 339(6121):823–826.

[172] Maller Schulman, B. R., Liang, X., Stahlhut, C., DelConte, C., Stefani, G., and Slack, F. J. (2008). The let-7 microRNA target gene, Mlin41/Trim71 is required for mouse embryonic survival and neural tube closure. *Cell Cycle* 7(24):3935–3942.

[173] Mannelli, G. and Gallo, O. (2012). Cancer stem cells hypothesis and stem cells in head and neck cancers. *Cancer Treat Rev* 38(5):515–539.

[174] Marión, R. M., Strati, K., Li, H., Murga, M., Blanco, R., Ortega, S., Fernandez-Capetillo, O., Serrano, M., and Blasco, M. A. (2009). A p53-mediated DNA damage response limits reprogramming to ensure iPS cell genomic integrity. *Nature* 460(7259):1149–1153.

[175] Martin, G. R. (1980). Teratocarcinomas and mammalian embryogenesis. *Science* 209(4458):768–776.

[176] Mason, I. (2007). Initiation to end point: the multiple roles of fibroblast growth factors in neural development. *Nat Rev Neurosci* 8(8):583–596.

[177] Mason, J. M. and Arndt, K. M. (2004). Coiled coil domains: stability, specificity, and biological implications. *Chembiochem* 5(2):170–176.

[178] Massiah, M. A., Matts, J. A. B., Short, K. M., Simmons, B. N., Singireddy, S., Yi, Z., and Cox, T. C. (2007). Solution structure of the MID1 B-box2 CHC(D/C)C(2)H(2) zinc-binding domain: insights into an evolutionarily conserved RING fold. *J Mol Biol* 369(1):1–10.

[179] Massiah, M. A., Simmons, B. N., Short, K. M., and Cox, T. C. (2006). Solution structure of the RBCC/TRIM B-box1 domain of human MID1: B-box with a RING. *J Mol Biol* 358(2):532–545.

[180] Matsui, Y., Zsebo, K., and Hogan, B. L. (1992). Derivation of pluripotential embryonic stem cells from murine primordial germ cells in culture. *Cell* 70(5):841–847.

[181] McLaren, A. (2003). Primordial germ cells in the mouse. *Dev Biol* 262(1):1–15.

[182] Meistrich, M. L. and van Beek, M. E. A. B. (1993). Spermatogonial stem cells. In: Cell and molecular biology of the testis, Desjardins, C. and Ewing, L. L. (Eds.), 266–295. Oxford Univ. Press, New York, NY.

[183] Meroni, G. and Diez-Roux, G. (2005). TRIM/RBCC, a novel class of 'single protein RING finger' E3 ubiquitin ligases. *Bioessays* 27(11):1147–1157.

[184] Meselson, M., Stahl, F. W., and Vinograd, J. (1957). EQUILIBRIUM SEDIMENTATION OF MACROMOLECULES IN DENSITY GRADIENTS. *Proc Natl Acad Sci U S A* 43(7):581–588.

[185] Micale, L., Chaignat, E., Fusco, C., Reymond, A., and Merla, G. (2012). The Tripartite Motif: Structure and Function. In: TRIM/RBCC Proteins, Meroni, G. (Ed.). *Advances in Experimental Medicine and Biology*, vol 770, 11–25. Springer, New York, NY.

[186] Min, I. M., Pietramaggiori, G., Kim, F. S., Passegué, E., Stevenson, K. E., and Wagers, A. J. (2008). The transcription factor EGR1 controls both the proliferation and localization of hematopoietic stem cells. *Cell Stem Cell* 2(4):380–391.

[187] Mitschka, S. (2015). *The role of Trim71 in cell fate determination of embryonic stem cells and germline development* Dissertation: Rheinische Friedrich-Wilhelms-Universität Bonn.

[188] Mitschka, S., Ulas, T., Goller, T., Schneider, K., Egert, A., Mertens, J., Brüstle, O., Schorle, H., Beyer, M., Klee, K., Xue, J., Günther, P., Bassler, K., Schultze, J. L., and Kolanus, W. (2015). Co-existence of intact stemness and priming of neural differentiation programs in mES cells lacking Trim71. *Sci Rep* 5:11126.

[189] Mizuno, Y., Gotoh, A., Kamidono, S., and Kitazawa, S. (1993). Establishment and characterization of a new human testicular germ cell tumor cell line (TCam-2). *Nippon Hinyokika Gakkai Zasshi* 84(7):1211–1218.

[190] Moch, H., Cubilla, A. L., Humphrey, P. A., Reuter, V. E., and Ulbright, T. M. (2016). The 2016 WHO Classification of Tumours of the Urinary System and Male Genital Organs-Part A: Renal, Penile, and Testicular Tumours. *Eur Urol* 70(1):93–105.

[191] Mochizuki, K., Hayashi, Y., Sekinaka, T., Otsuka, K., Ito-Matsuoka, Y., Kobayashi, H., Oki, S., Takehara, A., Kono, T., Osumi, N., and Matsui, Y. (2018). Repression of Somatic Genes by Selective Recruitment of HDAC3 by BLIMP1 Is Essential for Mouse Primordial Germ Cell Fate Determination. *Cell Rep* 24(10):2682-2693.e6.

[192] Mochizuki, K., Sano, H., Kobayashi, S., Nishimiya-Fujisawa, C., and Fujisawa, T. (2000). Expression and evolutionary conservation of nanos-related genes in Hydra. *Dev Genes Evol* 210(12):591–602.

[193] Mojica, F. J., Díez-Villaseñor, C., Soria, E., and Juez, G. (2000). Biological significance of a family of regularly spaced repeats in the genomes of Archaea, Bacteria and mitochondria. *Mol Microbiol* 36(1):244–246.

[194] Molyneaux, K. A., Stallock, J., Schaible, K., and Wylie, C. (2001). Time-lapse analysis of living mouse germ cell migration. *Dev Biol* 240(2):488–498.

[195] Mosquera, L., Forristall, C., Zhou, Y., and King, M. L. (1993). A mRNA localized to the vegetal cortex of Xenopus oocytes encodes a protein with a nanos-like zinc finger domain. *Development* 117(1):377–386.

[196] Müller, J., Skakkebaek, N. E., and Parkinson, M. C. (1987). The spermatocytic seminoma: views on pathogenesis. *Int J Androl* 10(1):147–156.

[197] Nagano, R., Tabata, S., Nakanishi, Y., Ohsako, S., Kurohmaru, M., and Hayashi, Y. (2000). Reproliferation and relocation of mouse male germ cells (gonocytes) during prespermatogenesis. *Anat Rec* 258(2):210–220.

[198] Nakagawa, T., Nabeshima, Y.-I., and Yoshida, S. (2007). Functional identification of the actual and potential stem cell compartments in mouse spermatogenesis. *Dev Cell* 12(2):195–206.

[199] Nakagawa, T., Sharma, M., Nabeshima, Y.-I., Braun, R. E., and Yoshida, S. (2010). Functional hierarchy and reversibility within the murine spermatogenic stem cell compartment. *Science* 328(5974):62–67.

[200] Nam, Y., Chen, C., Gregory, R. I., Chou, J. J., and Sliz, P. (2011). Molecular basis for interaction of let-7 microRNAs with Lin28. *Cell* 147(5):1080–1091.

[201] Nettersheim, D., Jostes, S., Schneider, S., and Schorle, H. (2016). Elucidating human male germ cell development by studying germ cell cancer. *Reproduction* 152(4):R101-13.

[202] Nettersheim, D., Westernströer, B., Haas, N., Leinhaas, A., Brüstle, O., Schlatt, S., and Schorle, H. (2012). Establishment of a versatile seminoma model indicates cellular plasticity of germ cell tumor cells. *Genes Chromosomes Cancer* 51(7):717–726.

[203] Neumüller, R. A., Betschinger, J., Fischer, A., Bushati, N., Poernbacher, I., Mechtler, K., Cohen, S. M., and Knoblich, J. A. (2008). Mei-P26 regulates microRNAs and cell growth in the Drosophila ovarian stem cell lineage. *Nature* 454(7201):241–245.

[204] Nguyen, D. T. T., Richter, D., Michel, G., Mitschka, S., Kolanus, W., Cuevas, E., and Wulczyn, F. G. (2017). The ubiquitin ligase LIN41/TRIM71 targets p53 to antagonize cell death and differentiation pathways during stem cell differentiation. *Cell Death Differ* 24(6):1063–1078.

[205] Nguyen, H. Q., Hoffman-Liebermann, B., and Liebermann, D. A. (1993). The zinc finger transcription factor Egr-1 is essential for and restricts differentiation along the macrophage lineage. *Cell* 72(2):197–209.

[206] Nielsen, H., Nielsen, M., and Skakkebaek, N. E. (1974). The fine structure of possible carcinoma-in-situ in the seminiferous tubules in the testis of four infertile men. *Acta Pathol Microbiol Scand A* 82(2):235–248.

[207] Nikolopoulou, E., Galea, G. L., Rolo, A., Greene, N. D. E., and Copp, A. J. (2017). Neural tube closure: cellular, molecular and biomechanical mechanisms. *Development* 144(4):552–566.

[208] Oakberg, E. F. (1971). Spermatogonial stem-cell renewal in the mouse. *Anat Rec* 169(3):515–531.

[209] O'Donnell, L. (2014). Mechanisms of spermiogenesis and spermiation and how they are disturbed. *Spermatogenesis* 4(2):e979623.

[210] O'Donnell, L., Nicholls, P. K., O'Bryan, M. K., McLachlan, R. I., and Stanton, P. G. (2011). Spermiation: The process of sperm release. *Spermatogenesis* 1(1):14–35.

[211] O'Farrell, F., Esfahani, S. S., Engström, Y., and Kylsten, P. (2008). Regulation of the Drosophila lin-41 homologue dappled by let-7 reveals conservation of a regulatory mechanism within the LIN-41 subclade. *Dev Dyn* 237(1):196–208.

[212] Ohinata, Y., Payer, B., O'Carroll, D., Ancelin, K., Ono, Y., Sano, M., Barton, S. C., Obukhanych, T., Nussenzweig, M., Tarakhovsky, A., Saitou, M., and Surani, M. A. (2005). Blimp1 is a critical determinant of the germ cell lineage in mice. *Nature* 436(7048):207–213.

[213] Oosterhuis, J. W. and Looijenga, L. H. J. (2005). Testicular germ-cell tumours in a broader perspective. *Nat Rev Cancer* 5(3):210–222.

[214] Oosterhuis, J. W. and Looijenga, L. H. J. (2019). Human germ cell tumours from a developmental perspective. *Nat Rev Cancer* 19(9):522–537.

[215] Paniagua, R., Codesal, J., Nistal, M., Rodríguez, M. C., and Santamaría, L. (1987). Quantification of cell types throughout the cycle of the human seminiferous epithelium and their DNA content. A new approach to the spermatogonial stem cell in man. *Anat Embryol* 176(2):225–230.

[216] Park, J. S., Kim, J., Elghiaty, A., and Ham, W. S. (2018). Recent global trends in testicular cancer incidence and mortality. *Medicine (Baltimore)* 97(37):e12390.

[217] Pauls, K., Jäger, R., Weber, S., Wardelmann, E., Koch, A., Büttner, R., and Schorle, H. (2005). Transcription factor AP-2gamma, a novel marker of gonocytes and seminomatous germ cell tumors. *Int J Cancer* 115(3):470–477.

[218] Pennisi, E. (2013). The CRISPR craze. *Science* 341(6148):833–836.

[219] Pesce, M., Wang, X., Wolgemuth, D. J., and Schöler, H. (1998). Differential expression of the Oct-4 transcription factor during mouse germ cell differentiation. *Mech Dev* 71(1-2):89–98.

[220] Phillips, B. T., Gassei, K., and Orwig, K. E. (2010). Spermatogonial stem cell regulation and spermatogenesis. *Philos Trans R Soc Lond B Biol Sci* 365(1546):1663–1678.

[221] Pilon, M. and Weisblat, D. A. (1997). A nanos homolog in leech. *Development* 124(9):1771–1780.

[222] Pinello, L., Canver, M. C., Hoban, M. D., Orkin, S. H., Kohn, D. B., Bauer, D. E., and Yuan, G.-C. (2016). Analyzing CRISPR genome-editing experiments with CRISPResso. *Nat Biotechnol* 34(7):695–697.

[223] Pucci, B., Kasten, M., and Giordano, A. (2000). Cell cycle and apoptosis. *Neoplasia* 2(4):291–299.

[224] Rajpert-De Meyts, E. (2006). Developmental model for the pathogenesis of testicular carcinoma in situ: genetic and environmental aspects. *Hum Reprod Update* 12(3):303–323.

[225] Rajpert-De Meyts, E., Hanstein, R., Jørgensen, N., Graem, N., Vogt, P. H., and Skakkebaek, N. E. (2004). Developmental expression of POU5F1 (OCT-3/4) in normal and dysgenetic human gonads. *Hum Reprod* 19(6):1338–1344.

[226] Rajpert-De Meyts, E., McGlynn, K. A., Okamoto, K., Jewett, M. A. S., and Bokemeyer, C. (2016). Testicular germ cell tumours. *Lancet* 387(10029):1762–1774.

[227] Rajpert-De Meyts, E., Nielsen, J. E., Skakkebaek, N. E., and Almstrup, K. (2015). Diagnostic markers for germ cell neoplasms: from placental-like alkaline phosphatase to micro-RNAs. *Folia Histochem Cytobiol* 53(3):177–188.

[228] Rajpert-De Meyts, E. and Skakkebaek, N. E. (1994). Expression of the c-kit protein product in carcinoma-in-situ and invasive testicular germ cell tumours. *Int J Androl* 17(2):85–92.

[229] Raman, J. D., Nobert, C. F., and Goldstein, M. (2005). Increased incidence of testicular cancer in men presenting with infertility and abnormal semen analysis. *J Urol* 174(5):1819-22; discussion 1822.

[230] Ran, F. A., Hsu, P. D., Wright, J., Agarwala, V., Scott, D. A., and Zhang, F. (2013). Genome engineering using the CRISPR-Cas9 system. *Nat Protoc* 8(11):2281–2308.

[231] Reddy, B. A. and Etkin, L. D. (1991). A unique bipartite cysteine-histidine motif defines a subfamily of potential zinc-finger proteins. *Nucleic Acids Res* 19(22):6330.

[232] Reddy, B. A., Etkin, L. D., and Freemont, P. S. (1992). A novel zinc finger coiled-coil domain in a family of nuclear proteins. *Trends Biochem Sci* 17(9):344–345.

[233] Reinhart, B. J., Slack, F. J., Basson, M., Pasquinelli, A. E., Bettinger, J. C., Rougvie, A. E., Horvitz, H. R., and Ruvkun, G. (2000). The 21-nucleotide let-7 RNA regulates developmental timing in Caenorhabditis elegans. *Nature* 403(6772):901–906.

[234] Resnick, J. L., Bixler, L. S., Cheng, L., and Donovan, P. J. (1992). Long-term proliferation of mouse primordial germ cells in culture. *Nature* 359(6395):550–551.

[235] Reya, T., Morrison, S. J., Clarke, M. F., and Weissman, I. L. (2001). Stem cells, cancer, and cancer stem cells. *Nature* 414(6859):105–111.

[236] Reymond, A., Meroni, G., Fantozzi, A., Merla, G., Cairo, S., Luzi, L., Riganelli, D., Zanaria, E., Messali, S., Cainarca, S., Guffanti, A., Minucci, S., Pelicci, P. G., and Ballabio, A. (2001). The tripartite motif family identifies cell compartments. *EMBO J* 20(9):2140–2151.

[237] Richardson, B. E. and Lehmann, R. (2010). Mechanisms guiding primordial germ cell migration: strategies from different organisms. *Nat Rev Mol Cell Biol* 11(1):37–49.

[238] Rooij, D. G. de. (1998). Stem cells in the testis. *Int J Exp Pathol* 79(2):67–80.

[239] Rooij, D. G. de. (2017). The nature and dynamics of spermatogonial stem cells. *Development* 144(17):3022–3030.

[240] Rooij, D. G. de and Griswold, M. D. (2012). Questions about spermatogonia posed and answered since 2000. *J Androl* 33(6):1085–1095.

[241] Rooij, D. G. de and Russell, L. D. (2000). All you wanted to know about spermatogonia but were afraid to ask. *J Androl* 21(6):776–798.

[242] Rotter, V., Schwartz, D., Almon, E., Goldfinger, N., Kapon, A., Meshorer, A., Donehower, L. A., and Levine, A. J. (1993). Mice with reduced levels of p53 protein exhibit the testicular giant-cell degenerative syndrome. *Proc Natl Acad Sci U S A* 90(19):9075–9079.

[243] Roy, S. and Majumdar, A. P. N. (2012). Colon Cancer Stem Cells: A Therapeutic Target. In: Stem Cells and Cancer Stem Cells, Volume 8, Therapeutic Applications in Disease and Injury, Hayat, M. A. (Ed.). *Stem Cells and Cancer Stem Cells*, vol 8, 217–225. Springer, Dordrecht.

[244] Runyan, C., Schaible, K., Molyneaux, K., Wang, Z., Levin, L., and Wylie, C. (2006). Steel factor controls midline cell death of primordial germ cells and is essential for their normal proliferation and migration. *Development* 133(24):4861–4869.

[245] Russell, L. D., Ettlin, R. A., Sinha Hikim, A. P., and Clegg, E. D. (1990). Histological and histopathological evaluation of the testis. Cache River Press, Clearwater, Fl.

[246] Rybak, A., Fuchs, H., Hadian, K., Smirnova, L., Wulczyn, E. A., Michel, G., Nitsch, R., Krappmann, D., and Wulczyn, F. G. (2009). The let-7 target gene mouse lin-41 is a stem cell specific E3 ubiquitin ligase for the miRNA pathway protein Ago2. *Nat Cell Biol* 11(12):1411–1420.

[247] Saitou, M., Barton, S. C., and Surani, M. A. (2002). A molecular programme for the specification of germ cell fate in mice. *Nature* 418(6895):293–300.

[248] Saitou, M., Kagiwada, S., and Kurimoto, K. (2012). Epigenetic reprogramming in mouse pre-implantation development and primordial germ cells. *Development* 139(1):15–31.

[249] Saitou, M., Payer, B., O'Carroll, D., Ohinata, Y., and Surani, M. A. (2005). Blimp1 and the emergence of the germ line during development in the mouse. *Cell Cycle* 4(12):1736–1740.

[250] Saitou, M. and Yamaji, M. (2012). Primordial germ cells in mice. *Cold Spring Harb Perspect Biol* 4(11).

[251] Sander, J. D. and Joung, J. K. (2014). CRISPR-Cas systems for editing, regulating and targeting genomes. *Nat Biotechnol* 32(4):347–355.

[252] Sapsford, C. S. (1962). Changes in the cells of the Sex Cords and Seminiferous Tubules during the development of the Testis of the rat and mouse. *Aust. J. Zool.* 10(2):178.

[253] Schindelin, J., Arganda-Carreras, I., Frise, E., Kaynig, V., Longair, M., Pietzsch, T., Preibisch, S., Rueden, C., Saalfeld, S., Schmid, B., Tinevez, J.-Y., White, D. J., Hartenstein, V., Eliceiri, K., Tomancak, P., and Cardona, A. (2012). Fiji: an open-source platform for biological-image analysis. *Nat Methods* 9(7):676–682.

[254] Schneider, D. T., Schuster, A. E., Fritsch, M. K., Hu, J., Olson, T., Lauer, S., Göbel, U., and Perlman, E. J. (2001). Multipoint imprinting analysis indicates a common precursor cell for gonadal and nongonadal pediatric germ cell tumors. *Cancer Res* 61(19):7268–7276.

[255] Schnell, J. D. and Hicke, L. (2003). Non-traditional functions of ubiquitin and ubiquitin-binding proteins. *J Biol Chem* 278(38):35857–35860.

[256] Schulman, B. R. M., Esquela-Kerscher, A., and Slack, F. J. (2005). Reciprocal expression of lin-41 and the microRNAs let-7 and mir-125 during mouse embryogenesis. *Dev Dyn* 234(4):1046–1054.

[257] Schwamborn, J. C., Berezikov, E., and Knoblich, J. A. (2009). The TRIM-NHL protein TRIM32 activates microRNAs and prevents self-renewal in mouse neural progenitors. *Cell* 136(5):913–925.

[258] Schwartz, D. C. and Hochstrasser, M. (2003). A superfamily of protein tags: ubiquitin, SUMO and related modifiers. *Trends Biochem Sci* 28(6):321–328.

[259] Seki, Y., Yamaji, M., Yabuta, Y., Sano, M., Shigeta, M., Matsui, Y., Saga, Y., Tachibana, M., Shinkai, Y., and Saitou, M. (2007). Cellular dynamics associated with the genome-wide epigenetic reprogramming in migrating primordial germ cells in mice. *Development* 134(14):2627–2638.

[260] (2011). Sertoli Cells. In: Encyclopedia of Cancer, Schwab, M. (Ed.), 3389–3390. Springer-Verlag, Berlin, Heidelberg.

[261] Shan, Z., Liu, Q., Li, Y., Wu, J., Sun, D., and Gao, Z. (2017). PUMA decreases the growth of prostate cancer PC-3 cells independent of p53. *Oncol Lett* 13(3):1885–1890.

[262] Sheth, U. and Parker, R. (2003). Decapping and decay of messenger RNA occur in cytoplasmic processing bodies. *Science* 300(5620):805–808.

[263] Skakkebaek, N. E. (1972). Possible carcinoma-in-situ of the testis. *Lancet* 2(7776):516–517.

[264] Skakkebaek, N. E., Berthelsen, J. G., Giwercman, A., and Müller, J. (1987). Carcinoma-in-situ of the testis: possible origin from gonocytes and precursor of all types of germ cell tumours except spermatocytoma. *Int J Androl* 10(1):19–28.

[265] Slack, F. J., Basson, M., Liu, Z., Ambros, V., Horvitz, H. R., and Ruvkun, G. (2000). The lin-41 RBCC gene acts in the C. elegans heterochronic pathway between the let-7 regulatory RNA and the LIN-29 transcription factor. *Mol Cell* 5(4):659–669.

[266] Slack, F. J. and Ruvkun, G. (1998). A novel repeat domain that is often associated with RING finger and B-box motifs. *Trends Biochem Sci* 23(12):474–475.

[267] Sonne, S. B., Almstrup, K., Dalgaard, M., Juncker, A. S., Edsgard, D., Ruban, L., Harrison, N. J., Schwager, C., Abdollahi, A., Huber, P. E., Brunak, S., Gjerdrum, L. M., Moore, H. D., Andrews, P. W., Skakkebaek, N. E., Rajpert-De Meyts, E., and Leffers, H. (2009). Analysis of gene expression profiles of microdissected cell populations indicates that testicular carcinoma in situ is an arrested gonocyte. *Cancer Res* 69(12):5241–5250.

[268] Sonoda, J. and Wharton, R. P. (2001). Drosophila Brain Tumor is a translational repressor. *Genes Dev* 15(6):762–773.

[269] Speed, R. M. (1982). Meiosis in the foetal mouse ovary. I. An analysis at the light microscope level using surface-spreading. *Chromosoma* 85(3):427–437.

[270] Spike, C. A., Coetzee, D., Eichten, C., Wang, X., Hansen, D., and Greenstein, D. (2014). The TRIM-NHL protein LIN-41 and the OMA RNA-binding proteins antagonistically control the prophase-to-metaphase transition and growth of Caenorhabditis elegans oocytes. *Genetics* 198(4):1535–1558.

[271] Spike, C. A., Huelgas-Morales, G., Tsukamoto, T., and Greenstein, D. (2018). Multiple Mechanisms Inactivate the LIN-41 RNA-Binding Protein To Ensure a Robust Oocyte-to-Embryo Transition in Caenorhabditis elegans. *Genetics* 210(3):1011–1037.

[272] Stallock, J., Molyneaux, K., Schaible, K., Knudson, C. M., and Wylie, C. (2003). The pro-apoptotic gene Bax is required for the death of ectopic primordial germ cells during their migration in the mouse embryo. *Development* 130(26):6589–6597.

[273] Stewart, C. L., Gadi, I., and Bhatt, H. (1994). Stem cells from primordial germ cells can reenter the germ line. *Dev Biol* 161(2):626–628.

[274] Subramaniam, K. and Seydoux, G. (1999). nos-1 and nos-2, two genes related to Drosophila nanos, regulate primordial germ cell development and survival in Caenorhabditis elegans. *Development* 126(21):4861–4871.

[275] Suzuki, A., Tsuda, M., and Saga, Y. (2007). Functional redundancy among Nanos proteins and a distinct role of Nanos2 during male germ cell development. *Development* 134(1):77–83.

[276] Suzuki, H., Tsuda, M., Kiso, M., and Saga, Y. (2008). Nanos3 maintains the germ cell lineage in the mouse by suppressing both Bax-dependent and -independent apoptotic pathways. *Dev Biol* 318(1):133–142.

[277] Tadokoro, Y., Yomogida, K., Ohta, H., Tohda, A., and Nishimune, Y. (2002). Homeostatic regulation of germinal stem cell proliferation by the GDNF/FSH pathway. *Mech Dev* 113(1):29–39.

[278] Takahashi, K. and Yamanaka, S. (2006). Induction of pluripotent stem cells from mouse embryonic and adult fibroblast cultures by defined factors. *Cell* 126(4):663–676.

[279] Tam, P. P. and Snow, M. H. (1981). Proliferation and migration of primordial germ cells during compensatory growth in mouse embryos. *J Embryol Exp Morphol* 64:133–147.

[280] Tanaka H., Pereira, L. A., NOZAKI, M., TSUCHIDA, J., SAWADA, K., MORI, H., and Nishimune, Y. (1997). A germ cell-specific nuclear antigen recognized by a monoclonal antibody raised against mouse testicular germ cells. *Int J Androl* 20(6):361–366.

[281] Tang, Z., Kang, B., Li, C., Chen, T., and Zhang, Z. (2019). GEPIA2: an enhanced web server for large-scale expression profiling and interactive analysis. *Nucleic Acids Res* 47(W1):W556-W560.

[282] Tao, H., Simmons, B. N., Singireddy, S., Jakkidi, M., Short, K. M., Cox, T. C., and Massiah, M. A. (2008). Structure of the MID1 tandem B-boxes reveals an interaction reminiscent of intermolecular ring heterodimers. *Biochemistry* 47(8):2450–2457.

[283] Tegelenbosch, R. A. and Rooij, D. G. de. (1993). A quantitative study of spermatogonial multiplication and stem cell renewal in the C3H/101 F1 hybrid mouse. *Mutat Res* 290(2):193–200.

[284] Teshima, S., Shimosato, Y., Hirohashi, S., Tome, Y., Hayashi, I., Kanazawa, H., and Kakizoe, T. (1988). Four new human germ cell tumor cell lines. *Lab Invest* 59(3):328–336.

[285] Thornton, J. E., Chang, H.-M., Piskounova, E., and Gregory, R. I. (2012). Lin28-mediated control of let-7 microRNA expression by alternative TUTases Zcchc11 (TUT4) and Zcchc6 (TUT7). *RNA* 18(10):1875–1885.

[286] Ting, S. B., Wilanowski, T., Auden, A., Hall, M., Voss, A. K., Thomas, T., Parekh, V., Cunningham, J. M., and Jane, S. M. (2003). Inositol- and folate-resistant neural tube defects in mice lacking the epithelial-specific factor Grhl-3. *Nat Med* 9(12):1513–1519.

[287] Tocchini, C. and Ciosk, R. (2015). TRIM-NHL proteins in development and disease. *Semin Cell Dev Biol* 47-48:52–59.

[288] Tocchini, C., Keusch, J. J., Miller, S. B., Finger, S., Gut, H., Stadler, M. B., and Ciosk, R. (2014). The TRIM-NHL protein LIN-41 controls the onset of developmental plasticity in Caenorhabditis elegans. *PLoS Genet* 10(8):e1004533.

[289] Torok, M. and Etkin, L. D. (2001). Two B or not two B? Overview of the rapidly expanding B-box family of proteins. *Differentiation* 67(3):63–71.

[290] Torres-Fernández, L. A., Jux, B., Bille, M., Port, Y., Schneider, K., Geyer, M., Mayer, G., and Kolanus, W. (2019). The mRNA repressor TRIM71 cooperates with Nonsense-Mediated Decay factors to destabilize the mRNA of CDKN1A/p21. *Nucleic Acids Res* 47(22):11861–11879.

[291] Tsuda, M., Sasaoka, Y., Kiso, M., Abe, K., Haraguchi, S., Kobayashi, S., and Saga, Y. (2003). Conserved role of nanos proteins in germ cell development. *Science* 301(5637):1239–1241.

[292] Tsukamoto, T., Gearhart, M. D., Spike, C. A., Huelgas-Morales, G., Mews, M., Boag, P. R., Beilharz, T. H., and Greenstein, D. (2017). LIN-41 and OMA Ribonucleoprotein Complexes Mediate a Translational Repression-to-Activation Switch Controlling Oocyte Meiotic Maturation and the Oocyte-to-Embryo Transition in Caenorhabditis elegans. *Genetics* 206(4):2007–2039.

[293] Ueno, T., Tanaka, Y. O., Nagata, M., Tsunoda, H., Anno, I., Ishikawa, S., Kawai, K., and Itai, Y. (2004). Spectrum of germ cell tumors: from head to toe. *Radiographics* 24(2):387–404.

[294] Vaiopoulos, A. G., Kostakis, I. D., Koutsilieris, M., and Papavassiliou, A. G. (2012). Colorectal cancer stem cells. *Stem Cells* 30(3):363–371.

[295] Vasdev, N., Moon, A., and Thorpe, A. C. (2013). Classification, epidemiology and therapies for testicular germ cell tumours. *Int J Dev Biol* 57(2-4):133–139.

[296] Vella, M. C., Choi, E.-Y., Lin, S.-Y., Reinert, K., and Slack, F. J. (2004). The C. elegans microRNA let-7 binds to imperfect let-7 complementary sites from the lin-41 3'UTR. *Genes Dev* 18(2):132–137.

[297] Vella, M. C., Reinert, K., and Slack, F. J. (2004). Architecture of a validated microRNA:target interaction. *Chem Biol* 11(12):1619–1623.

[298] Vergouwen, R. P., Jacobs, S. G., Huiskamp, R., Davids, J. A., and Rooij, D. G. de. (1991). Proliferative activity of gonocytes, Sertoli cells and interstitial cells during testicular development in mice. *J Reprod Fertil* 93(1):233–243.

[299] Vincent, S. D., Dunn, N. R., Sciammas, R., Shapiro-Shalef, M., Davis, M. M., Calame, K., Bikoff, E. K., and Robertson, E. J. (2005). The zinc finger transcriptional repressor Blimp1/Prdm1 is dispensable for early axis formation but is required for specification of primordial germ cells in the mouse. *Development* 132(6):1315–1325.

[300] Viswanathan, S. R., Daley, G. Q., and Gregory, R. I. (2008). Selective blockade of microRNA processing by Lin28. *Science* 320(5872):97–100.

[301] Wang, H., La Russa, M., and Qi, L. S. (2016). CRISPR/Cas9 in Genome Editing and Beyond. *Annu Rev Biochem* 85:227–264.

[302] Wang, L., Rowe, R. G., Jaimes, A., Yu, C., Nam, Y., Pearson, D. S., Zhang, J., Xie, X., Marion, W., Heffron, G. J., Daley, G. Q., and Sliz, P. (2018). Small-Molecule Inhibitors Disrupt let-7 Oligouridylation and Release the Selective Blockade of let-7 Processing by LIN28. *Cell Rep* 23(10):3091–3101.

[303] Wang, R. A., Nakane, P. K., and Koji, T. (1998). Autonomous cell death of mouse male germ cells during fetal and postnatal period. *Biol Reprod* 58(5):1250–1256.

[304] Weber, S., Eckert, D., Nettersheim, D., Gillis, A. J. M., Schäfer, S., Kuckenberg, P., Ehlermann, J., Werling, U., Biermann, K., Looijenga, L. H. J., and Schorle, H. (2010). Critical function of AP-2 gamma/TCFAP2C in mouse embryonic germ cell maintenance. *Biol Reprod* 82(1):214–223.

[305] Welte, T., Tuck, A. C., Papasaikas, P., Carl, S. H., Flemr, M., Knuckles, P., Rankova, A., Bühler, M., and Großhans, H. (2019). The RNA hairpin binder TRIM71 modulates alternative splicing by repressing MBNL1. *Genes Dev* 33(17-18):1221–1235.

[306] West, J. A., Viswanathan, S. R., Yabuuchi, A., Cunniff, K., Takeuchi, A., Park, I.-H., Sero, J. E., Zhu, H., Perez-Atayde, A., Frazier, A. L., Surani, M. A., and Daley, G. Q. (2009). A role for Lin28 in primordial germ-cell development and germ-cell malignancy. *Nature* 460(7257):909–913.

[307] Western, P. S., Miles, D. C., van den Bergen, J. A., Burton, M., and Sinclair, A. H. (2008). Dynamic regulation of mitotic arrest in fetal male germ cells. *Stem Cells* 26(2):339–347.

[308] Worringer, K. A., Rand, T. A., Hayashi, Y., Sami, S., Takahashi, K., Tanabe, K., Narita, M., Srivastava, D., and Yamanaka, S. (2014). The let-7/LIN-41 pathway regulates reprogramming to human induced pluripotent stem cells by controlling expression of prodifferentiation genes. *Cell Stem Cell* 14(1):40–52.

[309] Wulczyn, F. G., Cuevas, E., Franzoni, E., and Rybak, A. (2011). miRNAs Need a Trim: Regulation of miRNA Activity by Trim-NHL Proteins. In: Regulation of microRNAs, Großhans, H. (Ed.). *Advances in Experimental Medicine and Biology*, vol 700, 85–105. Landes Bioscience and Springer Science+Business Media LLC, New York, NY.

[310] Wyman, C. and Kanaar, R. (2006). DNA double-strand break repair: all's well that ends well. *Annu Rev Genet* 40:363–383.

[311] Yabuta, Y., Kurimoto, K., Ohinata, Y., Seki, Y., and Saitou, M. (2006). Gene expression dynamics during germline specification in mice identified by quantitative single-cell gene expression profiling. *Biol Reprod* 75(5):705–716.

[312] Yamada, Y., Davis, K. D., and Coffman, C. R. (2008). Programmed cell death of primordial germ cells in Drosophila is regulated by p53 and the Outsiders monocarboxylate transporter. *Development* 135(2):207–216.

[313] Yamaji, M., Seki, Y., Kurimoto, K., Yabuta, Y., Yuasa, M., Shigeta, M., Yamanaka, K., Ohinata, Y., and Saitou, M. (2008). Critical function of Prdm14 for the establishment of the germ cell lineage in mice. *Nat Genet* 40(8):1016–1022.

[314] Yamaji, M., Tanaka, T., Shigeta, M., Chuma, S., Saga, Y., and Saitou, M. (2010). Functional reconstruction of NANOS3 expression in the germ cell lineage by a novel transgenic reporter reveals distinct subcellular localizations of NANOS3. *Reproduction* 139(2):381–393.

[315] Yamashita, T. and Wang, X. W. (2013). Cancer stem cells in the development of liver cancer. *J Clin Invest* 123(5):1911–1918.

[316] Yang, Z. F., Ngai, P., Ho, D. W., Yu, W. C., Ng, M. N. P., Lau, C. K., Li, M. L. Y., Tam, K. H., Lam, C. T., Poon, R. T. P., and Fan, S. T. (2008). Identification of local and circulating cancer stem cells in human liver cancer. *Hepatology* 47(3):919–928.

[317] Yi, L., Lu, C., Hu, W., Sun, Y., and Levine, A. J. (2012). Multiple roles of p53-related pathways in somatic cell reprogramming and stem cell differentiation. *Cancer Res* 72(21):5635–5645.

[318] Yoshida, S. (2010). Stem cells in mammalian spermatogenesis. *Dev Growth Differ* 52(3):311–317.

[319] Yu, J. and Zhang, L. (2008). PUMA, a potent killer with or without p53. *Oncogene* 27(Suppl 1):S71-83.

[320] Yu, Z. K., Gervais, J. L., and Zhang, H. (1998). Human CUL-1 associates with the SKP1/SKP2 complex and regulates p21(CIP1/WAF1) and cyclin D proteins. *Proc Natl Acad Sci U S A* 95(19):11324–11329.

[321] Zhao, G.-Q. and Garbers, D. L. (2002). Male Germ Cell Specification and Differentiation. *Dev Cell* 2(5):537–547.

[322] Zheng, K., Wu, X., Kaestner, K. H., and Wang, P. J. (2009). The pluripotency factor LIN28 marks undifferentiated spermatogonia in mouse. *BMC Dev Biol* 9:38.

[323] Zhong, X., Li, N., Liang, S., Huang, Q., Coukos, G., and Zhang, L. (2010). Identification of microRNAs regulating reprogramming factor LIN28 in embryonic stem cells and cancer cells. *J Biol Chem* 285(53):41961–41971.

[324] Zorrilla, M. and Yatsenko, A. N. (2013). The Genetics of Infertility: Current Status of the Field. *Curr Genet Med Rep* 1(4).

[325] Zwaka, T. P. and Thomson, J. A. (2005). A germ cell origin of embryonic stem cells? *Development* 132(2):227–233.

Appendix

Supplementary figures

Supplementary figure S1

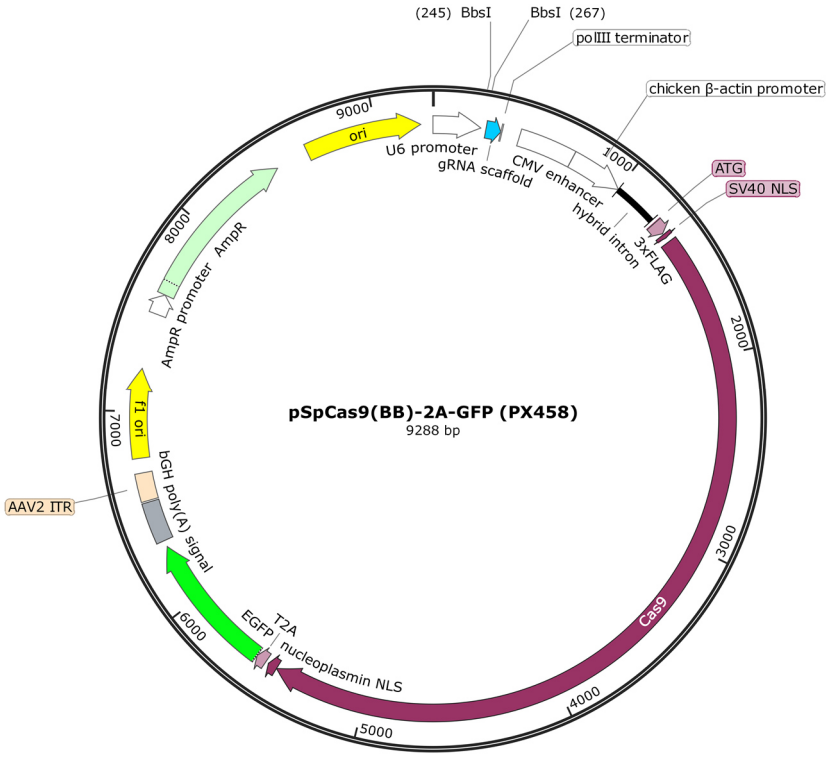

Figure S1 – Vector map of CRISPR/Cas9 plasmid pSpCas9-2A-GFP (PX458)
The PX458 plasmid was obtained as a gift from Feng Zhang (Addgene plasmid # 48138) and carries the cloning backbone for the sgRNAs together with the Cas9 from *S. pyogenes* and eGFP as a selection maker separated by the self-cleaving peptide T2A. The sgRNAs were inserted into the PX458 plasmid via *BbsI* restriction sites directly in front of the gRNA scaffold sequence. The ampicillin resistance gene (*AmpR*) served as the selection marker for cloning. The vector map was designed using the SnapGene software.

Supplementary figure S2

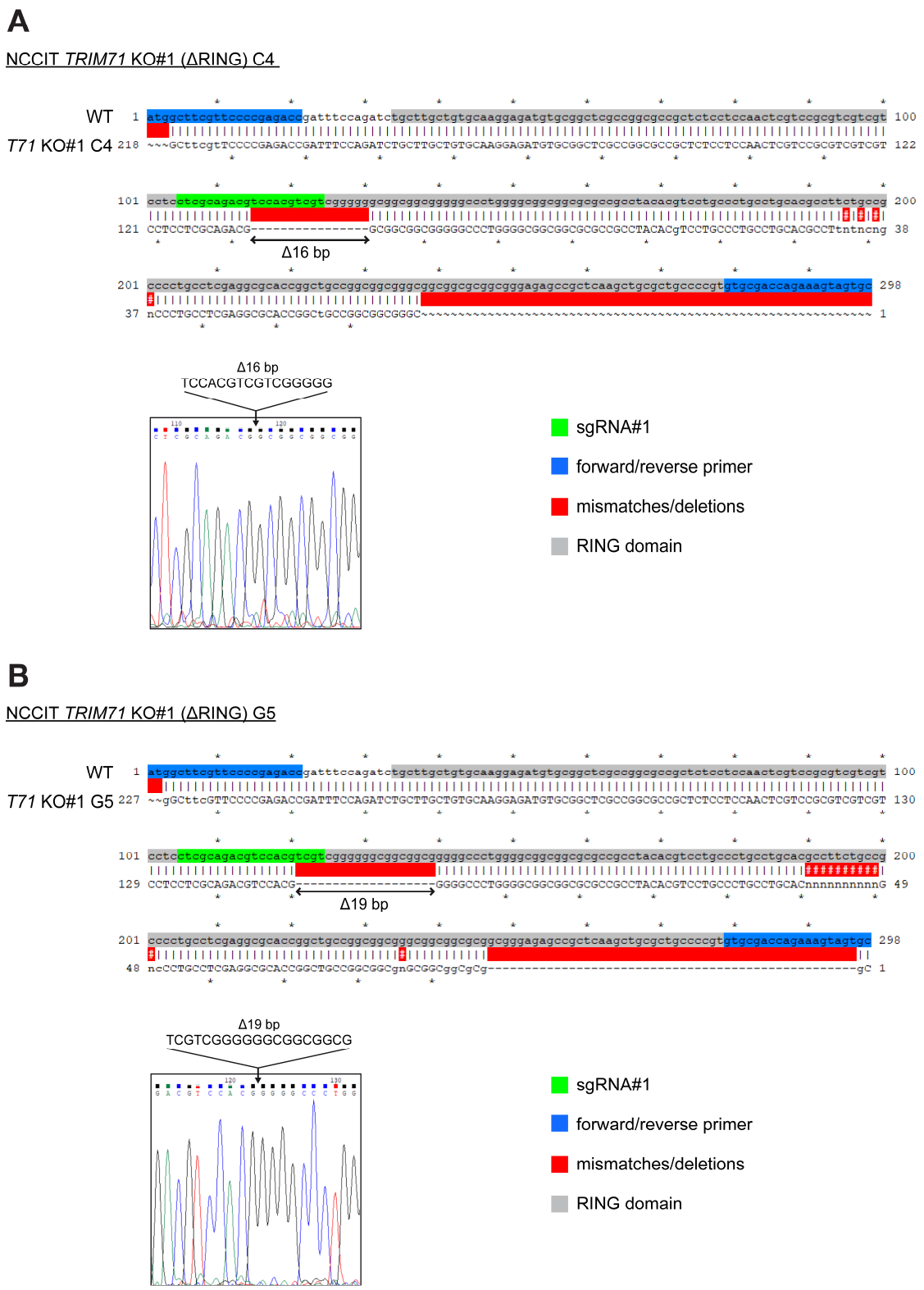

Figure S2 – Sanger sequencing of NCCIT *TRIM71* KO#1 (ΔRING) single cell clones
(A) Sequence alignment of Sanger sequencing results for the NCCIT *TRIM71* KO#1 (ΔRING) C4 single cell clone with wild type (WT) sequence using ApE plasmid editor (top) and the corresponding Sanger sequencing chromatogram (bottom). **(B)** Sequence alignment of Sanger sequencing results for the NCCIT *TRIM71* KO#1 (ΔRING) G5 single cell clone with wild type (WT) sequence using ApE plasmid editor (top) and the corresponding Sanger sequencing chromatogram (bottom). *T71*=*TRIM71*; WT=wild type.

Supplementary Figure S3

A

NCCIT *TRIM71* KO#2 (Δ6NHL) C5

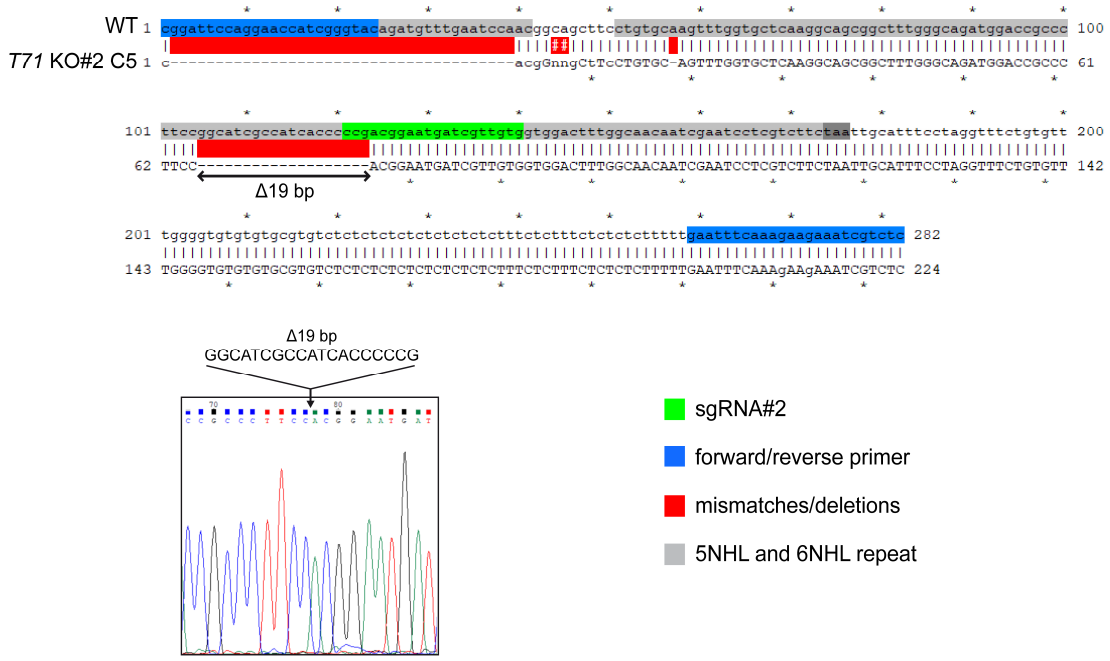

B

NCCIT *TRIM71* KO#2 (Δ6NHL) C8.2

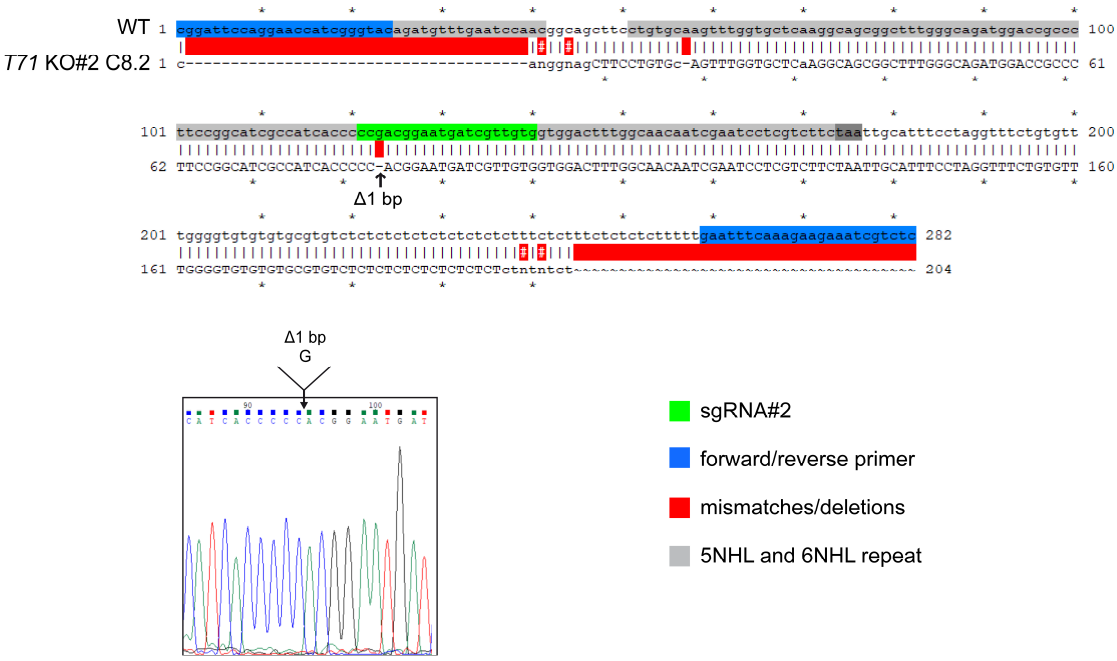

Figure S3 – Sanger sequencing of NCCIT *TRIM71* KO#2 (Δ6NHL) single cell clones
(A) Sequence alignment of Sanger sequencing results for the NCCIT *TRIM71* KO#2 (Δ6NHL) C5 single cell clone with wild type (WT) sequence using ApE plasmid editor (top) and the corresponding Sanger sequencing chromatogram (bottom). **(B)** Sequence alignment of Sanger sequencing results for the NCCIT *TRIM71* KO#2 (Δ6NHL) C8.2 single cell clone with wild type (WT) sequence using ApE plasmid editor (top) and the corresponding Sanger sequencing chromatogram (bottom). *T71*=*TRIM71*; WT=wild type.

Illumina MiSeq data

Alleles around cut-site for sgRNA#1 at day 0

bold Substitutions
Insertions
- Deletions
Predicted cleavage position

```
CTCCTCGCAGACGTCCACGTCGTCGGGGGGGCGGCGGCGGG Reference

CTCCTCGCAGACGTCCACGTCGTCGGGGGGGCGGCGGCGGG 60.96% (6423 reads)
CTCCTCGCAGACGTCCA---CGTCGGGGGGGCGGCGGCGGG 5.72% (603 reads)
CTCCTCGCAGA-------CGTCGGGGGGGCGGCGGCGGG 2.70% (284 reads)
TCCTCGCAGACGTCCACGTTCGTCGGGGGGGCGGCGGCGGG 1.93% (203 reads)
CTCCTCGCAGACGT------------------------------------------------ 1.22% (129 reads)
CTCCTCGCAGACGTCCACGT----------GCGGCGGG 1.15% (121 reads)
CTCCTCGCAGACGTCCACGT---------GCGGCGGCGGG 1.12% (118 reads)
CTCCTCGCAGACGTCCACGT-GTCGGGGGGGCGGCGGCGGG 1.10% (116 reads)
CTCCTCGCAGACGTCCACGT--TCGGGGGGGCGGCGGCGGG 0.80% (84 reads)
CTCCTCGCAGACGTCCACGT---------------------- 0.76% (80 reads)
CTCCTCGCAGA-------CGGGCGGCGGG 0.71% (75 reads)
---------------------------------------- 0.62% (65 reads)
-------------CGTCGTCGGGGGGGCGGCGGCGGG 0.61% (64 reads)
CTCCTCGCAGACGTC----CGTCGGGGGGGCGGCGGCGGG 0.51% (54 reads)
CTCCTCGCAGACGTCCA---------------------- 0.49% (52 reads)
CTCCTCGCAGA-------------------------- 0.49% (52 reads)
CTCCT-------------------------------- 0.47% (50 reads)
CTCCTCGCAGACGTCCA---------CGGGCGGCGGG 0.45% (47 reads)
CTCC-------------------------------- 0.44% (46 reads)
---------------------------------CGGG 0.43% (45 reads)
CTCCTCGCAGACGTCCACGT---------GGCGACGGG 0.43% (45 reads)
CTCCTCGCAGACGTCCACGTCCGTCGGGGGGCGGCGGCGG 0.42% (44 reads)
CTCCTCGCAGACGTCCAC--------GCGGCGGCGGG 0.42% (44 reads)
CTCCTCGCAGACGTC----------------------- 0.41% (43 reads)
CTCCTCGCAGACGTCCACGT-----------GGACGG 0.40% (42 reads)
CTCCTCGCA-------------GGCGGCGGCGGG 0.39% (41 reads)
CTCCTCGCAGACGTCCAC--CGTCGGGGGGGCGGCGGCGGG 0.38% (40 reads)
CTCCTCGCAGACGTCCACGTACGTCGGGGGGGCGGCGGCGGG 0.37% (39 reads)
CTCCTCGCAGACGTCCACGTGGACGTCGGGGGGGCGGCGGCG 0.37% (39 reads)
---------------------------CGGCGGCGGG 0.35% (37 reads)
CTCCTCGC-----------------CGTCGGG 0.35% (37 reads)
CTCCTCGCAGACGTCCACGT-----------CGGCGGG 0.29% (31 reads)
CTCCTCGCAGACGTCC----CGTCGGGGGGGCGGCGGCGGG 0.28% (30 reads)
CTCCTCGCAGACGTCCACGTCGGCG-----------GGG 0.28% (29 reads)
CTCCTCGCAGACGTCCACG-CGTCGGGGGGGCGGCGGCGGG 0.28% (29 reads)
CTCCTCGCAGACGTCCACGT-------GGGCGGCGGCGGG 0.28% (29 reads)
CTCCTCGCAG------ACGTCGTCGGGGGGGCGGCGGCGGG 0.26% (27 reads)
CTCCTCGCAGACGTCCACGTC-----------------G 0.26% (27 reads)
CTCCTCGCAGACGTCCACGTC---------------- 0.25% (26 reads)
CTCCTCGCAGACGTCCACGTAGTCGGGGGGGCGGCGGCGGG 0.25% (26 reads)
CTCCTCGCAGACGTCCAC--------GGGCGGCGGG 0.25% (26 reads)
CTCCTCGCAGA-------------GGCGGCGGCGGG 0.24% (25 reads)
-------------------------CGGCGGG 0.22% (23 reads)
CTCCTCGCAGA-------------------CGGG 0.22% (23 reads)
CTCCTCGCAGAC------------GCGGCGGG 0.22% (23 reads)
CTCCTCGCAGACGTCCACGTCGTC-GGGGGGCGGCGGCGGG 0.22% (23 reads)
CTCCTCGCAGACGTCCACGT----GGGGGGCGGCGGC-GG 0.22% (23 reads)
CTC-------------------GGGGGCGGCGGCGGG 0.21% (22 reads)
CTCCTCGCAGACGTC-----------CGGCGGCGGG 0.21% (22 reads)
```

Alleles around cut-site for sgRNA#2 at day 0

bold Substitutions
Insertions
- Deletions
Predicted cleavage position

```
CGGCATCGCCATCACCCCCGACGGAATGATCGTTGTGGTG  Reference

CGGCATCGCCATCACCCCCGAACGGAATGATCGTTGTGGT  17.34% (5169 reads)
CGGCATCGCCATCACCCCC-ACGGAATGATCGTTGTGGTG  10.77% (3211 reads)
CGGCATCGCCATCACCCC--CGGAATGATCGTTGTGGTG  6.73% (2007 reads)
CGGCATCGCCATCACCCC--ACGGAATGATCGTTGTGGTG  2.99% (890 reads)
CGGCATCGCCATCACC----ACGGAATGATCGTTGTGGTG  2.94% (876 reads)
CGGCATCGCCATCACCCCC-------GATCGTTGTGGTG  2.67% (797 reads)
CGGCATCGCCATC------ACGGAATGATCGTTGTGGTG  2.55% (761 reads)
CGGCATCGCCATCACCC---ACGGAATGATCGTTGTGGTG  2.34% (697 reads)
CGGCATCGCCATCACCCCCG-CGGAATGATCGTTGTGGTG  2.07% (618 reads)
CGGCATCGCCATCACCCCCG--GGAATGATCGTTGTGGTG  1.95% (580 reads)
CGGCATCGCCATCACCCCCG-------GATCGTTGTGGTG  1.92% (571 reads)
CGGCATCGCCATCAC----ACGGAATGATCGTTGTGGTG  1.82% (544 reads)
----------------GACGGAATGATCGTTGTGGTG  1.79% (534 reads)
CGGCATCGCCAT-------ACGGAATGATCGTTGTGGTG  1.24% (370 reads)
CGGCATCGCCATCACCCCC---GAATGATCGTTGTGGTG  1.24% (370 reads)
CGGCATCGCCATCACCCCCGACGGAATGATCGTTGTGGTG  1.08% (323 reads)
CGGCATCGCCATCACCCC--------CGTTGTGGTG  1.05% (312 reads)
CGGCATCGCCATCACCCCCGA------GATCGTTGTGGTG  1.03% (307 reads)
CGGCATCGCC----------------ATCGTTGTGGTG  0.99% (296 reads)
CGGC----------------ACGGAATGATCGTTGTGGTG  0.92% (275 reads)
CGGCATCGCCATCACCCCCG--------CGTTGTGGTG  0.91% (270 reads)
CGGCATCGCCATCACC----CGGAATGATCGTTGTGGTG  0.83% (246 reads)
CGGCATCGCCATCACCCCCG-----TGATCGTTGTGGTG  0.77% (231 reads)
CGGCATCGCCATCACCCCCGA------CGTTGTGGTG  0.77% (230 reads)
CGGCAT----------------CGGAATGATCGTTGTGGTG  0.77% (229 reads)
----------------ACGGAATGATCGTTGTGGTG  0.75% (224 reads)
CGGCATCGCCATCACCCCCGA--GAATGATCGTTGTGGTG  0.71% (213 reads)
CGGCATCGCCATCACCCCCG----ATGATCGTTGTGGTG  0.68% (202 reads)
CGGCATCGCCATCACCCCCGA-GGAATGATCGTTGTGGTG  0.67% (201 reads)
CGGCATC----------------ACGGAATGATCGTTGTGGTG  0.67% (199 reads)
CGGCATCGCCATCA-CCCCGACGGAATGATCGTTGTGGTG  0.65% (193 reads)
CGGCATCGCCATCACCCCCGTACGGAATGATCGTTGTGGT  0.64% (192 reads)
CGGCATCGCCATCA-----ACGGAATGATCGTTGTGGTG  0.64% (191 reads)
CGGCATCGCCATCACCC---CGGAATGATCGTTGTGGTG  0.64% (190 reads)
----------------------------GTTGTGGTG  0.63% (187 reads)
CGGCATCGCC----------ACGGAATGATCGTTGTGGTG  0.63% (187 reads)
CGGCATCGCCATCACCCCCG----------TCGTTGTGGTG  0.62% (186 reads)
CGGCATCGCCATCACCCCC--CGGAATGATCGTTGTGGTG  0.58% (174 reads)
CGGCATCGCCATC-------------ATCGTTGTGGTG  0.56% (166 reads)
CGGCATCGCCA---------ACGGAATGATCGTTGTGGTG  0.55% (164 reads)
CGGCATCGCCATCACCCCC----------------GGT  0.47% (140 reads)
CGGCATCGCCATCACCCCCGTAACGGAATGATCGTTGTGG  0.46% (138 reads)
CGGCATCGCCATCAC-------------------------  0.40% (120 reads)
CGGCATCGCCA----------GATCGTTGTGGTG  0.39% (116 reads)
CGGCATCGCCATCACCCCCGCACGGAATGATCGTTGTGGT  0.37% (110 reads)
CGGCAT----------CGACGGAATGATCGTTGTGGTG  0.37% (109 reads)
CGGCATCGCCATCACCCC-----------------GTG  0.34% (102 reads)
CGGCATCGCCATCACCCCCG-----------------  0.34% (100 reads)
CGGCATCGCC----------ATGATCGTTGTGGTG  0.32% (94 reads)
CG----------------GATCGTTGTGGTG  0.32% (94 reads)
```

Plagiarism analysis

This dissertation was scanned for plagiarism using the online available plagiarism detection tool PlagScan (https://www.plagscan.com). The report was reviewed and text passages evaluated as non-plagiarised were excluded manually from the report. The final plagiarism results are depicted in Figure S4.

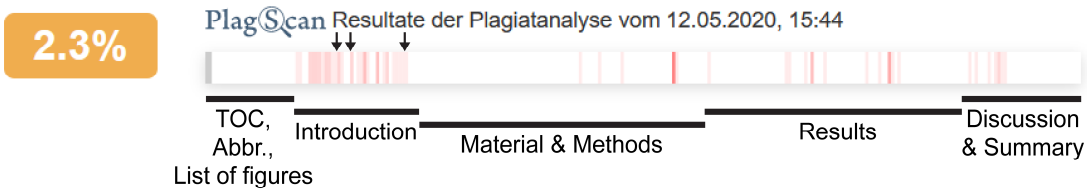

Figure S4 – Results of the plagiarism analysis
By scanning the present thesis for plagiarism using the online available plagiarism detection tool PlagScan (https://www.plagscan.com) and careful examination of the results, a PlagLevel of 2.3 % was obtained indicating the percentage of plagiarism within this work. The figure was obtained from PlagScan (https://www.plagscan.com). Arrows indicate short text passages which have been rephrased after the plagiarism analysis. TOC = Table of contents; Abbr. = Abbreviations.

Acknowledgement

First of all, I would like to thank Prof. Dr. Waldemar Kolanus for his scientific guidance and supervision of my PhD project.

Besides my supervisor, my sincere thanks go to my thesis committee: PD Dr. Heike Weighardt as second reviewer as well as Prof. Dr. Michael Hölzel and Prof. Dr. Anton Bovier as additional members of the examination board.

Special thanks go to the Jürgen Manchot Stiftung for their financial support which enabled my research project in the first place.

Furthermore, I want to thank Prof. Dr. Hubert Schorle for providing the germline-specific Trim71 knockout mice. My project also greatly benefited from the Illumina MiSeq analysis which was performed at Next Generation Sequencing Core Facility at the University Bonn with special thanks to Dr. André Heimbach for his technical expertise.

I would like to express my gratitude to all members of the Kolanus group who have supported me throughout my PhD studies. Especially I would like to thank the current and former “Trim-team”, including Dr. Lucia Torres Fernández, Dr. Stefan Weise, Dr. Karin Schneider and Dr. Sibylle Mitschka, for the helpful scientific advices and discussions. I am deeply grateful to Dr. Lucia Torres Fernández as one of the “Trim-team” members who always supported and encouraged me in all scientific as well as non-scientific aspects. I also want to thank Dr. Bettina Jux for her continuous scientific input and stimulating discussions. My further thanks go to Christa Mandel, Karolin Zölzer, Barbara Reichwein, Helga Ueing, Susanne Weese and Katrin Heße for their help and assistance in daily lab matters such as buffer preparation, genotyping, general organization of the lab or by simply their positive attitude. Not to forget, Gertrud Mierzwa and Katharina Fast who kept the lab running by their work in the scullery. Moreover, thanks to all present and former members of the Kolanus lab, also including Nicole Dörffer, Carsten Küsters, Dr. Thomas Quast, Dr. Johanna Kolanus, Dr. Anastasia Solomatina, Dr. Angrit Namislo, Dr. Michael Rieck, Dr. Felix Eppler and Dr. Felix Tolksdorf, for the really nice working atmosphere and the enjoyable times both inside and outside the lab.

Last but not least, a very special thanks to my family and friends for their endless support and encouragement over the last years. Especially to my parents and my brother who supported me emotionally and morally along the way and in my life in general.

“Our knowledge is a little island in a great ocean of nonknowledge”

Isaac Bashevis Singer